International Journal of Computational and Engineering

JUNE 2019 VOLUME4 NUMBER2

Publisher: ACADEMIC PUBLISHING HOUSE
Address: Quastisky Building, Road Town, Tortola, British Virgin Islands
UK Postal Code: VG1110

E-mail: editorial@ij-ce.com
www.ij-ce.com

ACADEMIC PUBLISHING HOUSE

CONTENTS

Design and Control Strategy of Chang'e-3 Soft Landing Orbit

Ai-ai Wang [1,2], Zhi-li Liu [1,2], Xiao-zhen Shi[1,3]
[1]North China University of Science and Technology, Tangshan, 063210, Hebei, China
[2]Yisheng Innovation Education Base, Tangshan, 063210, Hebei, China
[3]College of Chemical Engineering, Tangshan, Hebei, China
**E-mail: 1378817379@qq.com*

Abstract: The core task of Chang'e-3 is to achieve a high reliability and safety soft landing on the moon, requiring the lander to have the ability of autonomous obstacle identification and avoidance. In this paper, the flight dynamics models of the main deceleration stage, fast adjustment stage, obstacle avoidance stage and slow descent stage of the lunar soft landing are studied. According to the dynamic equation, the guidance laws of each stage are optimized, and the descent trajectory is optimized. Combining with engineering practice, the control strategy of Chang'e 3 soft landing orbit is established.

The first step is to determine the position and velocity of the near and far moons of the landing preparation orbit. A fixed coordinate system (agreement lunar coordinate system) centered on the lunar center is established to analyze the forces on Chang'e 3 and establish a two-dimensional dynamic model. Finally, the position of the nearest point is (19.43 degrees W, 29.01 degrees N) and the far point is (160.57 degrees E, 29.01 degrees S). The velocity of the perilunar point is 1.692 km/s and that of the far point is 1.614 km/s. The results show that T = 530, Q has a relatively small value of 1098.6 kg.

The second step is to optimize the fuel consumption in the landing preparation stage and the main deceleration stage. Take the nearest point to the center, coordinate A (1149, 1153). In the fast adjustment stage, the guidance law with linear variation of thrust magnitude and direction is used. For the rough obstacle avoidance section, the optimal switching guidance law is adopted first, and then the optical image-based rough obstacle detection algorithm is adopted. Through the analysis and processing of the image, the over-bright and over-dark obstacles are judged, and the major obstacles in the current falling area are identified, so as to determine the safe area. For avoiding obstacles, the main task is to avoid obstacles on the lunar surface. The method of obstacle avoidance recognition and safe landing area selection based on three-dimensional image is used to determine the safe area. In the slow descent stage, the main task is to achieve the relative rest of the moon at a distance of 4 M. The vertical soft landing model and the equivalent continuous variable thrust guidance rate are used to analyze the free landing of Chang'e 3 to the precise landing point.

Keywords: Orbital optimization; Lunar soft landing; Flight dynamics model; Two-dimensional analytical dynamic model

1. RESTATEMENT OF THE PROBLEM

1.1. Background introduction

Soft landing on the lunar surface is an important step in the lunar exploration program. The so-called lunar soft landing means that the lander, under the action of the braking system, landed at a small speed and accurately in the designated area of the moon to ensure the safety of test equipment and astronauts[1-3]. Because there is no atmosphere on the lunar surface, the entire soft landing process needs to guide the engine. The flight dynamics model of the lander is established correctly, and the descent trajectory and guidance law of the lander are optimized on this basis. It has important guiding significance for the design of lander flight procedure and fuel consumption[4-8].

1.2. Problems to be solved

According to the topic of information and the attachment content, we need to analyze the goddess of the moon landing number three six stages of the process, and establish reasonable lander flight dynamics equation, and then according to the different characteristics of six stages in the process of soft landing and declining trajectory of chang 3 requirements established and various stages of the optimal control strategy, finally, the model for the error analysis and sensitivity analysis.

2. PROBLEM ANALYSIS

Fuel consumption optimization is the main optimization objective in the landing preparation stage and the main deceleration stage. Quick adjustment period, using the linear change of size and direction of thrust guidance law, for coarse obstacle avoidance, first using the optimal guidance law, and then the coarse obstacle detection algorithm based on optical image, the imaging based on optical image, based on image analysis and processing, the judge had bright and the dark obstacles, identify the current decline in area of obstacle, to determine the safety area[9]. For the fine obstacle avoidance segment, the main task is to fine avoid obstacles on the lunar surface. The method of obstacle avoidance recognition and safe landing area selection based on

3D image is adopted to determine the safe area. The main task of the slow descent stage is to achieve a static position relative to the lunar surface at a distance of 4m[10-12].The model of vertical soft landing and the equivalent continuous variable thrust guidance rate are used to analyze the chang'e-3 free fall to the exact point of the moon.

Then, the error analysis of the engine thrust, initial velocity and initial height in the designed landing orbit and control strategy is required, and the influence of the different terrain heights of the lunar surface in the rough obstacle avoidance stage and the fine obstacle avoidance stage on the required adjustment probability of chang'e-3 landing is called sensitivity analysis.

3. ASSUMPTIONS OF THE MODEL

1) The fuel consumption of attitude engine is not considered.

2) All external forces acting on the detector pass through its center of mass.

3) The influence of lunar oblateness on Chang'e-3 soft landing is not considered.2

Symbol	Meaning
F	Main thrust
G_m	The Moon's Gravitation
a	acceleration
a_x	Horizontal acceleration
a_y	Vertical acceleration
G	Universal Gravitation Constant
n	Fuel consumption per unit time (kg)
v	Specific impulse in m/s unit
θ	Direction angle of main driving force
φ	Direction of acceleration
Q	otal fuel consumption of Chang'e-3 (kg)
M_0	Initial mass of Chang'e 3
m_t	Quality of Chang'e 3

4) The soft landing process of Chang'e-3 is only affected by the general gravity of the moon, without considering the influence of the sun, the earth disturbance and the aspheric gravity disturbance of the moon.

4. ESTABLISHMENT AND SOLUTION OF MODEL

4.1 Model preparation

The flow chart of this question is shown fig.1 below.

4.2. Solution of model

4.2.1. Rapid adjustment phase

In order to meet the requirement of uniform transition of thrust and attitude of the main engine, the thrust model of the rapid adjustment stage is established as follows

$$\begin{cases} F = k_1 t + b_1 \\ \lambda = k_2 t + b_2 \end{cases} \tag{1}$$

In this expression, F is the thrust, λ is thrust direction angle,that is, the angle between the thrust direction and the local horizontal line.

Assume that the initial moment of the fast-tuning phase is t_2' Termination time is t_3. The dynamic equation of this stage is

$$\begin{cases} v_x(t_2)=v(t_2)\cos\lambda(t_2) \\ v_y(t_3)=v(t_3)\sin\lambda(t_3) \end{cases} \tag{2}$$

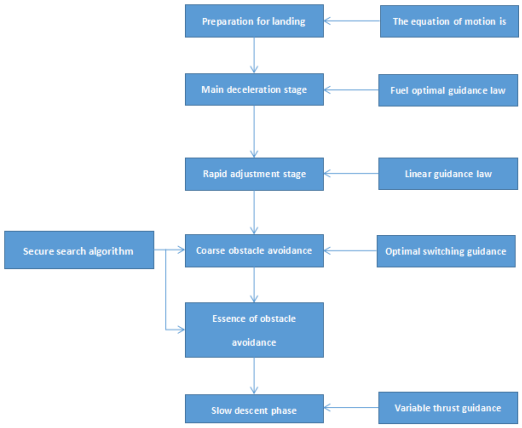

Figure 1. Question 2 Flow chart

4.2.2. Rough obstacle avoidance section

4.2.3. Optimal switching conductivity

Assume that the initial moment of the rough avoidance segment is t_3, termination time is t_4, Based on Planar Moon Model[6] , the equation of motion is as follows:

$$\begin{cases} h = -v\cos\gamma \\ v = -\dfrac{FS}{m} + g_m\cos\gamma \\ \gamma = -\dfrac{g_m\sin\gamma}{v} \\ m = -\dot{m}S \end{cases} \tag{3}$$

Among h is the height of the moon, γ angle between falling velocity v and vertical direction, Called drop Angle, g_m is the moon's gravitational acceleration, S is the switching value for braking force, It is defined as follows

$$S = \begin{cases} 0 & t \in [0, \ell] \\ 1 & t \in [\ell, t_f] \end{cases} \tag{4}$$

The type (14) indicates that the lander in the coarse avoidance section will first do a free fall motion and then fall down to the near-segment terminal by means of a starting mechanism.

In order to simplify the process, two simplification co nditions are introduced within a certain range of error s:

1) The lander approaches a vertical descent at this sta ge, γ treated as a small quantity, so

$$\begin{cases}\sin\gamma \approx \gamma \\ \cos\gamma \approx 1\end{cases} \tag{5}$$

2) The duration of this phase is shorter, and the assumption of quality invariance is introduced.

$$\frac{F}{m_{0a}-\dot{m}(t_{fa}-\ell)} \approx \frac{F}{m_{0a}} = a_{Fa} \tag{6}$$

*a*indicates the initial state of the coarse avoidance seg ment, f indicates coarse avoidance segment termination statu.

Finally, we obtain the simplified equation of motion as shown below.

$$\ell^2 + \frac{2v_{0a}}{g_m}\ell - \frac{2(a_{Fa}-g_m)(h_{0a}-h_{fa})-(v_{0a}-v_{fa})^2}{a_{Fa}-g_m} = 0 \tag{7}$$

4.2.4. Rough obstacle Detection algorithm based on Optical Image

The features of the rock pit images on the lunar surface are as follows:

1) the rock on the crater surface has a high brightness. 2) there are obvious shaded areas in the crater. 3) there is a strong contrast between the bright areas and the shadows, which are the targets of our elimination.

1. The Segmentation of Optical Image and the recognition of obstacle area

The optical image will be divided into *m*×*n* equal squares，The *TIF* diagram provided is 2300×2300 resolution， divide the gray value into 23×23， each pixel is 100×100, and then count the gray values of each grid.

There are 100×100 grayscale levels per cell，too large a grayscale means too bright, that is, rock on the surface of a rock pit, too small to represent a rock pit, is a dark area, when the gray scale of a grid is too large or too small points, this grid is identified as a barrier area, can not land. You need to count points that are too large and too small for grayscale, as follows

Let the initial value of the number of obstacle are *sum* as be 0 Barrier number threshold is $threshold$， the critical value of overdark grayscale is Dark, the overlighted gray value is Light, within a lattice 100×100 of grayscale points *x* if,

$$x < Dark \quad or \quad x > Light$$

Indicates that the gray point x is a barrier point， sum the statistical value plus one, when a lattice of statistics is complete, if

$$sum \geq threshold$$

That is, the number of obstacles exceeds the threshold, and then the lattice is judged to be a barrier area. For convenience, the mark barrier area is located in the lattice 0, the non-barrier area is 1.

Search safe Landing area by Spiral search algorithm

A spiral search algorithm, Fig.2, is used to search the barrier-free area from the middle of the table. Once the barrier-free area is found, set a security radius for it. Continue searching, and if you have a barrier-free area within a safe radius, the area within that radius is set to a safe landing area.

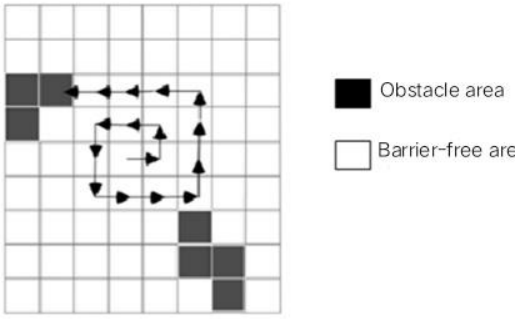

Figure 2. Spiral search algorithm diagram

4.2.5. Fine avoidance section

Selection of fine avoidance obstacle recognition area and safe landing area based on three-dimensional image

The designed algorithms of precision obstacle identification and safe landing selection are as follows: 1) pre-processing data, constructing terrain three-dimensional elevation map in survey coordinate system (2) average slope surface construction, using least square method to fit the average slope surface of a certain unit area; 3) calculating the average slope, calculating the average slope of the region according to the average slope, 4) calculating the obstacle height, estimating the barrier height of each cell in the region according to the average slope surface; 5) the safe landing zone constituency uses a clockwise forward search method starting from the center of the landing area until the location of the area that meets the landing requirements is found.

4.2.6. Slow descent stage

4.2.6.1. Vertical soft landing model

Near the end of the segment, the lander is very close to the lunar surface, and the descent rate is almost perpendicular to the local horizontal level. By means of piecewise control, the lander goes through several processes, namely, hovering, uniform acceleration, uniform deceleration and mechanism landing. The acceleration distribution of each segment is as follows:

$$\begin{cases} a_{ol} = a_{F_0 l} - g_m = 0 \\ a_{1l} = a_{F_1 l} - g_m < 0 \\ a_{2l} = a_{F_2 l} - g_m > 0 \\ a_{3l} = -g_m \end{cases} \tag{8}$$

4.2.6.1. Equivalent continuous variable thrust guidance law

Assuming that the acceleration of the equivalent thrus t varies linearly, the orientation is positive, and there a re

$$a_{Fl} = K \cdot t + (a_0 + g_m)$$

Among, K slope representing equivalent thrust acceleration，K>0 indicates a gradual increase in thrust，K<0 indicates a gradual decrease in thrust；a_0 represents the equivalent thrust acceleration relative to the lunar gravity acceleration g_m initial offset. $a_0>0$ indicates that the initial thrust acceleration is greater than g_m, $a_0<0$, indicates that the initial thrust acceleration is less than or equal to g_m.

Combining shutdown conditions

$$\begin{cases} v(t_{ft}) = v_{off} \\ \mathrm{h}(t_{ft}) = h_{off} \end{cases} \tag{9}$$

For equation (19), two consecutive integrals on both sides of equation (19) are obtained.

$$\begin{cases} K = 12 \times \dfrac{h_{0l} - h_{off}}{t_{fl}^3} + 6 \times \dfrac{v_0 + v_{off}}{t_{fl}^2} \\ a_0 = 6 \times \dfrac{h_{off} - h_{0l}}{t_{fl}^3} - 2 \times \dfrac{2v_0 + v_{off}}{t_{fl}} \end{cases} \tag{10}$$

Among them, subscript 0 and *f* denote the initial landing and shutdown state respectively, subscript *l* denotes the landing stage, subscript *off* denotes the shutdown time.

4.3. Solution of model

4.3.1. Coarse obstacle avoidance optical image segmentation and recognition of obstacle area

The imread function is obtained by MATLB, and the gray image of the rough obstacle avoidance optical image is read. Considering the gray scale image element, it is rather slow to judge the obstacle area with MATLB, so the gray scale image is input into C++ to solve the model.

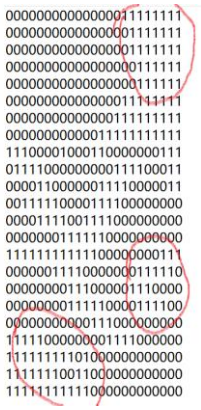

Figure 3. Comparison of obstacle area 0-1 with original TIF map

When using C++ to partition and identify obstacle areas, the values are set after many tests: The threshold value is 80, the critical value of over-dark gray level is 84, and the critical value of over-bright gray level is 105. The 0-1 figure of obstacle area is obtained as follows in fig.3 , and its correctness can be verified by comparing with TIF in fig.4.

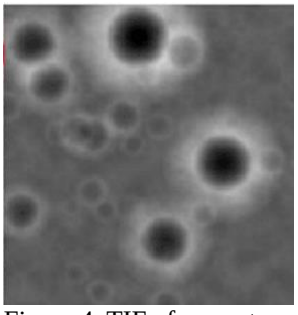

Figure 4. TIF of correctness

Area 0 corresponds to the rock pit area of the original map, area 1 corresponds to the flat area of the original map, and area 1 is the suitable safe area. The calculated results are in good agreement with the actual TIF diagram. The area included in the circle is the area where the final coarse obstacle avoidance process is suitable for safe landing.

5.EVALUATION AND IMPROVEMENT OF THE MODEL

5.1. Model evaluation

For the near-moon point and far-moon point in problem 1, it is necessary to establish the dynamic model, followed by the linear programming model. It is necessary to analyze the force of Chang'e-3 in detail, and to determine the objective function and the constraint conditions. Therefore, the data of near and far meniscus are not solved directly in theory. The advantages of the above-mentioned model are simple and clear, and the problem is directly transformed into solving the maximum value on the two-dimensional plane, which simplifies the solution of the practical problem.

For solving the optimal landing point by using the maximum slope model, in order to reduce the data processing, this paper does not deal with all the points of the elevation map given in all the problems. Instead, a range is determined first according to the constraints and observations of nonlinear programming, then further verified, and then the optimal landing point is found. Although the elevation map data is more accurate, but will still have a certain impact on the results, this is the source of the error. This paper not only considers the least fuel consumption, but also considers how to find the most reasonable landing point. The minimum fuel is the optimal condition to determine the landing point, and then the orbit is determined.

REFERENCES

[1]Editorial Department of this magazine. Chang'e is precisely recommended to run to the back of the moon by Long March 3A series rockets. China Aerospace, 2019 (01): 24-25.

[2]Sun Liping, Yang Jingchao, Liu Shilong, Zhao Jing, Wang Changting, Chang'e 3 soft landing orbit design and control strategy. New Industrialization, 2018, 8 (12): 108-112+122.

[3]Zhou Zheze, Zhao Meng, Shifan, Chen Shengyong,

Luan Hao. A method for estimating the elevation of Chang'e 3. Journal of Xi'an University of Electronic Science and Technology: 1-7 [2019-04-21]. http://kns.cnki.net/kcms/detail/61.1076.TN.20181217.1102.004.html.

[4]Yan Jin, Xu Xinchao, Zhang Jichao. Research on image matching method of descent sequence of Chang'e-3 lander. Surveying and spatial geographic information, 2018, 41(10): 140-144.

[5]Zhang Xiuzhi, Zhang Yumei, Zheng Cong, Liao Wenkai-Chang'e-3 soft landing orbit design and control strategy model. Science and technology innovation, 2018, (25): 44-45.

[6]Han Puxia. Calculating the lunar elevation of Chang'e-3 based on binocular vision. Tianjin University of Technology, 2018.

[7]Analysis of Key Mechanics Problems in the Release and Separation Process of Zou Huaiwu, Yang Wenzhao, Liu Dianfu, Xiao Jie, Hu Zhenyu, Chang'e 3 Patrol-Lander. Journal of Astronautics, 2018, 39 (01): 9-16.

[8]Qin Jiayong, Pei Yifei, Wang Jing, Yin Xiaofang, Gao Qinghua. Spacecraft Environmental Engineering, 2017, 34 (06): 656-661.

[9]Dingdan. Discussion on the design and control of Chang'e 3 soft landing orbit. Science and Technology Wind, 2017, (23): 7.

[10]Tong Shanshan, Niu Yujun, Chang'e 3 soft landing trajectory model and optimal control strategy. Journal of Nanyang Institute of Technology, 2017, 9 (04): 125-128.

[11]He Jinyang. Optimized Solution of Chang'e 3 Perigee Apogee Model. Enterprise Technology Development, 2017, 36 (07): 30-31+35.

[12]Zhang Qiaoling. The mission of Chang'e 3 and its preliminary scientific achievements. Journal of the Chinese Academy of Sciences, 2017, 32 (01): 85-90.

Design and Implementation of Intelligent Cultivation Plan and Syllabus Arrangement System

Wen-xiang Hou, Bo-tao Liu, Li Lu, Shi-mian Li, Kai-hong Xiao, Fan Gao*
College of Computer Science, Yangtze University, Jing Zhou, China
**E-mail:liubotao920@163.com*

Abstract: The development of cultivation plan and syllabus is of great importance to a school. The traditional manual arrangement method is prone to such problems as inconsistent arrangement contents, low work efficiency, long arrangement period and poor information sharing. Therefore, it is of practical application value and social benefit to compile a cultivation plan and syllabus arrangement system based on process and network.

This paper makes a comprehensive use of the knowledge of software engineering, database and software development, and on the basis of in-depth research on the cultivation plan and the preparation and audit process of the syllabus, puts forward a detailed demand analysis of the system, and develops a cultivation plan and syllabus arrangement system with Java. The main function of the system is to complete the Making, audit and publishing of cultivation plan, course information and syllabus online, and the requirements, design, implementation and testing of the system are discussed in detail in this paper. The test results of its functionality and robustness show that the system function is basically completed and the operation is stable and reliable.

Keywords: Cultivation plan arrangement system; Curriculum syllabus arrangement system; Curriculum information arrangement system; SSH

1. INTODUCTION

At present, the departments of Colleges and universities use the traditional manual way to arrange the cultivation plan and syllabus, the traditional way has the arrangement content inconsistency and the arrangement work inefficiency flaw [1-2]. After adopting this system, the inconsistency between cultivation plan and syllabus will be solved, and the efficiency of cultivation plan and syllabus will be greatly improved.

Although most of the universities' educational administration system have related modules, but most of the function is not complete, cultivation programs, curriculum information and course syllabus, three only one or the other, and because there are a large number of text messages, most of them choose to write cultivation plans and syllabuses as static web pages, and make it into the web site of the departments [3-5]. This not only can not quickly access to relevant information, but also the maintenance of the site caused great inconvenience. This system saves the information in the database, the dynamic management, can realize the on-line manufacture and the audit, will greatly enhance the work efficiency. This system uses the program of graduate school of Tianjin University for reference, displays all the cultivation plans and teaching syllabus in a centralized way, and manages them uniformly.

2. DEMAND ANALYSIS

The system can be divided into three modules: general manager module, foreground module and database module. The block diagram of its functional modules is shown in figure 1.

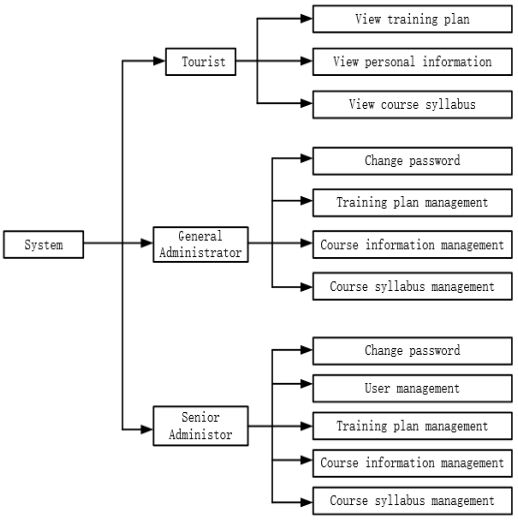

Figure 1. System function block diagram

2.1. General Manager Module

Submit: write cultivation plan, course information sheet and course syllabus and submit to senior manager for audit.

View: view the status of the cultivation plan, course information sheet, and course syllabus.

Revision: revise the failed cultivation plan, course information sheet and course syllabus and submit them to the senior manager for audit.

Deletion: have the authority to delete the failed cultivation plan, course information sheet and course syllabus.

Change password: General manager can change their own password.

2.2. Foreground Module

For all users, without login, any user can access.

Query classification: the user realizes the navigation function by querying the first level classification and the second level classification.

Query module: users can query the approved culvation plan, course information sheet and course syllabus

2.3. Database Module

The operation of the general manager is different from that of the senior manager, and the general manager can only submit and modify the cultivation plan, course information sheet and course syllabus. The senior manager completes the audit function and system maintenance, because the foreground of the system is open, no registration is required, the manager is only for a small number of teachers and management workers, so no registration is provided, the general manager is managed by the senior manager [10] .

According to the above demand analysis and the hand-made table of cultivation plan and syllabus, the relationship between the main entities and attributes can be analyzed. Figure 2 to figure 5 respectively represent the E-R diagram of users, course information, syllabus and cultivation plan.

3. SYSTEM DESIGN AND IMPLEMENTATION

3.1. Technical Roadmap

The technical roadmap of this project is shown in figure 6. Html+CSS3+JavaScript is adopted in the front end, SSH framework is adopted in the background, and Mysql [8-9] is selected as the database.

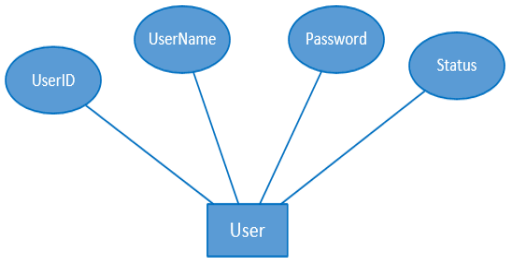

Figure 2. User E-R diagram

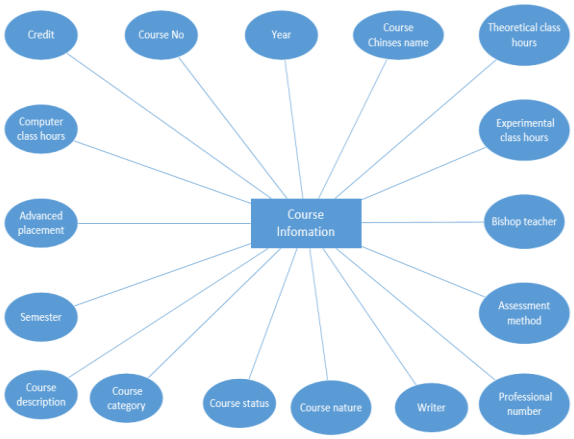

Figure 3. E-R diagram of course information table

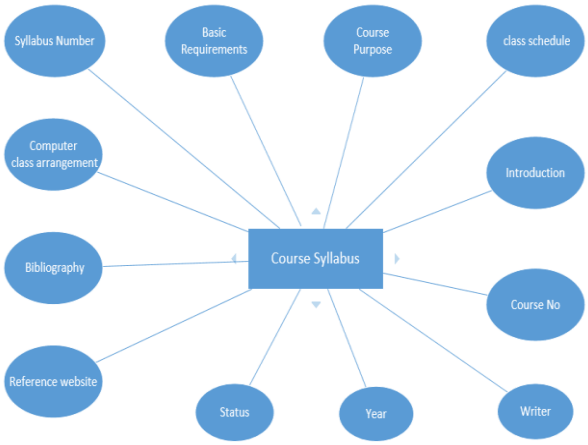

Figure 4. E-R diagram of the course syllabus

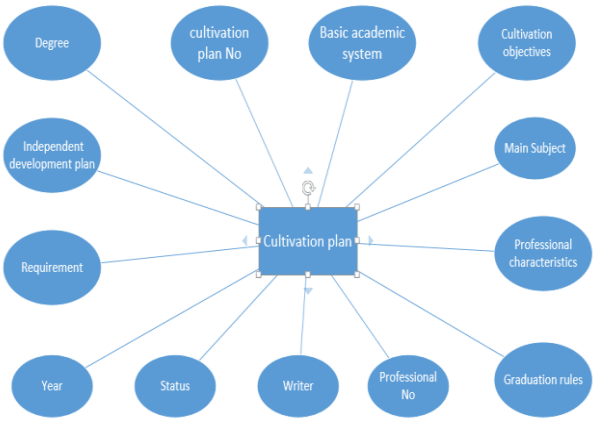

Figure 5. E-R diagram of the cultivation plan

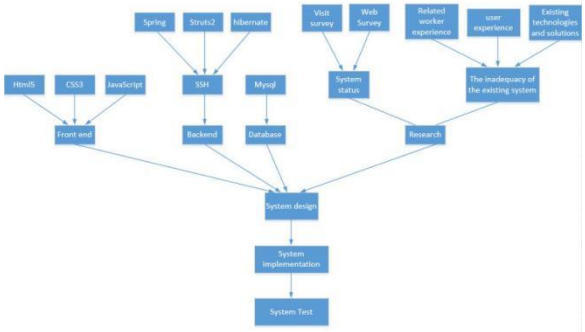

Figure 6. Technology roadmap

3.2. Whole Design

In the whole design process of this system, the database is named after t_+ module. The system is divided into four packages, action, service, dao and entity, entity class object, and the mapping relationship between entity and table is placed under entity package. Interactive actions with the foreground JSP are placed in the action package, service layer is responsible for business logic management, database operations are classified in the dao package. Spring's configuration files are named after entity classes and imported into the main configuration file. JSPS for different modules are also placed under packages named after entity classes.

The system flow is shown in figure 7 below.

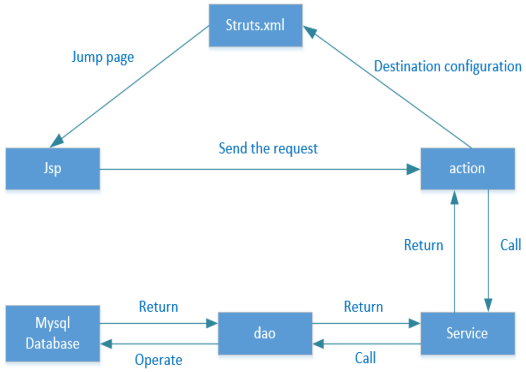

Figure 7. System module logic diagram

3.3. Logical Realization of System Module

3.3.1. User login module

User input user name, password, and through the drop-down boxes to select identity, wrapped it in Action, in turn into the Dao layer, and to query the database as a parameter, if there is a corresponding user returns the object, if there is no corresponding user returns null, determine the user's identity in the Action, then in the session, keep the login, and return a different string, according to the string, jump to different operating interface, its main node block diagram are shown in figure 8 below.

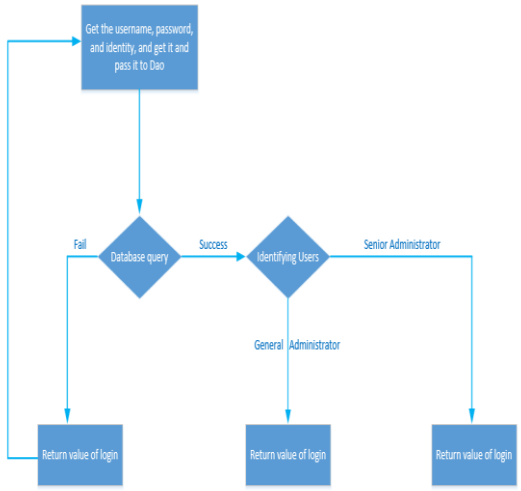

Figure 8. Schematic diagram of user login process

3.3.2. General manager module

The main node flow for a general manager to change a password is shown in figure 9 below.

The general manager modifies the password, first obtains the own id through the session, then obtains the personal information through the id query database and displays the password, then updates the personal information through the id. This content senior manager process and general managers are exactly the same.

General managers draft course information, course syllabus and cultivation plan, in which the foreign key related major is the dropdown box obtained by database query, the other dropdown boxes are the values limited by the page, the author cannot edit, must be the login user, and the default is the current user [11]. The main node for the general manager implementation to add course information is shown in figure 10.

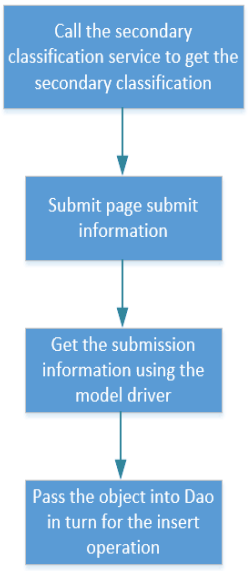

Figure 9. Schematic diagram of password modification process

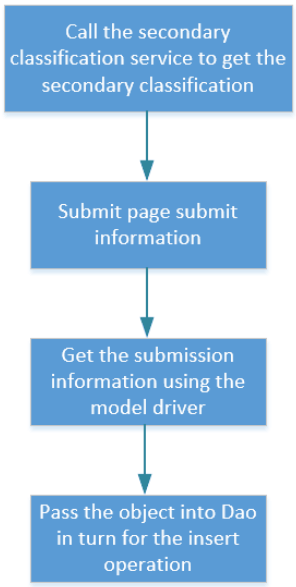

Figure 10. Schematic diagram of adding course information flow

The general manager has the right to modify and delete the failed cultivation plan, course information sheet and course syllabus. First query status to the query conditions had not been approved to cultivation plan, course information table and the list of the syllabus, by adding hyperlinks, and pass the primary key as a parameter, to remove, or modify its record, revised and resubmitted to senior manager audit, so until the audit by publishing to the foreground or delete the record.

3.3.3. Senior manager module

The senior manager of the user management, through the model-driven access to the page to add information, successively transferred to the dao layer for insertion operations; Through the writer query list, and in the form of hyperlink, get the primary key to delete the general manager [12].

Figure 11 is the main node-block diagram of the audit. First, the collection is returned through query and displayed in the interface, and then the status of each table is updated by obtaining the primary key to realize its audit function.

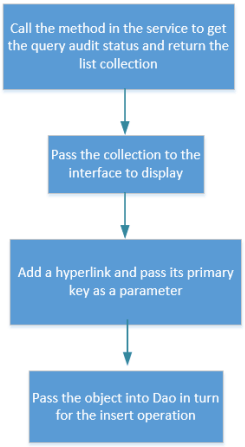

Figure 11. Schematic diagram of audit process

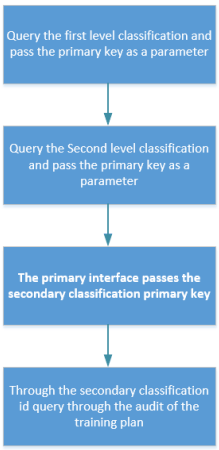

Figure 12. Schematic diagram of general tourist inquiry

3.3.4. Tourists module

Ordinary tourists can query the first level classification list and the second level classification list successively through the navigation window, and query the course information list, course syllabus and cultivation plan information through the second level classification id [13], its main nodes are shown in figure 12.

3.3.5. Database design and implementation

Through the analysis of database requirements, the relational model can be transformed into the relational data model supported by a specific database -- database tables [14-15], the above main entities can be transformed into database tables, such as the user t_user table, the t_courseinfo table, the t_ outline table, and the t_trainingplan table. Due to space limitations, I will not elaborate here.

4. SYSTEM TEST

All the functions of the system were tested according to the requirement analysis. Due to space limitations, only major functional tests are listed here as shown in table 1 below.

Test the modules involved	Test feature	Test purposes	The test results	The test results
Tourist/general manager/senior manager	Log on to the test	Can you login	Can login, whether the normal maintenance of personal information	The module works normally
General manager/senior manager	Develop a cultivation plan to test	Test whether the cultivation plan can be submitted to the senior manager correctly	Senior manager can review, modify and call back the cultivation plan	The module works normally
General manager/senior manager	Develo a syllabus	Test for correct submission of syllabus values to the senior manager	Senior managers can review, modify and type back the syllabus	The module works normally
Tourist/general manager/senior manager	Foreground syllabus query test	Test whether the user can query the syllabus of the specified course	Users can query the designated and approved syllabus	The module works normally

The test results show that the basic functions of the system are complete and basically meet the requirements of demand analysis, and the system runs stably with good robustness.

5. CONCLUSION

This paper mainly discusses the design and implementation of intelligent cultivation plan and syllabus arrangement system. Through this system, the making and modification of cultivation plan and syllabus, the audit and publishing of superior leaders, and the visit of foreground tourists can be realized online. The system uses Java as the development language, SSH as the development framework, Mysql

as the database [20]. Compared with the traditional manual production method, this system can greatly improve the work efficiency and data accuracy, and compared with the current market equivalent system, has the advantages of cross-platform, comprehensive functions, system maintenance difficulty is small.

ACKNOWLEDGEMENTS

This paper was financially supported by four projects: The project of young people in the Education Hall of Hubei (No. Q20161311), The Yangtze Youth Fund (No. 2015cqn53), Teaching and research project of Yangtze University (No. JY2015038), the Yangtze University Students' Innovation and Entrepreneurship Training Program Project (No. 2016081)

REFERENCES

[1]LI Hai-jian, TIAN Yue-xin, LI Wen-jie Mobile Internet Thinking and Traditional Business Reengineering. China Industrial Economics, 2014(10).

[2]ZHOU Hong-duo. I understand that the "Internet +" - "Internet +" is a kind of fusion. Modern Communication, 2015 (08).

[3]HU Wen, LI Yan. Analysis of MySQL DataBase Storage Engine. Software Guide, 2012(12).

[4]XUE Zhi-liang. Configuration of JSP and Servlet development environment under Tomcat. China Science and Technology Information, 2006(20).

[5](Germany) Christian Bauer. Java Persistence with Hibernate. People Post Press, 2007.

[6]ZHOU Hong-jing, YANG Jin-min. Object persistence implementation based on Hibernate. Computer Era, 2009(03).

[7](America)Rod Johnson etc. Professional Java Development with the Spring Framework. Mechanical industry press, 2006.

[8]ZOU Cun-jie. The researc and application of the Spring framework which based on MVC pattern. Dalian Maritime University, 2006.

[9]WANG Tao-tao, LI Xiao-yu, SHI Wei-li. Design and Implementation of Authority by Struts 2 Intercept. Computer and Modernization, 2009(01).

[10]LI Xiang. Design and Implementation of Web Application System Among Struts2 Framework. Southwestern University of Finance and Economics. 2010.

[11]Brown D, Davis c. Struts2 in Action, 2008.

[12]CHEN Hui-min, ZHANG Rui. Theory and Application of Software Engineering. Journal of Xi'an Petrdleum Institute (Social Sciences Edition), 2001(04).

[13]LIU Hong-mei. Development of Application System Based on C/S and B/S Architecture. Computer and Modernization, 2007(11)

[14]WU Wen. Analysis of Web Development Techniques based on Java. Science Mosaic, 2013(05)

[15]CHANG Jin, ZHENG Ke, XU Yan-qun. Research and Application of Lightweight Framework Based on SSH. Coal Mine Machinery, 2010(08).

[16]LI Yang. Design and Implementation of SSMin Web Application Development. Computer Technology and Development, 2016(12).

[17]LIU Tian-yin. HTML5 and Web Application Platform in the Future. Yinshan Academic Journal (Natural Science Edition), 2010(02).

[18]Gong Yun-zhan. Software testing course. Mechanical industry press, 2008.

[19]Wang Xiao-hua. Software Testing Technology Application Research. Defence Science & Technology Industry, 2012(03).

[20]Bruce Eckel. Thinking in Java. Mechanical industry press, 2007.6.

Research on High Precision Detection System Based on Infrared Sensing Technology

Jing Zhao
Electric and Electronic Engineering Department, Zibo Vocational Institute, Zibo, 255314, China
E-mail: 1827735183@.qq.com

Abstract：The system is based on infrared sensing technology and is used to detect the diameter of objects. Through the debugging of the selection, the system installation can achieve an impact distance of 5mm-30m.Adjusting the system accuracy, the system can automatically detect the diameter $\Phi \geqslant$ 0.05mm.The article introduces the workflow of the system and the design principles of the main functional modules.
Keywords: Photoelectric control; Pulse modulation/synchronous demodulation; Detection system

1. INTRODUCTION

The detection control circuit is one of the core technologies of the automation control system. Its sensitivity, accuracy, service life, safety, stability and other factors directly determine the advantages and disadvantages of the automation control process.

Through the investigation of cotton textile enterprises, it was found that some spinning equipment still uses on-site manual quality inspection. Because manual testing can not guarantee the timely splicing of cotton sliver and the stability of cotton yarn diameter, it causes problems such as product quality and low production efficiency.

In order to ensure the improvement of product quality and efficiency, a high-precision detection and control system based on infrared sensing technology is adopted. The system can be used not only in textile machinery, but also in traditional forging machines and machine tools by adjusting the system accuracy, sensitivity and measuring range. It can also effectively protect personal safety.

Because infrared has strong penetrating ability andanti-interference ability, it is not easy to scatter and is not easy to cause crosstalk. The system uses infrared-based sensing and uses modulation/demodulation technology to complete the system signal transmission and reception design.

2. SIGNAL FLOW AND PRINCIPLE OF THE SYSTEM

From the infrared emission tube to the relay control device to stop and start, it is the main channel for processing the unit signal.In the main channel, electrical signals are transmitted in the order shown in Figure 1.

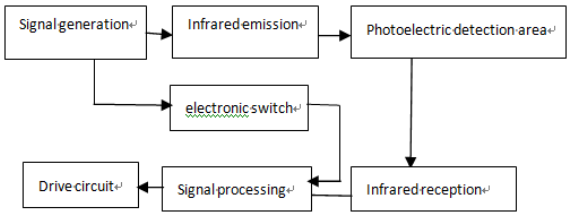

Figure 1.Signal main channel

Infrared luminescent tube and infrared receiving tube are separated on both sides of photoelectric detection area, which need little maintenance. Infrared receiver is a photosensitive current source. The photosensitive current increases with the increase of light flux. When the photosensitive current charges the capacitor, the electrical signal changes with the change of light flux can be obtained.

When there is no shield, the light path is unimpeded and the photosensitive current is the largest; when there is a shield passing through the detection area, the part of the light path is blocked, the output potential increases, and the larger the shading area, the higher the output potential.

By adjusting the sensitivity of the detection system, the principle can be used to measure and control the diameter or area of the object to be measured, so as to realize quality inspection or safety protection. Multi-station monitoring can be realized through the connector [1].

In this design, pulse modulation and synchronous demodulation are used to generate and pick up infrared light. Compared with dc light, pulse-modulated light enhances the ability towithstand stray light and electromechanical interference in the workshop.On the other hand, the life of the illuminating tube is relatively prolonged due to the pulse state.When a shield enters the detection area, the intensity of the light received by the infrared receiver will change abruptly. Therefore, the estimated value of the variable light is used as the occlusion signal.

Traditional safety protectors are prone to misoperation, such as when lighting is turned on or off, signal processing unit will judge them as occlusion signal and misoperation. In the design of the system, pulse modulation/synchronous demodulation is used to make the infrared luminescent tube emit signal for a period of time and turn off the signal for a period of time, that is, to emit infrared light in the form of pulse. Similarly, the

infrared receiving tube is only turned on during the period when the infrared luminescent tube transmits the pulse signal. Luminescence and reception are synchronized in time, so only the light emitted by the infrared light emitting tube can be detected, and the stray light from the outside can be excluded from the screen, which greatly improves the anti-interference ability of the control system and greatly reduces the misoperation.

3. DESIGN OF MAIN FUNCTION MODULES

The control system mainly consists of the following circuit modules: high stability and low power DC power supply system, signal generation system, infrared pulse transmission system, electronic self-locking switch system, infrared receiving system, signal processing system, status indicator panel, etc. This paper only explains the design principle of the important functional modules of the system [3].

3.1. Infrared pulse emission

The square wave from the signal generator is buffered, amplified, and frequency-converted to obtain a pulse wave with a smaller duty cycle to drive the infrared transmitting tube to work. This allows the infrared light tube to operate in a pulsed state, greatly extending its service life. The schematic diagram is shown in Figure 2.

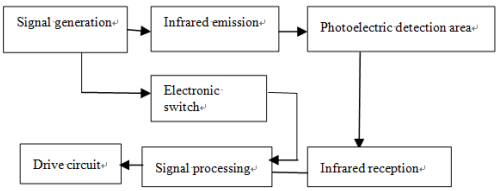

Figure 2.Infrared Pulse Emission

In order to meet the working requirements of the device, more than two infrared luminescent tubes can be connected in series to improve the output power and operating distance, and reduce the required current.

3.2. Infrared reception

When there is no shield in the detection area, the pulsed light emitted by the infrared emitter is received by the receiving tube without shield, and a negative polarity photosensitive voltage is generated on the front capacitor. This voltage is opposite to the voltage at both ends of the front capacitor, and no signal passes through the rear capacitor. When the shield enters the detection area, the intensity of the infrared light received by the receiving tube changes. Thus, a signal passes through the post-capacitor and enters the subsequent signal processing unit. The output signal of the receiver is very weak, so the signal passing through the post-capacitor is very small, which needs to be demodulated and amplified. In order to meet the working requirements, infrared filters can be installed at the front end of the receiving tube to remove visible light and make the infrared receiving tube constitute the maximum light receiving area. Electrical filter is added to the front end of the amplifier to eliminate low-frequency interference and high-frequency interference. Through the signal comparison circuit, the new level signal is output for processing [2]. The schematic diagram is shown in Figure 3.

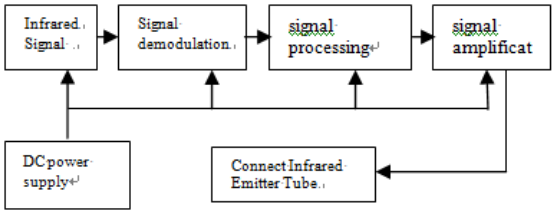

Figure 3.Infrared reception

3.3. Signal processing

The system uses four operational amplifier integrated chips with low power consumption, high gain and internal frequency compensation. When no shield enters the detection area, there is only DC signal in the circuit, which can not pass through the isolation capacitance; when there is shield enters the detection area, the receiving circuit outputs abrupt electrical signal, which is transmitted to the successor circuit through the capacitance, initially amplified by the transistor, and then sent to the amplifier circuit for secondary amplification. The schematic diagram is shown in Figure 4.

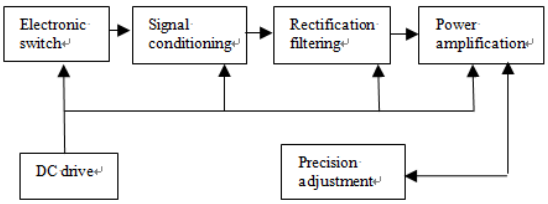

Figure 4.Signal processing

Because the demodulation square wave keeps synchronization with the infrared transmitter in time and the electronic switch is only turned on when the infrared transmitter works, only the optical signal from the infrared transmitter is received and the stray light is blocked. The square wave signal filtered by the electronic switch is smoothed by the resistance-capacitance network, leaving the DC component, so the light-shielding area signal of the shield is restored, that is, the light-shielding area of the shield is large, the DC component is large, the light-shielding area of the shield is small, and the DC component is small. The resistance network is used to adjust the high and low level of the pulse signal to get the appropriate voltage to drive the subsequent circuit. Based on the negative feedback principle of integrated operational amplifier, a sensitivity subsystem circuit is added to the signal processing circuit to adjust the detection accuracy. After adjusting the accuracy, the system can be widely used in other quality inspection and safety protection machinery and equipment, such as the transformation of traditional machine tools without safety protection device, forging machine, etc.

4. TEST RESULTS AND DATA ANALYSIS

The schematic drawing, simulation debugging and PCB board drawing of the testing system are all designed by EDA (Protel) software. The parts are selected, debugged and welded. Under normal temperature, humidity and fluorescent lamp environment, the infrared sensor is used to detect the measured object. By changing the measuring distance and the diameter of the measured object, several groups of experimental data are obtained, as shown in Table 1.

Table 1. Detection of automatic parking results under different conditions

Detection distance/m	Diameter of detector/mm	Detection Times/times	Diameter change of measured object/mm	Stopping times/times
0.05	0.05	20/20	d>0.05/d<0.05	20/20
0.5	0.05	20/20	d>0.05/d<0.05	20/20
1	0.05	20/20	d>0.05/d<0.05	20/19
1.5	0.05	50/50	d>0.05/d<0.05	47/49
3	0.1	20/20	d>0.1/d<0.1	20/20
10	0.25	20/20	d>0.25/d<0.25	20/18
15	0.5	20/20	d>0.5/d<0.5	20/19
15<L<30	0.5	50/50	d>2/d<2	40/38
15<L<30	2	50/50	d>2/d<2	48/49

From the experimental data, it can be seen that the diameter of the test object decreases with the increase of the test distance due to the divergence of the infrared light emitted by the infrared emitter in the air and other effects such as air flow, dust and density difference. By increasing the transmitting power and improving the demodulation and detection function of the receiver, the detection distance is 30m, the diameter of the test object is 2mm, and the detection accuracy is 95%. However, the accurate detection rate below 1 mm is low. Therefore, how to improve the detection accuracy is the focus of this project in the future, and also the key to continue to expand the detection field [4].

Considering that the infrared sensor is greatly affected by the environmental temperature, illumination, humidity and other properties, the stability of the environmental temperature, humidity, illumination, light stroboscopic detection system is adjusted. In the range of ambient illumination <20000LX, ambient temperature-15-60 C, ambient humidity <90% RH, stroboscopic <1500 RPM, the test detection rate (correct parking percentage) is not less than 90%.

5. CONCLUSION

The detection system works with 380 or 220V, 50-60Hz AC. It has good universality with mechanical equipment and does not need any other power supply. The installation frame is easy to install. It uses light display circuit to adjust the firing accuracy of transmitter and receiver tubes, which is simple and fast. The high precision detection system is based on infrared sensing technology. It can be used in the fields of textile, machinery, food production, product quality monitoring and safety protection. It effectively guarantees the improvement of product quality and normal production. The system has wide application prospects.

REFERENCES

[1]Liu Chuanqing. Wireless sensor networktechnology. Electronic Industry Press2015.

[2]Sun Ting, Yang Yongtian, Li Lihong. The Development Status of Wireless Sensor Network Technology. Application of Electronic Technology, 2006-06.

[3]Zhao Bing, Yang Jifeng, Sun Shulin, Wang Shuai.Laboratory Static Characteristics Calibration System Based on LabVIEW. Instrument Technique and Sensor, 2011-06.

[4]Yang Sanxu, Xu Shushan, Yin Baozhong. Study on the stability of capacitive sensor measurement circuit. Sensor and Microsystem, 2006-07

The Optimization Simulation of Casting Process for Compressor Crosshead

Gaojian Li
Zibo Vocational Institute, Shandong, China
E-mail: gaojian4099@126.com

Abstract: The casting process for compressor crosshead of ductile cast iron was analyzed, and the suitable pouring gate position gate position and parting surface were chosen. The casting forming process of the crosshead was simulated by procast software and the casting process was optimized. Finally, the self-forming riser which makes full use of nodular cast iron eutectic expansion effect was designed to improve the crosshead surface puality and internal defects, and improve the casting efficiency of the crosshead.

1. INTRODUCTION

Based on computer simulation technology, Procast casting molding software is used to simulate the casting process of spheroidal graphite crossheads, analyze the existing problems of existing process methods, and assist in finding out the causes and solutions [1-2] to optimize the crosshead casting process. Finally, the riser that makes full use of the eutectic expansion of ductile iron to achieve self-feeding is designed, which improves the surface quality and internal defects of the crosshead and greatly improves the casting efficiency of the crosshead.

2. PROCESS PLAN DETERMINATION

2.1. Process analysis

Figure 1 shows the three-dimensional shape of the crosshead of the compressor.

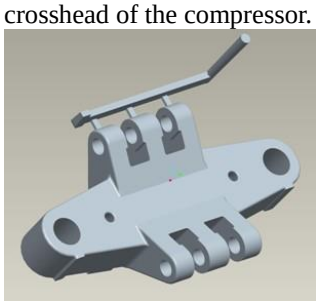

Figure 1 Three-dimensional model of the compressor crosshead

The crosshead is cast by ductile iron 80-55-06. Table 1 lists the chemical composition and mass fraction of ductile iron 80-55-06. The geometry of the crosshead is 1150mm × 610mm × 257.5mm, according to the "casting process design" manual, the processing grade is EG grade, based on geometric modeling considerations, determine the machining allowance level of the crosshead casting is G grade, the machining allowance value is set to 5mm; After the machining of the crosshead casting of the compressor, the casting surface of the crosshead is not allowed to have casting defects, and the non-machined surface is not allowed to have defects such as slag inclusions and depressions, and the distance between the upper and lower molds is not more than 1 mm. Since the cross-head castings of the research are used in the production of compressors in large quantities, combined with the material and geometry of the cross-head castings and the technical requirements of the process, this paper uses self-hardening resin sand to cast wooden molds to meet the needs of large quantities. Claim. Due to the large geometric length of the crosshead of the compressor, it is difficult to fill the molten metal. We have an internal sprue design on the sides of the crosshead. For the convenience of modeling, the grate is established on the sanding parting surface. Design, the molten metal flows from the side of the cavity, so that setting 3 internal runners according to the crosshead structure shortens the flow of molten metal in the cavity, which is beneficial to fast and smooth filling; at the same time, at both ends of the crosshead The runner is inclined to inject the molten metal, which can also reduce the temperature difference of the molten metal in the model cavity and ensure the uniformity of filling. In addition, the crosshead runner needs to be spaced from the lug to avoid collisions between the runner and the lug[3].

Table 1. Chemical composition of its mass fraction

components	C	Ce	Cr	Cu	Fe	Mg	Mn	Mo	Ni
Content%	3.7	0.11	0.04	0.4	93.1	0.04	0.56	0.08	0.13

(2) The position selection of cross head casting

The casting position is an important factor affecting the casting quality and dimensional accuracy of the casting. It is necessary to determine the pouring position of the crosshead according to the state and position of the casting in the cavity when the molten metal is poured [4]. Taking into account the above-mentioned influencing factors, according to the geometry of the crosshead, this paper preliminarily determines the choice of two crosshead casting positions, as shown in Figure 2.

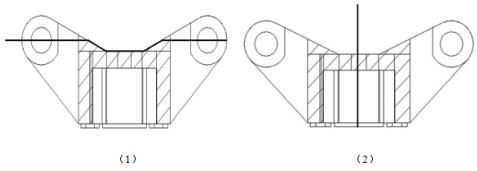

Figure 2. Optimization options of the die joint

position

For the pouring position scheme 1: the main part of the crosshead is located in the lower box, so that most of the crosshead can receive the static pressure from the upper pouring liquid to solidify and shape and serve to supplement the feeding. The distribution is uniform and the temperature difference is small, which makes the cross-head boss obtain a finer structure, reduces the probability of defects such as shrinkage and shrinkage, and improves the surface and internal quality of the casting. In addition, the casting position setting scheme of Fig. 3(1) is adopted, so that the large plane is located at the lower part or the inclined position of the sprue position, thereby avoiding sanding, hanging sand, and the like. The disadvantage is that the lug portion with high quality requirements is located at the upper part of the cavity, which seriously affects the casting quality of the lug.

For the pouring position scheme 2: the important part of the crosshead is located in the lower box, so that the forming quality is better. However, the cavity of the crosshead and the main processing surface are located in the upper box, and the castings are prone to defects such as shrinkage and shrinkage, pores and non-metallic inclusions, which affect the quality of the casting. In addition, using the casting position setting scheme of Fig. 3 (2), the main portion of the crosshead casting is located at the upper portion of the runner position, so that the crosshead increases the probability of casting defects during the casting process, and is prone to run fire.

Therefore, in combination with the analysis and comparison of the selection schemes of the above two casting casting positions, the casting forming effect using the casting position scheme 1 is obviously superior to the casting position scheme 2, so the casting position is selected.

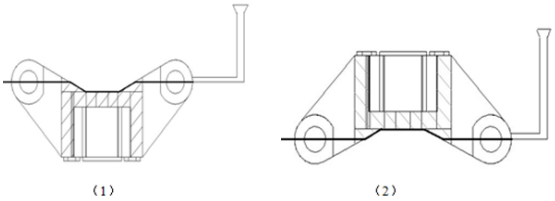

Figure 3 Optimization options of the crosshead pouring position.

2.2. Crosshead parting surface selection

The parting surface is an important factor in determining the dimensional accuracy, production cost and yield of parts. At the position of the yoke lug, its plane is convex, but the plane of the surrounding portion is relatively horizontal, which is advantageous for mold-making and box-forming during the processing and casting process. In addition, it is worth noting that the parting surface should be selected according to the choice of casting position in Figure 3, to maintain consistency to avoid flipping the sand type after the forming. According to the principle of maximum cross section.

For the parting surface position scheme 1: most of the castings are in the same box, which reduces the dimensional deviation caused by the misshape and inconvenience; the parting surface is located at the largest section of the casting, which is convenient for the mold; the selection of the parting surface It is in the same position as the pouring position, which avoids turning the sand mold after the box is closed.

For the parting surface position scheme 2: the castings can not be located in the same half of the mold as much as possible, so that the castings will be biased due to the alignment error of the joints; it is also possible to increase the casting size in the vertical plane because of the tight fitting of the joints, It is convenient to take the mold; the selection of the parting surface and the casting position are inconsistent, so that the sand type needs to be reversed after the box is assembled.

Comprehensive analysis of the above two types of parting surface scheme, the parting surface of the first scheme is obviously superior to the second scheme, and the selection scheme has a parting surface.

3. SIMULATION RESULTS AND DISCUSSION

According to the cross-head casting process of the above analysis, the cross-head casting model is established by Procast casting simulation software, and the cloud diagram of the solidification cooling process of the cross-head casting shown in Figure 4 is obtained through solution calculation. As can be seen from the figure, solidification begins to solidify from the runner position and then begins to solidify inside the crosshead, but there is a shrinkage at the runner position, which may cause casting defects.

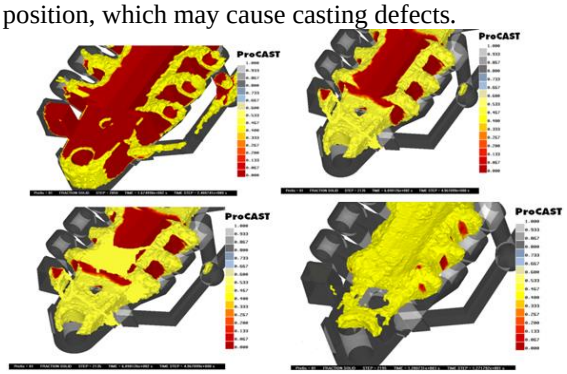

Figure 4. Cloud picture of crosshead casting solidification cooling process

Figure 5 shows the cross-head casting defect distribution. From the surface quality of Figure 5(1), there are defects such as depressions in the local area on the upper surface of the cross-head casting. This surface ductile casting cannot fully self-complement despite the eutectic expansion. From the internal quality of Figure 5 (2), there is no large shrinkage and shrinkage hole inside the crosshead casting, but shrinkage defects occur at some hot sections, because the liquid shrinkage of the lower part of the crosshead can be provided through the upper part of the casting. The molten iron, therefore, the internal forming quality of the lower half of the crosshead is very good.

However, due to the use of the casting position scheme, the higher the position of the lug cannot be replenished, resulting in the formation of shrinkage cavities.

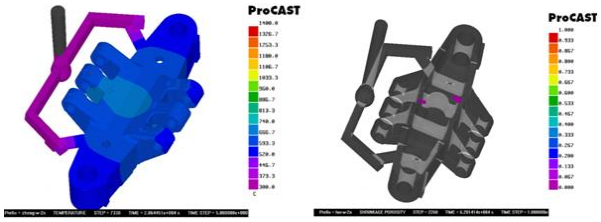

（1）surface （2）struct

Figure 5. Castingn defects distribution of the crosshead

4. RISER DESIGN AND ITS CASTING QUALITY

Ductile iron has the characteristics of paste-like solidification during solidification. If the riser is designed according to the traditional riser design, the riser should be placed at the hot section of the crosshead, so that the riser will introduce the defect into the riser; the spheroid during the solidification process The cast iron has a graphitization expansion phenomenon, which can compensate the shrinkage defect of the casting by the eutectic expansion of the ductile iron. Therefore, the riser arrangement shown in Fig. 6 is adopted in this paper, and the riser design idea is utilized to fully utilize the solidification of the ductile iron. The eutectic expansion effect realizes self-feeding, and the riser greatly improves the yield. After adding the riser as shown in Fig. 6, the cross-head casting effect is as shown in Fig. 7, and the surface quality and internal defects of the crosshead are improved by the riser.

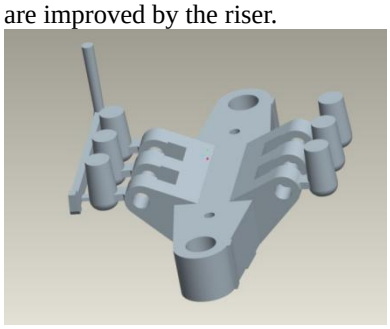

Figure 6. Schematic diagram of running and feeding layout

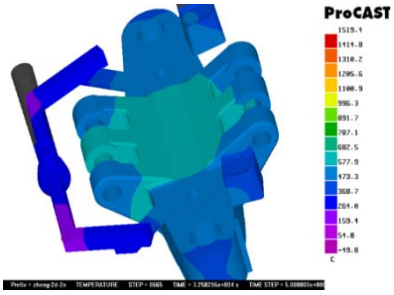

Figure 7. Casting quality after added the feeding riser

5. CONCLUSION

Based on the analysis of the crosshead process of the compressor, based on the computer simulation technology, the casting model of ductile iron crosshead was established by Procast casting molding software, and the crosshead casting process was optimized. In the past, the riser should be placed at the hot section of the crosshead, and the riser design that makes full use of the eutectic expansion of ductile iron to achieve self-feeding is designed, which improves the surface quality and internal defects of the crosshead. Greatly improve the casting efficiency of the crosshead.

REFERENCES

[1]Zhang Fuquan, Wang Yang, Zhou Yiwu, et al. Numerical simulation of casting process of large section ductile iron and prediction of shrinkage shrinkage. Foundry technology, 2013, 34(8): 1027-1030.

[2]Chen Wenbiao, Cheng Hefa, Zhou Yunhai, et al. Application of Numerical Simulation Technology in Optimization of Casting Process of Ductile Iron Abutment. Foundry Technology, 2013, 34(1): 102-104.

[3]Liu Baozhong, Wang Youchao, Mi Guofa. Casting Simulation and Process Optimization of Cross-head Cast Steel Parts. Thermal Engineering, 2012, 41(7): 42-47.

[4]You Zhiyong, Li Wei, Ma Tao et al. Process design and numerical simulation of crosshead casting based on PRO/E. China Foundry Machinery and Technology, 2011, (6): 31-33

Discussion on Anti-jamming Technology of Intelligent Medical Paging System

Lingling Ding
Information Engineering Department, Zibo Vocational Institute, Zibo, Shandong Province, 255000, China
E-mail: svg00@163.com

Abstract: This paper first describes the source and consequences of medical paging system interference, and then gives solutions from both the host and the extension. These methods can improve the stability and reliability of the medical paging system.
Keywords: Medical paging system; Hardware; Software; Anti-jamming technology

1. INTRODUCTION

With the development of society, intelligent medical paging intercom system is applied to various fields, such as hospital wards, nursing homes and other occasions. At present, the general functions of the bus two-wire products on the market are relatively simple, and the anti-interference and reliability are poor. Due to the limited design level and testing equipment, in the complex electromagnetic environment of the hospital, the products often fail, which affects the normal use. The reliability of the intelligent medical paging intercom system is determined by many factors, and the system anti-interference performance is one of the important indicators of system reliability. Even the control system designed in the company's laboratory, after installation and commissioning, fully meets the design requirements, but after entering the site, the system is often unable to work stably for a long time. The reason for this situation is that the site environment is more complicated and there are various electromagnetic interferences [1]. Therefore, the reliability design of the paging intercom system and the application of anti-interference technology are more and more important.

2. SOURCES AND CONSEQUENCES OF INTERFERENCE

Interference in the field environment enters the MCU system in the form of pulses. There are three main channels, namely, spatial interference, power supply system interference, and process channel interference.

Consequences of interference: (1) Increased data acquisition error. (2) The program runs out of order, and the control state fails or crashes. (3) The system controlled object is mishandled. (4) The state of the controlled object is unstable. (5) Timing is not allowed. (6) Changes in data [2].

In view of the above problems, this paper discusses some methods to improve the anti-interference ability of single-chip application system from hardware and software.

3. HARDWARE ANTI-INTERFERENCE

3.1. Reasonable selection of components

The device is reasonably selected based on system parameters to meet system performance requirements. As far as possible, select components with high integration, low temperature drift, good anti-interference performance and low power consumption, and choose a CPU with strong anti-interference performance.

3.2. Suppress power interference

Connect the TVS or varistor at the incoming end of the AC grid, Absorb surge voltage; use low-pass filter to suppress high frequency noise introduced by power grid. When designing filter, pay attention to make resonance frequency much smaller than interference frequency; use analog circuit and digital circuit power supply separately, power supply floating technology, use power supply Isolation transformer and power supply filtering technology.

3.3. Suppress electromagnetic field interference

When the metal with good electrical conductivity is used as the shielding box and grounded, the power line inside the shielding box will not affect the outside, and the external power line will not penetrate the shielding box into the inside, which can suppress the interference source and block the transmission path of the interference. The role of electric field isolation. The magnetic circuit shielding is made of a highly magnetically conductive material and is enclosed in a closed structure [3-4].

3.4. Good grounding

Good grounding can greatly inhibit the internal noise coupling of the system, prevent the intrusion of external interference, and improve the anti-interference ability of the system.

3.5. Take isolation measures

Isolation of digital signals typically employs optocouplers. In the specific circuit design, the optocoupler is added after the ADC and before the DAC. The power supply of the power supply and the microcomputer must be independent, and the ground line must be separated. For the isolation of analog signals, an isolation amplifier is usually used, and the signal is magnetically coupled by a transformer in the isolation amplifier to block the line connection of the path, thereby cutting off the interference source[5].

3.6. Overvoltage protection circuit

The overvoltage protection circuit is composed of a current limiting resistor and a voltage stabilizing tube. The current limiting resistor should be selected

appropriately. If it is too large, it will cause signal attenuation. If it is too small, it will not protect the regulator tube. The voltage regulator value of the Zener is selected to be slightly higher than the highest transmitted signal voltage. Too low will limit the effective signal and make the signal distorted.

3.7. Wiring and process of printed circuit board

Design the printed circuit board and wiring in accordance with the three principles of controlling the noise source as much as possible, minimizing the propagation and coupling of noise, and minimizing the absorption of noise.

3.8. Improvement of host anti-interference performance

Due to the complexity of the hospital's electromagnetic environment, this design uses several measures to enhance its anti-interference ability, the main means are as follows:

1) Shielding: the outer frame is made of aluminum metal, the joints are tightly connected; the bus adopts shielded twisted pair;

2) Grounding: the outer frame is connected to the earth, and the bus shielding layer is connected to the earth;

3) Filtering: 104 chip capacitors are added between all digital IC power pins and ground, and placed close to the chip;

4) Adopt chips and components with strong anti-interference ability;

5) The external interface is separated and protected by magnetic beads, TVS, varistor and other components;

6) The chip and the external input and output pins plus TVS or fast diodes for limiting, or add optocouplers, optical relays, etc. to isolate;

7) Reasonably arrange the devices on the circuit board, following the principle of small electrical interference between devices and easy to dissipate heat;

8) The layout of the circuit board is reasonably divided. The analog circuit area, digital circuit area, and power drive area are separated as much as possible. The ground lines are not mixed and connected to the ground of the power supply. The ground and power lines are as thick as possible, and many more;

9) Communication timeout automatic reset function: If the communication between the CPU of the main control board and the CPU of the display board times out, it is considered that the other party is dead. At this time, the automatic reset function is activated, and the +5V power supply is cut off for about 1 second to make the voltage of the single-chip microcomputer rapidly decrease, ensuring power failure. After the automatic power-on restart [6].

After the instrument (all products of Shanghai Sanji SANKI Electronics: electrostatic generator: NS61000-2K, pulse group generator: NS61000-4K, lightning surge generator: LSG-728), the anti-interference ability of each test There has been a substantial increase.

Electrostatic discharge ESD: from the original 2 (contact discharge 2KV, air gap discharge 4KV) to level 4 (contact discharge 8KV, air gap discharge 15KV) [52];

Electric fast transient pulse group EFT: from the original level 1 (500V/5KHz on the power line, 250 V/5KHz on the signal line) to level 3 (2KV/5KHz on the power line, 1KV/5KHz on the signal line);

Lightning Surge: Increased from the original level 2 (line-line 0.5KV, line-ground 1KV) to level 3 (line-line 1.0KV, line-ground 2.0KV).

3.9. Improvement of anti-jamming performance of extension and display

1) From the original single panel, the full plug-in is changed to double-panel, patch technology, and the chip STC12C2052 with strong anti-interference ability is selected as the CPU;

2) Add anti-interference components at the input and output port lines, such as input to increase TVS, varistor, etc. to suppress the transient high-voltage stringing; use optocoupler to isolate the external pins connected to the CPU; extension, door light The input is connected to the self-recovery fuse. When the internal components of the extension are damaged and the short circuit exceeds the critical operating current of the fuse, the protection will be activated, and the connection between the extension and the bus will be disconnected to prevent the entire system from being affected. , and can be automatically restored [7].

3)When the circuit board is typeset, place components according to function, power, etc., rational layout and wiring, thicken power and ground lines, and cover copper on a large area, and so on.

4. SOFTWARE ANTI-INTERFERENCE

4.1. CPU anti-interference measures

The CPU anti-interference needs to be solved. The following methods can be used.

1) Manual reset

2) Power failure protection

3) Sleep anti-interference

4.2. Instruction redundancy

Manually insert some single-byte instructions at key locations, or rewrite valid single-byte instructions, which is called "instruction redundancy". Usually, a two-byte or more empty operation instruction NOP is inserted after a two-byte instruction and a three-byte instruction, so that even if the random program flies to the operand. Due to the existence of NOP, the subsequent instructions are prevented from being executed as operands, and the program is automatically put on the track.

4.3. Setting Software Traps

When the random program enters the non-program area, the redundant instructions will not work. Through software traps, intercept the random program, direct it to the specified location, and then handle the error. A software trap is an instruction that directs the captured random program to the reset entry address 0000H.

4.4. “Watchdog” technology

The “watchdog” technology continuously monitors the program cycle running time. If the time exceeds the known cycle setting time, the system is considered to be in an “infinite loop”, then the program is forced to return to the 0000H entry, and an error is scheduled at 0000H. Process the program to get the system running on the right track.

4.5. Digital filtering

Digital filtering is to process the signal input to the data acquisition part of the single-chip microcomputer through program design to achieve anti-interference.

5. CONCLUSION

In engineering practice, several anti-interference methods are usually used together and complement each other to achieve good anti-interference effects. Fundamentally, hardware anti-jamming is active, and software anti-jamming is passive. Detailed analysis of interference sources, hardware and software anti-interference measures, improve system monitoring procedures, you can ensure that the system runs accurately and reliably.

REFERENCES

[1]Practical anti-jamming technology of single-chip system. Beijing: People’s Posts and Telecommunications Press, 2004.

[2]Jhong Sam Lee & Leonard E. Miller. CDMA System Engineering Handbook. 2002, 56-65.

[3]Bingyun Qian, Jianping Wang. Anti-jamming technology in single-chip application system. Modern electronic technology, 2005, No. 2.

[4]Lal C. Godora. Application of Antenna Arrays to Mobile Communication, Part 1: Performance Improvement, Feasibility, and System Considerations. Proc IEEE, 1997, 85: 1031-1060.

[5]Guojin Li, Xiaokui Ren. Anti-jamming technology of single-chip microcomputer. Modern electronic technology, No.15, 2003.

[6]Hoyoung Choi, Jaeseong Bae, Sangho lee, Sangjun Lee. Simulation Results for Coverage and Performance Improvements for CDMA2000 1X Networking Using Smart Antenna System. VTC, 2002, 1574-1578.

[7]J.C. Liberti, T.S. Rappaport. Analytical Results for Capacity Improvement in CDMA. IEEE Trans. On Veh. Tech., August, 1994, 43(3).

Simulation Experiment and Analysis of Oil-Water Two-Phase Fluid Imager in Near Horizontal Well

Hang Chen[1], Junfeng Liu[1,2,], Jinyu Meng[1], Guoqiang Cheng[1], Yu Xie[1]*
[1]School of Geophysics and Oil Resources, Yangtze University (Wuhan Campus), Wuhan, Hubei, 430100, China
[2]Key Laboratory of Exploration Technologies for Oil & Gas Resources (Yangtze University), Ministry of Education, Wuhan, Hubei, 430100, China
**E-mail: kg2004002@163.com*

Abstract: The interpretation of multiphase flow in horizontal wells is recognized as a difficult problem at present. The measurement of single probe centering in conventional instruments cannot reflect the true situation of the well because of the uncertainty of the measurements of the phase holdup and the velocity of flow. In order to solve this problem, based on the flow loop, a series of physical simulation experiments have been carried out using the newly developed single probe fluid imager, which consists of a single turbine flowmeter and a single capacitance water holdup tool, which is composed of a single turbine Flowmeter and a single capacitance water holdup tool. Continuous measurements can be made on the wellbore section. First, the well deviation is 85 °, 88 °and 90 °, and the total flow rate of oil and water is 50, 70, 100, 120, 160, 200, 250, 300 m³/d simulation experiments were carried out and fixed-point measurements were carried out at five different height positions on the cross-section of the wellbore. Secondly, the counting rate of the holdup probe at different positions and the rotating speed of the turbine were collected under different flow conditions. Then, (1) the Trallero flow pattern classification method is used to divide the flow pattern. (2) the local water holdup is calculated according to the response value of the holdup probe in pure oil and pure water, and the response coefficient and start-up speed of the turbine are calculated according to the response value of the turbine in pure oil and pure water, and then the starting speed of the turbine is calculated. Local velocity. Finally, the holdup profile imaging is analyzed by using MATLAB software. The results show that the simple inverse range ratio algorithm is the best for smooth stratified flow. For wavy stratified flow, Gaussian Radial basis algorithm has the best imaging effect, which provides a theoretical basis for the interpretation of oil-water two-phase flow profile in near horizontal wells.

Keywords: horizontal well; oil-water; flow pattern; local water holdup; local velocity; flow imaging

1. INTRODUCTION

The oil-water two-phase flow pattern, local velocity and local water holdup have complicated changes in horizontal and high deviated wells due to gravity differentiation and the influence of well deviation [1-2], and the response characteristics of two-phase flow pattern to the instrument have taken place. Subsequent flowrate calculation, dynamic monitoring and interpretation of production profile will have a great impact. Therefore, the commercial multi-phase flow logging tools for horizontal wells are mainly measured by array probes. Schlumberger has introduced the FSI fluid Imager [3], which consists of six optical probes, six electric probes and five micro flowmeters. The probe and flowmeter are distributed on the triangle hydraulic arm, which can be achieved by extending the hydraulic arm. Borehole coverage measurement. In addition, Halliburton also introduced the SONDEX-MAPS fluid imager. The instrument consists of Capacitance Array Tool (CAT), Resistance Array Tool (RAT), and Spinner Array Tool (SAT) [4-5]. CAT is composed of 12 capacitance sensors, which is used to distinguish the light phase from the heavy oil and water. RAT is composed of 12 micro-resistivity sensors to distinguish non-conductive hydrocarbon (oil and gas) and water with good conductivity. SAT consists of 6 micro-rotors for measuring flow the velocity of the body.

Different from the above-mentioned instruments, the single probe fluid imager used in this experiment consists of a single turbine flowmeter and a single capacitance water holdup tool, which can be continuously measured on the wellbore section. By changing the position measurement of the single probe on the wellbore cross-section, the coverage measurement of the whole hole cross-section can be realized, and then several local holdup and local velocity can be obtained.

2. GENERAL SITUATION OF EXPERIMENT

As shown in figure 1, Yangtze University multiphase flow simulation loop is used for this experiment. The simulated well bore is 12m long and the inner diameter is 124mm. The temperature is 5°C and 12°C, the pressure is normal pressure. The medium is tap water (density 1000kg/m^3, viscosity 1.16mPa·s) and white oil (density 842.5kg/m^3, viscosity 9.26mPa·s). The total flow rate of oil and water is 50, 70, 100, 120,

160, 200, 250, 300 m^3/d. Water cut is 0%, 10%, 20%, 40%, 50%, 60%, 70%, 80%, 90%, 100%. The horizontal well is not completely horizontal in the actual production process. In order to get closer to the real situation, the deviation angle is designed to be 85°,88°and 90°(horizontal). As shown in figure 2, the measuring instrument is a single probe fluid imager. As shown in figure 3, the capacitance and turbine response values at five different positions are measured, the total oil-water flow rate, water cut, well deviation and tool rotation angle are recorded, and the experiments are recorded and photographed.

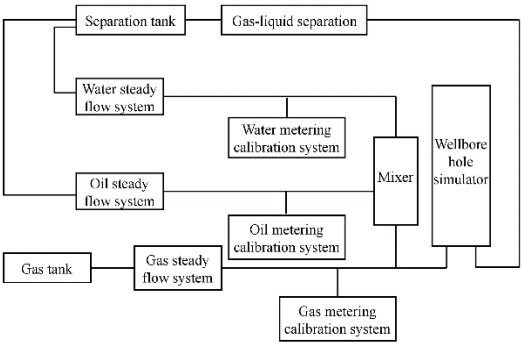

Figure 1. Schematic diagram of multiphase flow simulation loop of Yangtze University

Figure 2. Single probe fluid flow imaging instrument

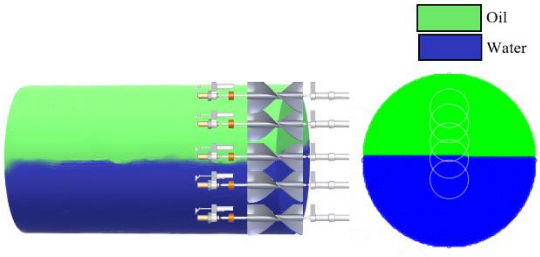

Figure 3. Five different measurement locations

3. ANALYSIS OF FLOW PATTERN

3.1 Classification of the oil-water two-phase flow pattern

There are six flow patterns were obtained by Trallero et al [6]. In the experiment on oil-water two-phase flow. And the experiment was conducted under the condition of a horizontal tube diameter of 50.13mm and a tube length of 15.54m. In this experiment, only four flow patterns appeared due to the large pipe diameter and small flowrate, as shown in Table 1.

3.2 The cross-section imaging of holdup and velocity of flow

Table 1 (a) OW-PD85 flow pattern

	O/W Ratio	Experimental photo	Flow pattern
1	L100CW20		ST&MI
2	L120CW60		W-O/W
3	L300CW20		W/O

Table 1 (b) OW-PD88 flow pattern

	O/W Ratio	Experimental photo	Flow pattern
1	L50CW20		ST
2	L100CW40		ST&MI
3	L160CW80		W-O/W
4	L300CW20		W/O

Table 1 (c) OW-PD90 flow pattern

	O/W Ratio	Experimental photo	Flow pattern
1	L50CW20		ST
2	L100CW60		ST&MI
3	L120CW80		W-O/W
4	L200CW20		W/O

In the Table, OW-PD85 is oil-water two-phase, and the well is inclined at 85 degree. L100CW20 is a total oil-water flow rate of 100 m^3/d and a water cut of 20%.

3.3 The calculation holdup

In the single-probe fluid imager tool, a capacitance water holdup tool primarily uses the difference in dielectric constant between water and hydrocarbons (oil and gas) to distinguish between water and hydrocarbons, which differ by an order of magnitude. The water holdup calculation method is:

$$HYD = Y_w \cdot HYD_w + (1 - Y_w) \cdot HYD_o \quad (1)$$

$$Y_w = \frac{HYD - HYD_o}{HYD_w - HYD_o} \quad (2)$$

Where HYD is the counting rate of mixed fluids measured by the capacitance water holdup tool, cps. HYD_w is scale value of the total water counting rate, cps. HYD_O is the calibration value of the total oil count rate, cps.

3.4 Velocity calculation

$$V_i = k_i' \cdot RPS_i + V_{ti}' \quad (3)$$

Where V_i is the local velocity of the fluid at position i, m/min. k_i' is position i turbine response factor, dimensionless. RPS_i is the speed of the turbine at position i, rps. V_{ti}' is turbine start-up speed, m/min.

3.5 Holdup mad velocity profile imaging

In this experiment, MATLAB software was used to image the holdup and velocity profile [7]. The holdup profile imaging was performed by simple distance inverse ratio method and Gaussian radial basis algorithm [8]. The publicity is as follows, and the imaging results are shown in Table 2. Velocity profile imaging is shown in Table 3.

Table 2 Holdup profile imaging

O/W Ratio	Photo	Simple distance	Gaussian radial
OW-PD85 L100CW20		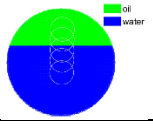	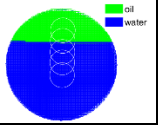

OW-PD88 L50CW20		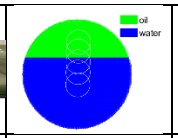	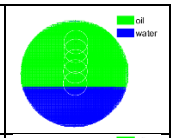
OW-PD90 L50CW20		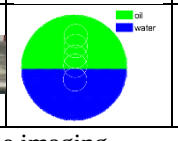	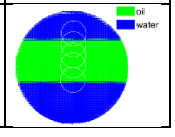

Table 3 Velocity profile imaging

O/W Ratio	Flow velocity section imaging
OW-PD85 L100CW2	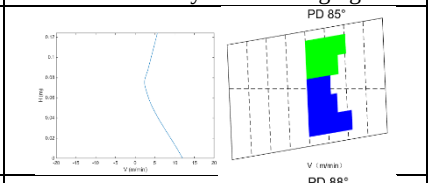
OW-PD88 L50CW20	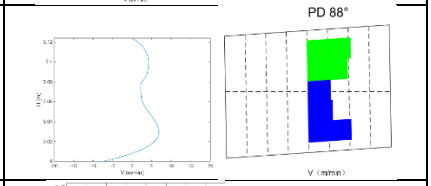
OW-PD90 L300CW20	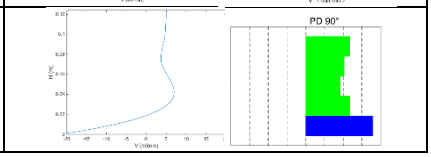

Simple distance inverse ratio method:

$$r_i = \frac{1}{\sqrt{(x-x_i)^2-(y-y_i)^2}} \quad (4)$$

$$Y_{wp} = \frac{\sum_{i=1}^{5} r_i^2 \cdot Y_{wi}}{\sum_{i=1}^{5} r_i^2} \quad (5)$$

Where Y_{wp} is the holdup of the interpolation point. Y_{wi} is the holdup measured by the i probe. r_i is the reciprocal of the interpolation point (x, y) to the distance of the i probe.

Gaussian Radial basis algorithm:

$$T_k = \sum_{i=1}^{5} D_{ik} \cdot C_i \cdot T_i \quad (6)$$

$$D_{ik} = \exp[-\left(\frac{x-a}{m}\right)^2 - \left(\frac{y-b}{n}\right)^2 \quad (7)$$

Where T_k is water holdup of interpolation point. D_{ik} is the weight coefficient between the interpolation point and the first probe. C_i is undetermined coefficient.

The undetermined coefficient Ci can be obtained by replacing the interpolation point water holdup Tk with the known water holdup value of the kth probe.

It can be seen that the simple distance inverse ratio method has a better imaging effect on the holdup profile of the smooth stratified flow, and the Gaussian radial basis algorithm has a better imaging effect on the holdup profile of the wavy stratified flow. Velocity imaging basically reflects the change in fluid stratification velocity.

4. CONCLUSIONS

(1) In this experiment, there are four flow patterns: smooth stratified flow (ST), wavy stratified flow (ST&MI), water and oil-in-water flow(W-O/W) and water-in-oil flow(W/O). Under the same physical parameters of the experimental medium, the variation of well deviation and apparent velocity of fluid have a great influence on the flow pattern.

(2) The simple distance inverse ratio method is suitable for the holdup profile imaging of smooth stratified flow, and Gaussian Radial basis algorithm is suitable for the holdup profile imaging of wavy stratified flow.

5. ACKNOWLEDGMENTS

The authors are grateful to production logging laboratory of Yangtze University. This paper is supported by Open Fund of Key Laboratory of Exploration Technologies for Oil and Gas Resources (Yangtze University), Ministry of Education (Grant No. K2018-10), Yangtze university undergraduate innovation and entrepreneurship training program (Grant No. 2016020).

REFERENCES

[1]Bian Xiaohang, Liu Junfeng, Ye Tianming, et al. Numerical simulation of oil-water two-phase flow pattern in large diameter and different inclined wells. Well Logging technology, 2016, 40(4): 399-403.

[2] Liu Junfeng, Xu Yazhong, Wu Qinxuan. Holdup flow imaging analysis for capacitance and resistance ring array probes. Progress in Geophysics (in Chinese), 2018, 33(5): 2141-2147.

[3]Vu-Hoang, D., Faur, M., Marcus, R., Cadenhead, et al. A novel approach to production logging in multiphase horizontal wells. Society of Petroleum Engineers, 2014.

[4]Jin Jianxun, Hu Haitao, Wu Lingmin, et al. Introduction and application of production logging tools for horizontal wells. Foreign logging technology, 2015, 3, 23-25.

[5]Liu Junfeng, Qin Ruize, Shi Hongbo, “Research and implementation of a three-dimensional flow imaging algorithm for multiphase flow in horizontal well,” Journal of Mines, Metals and Fuels, 2017, 65(12): 708-713, 762.

[6]Trallero J L, Sarica C, Brill J P. A Study of Oil-water Flow Pattern in Horizontal Pipes. SPE Production Facilities, 1996, 12(3): 165-172.

[7]Yu Shengwei, Wu Ting, Luo Jianqiao. MATLAB GUI Design introduction and practice. Beijing: Tsinghua University Press, 2016.

[8]Yang Rui. Study on MAPS holdup imaging processing method. Master’s thesis, Yangtze University, 2016.

Discussion on Mine Hoist Vector Control System Based on Three-Level Inverter

Yao Wang
Zibo Vocational Institute, ZiBo 255314, China
E-mail: anyo211@qq.com

Abstract: Mine hoist is an important transportation equipment for mines.Mine hoisting is the most important working procedure in mining. It is mainly responsible for the connection between the underground and the underground, as well as the collection of good coal through the shaft hoisting, and the release of materials and equipment needed underground. The staff also uses this equipment to achieve the connection between the wells and the wells. Once such transportation equipment fails, it will not only cause the mines to work normally, but even endanger the lives of the workers.Therefore, the requirements of the mine hoist for its own electrical control devices are very strict, and the electric drive equipment of the mine is also a research hotspot of researchers today.This paper mainly analyzes the application principle and mechanism of the new inverter three-level inverter in the mine hoist, and analyzes the function of the three-level inverter on the mine hoist and the improvement of the hoist vector control system.
Keywords: Mine hoist; Three-level inverter; Vector control system

1. INTRODUCTION

Mine work is a large-scale equipment consisting of various electromechanical equipment. The mine hoist is not only the transmission equipment for mine work but also the largest fixed equipment for mines. Its power consumption accounts for 30% to 40% of the total power consumption of the mine. The huge power consumption makes the mine hoist have high requirements for its own electrical control devices. In addition, it has large inertia, high speed and complex operation requirements [1]. Therefore, in order to ensure the normal and efficient operation of coal mine production, the electric drive of the mine hoist should be further researched and improved to promote the coal production efficiency of the entire mine.

2. THE CURRENT DEVELOPMENT STATUS OF MINE HOIST

After 30 years of development, the mine hoist has developed from the original motor through the reducer drive reel system to the IGBT pulse width modulation high-performance inverter with direct torque control technology and the IGCTU_ level high-voltage inverter. Large-capacity synchronous motor variable frequency speed control system [2].The development and application of this electric transmission device enables high efficiency and low accident rate in today's mines. However, due to China's own national conditions, today's mines have a large gap with foreign countries in automation and equipment manufacturing processes. Some high-performance AC speed control systems are still imported from abroad.

Therefore, this also puts strict requirements on the development of electric drive equipment for mine hoists in China.Strengthening the research on electric drive equipment and developing its own first-class electric drive technology has become the main subject of today's researchers. Here, the author combines the development status of domestic and foreign hoisting machines, and briefly analyzes the requirements and improvements of electrical equipment required for mine lifting equipment.

3. MINE HOIST REQUIREMENTS FOR ELECTRIC DRIVES

The operating characteristics of the mine hoist and its huge power consumption have placed great demands on its own electric drive.In view of the important position of mine hoist in mine production, in order to ensure the normal operation of the hoist to ensure the normal operation of the mine, the author puts forward the following requirements for the electric drive unit in combination with the operating characteristics of the mine hoist:

3.1. Reliability

The normal operation of the mine hoist is not only related to the normal operation of the mine but also the life of each miner. Therefore, the electric drive system of the hoist itself has high reliability.Interference from external factors also has certain exclusion functions, and the key equipment needs to be redundantly protected.Only by comprehensive consideration can we ensure the normal operation of the mine [3-4].

3.2. Four quadrant operation

In the mine hoist's drag system, both the bucket lifting system and the cage lifting system must meet the four-quadrant operation, and the four stages of acceleration, constant speed, deceleration and crawling are required in one cycle.The specific working principle is to drive the driving wheel by using the driving motor, and then to pull the lifting container through the traction wire connected with the driving wheel, and at the same time, use the speed regulating system connected with the motor to play

the role of shifting the entire drag system.Generally, the relationship between different torques and speeds required for different time periods can be calculated by formula (1).

$$T_e - T_L = \frac{GD^2}{375}\frac{dn}{dt} \quad (1)$$

T_e is the drag torque; T_L is the static load torque; and GD^2 is the positive torque of the drag system[5].

3.3. Speed range

In order to make the hoist work normally, there are certain requirements for the speed range and characteristic hardness of the electric system. Generally, the electrical system is required to have a characteristic hardness of 0.5% within the speed range of 1:25.The speed range is generally calculated from the ratio of the highest running speed to the creeping speed in different hoisting processes.The requirement for the characteristic hardness is to ensure that the crawling speed can meet less than 0.5m/s under the rated load, so that the hoist can work normally.

3.4. Speed and stability

Whether the hoist is in a negative or positive load state, the transmission system is required to quickly establish the torque, which requires the transmission system itself to have a fast adjustment speed.However, because the hoist is mainly connected by the elastic connection of the wire rope and the load, the main disadvantage of this connection is that the shock absorbing ability of the connection is poor, and simply increasing the adjustment speed will only cause the wire rope to vibrate and slip.Therefore, in the adjustment can not be blindly fast, but on the basis of maintaining stability, the application of the optimal adjustment speed can not only maintain the ability to quickly establish the torque but also meet the speed without oscillation and no overshoot[6].

4. BRIEF INTRODUCTION OF THREE-LEVEL INVERTER TECHNOLOGY

In order to realize the requirements of mine hoist for high-power high-voltage frequency conversion speed regulation, Sanping inverter has been well developed and popularized in recent years.Its output has low harmonic content, high output quality, and low electrical stress of each power device.In addition, because it can solve the electromagnetic interference problem well, it is also suitable for the high voltage of the hoist and the development direction of the large capacity.Compared with the shortcomings of the past two-level inverter technology, these excellent functions can not only effectively realize high-voltage variable frequency speed regulation, but also its simple circuit topology also facilitates the research work of researchers.It is called a typical circuit in the multi-level inverter control principle.

5. BRIEF ANALYSIS OF THREE-LEVEL INVERTER

5.1. Basic principle of three-level inverter

The judgment of the area where the reference voltage falls is as follows:

When receiving the reference space vector V_{ref}, the first consideration of the three-level inverter control system is the specific position where the space vector falls, as shown in Figure 1:

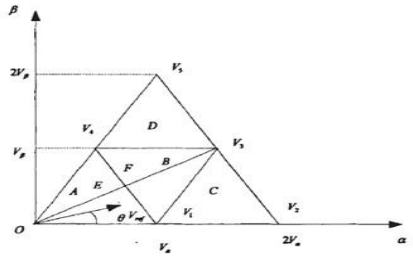

Figure 1. Voltage space vector

In the figure 1, it is necessary to first determine the sector of the vector, and then determine which triangle of A, B, C, D is in the triangle area.In the analysis, we take the vector as the example of sector 1, and then there are four cases in the four triangles A, B, C, and D.Below we take S = 1, R = A for the corresponding analysis, in this case, mainly meet | OE | < | OF | can be, at this time through the corresponding geometric analysis can get the following relationship:

$$V_{ref}\cos(\frac{\pi}{6}-\theta) \le V_{ref}\sin\frac{\pi}{3}(0° \le \theta \le 30°) \quad (2)$$

$$V_{ref}\cos(\theta-\frac{\pi}{6}) \le V_{\alpha}\sin\frac{\pi}{3}(30° \le \theta \le 60°)$$

Obtained by Formula (2)

$$u_{s\alpha} + u_{s\beta}\Big/\sqrt{3} \le V_{\partial} \quad (3)$$

In the formula (3), $u_{s\alpha} = V_{ref}\cos\theta$ is the component of the reference voltage vector on the α-axis, and $u_{s\beta} = V_{ref}\sin\theta$ is the component of the reference voltage vector on the β-axis.Similarly, a similar geometric analysis can be performed when S=1, the vector falls in the three triangular regions B, C, and D[7-8].

By analyzing the triangle regions with different sectors, the following three rules can be obtained:

$$u_{sa} + u_{s\beta}/\sqrt{3} \le V_a \quad (4)$$

$$u_{sa} - u_{s\beta}/\sqrt{3} \ge V_a \quad (5)$$

$$u_{s\beta} < V_{\beta} \quad (6)$$

In addition, for the judgment of the reference voltage vector of different sectors, it is also possible to convert each different sector into one sector for corresponding analysis.

After the voltage vector is sent to the inverter, the position of the voltage vector in the sector and the triangle region is first determined according to the above analysis, and then the synthesis order of the triangle fixed-point space vector is scheduled according to the NTV rule and synthesized.In the synthesis process, if it is noted that the spatial voltage vector including the PO state is taken as the initial vector, the vector mutation problem in which the region switching occurs can be effectively solved.

5.2. Inverter development and problem analysis

5.2.1. Development of three-level inverter

The three-level inverter has three level states, so that its output harmonics are significantly less than the two-level inverter, and its own asymmetric bidirectional switch ensures the two-way flow of energy, which largely guarantees The hoist is required for four-quadrant operation in electric drive control.In addition, the three-level inverter embedded in the diode can also realize the function of converting the medium-low voltage device into a high-capacity converter. Based on the performance characteristics of the three-level inverter itself, it has broad prospects in medium and high voltage variable frequency speed regulation and power system reactive power compensation.

However, while seeing the advantages of the three-level inverter itself, its own shortcomings have also brought certain constraints to its development.

First of all, its topology uses 12 power tubes, which brings inconvenience to the control of the three levels itself. Secondly, the imbalance of the midpoint potential on the DC side also restricts the development of the topology.Nowadays, SVPMW is the main control strategy for the three-level topology.

Three-level inverters have entered a practical stage abroad, but their development and application in China are still in the initial stage. Traditional DC voltage source power supply and DC voltage source power supply GT0 inverter is replaced by IGBT and IGCT two-level or three-level PWM inverter. It is also a development trend, which can meet high-power, high-voltage AC frequency conversion control. The system also certifies its important position in the electrical equipment of the hoist.

5.2.2. Difficulty analysis of three-level inverter

The topology of the three-level inverter uses 12 power tubes, and the topology itself has a variety of structures. Therefore, the control strategy for the topology is much more complicated than that of the two-level inverter.Nowadays, the main influence on the development of the topology is the imbalance of the midpoint potential on the DC side. For this problem, this paper also gives a corresponding solution strategy.

The balance of the midpoint potential on the DC side is related to the performance of the inverter. If the effective regulation cannot be performed, it will not only affect the efficiency of the inverter, but also the speed regulation performance of the motor. Therefore, the DC side focus potential balance effect directly affects the entire production process.

5.3. Control Strategy of Space Vector for Three-Level Inverter

The three-level control strategy for space vector is currently the most widely used PWM.This control strategy is mainly based on the synthesis of space vectors. Firstly, the utilization of voltage is much higher than other control strategies. Secondly, the output waveform is of high quality, almost close to sinusoidal. In addition, its control itself can make rational use of space vectors to reduce the use of switches. The effective control of the space vector by the three-level inverter is almost perfect in line with the high requirements of the mine hoist for electric drive equipment.Therefore, the application of three-level inverters in mine hoist equipment is also the first choice of electrical equipment of mine hoist nowadays.

6. CONCLUSION

Mine hoist is an important transmission equipment in mine production. In order to complete mine work with high quality, to ensure low mine operation and high efficiency, mine hoist also needs certain development.In order to improve the operation quality of the hoist, controlling the electric drive equipment of the hoist plays an indispensable role. Based on this, this paper further analyzes the three-level inverter suitable for high voltage and large capacity and low harmonic at the output end. The working principle of three-level inverter, how to solve the problem of neutral-point potential balance which restricts the development of its own topology, and the control strategy of space vector are analyzed accordingly, which effectively solves the performance requirement of high voltage frequency conversion in electric drive equipment of hoist.

REFERENCES

[1]Annette Von Jouance, Shaoan Dai, Haoran Zhang. A Simple Method for Balancing the DC-link Voltage of Three-level Inverters, 2001.

[2]Jae Hyeong Seo, Cang Ho Choi, Dong Seok Hyun. A new simplified Space-Vector PWM Method for Three-Level-Inverters, IEEE Transactions on Power Electronics, 2001.

[3]Fang Xiang. Vector control system of mine hoist based on three-level inverters. Anhui University of Technology: Control Theory and Control Engineering, 2009.

[4]Zhang Li. Research and Application of Three-level Inverter Synchronous Motor Speed Regulation System. Anhui University of Technology: Power Electronics and Power Drive, 2009.

[5]Lanyun, Zhangli. Application of IGCT Frequency Converter in Speed Regulation System of Mine Hoist. Electrical Drive, Nov 2008.

[6]Zhang Li, Li Shuangliu, Liu Fayun. Application of IGCT in Frequency Conversion Speed Regulation System of Mine Hoist. Coal mine machinery, Apr 2002.

[7]Li Chongjian. AC Synchronous Motor Speed Regulation System. Science Press, 2006.

[8]Katsutoshi Yamanaka, AhmetM ava, HiroshiKirino, YoshiyukiTanaka, NoritakaKoga, Tsuneo Kume. A Novel Neutral Point Potential Stabilization Technique Using the Information of Output Current Polarities and Voltage vector. IEEE Transactions on Industry Applications, 2002.

Design and Implementation of a Building Foundation Construction Virtual Simulation Training System

Wenzhen Wang
Zibo Vocational College, Zibo, Shandong 255314, China
E-mail: xbot@sina.com

Abstract: Construction foundation construction is the core knowledge that construction engineering students should master. It has important significance in the development of students' professional ability. The traditional on-site learning method is affected by many factors such as time and cost, and it is difficult to meet the needs of actual learning. The development of a related virtual simulation training system can simulate the actual situation of the construction site, so that students can experience the experience similar to the actual operation, making the teaching more intuitive, improving the interest of learning and deepening the mastery of relevant knowledge.
Keywords: building foundation construction; virtual simulation; training system

1. INTRODUCTION

Virtual simulation is a new technology developed after the 1980s. It forms a three-dimensional digital graphical model through software programming to generate a man-made virtual environment. It involves disciplines such as artificial intelligence, sensing technology, human-computer interaction, and computer graphics. The application of virtual simulation technology in education and teaching can not only present the knowledge learned more intuitively, mobilize the enthusiasm of students, but also change the traditional teaching mode and improve the students' practical ability[1].

Construction foundation construction is the core teaching content of civil engineering related majors, and it has strong practical characteristics, especially the main project, namely the construction of reinforced concrete engineering. For the frontline personnel at the construction site, mastering the craft and method is also should have the basic qualities. At present, the main problems in the construction of building foundation construction are:

(1) The practical teaching link is difficult to meet the actual teaching needs: due to the characteristics of the architectural profession, the teaching plan is difficult to correspond to the actual production time of the enterprise; the period of infrastructure construction is long, the amount of engineering is large, and the short-term training cannot be truly comprehensive. Understand the construction process.

(2) Students are difficult to actually operate, and the learning effect is not good: internships at off-campus construction sites, due to time and cost constraints, and construction units for personal safety considerations, students often cannot actually complete construction operations. It is difficult to achieve the expected learning effect.

(3) The assessment of academic performance is not reasonable: the learning of infrastructure construction content is generally through off-campus practice. The academic performance is generally based on the student's attendance and relevant reports and summary materials issued by the trainee, which is subjective. Sex is not conducive to the development of students' enthusiasm for learning.

The development of building foundation construction simulation teaching software can use the current advanced virtual simulation technology to apply 3D visualization technology to teaching, so that students can simulate and post training in the learning process, and can fully understand the whole construction foundation. process. Through the construction of this virtual simulation software, the practice and theory can be combined with the actual situation of the construction site, and the real working environment can be simulated and developed by using software, so that students can truly experience the technology and skills of the construction site, thus reducing the students. The unfamiliarity of the scene makes the teaching more intuitive [2-3].

2. DOMESTIC AND FOREIGN RESEARCH OVERVIEW AND DEVELOPMENT TREND

The application of virtual simulation technology in architecture at home and abroad is mainly reflected in the following two aspects:

2.1. Research on the theory of building construction simulation

In 1991, American scholars proposed the definition of virtual enterprise. Tsinghua University and Tongji University had scholars in this area. In 1997, domestic research on virtual enterprises received attention in various aspects. At present, the relevant theoretical framework has been formed, virtual enterprises have also begun to expand from the manufacturing industry to other industries. In terms of virtual construction, from the first introduction of the concept by the American Inventors Association in 1996 to the emergence of the TFV (Transformation-Flow-Value)

theory in 2000, the possibility of applying virtual enterprise theory in the construction industry was demonstrated. Domestic researchers' research on virtual construction is mostly at the organizational management level, and less research on the realization of specific technologies [4-5].

2.2. Research on simulation methods of building construction

Building construction simulation technology is a specific application in virtual construction, mainly through virtual simulation and virtual reality technology. Virtual simulation technology generally describes the whole system by establishing a model, and then obtains some regular data through some repeated experiments. The domestic researcher Yu Xinfu studied the dynamic simulation of super high-rise building construction, and Zhang Zhengfeng applied the graphic technology in visual simulation to study the construction process of complex group buildings [6]. Virtual reality is the transformation of boring data into intuitive images in virtual construction, which facilitates operations and comparative analysis, and enables the study of deeper content in the data. Zhao Lingjun studied the identification of buildings and the extraction of geometric dimensions. Wang Chenhui simulated the working scene of hydraulic excavators. Zhong Denghua and others analyzed the visual simulation of hydropower projects, and their research results have been successfully applied. Virtual reality technology is widely used in building construction, and its development direction is mainly event-driven immersion and time-driven immersion.

3. RESEARCH AND ANALYSIS ON THE STATUS QUO OF CONSTRUCTION TRAINING FOR BUILDING FOUNDATION CONSTRUCTION

"Construction Engineering Construction Technology" is the core course of civil engineering related majors. The main project, that is, the construction of reinforced concrete engineering, is even more important. For the construction of this part of the project, for the first-line personnel at the construction site, master the process and method. It is the basic quality that should be possessed, especially for the construction workers. In the training of students, the teaching hours and credits, teaching equipment and training places, and the number of teachers are the first in each course [7]. This course is also a compulsory course for other civil engineering majors. It plays a role in the formation of students' professional ability. Decisive significance, in the construction industry, the demand for talent skills is getting higher and higher, its status and role is increasingly prominent, so how to make students more accurately master the skills of building foundation is particularly important.

4. CONSTRUCTION AND DEVELOPMENT OF VIRTUAL SIMULATION TRAINING SYSTEM FOR BUILDING FOUNDATION CONSTRUCTION

The system uses Unity3D and 3ds Max as the development platform to realize the system logic function and 3D model design and production; use SQL Server 2008 to realize the storage of identity information and training progress information; the specific virtual training system can support the above technical support. Run on PCs, mobile devices, and the web.

The design framework uses the classic MVC design pattern to divide the entire system development into three major modules: the model component, the view component, and the controller component. The model component is the communication bridge between the view component and the controller component. The specific operation information sent by the controller is transmitted to the model component. After a series of logical calculations, the model component sends a calculated series of related information to the view. A component that receives information from the view component and ultimately presents it to the user. In this system, the model component is implemented by C# function script, the view component is jointly completed by UGUI interface development technology and 3ds Max, and the controller component is responsible for hardware devices such as mouse and keyboard. The MVC design pattern reasonably divides the software development process and abides by the principle of "low coupling and high cohesion" of software development. The developer can develop different system components in parallel according to the interface mode of the overall design of the system, effectively improving System development efficiency.

The building foundation construction virtual simulation training system consists of 6 modules, as follows:

(1) Identity authentication module

Its main functions are: judging the identity of the logged-in user, recalling the progress of the corresponding learning module, and learning scores.

(2) Common module

Its main functions are: engineering drawings, technical specifications, knowledge learning, video library, test question bank, toolbox.

(3) Earthwork excavation engineering module

Its main functions are: site requirements, site cleaning, line positioning, mechanical excavation, trimming and inspection.

(4) Reinforcement engineering module

Its main functions are: elastic steel wire, placing steel bars, tying steel bars, placing blocks, placing vertical ribs, welding steel bars, and hoop binding.

(5) Template Engineering Module

Its main functions are: preparation work before construction, formwork installation, quality inspection and acceptance, formwork demolition, and project acceptance.

(6) Concrete engineering module

Its main functions are: concrete preparation, concrete

transportation, pouring and compaction, concrete maintenance, engineering acceptance.

In short, the virtual simulation training system of building foundation construction has built a teaching platform combining the theoretical study and production practice of higher vocational building majors, making up for the teaching methods, training conditions, time and space constraints, and realizing teaching in the classroom. Project and construction projects, teaching process and construction process, school learning and actual work consistency. However, this kind of simulation teaching system also has problems such as poor student's on-site safety production awareness and inability to perform on-site operations, etc., which should be paid attention to. Through the rational design of each teaching link, the virtual simulation training combined with the theoretical teaching and production practice can improve the teaching efficiency, broaden the practical teaching channels, and play an active role in promoting the vocational school's ability and development.

REFERENCES

[1]Hua L.F., Adviser-Su, Jun C. The development of intelligent virtual reality-based industrial training systems. Hong Kong: Hong Kong University of Science and Technology, 1998, 100-102.

[2]Hang Y.Y., Zhong L.Z., Li Z. Survey of virtual maintenance. Acta Simulata Systematica Sinica, 2005, 9(15): 38-39.

[3]Fang Xiaofeng. 3D Simulation Design System for Urban Planning Based on Virtual Reality. Computer Simulation, 2007, 24(3): 230-235.

[4]Wang Jianjian, Zhang Xu, Wang Yong, et al. Development status, policies and implications for virtual reality technology in the United States. Science and Technology Management Research, 2010, 30(14): 37-40, 56.

[5]Jiang Xuezhi, Li Zhonghua. Research Status of Virtual Reality Technology at Home and Abroad[j]. Journal of Liaoning Technical University (Natural Science Edition), 2004, 23(2): 238-240.

[6]Talking about the research status and development trend of virtual reality technology [EB/OL]. http://blog.sina.com.cn/s/blog_5ddbd1060100ec6r.html, 2009-07-01.

[7]Grigore C. Burdea, Philippe Coiffet. Virtual Reality Technology. 2nd ed. Wei Yingmei, Luan Daodao, etc.. Beijing: Publishing House of Electronics Industry, 2005.

Electrical Control of Tunnel Kiln Based on Industrial Network

Shisheng Zhang
Zibo vocational institute, Zibo, Shandong, 255314, China
E-mail: zsszdm@163.com

Abstract: According to the control technology of zirconia zunnel ziln, it is proposed a solution of remote control based on CC_Link bus. Configuration via the substrate module,Configure network parameters and inverter parameters,Using Q series PLC to control system,GOT touch screen for interactivecontrol.The network is stable and reliable,stronganti-interference ability,Convenient programming. The system is easy to operate,Kiln atmosphere is easy to control.
Keywords: CC_Link; zunnel ziln;inverter

1. ANALYSIS OF ELECTRICAL CONTROL TECHNOLOGY OF TUNNEL KILN

Tunnel kiln is a continuous firing equipment, which has the advantages of continuity, short cycle, good quality, high thermal efficiency, uniform temperature, labor saving and long service life.This project uses a tunnel kiln with a length of 41 meters and an annual output of 3,000 tons of zirconia.It has 68 kiln cars and its electrical control is divided into seven areas (lines).The structural diagram is shown in figure 1.

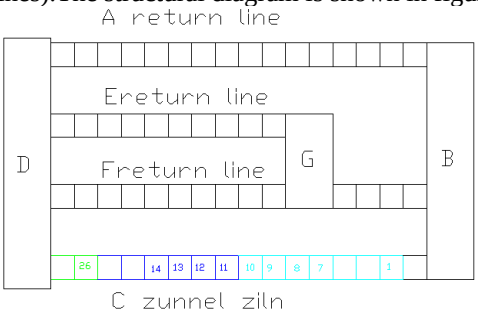

Figure 1.The structural diagram

Area A (return line) is used for loading and unloading of kiln trucks to ensure that there are trucks at the end of the line.Area B ferry is used to transport zone A kiln car to kiln head.The kiln in zone C is used for sintering incoming materials, pushing a kiln truck every 72 minutes.Zone D ferry is used to transfer the sintering completion of zone C to the kiln car parked at the end of the kiln to the F line for cooling.When there is a call order, the kiln car cooled in zone E will stop at the end of the line and be transported to line A.E, F area return line for kiln car cooling, buffer storage to ensure that there is a car at the end of the line.G zone ferry is used to transport F zone kiln car to E line for further cooling and storage [1].

2. MITSUBISHI CC-LINK BUS

In the industrial control system, data and control information can be transmitted simultaneously in a 10 Mbps high-speed field network by CC-Link Bus.It has outstanding advantages such as excellent performance, strong anti-interference ability, simple use and cost saving.

Its bottom layer follows RS485 communication protocol and mainly uses broadcasting-polling (circular transmission) mode to communicate.The master station sends the refresh data (RY/RWw) to all slave stations and polls slave stations at the same time; the slave station responds to the master station's polling (RX/RWr) and informs other slave stations of the response; and then the master station polls other slave stations (which do not send refresh data at this time) and informs other slave stations of the response.

This project space does not exceed 100 meters, according to its maximum data transmission speed of 10 Mbps, its performance is quite stable; and it can also connect various local control stations as intelligent equipment stations, using CC-Link can form a simple PLC control network, the price is extremely low.

3. HARDWARE CONFIGURATION

The control system uses Mitsubishi Q series PLC and CC_Link module to configure on the base. Connect stations on CC_Link network module as shown in Table 1.

Table 1. CC-link Hardware Configuration

Station	Modular	Function
0	QJ61BT11N	CC-Link Master
1	AJ65SBTB1-32D	Input
2	AJ65SBTB2N-16RD	Output
3	AJ65SBTB1-32DR	B Ferry
4	AJ65SBTB1-32DR	D Ferry
5	AJ65SBTB1-32DR	G Ferry
6	FR-A740-7.5K	Preheating Fan
7	FR-A740-5.5K	Combustion Supporting Fan
8	FR-A740-22K	Smoke Exhausting Fan
9	FR-A740-7.5K	Cooling Fan

4.NET CONFIGURATION

After setting up the PLC project in GX-Work2, all the modules on the board are configurated. Under the monitoring of diagnosis_system, the installation location and address distribution of each module can be seen. The address of CC_Link module on the

board is 80H.The netconfiguration is shown in figure 2.

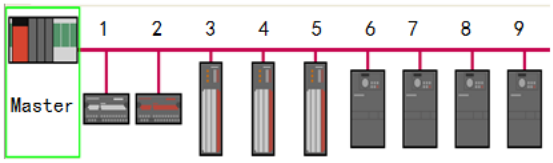

Figure 2.The netconfiguration

Then set network parameters, in the project parameters network parameters CC-link, indicate the meaning of each parameter.

For the converter, it is necessary to install additional CC-link interface board on the converter, wiring the network on the interface board, and then setting the parameters of the converter.

Select transmission speed of 156 kbps, other parameters are default, click "Reflect Settings and Close" to save information.

Pull out "X/Y Assignment Confirmation" and you can see that the slave address is assigned as Table 4, which is the mapping address to be used in programming [1]. The X/Y initial address assignmentis shown in Table 2.

Table 2. X/Y initial address assignment

Station	X	Y
1	1→X1000	1→Y1000
1	1→X1010	1→Y1010
2	2→X1020	2→Y1020
2	2→X1030	2→Y1030
3	3→X1040	3→Y1040
3	3→X1050	3→Y1050
4	4→X1060	4→Y1060
4	4→X1070	4→Y1070
5	5→X1080	5→Y1080
5	5→X1090	5→Y1090
6	6→X10A0	6→Y10A0
6	6→X10B0	6→Y10B0
7	7→X10C0	7→Y10C0
7	7→X10D0	7→Y10D0
8	8→X10E0	8→Y10E0
8	8→X10F0	8→Y10F0
9	9→X1100	9→Y1100
9	9→X1110	9→Y1110

5. COMMUNICATION CONTROL

The remote I/O module settings take the B area ferry as an example. Its module model is AJ65SBTB1-32DR, and its CC-link station is set to No. 3. The module I/O address corresponds to the actual programming address. The action of the module Y00 can be controlled by controlling Y1050 in the program [2].

After the initialization of PLC, after a period of time, ensure that the frequency converter is ready to start, and then write frequency to enable the frequency converter, otherwise the operation is complex or the frequency converter can not carry out network communication.

When the system is debugged, the converter controls the fan to form the thermal atmosphere in the kiln, which is operated by the thermal engineer to determine the working frequency of each converter[3]. It can be configurated on touch screen, the interface should have permission to avoid non-professional operation and clear responsibility; the change of frequency value can be increased or decreased by buttons to meet the requirements of thermal engineers; and the upper and lower limits of frequency should be set to protect the thermal atmosphere of equipment and kiln. If the control mode of the converter needs to be changed, the mode button of the panel can be directly operated without temporarily stopping the work of the converter, so as to avoid the change of gas concentration, insufficient oxygen supply and danger during start-up and shutdown.

6.PROGRAM STRUCTURE

The system has three return lines, three ferry cars, four frequency converters, 10 gas valves, three kiln doors and one cylinder to be controlled. The program structure is shown in Figure 11-20. In addition, there are test procedures, alarm management, password management and so on.

Each program block should be controlled sequentially to avoid interaction. A unified resource allocation library, equipment component library and alarm information database are established to facilitate adding and modifying and avoid resource conflicts.

Taking A return line as an example, the program flow is analyzed. Initial state (M102) A car is waiting between parking spaces 3 and 4, and the running judgment is made to decide which process to enter (waiting, manual delivery, regular delivery).

Manual delivery is the process of moving a parking space from the kiln car with full material at the tail of the return line to the first one (condition: there are manual delivery signals and fewer than 26 kiln cars on the return line (up to 26 on this line). The car goes westward (M110) to position 3 and is automatically crashed into the kiln car by mechanical device, stopping westward. Start eastbound (M111), reach position 4, delay eastbound (M112) 2 seconds, stop eastbound. Start westbound (M113) (automatically decoupled from kiln car by mechanical device) return, westbound to position 4, stop westbound, enter the waiting state (M102), ready for the next time.

Timing delivery is the process of sending a car to the first car every 72 minutes: if there is no manual signal, more than 10 kiln cars on the return line (less than 10 can not be delivered), B ferry is in a waiting state, and there is no car at the exit of the return line, it can be delivered; first, the car travels eastward (M120), meets the kiln car's automatic loading, stops eastbound when there is a car at the rear; and starts westbound (M113) from the mechanical device. Return to No. 4 westbound, stop westbound, enter the

waiting state (M102), prepare for the next time.

In order to ensure the operation and maintenance of the system, fault alarm is essential. The possible failure states are: car override on return line, inclination of kiln box, number saturation of kiln car, alarm test, ferry override, unloading fault, kiln door lifting override, cylinder expansion fault, temperature abnormality, pressure abnormality, return line overtime, ferry overtime, kiln head urgent need kiln car, kiln tail urgent need to leave, a total of 61 failure points.

When a fault occurs, the corresponding state is positioned. On the one hand, the alarm is driven. On the other hand, the state is configurated to the touch screen alarm group, and the fault number, location and treatment method are prompted on the touch screen. When the staff has finished handling the malfunction, press the reset button on the touch screen, and the alarm will be released.

In addition, the duty personnel can inquire the fault number, fault location and treatment methods in the work manual to ensure the normal operation of the system.

Through operation, it is found that most of the causes of failure are caused by sensors or mechanical reasons, and the PLC itself has no fault.

7. CONCLUSION

Based on the research and analysis of the control technology of zirconia tunnel kiln, the solution of long-distance control with CC_Link bus is put forward. This requires the configuration of the substrate, the configuration of network parameters, the use of Q series PLC for system control, GOT touch screen for interactive control. The actual results show that the network is stable and reliable, anti-interference ability is strong, simple and easy to operate, the programming is convenient, the operation is easy, the system runs well, the failure rate is very low, the kiln atmosphere is easy to control, and the product quality and output fully meet the design requirements of the factory.

REFERENCES

[1]Zhang shisheng. PLC Applied Technology, Xian:Xidian University Press,2018, 252-260.

[2]Qiao yuanfeng.CC-Link Communication Technology between Mitsubishi PLC and Mitsubishi Inverter.NanNing:Equipment Manufacturing Technology, Phase 2, 2012, 82-83.

[3]Hou Lu. Design and Temperature Control of Tunnel Kiln Control System, Phil. Trans. Roy. Shenyang:Northeastern University, 2008.

Classification of Color Images Based on Vgg16 Network Model and Lib-SVM

Zhi Chen, Zhijiang Bai*
College of Information Engineering, Shanghai Maritime University, Shanghai 201306, China
Research Center of Intelligent Information Processing and Quantum Intelligent Computing, Shanghai 201306, China
**E-mail:1589236696@qq.com*

Abstract: In recent, image classification has become an important field of artificial intelligence, and the method and precision of image classification are also increasing. This paper proposes a vgg16-based network model and Lib-SVM classification method. First, the vgg16 model is used to train data. Then extract the shallow and deep features, fuse their features, perform PCA dimensionality reduction, and use the specific implementation of the support vector machine Lib-SVM toolkit to classify it. Experiments show that this method has better accuracy compared with traditional methods.
Keywords: vgg16; PCA; feature fusion; SVM

1. INTRODUCTION

Now image classification has become an important topic in the current society, and image classification is also an important branch of image processing. Image classification is also widely used, such as face recognition, vehicle detection, pedestrian detection, medical and military applications. Although image classification has achieved good results at this stage, image classification is a complex process, which contains a lot of information for the image itself, so it is a challenge to get these information completely, then to better classify and obtain better accuracy. There are many methods for image classification, such as neural network classification, but there are also some shortcomings. When using neural network to directly classify, the extracted image features are not very complete, some details of the features will be ignored, so sometimes the effect of classification is not very good. On the other hand, the traditional manual feature extraction method for classification usually requires very complex. Computing and generalization ability of the algorithm is not very good, so in this paper, we use the method of multi-layer vgg16 fusion feature processed by PCA combined with SVM (MVP-Lib-SVM) to realize image classification. Firstly, we use the model of vgg16 to train, and then extract the shallow and deep features for image classification. Multiple Feature Fusion (MFF), feature fusion can obtain more image information, and the classification effect is better [1]. After fusion, the features are reduced by PCA. Finally, the Lib-SVM toolkit is realized by support vector machine.

2. MVP-LIB-SVM MODEL

The accuracy of image classification is an important indicator for testing image models. However, extracting image features is the premise of accuracy. In recent years, CNN as a method of deep learning has greatly improved the efficiency of classification. CNN As a multi-level model, image input, through the stacking of convolution pooling and a series of operations of non-linear activation functions, can mine the multi-layer features of the image, but the traditional CNN usually sends the features of the last layer mapping into the classifier for classification. If only the features of the last layer are classified, it will inevitably miss a lot of detail features, which will certainly have an impact on the results of classification. So we will use the network model of vgg16 to extract and fuse the features of images, but the features are different. The more extracted, the less effective it is, so PCAis adopted to reduce dimensionality, remove redundant information of features, and then classify by Lib-SVM. The framework of this paper is as Figure 1:

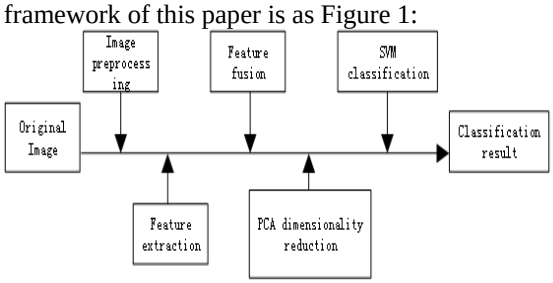

Figure 1. Frame diagram of this paper

The algorithm structure diagram is shown in Figure 2:

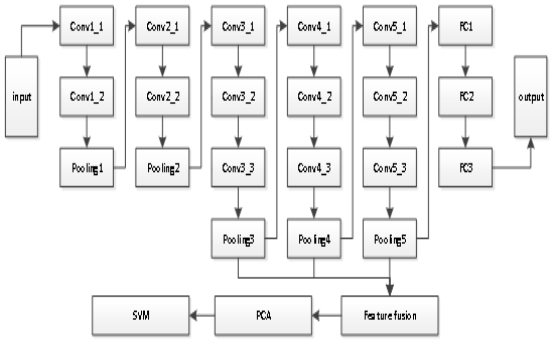

Figure 2. MVP-Lib-SVM

2.1. Image preprocessing

The data set used in this experiment is 80 images of

flowers, food, buildings, animals and cars from the Corel database, but because the image used by vgg16 is 224 X 224 input, the image is normalized to 224 X 224 image pixels as input.

In deep learning, a large number of experiments show that the size of data sets directly affects the performance of deep learning. If the data sets are too small, it is easy to cause over-fitting. In order to get more data, we will use data enhancement to expand the size of the data set [2]. Data enhancement methods include flipping, clipping, rotation, scaling deformation, affine change, visual change and so on. In this experiment, we will use rotation to enhance the data, which can not only enhance the size of the data, but also keep the pixels of the image unchanged. This will preserve more information about the image. Rotation enhancement will rotate the image as the center, and the enhancement is as follows: rotate the picture 90°, 180°, 270°, so that the number of images will be 3 times, which are 240 sheets, and then 70% of the image will be used. The training set, the remaining 30% as a test set.

2.2. Feature extraction

Because of the nature of convolution and pooling computation, the translation part of the image has no effect on the final eigenvector. From this point of view, the extracted features are more difficult to over-fit. Because of the invariance of translation, it is meaningless to alter the translation character, which eliminates the process of altering the sample. The features extracted by CNN are more scientific than simple projection and direction. Feature extraction will not become the bottleneck of the final improvement of accuracy. The ceiling can use different convolution, pooling and the size of the final output eigenvector to control the fitting ability of the overall model. The dimension of eigenvectors can be reduced in over-fitting, and the output dimension of convolution layer can be increased in under-fitting. Compared with other feature extraction methods, vgg16 is more flexible. In this paper, we use vgg16 to extract features [3]. We will extract features from pool 3, pool 4 and pool 5 layers [4]. The operation of pool layer is image resize. The information removed during image compression is only some insignificant information, while the information left behind is a scale invariant feature, which is the most capable of expressing image features. Feature dimensionality reduction, we know that an image contains a lot of information and features, but some information for us to do image tasks without too much use or duplication, we can remove such redundant information, extract the most important features, which is also a major role of pooling operations. To a certain extent, it can prevent over-fitting and is more convenient to optimize. The pooling layer is to do some optimization under the condition of feature invariance.

2.3. Feature fusion

The model of convolution neural network will filter the image features. If some valuable features are ignored, it will affect the experimental results and degrade its performance. The traditional convolution neural network only considers the feature map of the last layer after layer convolution, and does not fully mine the information of each layer of convolution neural network, which will be one. The neglect of the shallow features of some images results in the reduction of classification accuracy. Therefore, combining the shallow features with the deep features and using the fused features to classify will achieve better results. In this paper, feature fusion will be carried out by serial fusion. The fused feature vectors can be expressed by the following expressions (1):

$$Z = \left\lfloor X^{l-2}, X^{l-1}, X^{l} \right\rfloor \quad (1)$$

2.4. PCA dimension reduction

The feature is merged by serial fusion, and the redundant information is increased. We need to reduce the dimension of the fused feature vector. The dimension reduction can remove noise and unimportant features, making the data set easier to use and reducing the calculation of the algorithm. There are many dimension reduction algorithms, such as singular value decomposition, principal component analysis, factor analysis, etc. In this paper, PCA is used to reduce the features [6], and a k-dimensional image feature is obtained. The value of K is determined by the cumulative contribution rate of the principal component. Combining with the experiment, the first k eigenvectors with cumulative contribution rate of 0.85 are selected to form a new image feature map to reduce the dimension without affecting the classification accuracy.

2.5. Lib-SVM classifier

SVM can analyze objects from the characteristics of samples. Support Vector can minimize the empirical error and maximize the geometric edge, which is characterized by solving the small sample size and non-linear classification to a certain extent, solving the problem of local minimum of classification model and improving the accuracy of classification. This article will use Lib-SVM instead of the output layer of vgg16 to classify images [7]. Lib-SVM is a toolkit designed and developed by Professor Lin Zhiren of Taiwan University. Download the lib-svm package first, then import the package into the python package to use.

3. EXPERIMENT AND RESULT ANALYSIS

3.1. Experimental platform

The experimental environment used in this paper is Windows operating system, using I5-6500 processor, the main frequency is 3.20GHz, the memory is 16GB, the deep learning framework is TensorFlow, and the software programming environment is Python3.6.

3.2. Evaluation criteria

This experiment mainly verifies the results of the experiment by the accuracy rate. The main formula is

as follows:

$$Accuracy = \frac{Identify\ he\ correct\ number\ of\ images}{Tota\ln umber\ \text{of pictures}} \times 100\% \quad (2)$$

3.3. Comparison with other methods

In order to verify the effectiveness of the method, it will be compared with the traditional method, the results are shown below:

Table 1. MVP-Lib-SVM

Sample type	Classification accuracy/%
flowers	93.6
food	90.7
building	93.3
animals	96.5
cars	89.6

Table 2. Manually extract-Lib-SVM

Sample type	Classification accuracy/%
flowers	86.4
food	88.5
building	92.7
animals	95.6
cars	90.5

Table 3. Vgg16-Lib-SVM

Sample type	Classification accuracy/%
flowers	89.5
food	89.3
building	90.1
animals	93.6
cars	90.8

Comparing the method of this paper with the above two methods, the comparison of Table 1 and 2 experiments shows that the features extracted by vgg16 are more complete than the features of manual extraction. Table 1 and 3, the feature fusion makes the information of the picture more specifically, the accuracy of the classification is higher.

4. CONCLUSION

This paper combines neural network and multi-feature fusion to classify images with support vector machine. The accuracy has been improved to a certain extent. After feature fusion, dimension reduction is carried out, which effectively reduces the redundant information of features and greatly improves the operational efficiency. Some samples are not very good when classifying, resulting in poor results. The more types, the lower the classification efficiency. The next step is to do so. Good samples can be selected for further experiments, and different classifiers can be selected for further experiments.

REFERENCES

[1]XuenaQiu. An adaptive kernel-based target tracking method based on multiple features fusion. Ieej Transactions on Electrical & Electronic Engineering, 2011, 7(1):91-97.

[2]ShengDaoqing. Research on image enhancement algorithm. Wuhan University of Science and Technology.

[3]Liu B., Zhang X., Gao Z., et al. Weld Defect Images Classification with VGG16-Based Neural Network. 2017.

[4]Sun W., Du H.J., Zang X.R., et al. Traffic Sign Recognition Based on CNN Multi-layer Feature and ELM. Journal of University of Electronic Science and Technology, 2018, 47(3): 343-349.

[5]QuanSen ZENG, Sheng Gen, et al. A new method of feature fusion and its application in image recognition. Pattern Recognition, 2005, 38(12): 2437-2448.

[6]LiLei. Method of SVM Face Detection Based on PCA Dimensionality Reduction. Journal of Qingdao University of Science and Technology (Natural Science), 2010, 31(5).

[7]Anonymous. Application of Lib SVM in Color Image Classification. Wireless Interconnect Technology, 2018, v.15, No. 140(16): 140-142.

Analysis of College-led College Student Work Management Mode

Xingzhong Li
Zibo Vocational Institute, Shandong, China
E-mail: 17569620@qq.com

Abstract: The college-led college student work management model is based on the school, with the secondary colleges as the main force, with clear powers and responsibilities, division of labor and cooperation, management and service of college students, and a new model of college students' work that highlights the functions of ideological and political education. Under this model, the work of college students presents a significant degree of autonomy, and the autonomy of college students is targeted, characteristic and educational.
Keywords: College student work; Education; X-ray energy spectrum

1. INTRODUCTION

College student work has multiple functions of management, service and education, and the function of ideological and political education is increasingly valued by people. For example, in 2004, the "Opinions on Further Strengthening and Improving College Students' Ideological and Political Education" jointly issued by the Central Committee of the Communist Party of China and the State Council required "putting the ideological and political education of college students at the top of the school's work." Counselors affiliated with colleges and universities are regarded as the "backbone strength" of college students' ideological and political education. The "study style construction", "social practice activities" and "solving the practical problems of college students" mentioned in these schools all depend on the work of college students. carry out. At present, the role of college students' work in the ideological and political education of college students is further exerted. Can not be separated from the optimization of its management. The "College of the College" model is a new exploration of the current development of student work management in colleges and universities [1]. We intend to examine the concepts related to it. Discuss the characteristics and value orientation of this management model College-led college student work management model connotation college-led college student work management model,

It is based on the school. A new mode of college student work management with colleges as the main force, clear powers and responsibilities, division of labor and cooperation, management and service of college students, and highlighting the objectives of ideological and political education.

2. THE MAIN TASKS OF COLLEGE STUDENTS' WORK

Main Tasks of College Student Work The work of college students in China is mainly composed of college student affairs management and college ideological and political education. The former mainly includes management and service in terms of student status, funding, class, employment, attendance, logistics, etc.; the latter is guided by Marxism, Mao Zedong Thought and the theory of socialism with Chinese characteristics. The implementation of the "student-oriented" value concept mainly includes college students' mental health education, situation policy education, employment guidance education, as well as organizing students to participate in party and group life, participating in various activities sponsored by colleges and schools, and participating in social practice activities. And implemented as a carrier [2-3].

Although all colleges and universities in China have set up special courses in ideological and political theory, which are taught by full-time teachers, the work teams of college students actually undertake the functions of ideological and political education for college students. Not only does it have courses related to it, but it is also close to student life and is integrated into education. The characteristics of education in practice play an irreplaceable role. It has become an important channel beyond the "main channel" of ideological and political education in colleges and universities.

3. COLLEGE STUDENT WORK MANAGEMENT MODE

Student work management mode in colleges and universities work management of college students is the realization of the tasks of the relevant functional departments around the work of college students. A kind of adjustment and control activities for the implementation of college students' work management of college students' work discussed in this paper mainly refers to the management implemented at the school level, that is, within the school. The university student work management mode is a set of relatively fixed management standards and operating systems formed in the management activities of college students' work [4].

It is precisely because of this relatively fixed and standardized characteristics. The management model has a tendency to become rigid. Directly affecting the

completion of organizational tasks and the realization of goals. Some scholars pointed out that from the perspective of organizational structure, the work of college students in China has long adopted a centralized and unified bureaucratic management model. This management model is "theoretically; the straight-line organizational structure": the school leader, the student work department, and the first-class student work group. There are problems such as excessive management functions, unclear division of labor, low degree of specialization, weak coordination and coordination, and poor communication of organizational information. What the king wants is that this management model makes the student staff business complicated [5]. The main function of student work has a negative impact on ideological and political education. This student work management model is school-led and innovation needs to be promoted.

4. EMPHASIZING THE RELEVANCE OF COLLEGE STUDENT WORK

Western modern management science that emerged in the 1950s. Such as Peter Drucker's epoch-making "goal management" thinking, the behavioral school advocates the human-centered "flexible management" concept. All of the current college students' work management innovation can be used for reference.

The work management mode of college students is an external condition for college students' work and operation, and can adapt to the current situation of college students' work. It will have an important impact on the orderly and efficient development of university students' work. Based on the above discussion. We try to put forward the "college-led college student work management model". And its connotation is defined as follows: the college-led college student work management mode is based on the school, with the college as the main force, clear powers and responsibilities, division of labor and cooperation, management and service of college students. A new mode of college student work management that highlights the objectives of ideological and political education.

College-led college student work management model characteristics College-led work management model for college students. In fact, the autonomy of student work is clearly, fully and appropriately assigned to colleges, further delineating the respective rights of schools and colleges responsibility [6]. Make the two work together and complement each other in student work. Under the college-led model, the college fully enjoys the autonomy of student work.

4.1. Emphasizing the pertinence of college students' work

First of all, contemporary college students often have distinct personalities in understanding problems, feeling the world, and living in the world, pursuing a different way: secondly, since the 1990s. China's higher education has become more popular from the elite, and the colleges and universities have greatly expanded their enrollment. The number of college students has increased year by year. Therefore, many new contradictions and new problems are faced. This requires that the work of college students can be carried out in a flexible and diverse manner. Can truly respect the different choices of college students. Solve the different types of difficulties it faces. In this case. Traditional school-led student work management model. It is often based on solving the problems of general and universal existence among college students. It is difficult to adapt to the needs of college students' personality development. The academic team of colleges and universities directly contacts and interacts with students. They leave students' lives, listen to students' opinions, answer questions and solve problems for students, and have unique advantages in dealing with the above situations; in fact. At present, the actual work of college students is more borne by the academic teams of various colleges.

4.2. Reflecting the characteristics of the student work of the college

Higher education in the world adopts a model of sub-disciplinary training for students, in order to enable the educational subjects to master certain professional skills to adapt to the increasingly fine social division of labor. Meet the needs of an increasingly diverse market, or try to cultivate specialized talents who are engaged in research in a particular subject area. In this case. The profession determines the future career direction of college students to some extent. The life vision, value orientation, thinking style and career ideals of college students are often closely related to the majors they are studying. Therefore, college students of different majors often have significant differences in the above aspects. College students with the same or similar majors have some commonality in these aspects. This objectively requires the university's academic system to manage and serve. When implementing ideological and political education. Must meet the reality of college students at different levels of professionalism.

5. CONCLUSION

As mentioned earlier, ideological and political education should be placed at the top of all work in colleges and universities, and this aspect of the work of college students is increasingly valued by people in the school-led mode. In all fairness. With the increasing enrollment of colleges and universities in recent years, the number of college academics is limited to the large number of "hard" jobs that can be investigated, and ideological and political education is often due to its own ambiguity, long-term and complexity. Ignored. Under the college-led model. It will give them more time to strengthen and improve the ideological and political education of the college, such as the guidance of the extracurricular activities of college students.

REFERENCES

[1]Li Zhongyan, Zhang Furong. Student Management and Thinking in Colleges and Universities in the New Period. Urban Construction Theory Research (electronic version), 2018, (24).

[2]Hu Jiangling. Reflections on doing a good job in the management of college students in the new era. Examination Weekly, 2009, (35), 181-182.

[3]Ye Chunqiao. Exploration and Reflection on College Student Management in the New Period. Journal of Ningbo University (Educational Science Edition), 2018, 28(1) 46-48.

[4]Li Jianpo. Strategic Thinking on Improving the Management Level of College Students in the New Period. Journal of Henan Normal University (Philosophy and Social Sciences), 2009, 36(5) 211-213.

[5]Zhang Xiaojun.Analysis of the Ideological and Political Education Function of Student Management Early Warning Mechanism in Private Colleges and Universitie. Science and Technology Economics Guide, 2016(18).

[6]Fan Wei. Analysis of ideological and political education in the management of students in higher vocational colleges. Cai Zhi, 2017(22).

Research on Channel Estimation Technology Based on OFDM in Wireless Communication Systems

Ke-jia Ji, Yi Sun
Institute of Information and Engineering, Zhengzhou University, Zhengzhou 450000, Henan, China

Abstract: Orthogonal frequency division multiplexing (OFDM) modulation technology is widely used in the fourth-generation mobile communication. It has strong anti-multipath fading capability and high spectrum utilization. However, OFDM system is very sensitive to channel estimation errors . The channel estimation accuracy is directly related to the detection, demodulation and equalization at the receiving end. Focus on OFDM channel estimation technology, the traditional performance based on pilot is discussed. And the channel estimation in high-speed mobile communication is proposed. Besides, for OFDM systems with different system uses, the parameters of the channel are different.
Keywords: OFDM; Wireless communication system; Channel estimation

1. INTRODUCTION

Orthogonal Frequency Division Multiplexing (OFDM) converts high-speed serial data flow into low-speed parallel data stream by dividing the channel into several sub-channels in the frequency domain. And each channel uses orthogonal sub-carriers to transmit data, and the receiver uses correlation technology to separate the data, which reduces the mutual interference between sub-carriers and improves the utilization of frequency band [1]. Therefore, OFDM is widely used in wireless communication.

However, OFDM system is very sensitive to channel estimation error and synchronization error, and channel estimation plays an important role in signal detection and coherent demodulation. Consequently, channel estimation has become a key part of wireless communication system. The accuracy of channel estimation in OFDM system will directly affect the performance of the whole wireless communication system.

Channel estimation is to estimate the impact response of the channel in order to study the impact of the physical channel on the input signal. In orthogonal frequency division multiplexing (OFDM) systems, the design of channel estimation mainly considers two factors: one is the complexity of the algorithm, the other is the arrangement of pilot patterns. The suitable channel estimation algorithm requires lower bit error rate and less mean square error, and the complexity of the algorithm should meet the requirements.

2. CONVENTIONAL CHANNEL ESTIMATION ALGORITH

Traditional pilot-based algorithms include least square method (LS), least mean square error method (MMSE) and discrete Fourier transform method (DFT) based on transform domain.

2.1. Least square method (LS)

The least squares algorithm is the basis of channel estimation algorithms for all OFDM systems because of its low complexity and simple computation. However, it dose not take into account the influence of noise so that it can only be used in the case of high signal-to-noise ratio (SNR). When the SNR is low, the influence of noise is great, and the accuracy of channel estimation is quickly decreased.

2.2. Minimum mean square error method (MMSE)

Unlike the LS algorithm, the MMSE algorithm consid ers the influence of noise. It makes full use of the statistical characteristics of the channel to deal with the noise, so it has a wider range of applications and higher estimation accuracy. Nevertheless, a difficulty is that the channel characteristics are often unknown in practical application. In addition, the MMSE algorithm requires the solution of the inverse matrix, and the computation is complex when the dimension of the matrix is large. Thus, its use is still limited to a certain extent.

2.3. Discrete fourier transform method (DFT)

The estimation accuracy of DFT algorithm is higher than that of LS algorithm, and the complexity of the algorithm is lower than that of MMSE algorithm. The algorithm is based on the feature that channel energy is more concentrated in time domain than in frequency domain. First, the LS algorithm is used to estimate the signal, and then the frequency domain value is converted to the time domain value by IDFT. After removing the noise in the time domain, the time domain is converted to the frequency domain by DFT, and finally the frequency domain response of the channel is estimated. Because DFT and IDFT can be implemented quickly by digital signal processing technology (DSP), the complexity of the algorithm is not high.

In fact, the three traditional channel estimation methods mentioned above show that pilot signals are inserted serially, and the bandwidth utilization is low, so they occupy valuable frequency band resources. In this case, the channel estimation method based on

decision feedback does not need pilot signal, and can effectively improve the transmission efficiency and band efficiency. However, due to the problem of error accumulation, the performance of the system is degraded and can not be realized quickly. In contrast, the blind channel estimation method does not need training sequence, and the transmission efficiency of the system is higher. Of course, we can also use the semi-blind channel estimation method with low complexity, which uses both specific training sequence and blind estimation method. This method not only ensures the system performance, but also has a good convergence rate [2].

3. CHANNEL ESTIMATION IN HIGH SPEED MOBILE ENVIRONMENT

The high-speed transmission system adopts coherent demodulation. In order to ensure the performance of the system, it is necessary to rely on the channel estimation to demodulate the signal at the starting end of the transmission system. In the high-speed mobile environment, the channel change speeds up and the traditional channel estimation method is no longer applicable. It is essential to design a method which can effectively resist the channel change, track the channel change quickly, improve the transmission efficiency and reduce the complexity of the algorithm [3]. Because DFT is an effective interpolation method with simple implementation and good estimation performance, we can interpolate the frequency response of the channel in the process of time-domain and frequency-domain transformation. Another method is to perform MMSE filtering in frequency domain and linear interpolation in time domain to adapt to the high-speed changing channel by means of MMSE algorithm. In a word, no matter which algorithm is adopted, it is sagacious to consider the channel change and the complexity of the algorithm to realize the fast tracking ability of the estimation algorithm according to the actual environment.

4. CHANNEL ESTIMATION FOR DIFFERENT OFDM SYSTEM

4.1. Multi-input multi-output orthogonal frequency division multiplexing system (MIMO-OFDM)

The MIMO-OFDM system has multiple transceiver terminals, which can generate independent parallel channels in space and transmit data simultaneously. It improves the transmission efficiency and channel capacity. The accurate estimation of the channel state will directly affect the data processing of coherent demodulation and channel equalization. Because the received signal at the receiving end of the MIMO system is the superposition of the multiple antenna signals, and the signals of other antennas are interference for the channel estimation of any pair of antennas, the proposed channel estimation algorithm should match the MIMO-OFDM channel model. Based on common channel estimation methods, blind estimation algorithm has high complexity, low convergence and poor tracking ability. Therefore, channel estimation is based on pilot insertion, that is, non-blind channel estimation algorithm, which requires not only the minimum number of pilots, but also the real-time tracking of channel changes [4]. Different from OFDM system, the pilot frequency of different antennas in MIMO-OFDM system should be orthogonal in order to avoid the interference between antennas.

4.2. Multi-band orthogonal frequency division multiplexing ultra-wideband system (MB-OFDM-UWB)

MB-OFDM-UWB system has the advantages of high bandwidth in frequency domain and high transmission rate. It can transmit data at high speed and is suitable for short-range wireless communication. Because of the sparse characteristics of UWB system, most of the impact response values are near zero. We can reduce the channel dimension by using compressed sensing technology to achieve channel estimation [4-7]. If compression sensing is carried out in the time domain, it is indispensable to add a qualified training sequence in the time domain and change the structure of the system in order to realize the channel estimation more accurately but the realization process is more complicated. Based on the above situation, compression sensing in frequency domain and reconstruction of OMP algorithm can be used to realize channel estimation. This method can obtain high estimation accuracy without using all the known training sequences.

4.3. Coherent Optical Orthogonal Frequency Division Multiplexing System (CO-OFDM)

For CO-OFDM system, easy to carry on signal processing and high-order modulation, it has become the research hotspot in the field of optical communication. Due to the dispersion of fiber, frequency shift and phase noise caused by transceiver laser, it is certainly worth considering the error rate (BER) as an important index to evaluate the system performance in the process of channel estimation [2].

In general, the above three different systems utilize the OFDM technology, but also because of the different system performance requirements, the influence of its own factors needs to be taken into account when the channel estimation is carried out, and the appropriate parameters are selected as the best index to measure the performance of the system.

5. CONCLUSION

Channel estimation has always been an important research topic in the field of mobile communication, and its accuracy will directly affect the results of signal processing and thus affect the performance of the system. OFDM technology is widely used in mobile communication because of its high band efficiency and high anti-jamming ability. For the three traditional channel estimation methods of wireless mobile communication: LS algorithm has low complexity, but its application range is limited; MMSE algorithm has high estimation precision, but

the algorithm is more complex; DFT is between the two methods, and DSP technology can be used to improve the computing speed. For high-speed wireless mobile communication, the channel estimation method needs to track the channel change in real time. And for the wireless communication system with different uses, it is necessary to find the corresponding channel estimation algorithm according to its unique system performance, and improve the algorithm according to each performance index.

REFERENCES

[1]Chen L. Research on Channel Estimation of Next Generation Wireless Communication System. Beijing University of Posts and Telecommunication, 2014

[2]Liu K, Liao S Y, Yin R M, Wang W. Research on Pilot-symbol-aided Channel Estimation in OFDM Wireless OFDM Wireless Communication system. Journal of Henan Polytechnic University (Natural Science), 2013, 32(4): 596-602.

[3]Jiang Z M. Key Technologies of OFDM Wireless Mobile Communication System. Communication design and application, 2015, 9: 16-16.

[4]Tian Q H, Research on key Technologies of High Speed Mobile Wireless Communication system and Broadband Satellite Communication system based on OFDM. Beijing University of Posts and Telecommunication, 2013.

[5]Shu S. Research on Pilot-Based Channel Estimation Technologies for MIMO-OFDM Wireless Communication System. Nanjing University of Aeronautics and Astronautics, 2017.

[6]Wang X M. Research and Implementation of the Channel Estimation in Wireless Communication Systems. Nankai University, 2015.

[7]Cong J. Study of the Synchronization and Channel Estimation Technique Incoherent Optical OFDM Communication System, Harbin Institute of Technology, 2014.

Quantum Particle Swarm Optimization Algorithm Based on Improved Migration Idea

Qianyu Chen[1], Yonglu Liu[1], Yiwei Zhao[1], Mingfang Wang[2], Yuhao Dong[3]
[1]PLA Dalian Naval Academy
[2]Unit 93861
[3]PLA Air Force Engineering University, Xi'an, Shanxi, 710051
E-mail: 821387717@qq.com

Abstract: In PSO algorithm, the search space of particles is the whole feasible solution space of the problem, but because of the aggregation of particle swarm, the loss of population diversity is inevitable. At the later stage of the search, the particles are clustered and the search space is very limited. Particle swarm may fall into local extreme point. In order to avoid falling into local extremum, an adaptive method is introduced based on QPSO algorithm. When using QPSO to solve practical problems, the parameters in formula (5.5) are usually reduced linearly[1].
Keywords: PSO algorithm, QPSO algorithm, convergence

1. INTRODUCTION

In order to make the standard particle swarm optimization algorithm get rid of the local extremum, this paper applies the migration strategy to the standard particle swarm optimization algorithm. The multi-generation population of the particle swarm optimization algorithm does not appear the phenomenon of individual gradually becoming better, which proves that the particle swarm optimization algorithm has been trapped in the local optimum. Therefore, guided by the best fitness particle, a goal is set as M, which is analyzed together with other particles in the collective. Then, the worst individual after migration is replaced by the best individual $Gbest$ before migration, thus the migration quantum particle swarm optimization algorithm is obtained.

2. MIGRATION THOUGHT

2.1. Particle swarm optimization (PSO) migration idea

In the D-dimensional search space, a community is composed of N particles, each particle contains a D-dimensional position vector, which is denoted as Xi, and is regarded as the group optimization, thus producing a random target point Pbest, denoted as M. Therefore, the migration strategy of PSO is to adjust its own position according to the formula:

$$X_{i\_new} = X_i + \sqrt{2-\varphi}\frac{(M - Pbest_i)}{|M - Pbest_i|} \qquad (1)$$

2.2. Algorithmic flow

The algorithmic flow is:
Step1: Initialize the position and velocity of particles
Step2: Calculate the fitness of each particle
Step3: The current position of the particle
Step4: Change the velocity and position of particles
Step5: Compare the fitness values. The current position of particles is regarded as the best position in the whole population.
Step6: Judging whether the PSO algorithm can fully satisfy the convergence conditions
Step7: Global Optimal Particle Individual Output, this is the end of the algorithm.

3. CONCLUSION

Power supply equipment optimization problem is a complex non-linear optimization problem, and its continuous and discrete variables are intermingled with each other, which makes optimization very difficult. Long-term research is based on traditional optimization methods, such as non-linear programming, linear programming and dynamic programming, which have strong model dependence and high requirements for the continuity of initial points and variables. In recent years, intelligent optimization algorithms widely used in academia can better overcome the shortcomings of traditional optimization algorithms. Particle swarm optimization (PSO) algorithm is a heuristic algorithm based on multi-point random search. It uses multi-point parallel search method and information exchange among particles. It can quickly converge to a point in the solution space. There are fewer parameters to be adjusted, and it is suitable for power supply equipment optimization[2]. Firstly, the improved particle swarm optimization (PSO) algorithm is used to optimize the reactive power of power supply equipment. Firstly, the optimization index is determined to be the stability of static voltage, thus a set of Multi-Objective Reactive power optimization model is established. At the same time, the comprehensive factors such as the minimum active power loss, the optimization of voltage level and the maximization of static voltage stability are considered. Particle swarm optimization (PSO) is used to optimize the model function. The experimental results show that the particle swarm optimization algorithm can realize the economic operation of power supply equipment and improve the stability of power supply equipment. Therefore, it proves that the particle swarm optimization algorithm has its unique

advantages and effectiveness[3].

Secondly, the improved particle swarm optimization algorithm is used to optimize the multi-objective dispatching model of power supply equipment failure. According to the relevant research, it is proved that the improved particle swarm optimization algorithm can greatly improve the feasibility of power supply equipment decision-making, provide strong support for decision-makers, and prove that the algorithm is very suitable for multi-objective dispatching optimization of power supply equipment.

Thirdly, according to the specific power loss problem of power supply equipment, the variant improved particle swarm optimization (PSO) algorithm is used to optimize the reactive power of multi-objective. Through a large number of related experiments, it is proved that PSO algorithm can express the specific relationship between voltage deviation and power loss in power supply equipment, and at the same time, provide users with a very uniform distribution of diverse alternatives. By stacking the results several times, it can be shown that the algorithm has reliable stability. Moreover, numerical experiments on the improved particle swarm optimization algorithm prove that the algorithm has strong search ability and convergence ability, and overcomes many shortcomings of the particle swarm optimization algorithm.

In summary, the improved particle swarm optimization (PSO) algorithm is applied to the power supply equipment fault problem, which can reduce the number of parameter settings and has strong operability in optimization. Therefore, this paper uses the PSO algorithm to optimize the parameters of the wide area damping controller.

REFERENCES

[1]Roman Lysecky, Frank Vahid. A Configurable Logic Architecture for Dynamic Hardware/ Software Partitioning. Proceedings of the Design, Automation and testing in Europe Conference and Exhibition (DATE04), 2004, IEEE, 01-06.

[2]William B. Andrew, Glenn Cart, Ravi K, Charath, James F.Hoff, Ron Modo,Hung Nguyen, William Smith, David Rhein, Joe Schulingkamp, Carolyn W. Spivak, James P. Steward, Akila Subramaniam. A Field Programmable System Chip which combines FPGA and ASIC circuitry. IEEE 1999 CUSTOM INTEGRATED CIRCUITS CONFERENCE, 183-186.

[3]Quartus II Installation & Licensing for PCs, Altera Corporation 101 Innovation Drive San Jose, CA 95134(408)544-7000, www.altera.com

Analysis of dragon migration based on Analogy and cluster Analysis

Suyun Wang, Yajun Zhang, Chongrun Wu, Yu Gao, Chunli Wang
Institute of Information Technology of Guilin University of Electronic Technology, Guilin, 541004, China
E-mail: xxkjxy@guet.edu.cn

Abstract: Firstly, it is supposed that there are many factors， which means overall ecological impact requirements, food, environment and the community and so on. After calculation, we can finally find that food is main factor. Secondly, our team establishes the transfer diagram of the external environment and energy of dragons. Then we find basic energy consumed by the three dragons. Thirdly，we use the way of analogy to calculate the body surface area of each dragon. That is equal to the coefficient multiplied by the height plus the coefficient multiplied by the weight. Then we use the figure of calculation subtracts the coefficient to get the area of three dragons. Fourthly, suppose that if the animal body is analogized with a flexible beam (cylinder), which is supported at the end of the extremities. Base on the elastic theory, we get the final calculated heat. Regarding question 5, we compare the living community of the Siberian Tigers to the dragon. Then get the communities supporting three dragon are 24,000 square kilometers. Finally, we analyze energy consumption of the dragon in different climates and areas, and then find the basic energy consumption of the dragon .

Keywords: The energy consumption of dragon; Analogy calculation; Cluster analysis; Principal component analysis; Nonlinear regression equation

1. THE RESTATEMENT OF PROBLEM

1.1. The background of problem

In “Game of Thrones”, the weight of three dragons was about 10 kg when they hatched, and their weight increased about 30-40 kg per year. They continued to grow throughout life, depending on the characteristics, behavior, habits, diet, and interaction with the environment.

1.2. The requirements of problem

Question 1: What are the ecological impacts and requirements of the dragon?

Question 2: What is the energy consumption of the dragon?

Question 3: How much area does it take to support the three dragons?

Question 4: What are their calorie intake requirements?

Question 5: How much community is needed to support the dragon to get different levels of assistance?

Question 6: Like other migratory animals, dragons may travel to different parts of the world in different climates?

Question 7: In arid regions, does dragons moving between warm temperate regions and the Arctic region have a major impact on the resources needed to sustain and grow dragons?

2. THE ASSUMPTIONS OF MODEL AND THE DESCRIPTION OF SYMBOL

1). Assume that the dragon's basic biology is accurate and obey the laws of conservation of energy in nature.

2). Assume that the ecological impact of the dragon is determined by four factors: food, environment, community, and geography.

3). Assume that the dragon is a warm-blooded animal and the environment has less impact on the dragon.

4). Assume that each dragon has the same habits, behavioral characteristics, and eating habits.

5). Assume that each dragon's intake is one percent of its own and the food is sufficient.

6). Assume that dragons live in the community and receive feeding.

7).

Symbol	The Meaning of Symbol
Y	Individual ecological impact and requirements of dragon
$x_i(\mathrm{i}=1.2.3\cdots n)$	Influencing factors
Y_M	The daily calorie needed
Y_J	The energy that dragons need to basal metabolism
Y_X	The energy that dragons need to digest food
Y_T	The energy that dragons need to physical activity

3. THE ANALYSIS OF PROBLEM

3.1. Analysis of question 1

In order to know and solve the ecological impact and requirements of the dragon and we can assume that the ecological impact of the dragon is determined by many factors such as food, environment, community, geography, humanities, space, and time.[1]

3.2. Analysis of question 2

We can use Figure 1, in which the three dragons absorb the external energy for growth, and the excess energy is excluded from the external energy. The amount of heat each dragon needs per day is equal to the basic energy required for each dragon's basal metabolism. Then, use the figure of calculation plus the calories needed for the physical activity of the dragon.[2] Finally use the results plus the energy

needed to digest the food.

The energy required for each dragon to digest food is equal to 10% multiplied by the amount of heat required for basal metabolism plus the amount of heat required for physical activity. The heat required for each dragon per day is equal to 1.1 times the basic energy required for basal metabolism plus the amount of heat required for each dragon's physical activity.[3]

3.3. Analysis of question 3

Regarding the question 3, we can calculate the body surface area of the dragon analogously to the surface area of human beings.[4] The analog surface calculation method is used to calculate the body surface area of each dragon.

The body surface area of each dragon is equal to the coefficient multiplied by the height of the dragon plus the coefficient multiplied by the weight of the dragon and finally subtracted from the coefficient.[5] The adult dragon can swallow a long mammoth in one bite, so we can know the height and volume of the dragon. It is known that area needed to support each dragon.

3.4. Analysis of question 4

For the calculation of the intake of the three dragons, we must first calculate the volume of each dragon. Besides, we have calculated how much energy is needed for the three dragons to maintain daily growth.[6] As long as the model changes, we can calculate the maximum basic intake per dragon and get the basic intake of the three dragons. .

3.5. Analysis of question 5

We refer to the current Siberian tiger, and analogy to the size and range of activities to calculate how large the active community of each dragon is. Then, we calculate how many areas of the three dragons require community giving activities.[7]

3.6. Analysis of questions 6 and 7

We refer to the current migratory birds, analogous to the migratory range of migratory birds to calculate the migration of dragons. As the species migrates, the resources also change. Considering the subsequent conditions, cluster analysis method in multivariate analysis is used to analyze the influence of different pairs on the dragon.[8]

4. THE ESTABLISH AND SOLUTION OF MODEL

4.1. The establish and solution of the problem one model

We can use the nonlinear programming to assume that the overall ecological impact and requirements of the dragon are Y, and many other influencing factors are x_i.

Then there are:

$$x_i = \begin{cases} 1 & \text{Determining ecological impacts and requiremen} \\ 0 & \text{Not determining ecological impacts and require} \end{cases}$$

So the total obtained is:

$$\sum_{i=1}^{n} x_i \le Y$$

Because of $x_i\,(i = 1 \cdots n)$ only values 0 or1, thus $x_i\,(1\text{-}x_i) = 0\,(i = 1 \cdots n)$, we have

$$0 \le \sum_{i=1}^{n} x_i \le Y$$

Principal component analysis is used to further optimize the model and the results are obtained. The overall ecological impact and requirements of the dragon are Y. The other influencing factors including: food x_1, environment x_2, community x_3, geography x_4, humanity x_5, space x_6, and time x_7 and so on.

$$Y = a_1 x_1 + a_2 x_2 + a_3 x_3 + \cdots + a_n x_n$$

$$x = \begin{Bmatrix} x_{11} & x_{12} \cdots x_{1n} \\ x_{21} & x_{22} \cdots x_{2n} \\ \vdots & \vdots \cdots \vdots \\ x_{n1} & x_{n2} \cdots x_{nn} \end{Bmatrix}$$

$$a_1 = \begin{bmatrix} a_{11} \\ a_{21} \\ \vdots \\ a_{n1} \end{bmatrix} \quad a_2 = \begin{bmatrix} a_{12} \\ a_{22} \\ \vdots \\ a_{n2} \end{bmatrix} \quad a_3 = \begin{bmatrix} a_{13} \\ a_{23} \\ \vdots \\ a_{n3} \end{bmatrix}$$

So get: $Y_i = a_i' x$

It is possible to get that the main factor is food, and the environmental, community and geographical are assistant.

4.2. The establish and solution of the problem two model

The amount of heat that each dragon needing per day is equal to the basic energy required for each dragon's basal metabolism plus the amount of heat required for each dragon's physical activity plus the energy needed to digest food, namely:

$$Y_M = Y_J + Y_X + Y_T$$

The energy required for each dragon must be greater than the daily basic calories needed to grow, namely:

$$Y_C > Y_M$$

The energy required for each dragon to digest food is equal to 10% multiplied by the amount of heat required for each dragon's basal metabolism plus the amount of heat required for physical activity, namely:

$$Y_X = 10\% \times (Y_J + Y_T)$$

The heat required for each dragon per day is equal to 1.1 times the basic energy required for each dragon's basal metabolism plus the heat required for each dragon's physical activity, namely:

$$Y_M = 1.1 \times (Y_J + Y_T)$$

From the above, we can know that if each adult dragon need to maintain growth, the basic energy every day are $2.5 \times 10^6 KJ$. The basic energy consumed by three dragons every day are $7.5 \times 10^6 KJ$.

4.3. The establish and solution of the problem three model

We use the analogy calculation method to calculate the body surface area of each dragon. It is equal to the coefficient multiplied by the dragon's height plus the

coefficient multiplied by the dragon's weight. Finally, we use this number to subtract the coefficient, namely:

$$Y_S = 0.0659 \times 28 \times 100cm + 0.126 \times 20000Kg - 1.603$$

The body surface area of each dragon is $3658.197m^2$

If the dragon want to fly，the dragon's wings must occupy two-thirds of the surface area. Their bodies can be thought of as a cuboid whose surface area are $2436.36m^2$ .Thus we can calculate the dragon to each dragon is $800m^2$，and three dragons are $2400m^2$

4.4. The establish and solution of the problem four model

If the animal body is analogous to a flexible beam (cylinder) supported at the end of the extremities, the flexible column theory has been extensively studied. Finally, many ready-made results are available.[9]

Let l mean the length of the torso. d means the diameter of the cross section of the torso，A means the area of the cross section，F means the weight of the dragon，δ indicates the maximum deflection of the dragon trunk under its own weight. Because the dragon's only elastic beam is the torso supported on the limbs and known by the theory of elasticity, the maximum deflection δ meets：

$$\delta \propto \frac{Fl^3}{Ad^2}$$

Because of $F \propto Al$ ，we can get：

$$\delta \propto \frac{Fl^3}{Ad^2} \propto \frac{Fl^4}{Ad^2} = \frac{l^4}{d^2}$$

Then，we can get：

$$\frac{\delta}{l} \propto \frac{l^3}{d^2}$$

Then, we have calculated basic energy consumed per dragon per day is $2.5 \times 10^6 KJ$ However, in the actual situation, up to 60% of the animal's intake is converted into energy, and only 80% is converted into energy consumed per day. Assume that the consumption can be expressed as Y_S .It can be calculated the maximum energy consumed per dragon per day. The intake is:

$$2.5 \times 10^6 KJ \div \frac{6}{10} \div \frac{8}{10} = 5.21 \times 10^6 KJ$$

$$Y_M \div \frac{6}{10} \div \frac{8}{10} = Y_S$$

$$Y_S = 5.21 \times 10^6 KJ$$

4.5. The establishment and solution of the problem five model

We can use the analogy of the scope of the activities of the Siberian tiger to get the dragon's range of activities:

We compare the weight, body length, and tail length of the Siberian tiger with the height, body length, tail length of dragon:

The weight of the Siberian tiger: D_{tz} ————the weight of the dragon: L_{tz} ;

The height of the Siberian tiger : D_{sg} ————The height of the dragon: L_{sg} ;

The body length of the Siberian tiger: D_{tc} ————The body length of the dragon: L_{tc} ;

The tail length of the Siberian tiger : D_{wc} ————The body length of the dragon: L_{wc} ;

The activity area of the Siberian Tiger D that has multiple locations is:

$$m_i (i = 123.....n)$$

The distance between the settlement of Siberian Tiger D and the location of the activity site is：

$$s_i (i = 123.....n)$$

Assuming that the weight, body length, tail length, and height of the Siberian tiger are proportional to the distance of the activity site, a model can be established:

$$D_{tz} \propto s_i (i = 123.....n)$$

$$D_{sg} \propto s_i (i = 123.....n)$$

$$D_{tc} \propto s_i (i = 123.....n)$$

$$D_{wc} \propto s_i (i = 123.....n)$$

We know that the current Siberian tiger can have a maximum of 350Kg, a body length of 2.8 meters, a tail length of 1 meter, a height of 1.3 meters, and a range of activities of 100 square kilometers. Therefore, the activity range of each dragon is calculated to be 8,000 square kilometers, and the activity range of the three dragons is 24,000 square kilometers.

4.6. The establishment and solution of the problem six or seven models

The climatic conditions are very important for the dragon, so we use cluster analysis to calculate the impact of different climates on the dragon. Throughout the world, migratory animals find that their migration route is the result of natural selection. It is mainly a theoretical or ideal migration route to the natural climate, geographical barriers and natural environment. In fact, no bird is moving in a straight line, mainly due to various factors such as ground structure, landscape type, vegetation, food and weather. So do the dragons.[10]

Between the warm temperate regions and the Arctic regions, the Seven Dragons in the arid regions have a great impact on the resources needed to maintain and raise the dragons. We calculate the dragons' flight in the arid regions and the warm zone flight, and the energy consumed while flying in the Arctic. Then we calculate the energy consumed by different regions during flight. Assume that the dragon flies for eight hours a day during migration. It is assumed that the physical activity of the dragon in the warm area is the first level f_1, the physical activity in the dry area is

the second level f_2, and the level of physical activity in the Arctic is f_3.

Then there are:

The basal metabolic rate (BMR) is:

$$BMR = Y_M \div \text{weight} \div 24h$$

The effect of food heat is:

$$\text{The effect of food heat} \approx BMR \times 10\%$$

The total energy that the dragon needed to fly every day in the warm zone is:

$$Y_W = Y_M \times BMR \times 8h \times f_1 + Y_M \times BMR \times 12h + BMR \times 10\%$$

$$Y_W = 2.5\times10^6 \times 3.72 \times 8h \times f_1 + 2.5\times10^6 \times 3.72 \times 12h + 2.5\times10^6 \times 10\%$$

$$Y_W = 1.86\times10^8 f_1$$

The total energy that the dragon required to fly daily in arid areas is:

$$Y_g = Y_M \times BMR \times 8h \times f_2 + Y_M \times BMR \times 12h + BMR \times 10\%$$

$$Y_g = 2.5\times10^6 \times 3.72 \times 8h \times f_2 + 2.5\times10^6 \times 3.72 \times 12h + 2.5\times10^6 \times 10\% \; Y_W = 1.86\times10^8 f_2$$

The total energy that the dragon needed to fly every day in the Arctic is:

$$Y_b = Y_M \times BMR \times 8h \times f_3 + Y_M \times BMR \times 12h + BMR \times 10\%$$

$$Y_W = 2.5\times10^6 \times 3.72 \times 8h \times f_1 + 2.5\times10^6 \times 3.72 \times 12h + 2.5\times10^6 \times 10\%$$

$$Y_W = 1.86\times10^8 f_3$$

Because f_1、f_2、f_3 mean that physical consumption of the dragon in different levels of environment, it is calculated that basic flight consumption is .

$$Y_W = 1.86\times10^8$$

5. EVALUATION AND PROMOTION OF THE MODEL

Because the analogy model method in the text belongs to the category of reasonable reasoning. Besides, there is the property of contingency, and the mathematical model established by the analogy method lacks reliability. The reliability depends on the similarity and the similarity of the two things and the degree of correlation between them. Therefore, this method requires a wealth of information, and requires some experience or a large number of experiments, as well as the correctness of the mathematical model built according to statistics. A practice test is also required. However, there is insufficient information in the text, and there are also contingent characteristics.[11]

Because the dragon is a virtual species in the novel, it is the most feasible way to combine the results of animals in real life.

6. ACKNOWLEDGMENT

The authors wish to thank Chunli Wang. This word was supported in part by a grant from the project of fund of teaching reform project of higher education undergraduate in Guangxi in 2018: research and practice of “handwriting pad +the teaching plan of PDF + MeiPai” hybrid teaching method for mathematics courses in independent colleges (2018JGA335).

REFERENCES

[1]Jiang Qiyuan, Xie Jinxing. Mathematical Model (Third Edition). Beijing: Higher Education Press, 2003.

[2]Li Mingzhen, Qi Jianhua. Establishing Mathematical Model by Analogy Method. Journal of Henan Institute of Education, 2003.

[3]Zhang Fuyun, Yang Ruoli. Chinese Bird Migration Research. China Forestry Publishing House, 1997.

[4]Chen Jun. Research on the relationship between urban rail transit and regional economic development based on cluster analysis. Science and Technology Economic Market, 2018.

[5]Wang Nanqi, Jiang Weibing. Comparison and Cluster Analysis of Photosynthetic Efficiency and Seasonal Changes of Different Li Resources. Journal of Nanjing Agricultural University, 2019.

[6]Hou Yuanwei. A new clustering analysis algorithm based on deep learning. Journal of Xinxian University, 2018.

[7]Xiang Yuyu, Liang Shu. Study on the relationship between wintering migratory birds and environmental factors in the East Dongting Lake wetland. Journal of Zhongnan University of Science and Technology, 2017.

[8]Li Huan, Xiong Mengying. Random forest analysis of fusion factor analysis. Computer Engineering and Applications: 2019.

[9]Yu Lei, Zhu Wenzhao. Research on Innovation Capability of High-tech Industry Based on Factor Analysis. Journal of Changchun University of Science and Technology, 2019.

[10]Zhang Yumeng. Research on Environmental Protection Evaluation of Anhui Province Based on Factor Analysis and Cluster Analysis. Modern Business & Trade, 2019.

[11]LIU Che. The Geographical Pattern of Bird Species Richness in China and Its Relationship with Environmental Factors. Journal of Peking University (Natural Science), 2014.

An Algorithm for Semantic Matching of Natural Language Environment Paragraph

Ying Li[1,], Yinghong Cai[2], Huijuan Liu[1]*
1China Comservice Public Information Industry Co. Ltd., Xinjiang, 830000, China
2Guilin University of Electronic Technology, Guilin, 541004, China
**E-mail：31800841@qq.com*

Abstract: Aiming at the problem that traditional text retrieval can only match texts by keywords, but not semantic matching, an algorithm for natural language environment paragraphs semantic matching with subject description sentences is proposed. Firstly, a method for quickly calculating semantic similarity is proposed. The Euclidean distance calculation is performed on the word vector of the topic sentence and the article so that the similarity is obtained efficiently. Secondly, a method of dimensionality learning to compare the loss of different features is proposed, which can keep the acquired sample features unchanged while the number of dimensions is reduced, so that the learned spatial features are more conducive for sentence matching. Experimental results show that the concatenated long Short-Term Memory (LSTM) framework provides promising results on the Sohu news dataset with an accuracy rate of 95%.
Keywords: Text retrieval; Semantic matching; Euclidean distance; Contrast loss

Semantic matching is an important research field in information retrieval. It has been in the application in the field of natural language. Compared with basic keyword matching, semantic matching is more challenging because of the different semantic information between different sentences. The problem that semantic matching needs to deal with is the similarity between sentences and sentences or between sentences and articles. The challenge of this problem mainly includes the influence of redundant information, the context of the sentence in which the sentence is located, the multi-sense of part of speech and the connotation of multiple words and other factors.

The text search that was first introduced and put into use is the index of the books used by the library. Readers can quickly find the book and its specific location in the library through the index. With the invention and emergence of computers, document matching is performed on a computer basis, and documents for retrieving keywords appear to be presented to the user as final retrieval results. The work [1] uses a keyword and a logical relationship (including "and", "or", "non") to form a Boolean expression. A document is a collection of index words. The criterion for judging whether the query is related to the document is whether the document satisfies the Boolean expression of the query. In [2], a VSM (vector space models) model is proposed, it uses the vocabulary to multiply the word frequency in the text and the reverse document frequency of the vocabulary to calculate the weight, and the search term is obtained. With the development of deep learning, Long Short-Term Memory Networks (LSTM) has been proven to have made breakthroughs in many aspects like sentence matching, information retrieval and machine translation. Deep learning does not require manual design of feature extractors, but is learned by computer autonomously. It is suitable for complex and changing data. It is robust and provides generalization ability. The cross-language automatic retrieval method based on semantic extension proposed in [3]. It is to complete the semantic retrieval by the original search instruction input by the user. In fact, many users express the retrieval requirements in this way, resulting in the decline of retrieval quality.

In [4], a document retrieval design method is proposed based on latent semantic analysis. This method solves the problem like multiple words and one meaning. Besides， it can effectively cluster documents in semantics and complete the similarity calculation between query statements and document sets. Reference [5] proposes a semantic retrieval method based on process ontology, which improves the fit of search results by using the content matching principle of reserved semantics in PQL statements.

Aiming at the method in [3-5], an algorithm for quickly calculating the similarity of sentences is proposed. By calculating the Euclidean distance between sentence vectors, the rate of sentence matching is effectively improved. At the same time, this paper also proposes a contrast loss method based on Euclidean distance, which adds the Euclidean distance and the threshold. In the process of network training, the learned feature class distance can better express the paired sentences and the degree of matching. In the end, the method can effectively improve the accuracy of sentence semantic matching.

1. THE OVERALL FRAMEWORK DESIGN

1.1. The designed scheme of LSTM sentence semantic based on euclidean diatance

The Euclidean distance method is usually used in similar layers. This paper uses the Manhanttan LSTM Model [6] proposed by Jonas Mueller and Aditya Thyagarajan to improve the connected LSTM backbone network. The Siamese LSTM structure

satisfies the needs of semantic retrieval by designing a set of paragraph and subject sentence matching algorithms. The network architecture used by the algorithm consists of two LSTM networks, each processing a given paragraph and subject sentence. LSTM is a network structure for learning long-term dependencies that handles long text data like paragraphs and subject sentences. Through the modeling of the latent semantic similarity of paragraphs and subject sentences, the accuracy of matching is improved. Each paragraph and subject sentence are represented as a sequence of word vectors, and are sequentially transmitted into the network by hiding the last layer of the network. The time point output state is used as the input of the similarity layer, and finally the similarity between the sentences is calculated to determine whether the paragraph and the subject sentence match, so as to realize the semantic retrieval of the text.

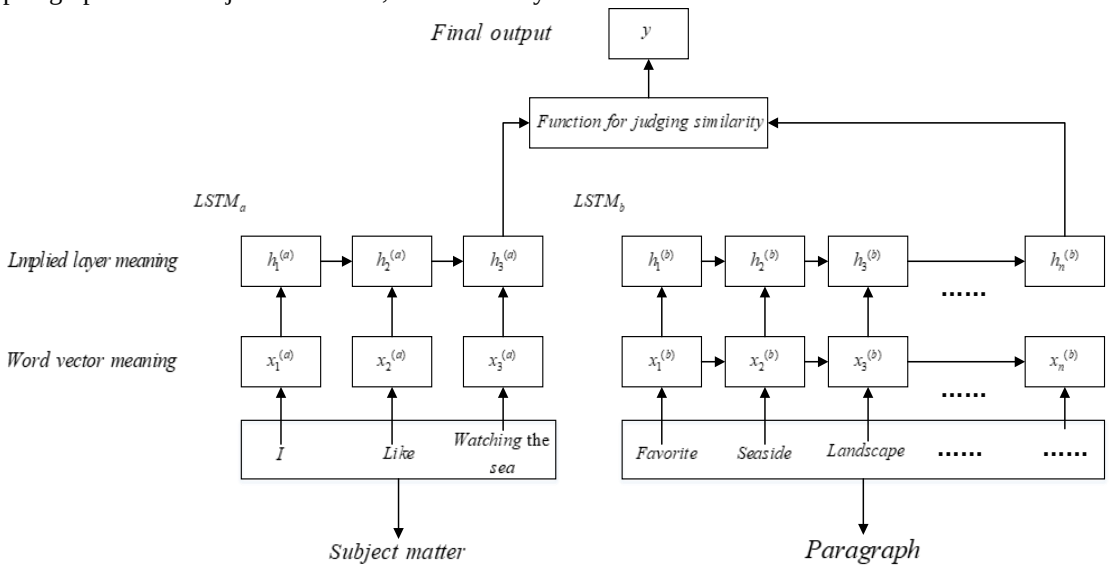

Figure 1. Conjoined LSTM sentence semantic matching framework based on Euclidean distance

1.1.1. Matching network of siamese lstm sentence semantic

This paper uses a conjoined LSTM network structure, which is composed of two networks LTSMa and LSTMb. Each of them processes a given paragraph and subject sentence. LSTM is also called long-term and short-term memory network, which can better learn the long-term dependency information. Compared with the general cyclic neural network, it adds three controllers: the input gate determines how much information is input to the memory cell c_t at the current moment input x_t . The forgetting gate determines that the memory cell c_{t-1} at the previous moment how much can be saved to the memory cellc_t; The output gate is used to control how much memory cells output to LSTM to the current output value h_t.

$$i_t = sigmoid(W_i x_t + U_i h_{t-1} + b_i) \quad (1)$$

$$f_t = sigmoid\left(W_f x_t + U_f h_{t-1} + b_f\right) \quad (2)$$

$$\widetilde{c_t} = \tanh(W_c x_t + U_c h_{t-1} + b_c) \quad (3)$$

$$c_t = i_t \odot \widetilde{c_t} + f_t \odot c_{t-1} \quad (4)$$

$$o_t = sigmoid(W_o x_t + U_o h_{t-1} + b_o) \quad (5)$$

$$h_t = o_t \odot \tanh(c_t) \quad (6)$$

W_i , W_f , W_c , W_o , U_i , U_f , U_c , U_o are weight parameters; b_i , b_f , b_c , b_o are offset parameters.

1.1.2. Calculation of euclidean distance similarity

The Euclidean distance [7] is used as a similar function for the similar layer, which is a formula used to calculate the distance. The distance between two points x_1, x_2 in the N-dimensional Euclidean space, the specific formula is as follows:

$$g\left(h_{Ta}^{(a)}, h_{Tb}^{(b)}\right) = \exp\left(-\left\|h_{Ta}^{(a)} - h_{Tb}^{(b)}\right\|_1\right) \in [0,1] \quad (7)$$

$$d = \sum_{i=1}^{N} \sqrt{(x_{1i} - x_{2i})^2} \quad (8)$$

g is a similar function, using Euclidean distance, x_{1i} is the subject sentence vector, x_{2i} is the paragraph word vector.

1.2. Design of contrast loss method based on euclidean distance

In the semantic matching task, because of the matching of paragraphs and sentences, for the task of matching sentences with complex semantic environment and word meaning diversity, the general mean square error is used as the loss function. The similarity between sentences cannot be well expressed, resulting in inaccurate sentence matching. In order to solve the above problems, this paper proposes a contrast loss function based on Euclidean distance. The contrast loss is mainly used in feature extraction. After the original two samples are extracted by feature, in the feature space, the two samples are still similar, and vice versa. In this paper, the idea of the Reference [6] is improved, and a loss function integrating Euclidean distance is designed as follows:

$$L = \frac{1}{2N} \sum_{n=1}^{N} yd^2 + (1-y)\max(margin - d, 0)^2 \quad (9)$$

y is the similarity label, d^2 is the Euclidean distance,, $margin$ is the set threshold. When$y = 1$according to

the formula, the contrast loss function only leaves $\sum_{n=1}^{N} yd^2$, their Euclidean distance of the original two samples in the feature space is relatively large. It shows that the current model is not good, so it should increase the loss. However, for $y = 0$， if the Euclidean distance of the sample in the feature space is small, the corresponding loss value will become larger. In this paper, we use the Adadalta [8] gradient optimization method for feedback learning. The formula is as follows:

$$\mathrm{E}[g^2]_t = \rho \mathrm{E}[g^2]_{t-1} + (1-\rho) g_t^2 \tag{10}$$

$$\mathrm{RMS}(g_t) = \sqrt{\mathrm{E}[g^2]_t + \epsilon} \tag{11}$$

$$\Delta x_t = -\frac{\eta}{\mathrm{RMS}(g_t)} g_t \tag{12}$$

g is the similarity function， ρ is the attenuation coefficient, RMS is value， Δx_t is the attenuation coefficient after each update iteration, ϵ is the minimum value to avoid the denominator zero added， g_t is the iterative gradient.

2. EXPERIMENTAL RESULTS AND ANALYSIS

The experimental platform configuration includes Intel i5-4460 quad-core 3.4GHZ processor, 8GB memory, GTX980Ti graphics card and Ubuntu14.04 operating system, and uses TensorFlow deep learning framework based on Python programming language.

2.1. The data of experimental; thesetting of parameter setting

2.1.1. Training database and test database

In order to obtain the network training of semantic sentence matching corpus, it is needed of the segment-sentence form data of paragraphs and subject sentences [9] . Considering the format of the news data "title and content", Sohu News is used as the data set.

2.1.2. The preprocessing of data

First, the title and content of each news item used should be extracted, and remove the information that only has the title but the content is empty. Besides, it should remove the content that has no title and does not meet the data format requirements. Secondly, the jieba word segmentation tool is used to accurately extract the extracted data [10] . In the format: subject (corresponding to the news headline) \t the paragraph described in the subject matter (corresponding to the content of the news) \ t tag, artificially mark the matching result of the paragraph and the subject, 1 is similar to 0 is not similar. The title and narrative content of news must be matched, then the tag value is set to 1; for the tag value 0, the total number of news lines is divided into two parts. For the number of lines greater than fifty, the content and the title are randomly selected in the number of lines less than fifty from the front. Otherwise, the 50 numbers of the following numbers are randomly selected for matching, and finally the processed data set is divided into a training set and a test set.

2.2. Experimental results and analysis

This experiment used three different sets of data to conduct experiments and analysis and comparison, shown in Table 1.

Table 1. Comparison of three sets of data sets

Dataset	Label value 1 and 0 ratio	Number of trained data sets	Experimental results
1	1：4	15965	TOP1：50.27%
2	1：1	6386	TOP1：71.96%
3	1：1	519263	TOP1：95.12%

2.2.1. A data set with a ratio of 1 to 0 with a label value of 1:4

Data set 1: The ratio is that 1 means right and 4 means errors. That is, the data with a ratio of "1" and "0" of 1:4, and a total of 15,965 are trained. The accuracy of the experimental results is TOP1: 50.2%.

Analysis of experimental results: The reason why the accuracy after analysis is low is that the proportion of data with a tag value of "0" in the dataset is too large, which leads to the fact that the conjoined LSTM structure does not learn the semantics of paragraphs and subject description sentences well match [11] .

2.2.2. Small data with a ratio of 1 to 0 with a label value of 1:1

Data set 2: Based on the data 1, the data is improved, and the ratio is that 1 means right and 1means error. That is, the data with the label value of "1" and "0" is 1:1, and a total of 6386 pieces of data are used for training. The accuracy of the experimental results is TOP1: 71.9%.

Analysis of experimental results: The experimental results prove the correctness of the improved ideas. When the data set contains a small value of "0", the accuracy will be significantly improved [12] . However, the amount of data in this data set is too small, only 6386 pieces of data. After analysis, the reason why the current accuracy is not high is that the trained data set is too small and the concatenated LSTM structure cannot learn more semantic similarity [13] .

2.2.3. Big data with a ratio of 1 to 0 with a label value of 1:1

Data set 3: The Sohu news data is used in a one-to-one error, that is, the data with a label value of "1" and "0" is 1:1. A total of 519,263 pieces are trained, and the test data set is 510,000. The accuracy of the experimental results is TOP1: 95%.

Analysis of experimental results: This experimental result proves the correctness of the improved thinking. Experiments show that when the data set contains a small value of "0" and the data set is large enough, the concatenated LSTM structure can capture the similarity between the semantics of the paragraph and the subject description sentence. The accuracy rate will be greatly improved [14] .

2.2.4. Comparison results of three different sets of data

Through the analysis of the training results of data set 1 and data set 2, the conclusion is that when the data

set contains a large proportion of data with a label value of "0", the trained model is not satisfactory. When the proportion of data with a tag value of "0" in the data set is large, the concatenated LSTM structure does not well learn the matching of the paragraph and the subject description sentence. The Sohu News Big Data Set uses data with label values of "1 and 0" to be processed in a ratio of 1:1. The data set is divided into training data sets with 519,263 and test data sets with 510,000. The accuracy of the experiment is accurate. The rate reaches TOP1: 95%. The results show that the conjoined LSTM structure has achieved good results in dealing with natural language environment paragraphs and subject description sentence matching. The concatenated LSTM based on word embedding can well learn the potential semantic similarity between the input paragraph and the subject description sentence. This result depends on the acquisition of a large amount of data and training, so that the Siamese LSTM structure can be fully learned, and a good predictive matching result can be obtained.

3. CONCLUTION

This paper proposes an matching algorithm for natural language environments paragraph semantic. The Euclidean distance is used as a similar function to calculate the degree of matching between the paragraph and the subject sentence. The degree of calculation is also improved while obtaining the similarity. Using the contrast loss function, the network can learn the matching features between sentences during the training process, and better express the consistency of sentence pairs. The experimental results of this method on Sohu news data matching task show that the accuracy of this method is as high as 95%. Further research can extract the subtle features of sentences through deep semantic analysis techniques to improve the accuracy of sentence semantic matching.

ACKNOWLEDGMENT

The authors wish to thank Cai Xiaodong. This word was supported in part by a grant from Cai Xiaodong.

REFERENCES

[1]Liu H.Q., Zhang L.F. Analysis of Boolean Logic Retrieval Model. Modern Information, 2004, 24(9): 4-6.

[2]Zhuang X.Y. Research and implementation of Chinese text classification system based on SVM. Jilin University, 2007.

[3]Mikolov T., Sutskever I., Chen K., et al. Distributed Representations of Words and Phrases and their Compositionality. Advances in Neural Information Processing Systems, 2013, 26:3111-3119.

[4]Ning L. A Design of Cross-Language Automatic Retrieval Method Based on Semantic Extension. Modern Information, 2014, 34(1): 155-158.

[5]Zhang Expo, Liu Boai, Liu Chaoyang, et al. Document retrieval design method based on latent semantic analysis. Journal of Beijing Institute of Petrochemical Technology, 2015, 23(2): 37-42. Jonas Mueller and Aditya Thyagarajan. 2016. Siamese recurrent architectures for learning sentence similarity. In Thirtieth AAAI Conference on Artificial Intelligence.

[6]Zhou Z.H. Machine Learning: Machine learning. Tsinghua University Press, 2016.

[7]Zeiler M.D. ADADELTA: An Adaptive Learning Rate Method. Computer Science, 2012.

[8]Graves A. Supervised Sequence Labelling with Recurrent Neural Networks. Springer Berlin Heidelberg, 2012.

[9]Bjerva J., Bos J., Goot R.V.D, et al. The Meaning Factory: Formal Semantics for Recognizing Textual Entailment and Determining Semantic Similarity. SemEval-2014 Workshop. 2014.

[10]He H., Gimpel K., Lin J. Multi-Perspective Sentence Similarity Modeling with Convolutional Neural Networks. Conference on Empirical Methods in Natural Language Processing. 2015: 1576-1586.

[11]Le Q.V., Mikolov T. Distributed Representations of Sentences and Documents. 2014, 4: II-1188.

[12]Li Y., Xu L., Tian F., et al. Word embedding revisited: a new representation learning and explicit matrix factorization perspective. International Conference on Artificial Intelligence. AAAI Press, 2015: 3650-3656.

[13]Lien E., Kouylekov M. Semantic Parsing for Textual Entailment. International Conference on Parsing Technologies. 2015: 40-49.

[14]Tai, K. S., Socher, R., and Manning, C.D. Improved Semantic Representations from Tree-Structured Long Short-Term Memory Networks, 2015, ACL 1556-1566.

Research on Endowment Insurance Management System Based on BS Architecture

Jiaqi Huo[1,], Tianyu Zhang[2], Jiahao Wang[3]*
[1]Yisheng College, North China University of Science and Technology, Tangshan, Hebei, China
[2]College of Metallurgy and Energy, North China University of Science and Technology, Tangshan, Hebei, China
[3]College of Science, North China University of Science and Technology, Tangshan, Hebei, China
**E-mail: jiaqihuo@qq.com*

Abstract: This paper studies the design and test of insurance business management system based on BS framework. First, the functional requirements of customer management, contract management, insurance category management and other nonfunctional requirements such as security and system environment are analyzed. Then, on the basis of BS technology framework, to meet the needs of endowment insurance management, the system design of endowment insurance management system is realized. Finally, the white box testing method is used to test the function and performance of the pension insurance management system, and determine whether the test results are consistent with the expected results of the software.
Keywords: BS framework; Functional requirement; White box testing

1. INTRODUCTION

When the traditional endowment insurance enterprise business management, the business data are recorded on the paper, the management efficiency is low [1-3]. Design and implementation of the pension insurance business management system based on BS framework, can help the old-age insurance enterprises a better understanding of customer needs, so as to formulate the corresponding pension insurance business plan better, laid the foundation for the first to occupy the market opportunities, through the implementation of the pension insurance business management system, through the network sharing all the better the pension insurance business resources, and thus laid the foundation for collaborative work, improve work efficiency and better.

Analysis of the pension insurance business management needs in the pension insurance business management system function, need to provide the main function of customer management [2-7], contract management, category management, pension insurance pension insurance business management, customer complaint management, user management and permissions management requirements and the system safety, environment and other nonfunctional requirements, to ensure that the endowment insurance business management system can satisfy the actual demand of pension insurance business management system, management organization structure specific figure endowment insurance business management system structure diagram, shown in Figure 1.

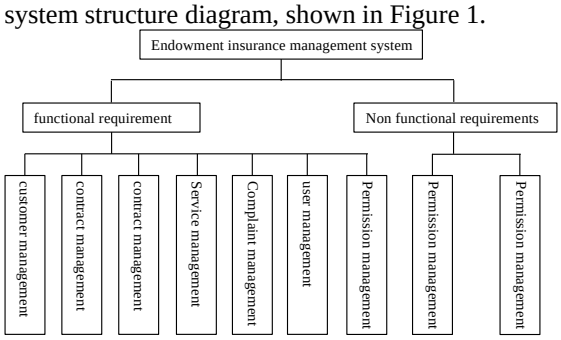

Figure 1. Organization chart of endowment insurance management system

2. DESIGN OF ENDOWMENT INSURANCE MANAGEMENT SYSTEM BASED ON BS FRAMEWORK

2.1. Logical structure

In the design and implementation of BS architecture [3] based on the insurance business management system, application framework is mainly used in the J2EE technology of Struts2, Spring and JDBC to build the system, guided by MVC, the system is divided into presentation layer, business logic layer and data access object domain, five different from the house, and then in the background data storage using SQL inch Server2005 as a data storage device. The specific technical route and implementation plan are shown in Figure 2.

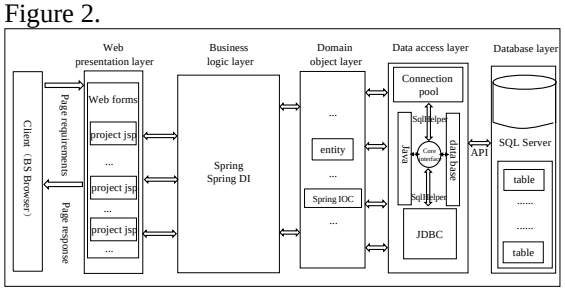

Figure 2. Insurance management system technology roadmap and implementation plan

2.2. System architecture design

Design and implementation of insurance business management system based on BS architecture, the

main purpose is to hope that through the application of the system to provide a reliable support for the insurance business management of insurance companies [4], to reduce the burden of work staff can also improve the management efficiency of the insurance business, system analysis and design from a number of different point of view, as shown in Figure 3 for the endowment insurance management system architecture design flow Figure 3.

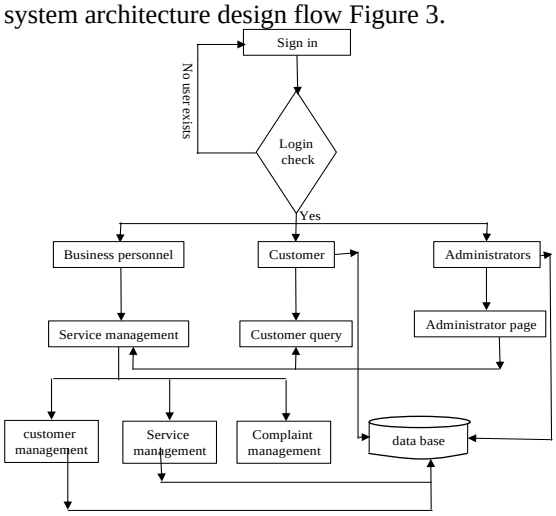

Figure 3. Framework design flow chart of insurance management system

The insurance business management system architecture design flow chart shows that in the design of the system application framework, provides the first login verification mechanism, only through legitimate users can check the login function of operation system, and when the user login through the check, the system will according to the different operating system login personnel identity permissions, and then the users can operate with different functions, and finally the insurance business management related data into the system database, when users need to extract operation through the system to provide the query interface, efficient data access.

2.3. Function module design

In the design of customer management module as an example, the main design of the customer information inquiry, customer information times, modify customer information and delete several clients add information such as different operating functions, function of the specific design of the IPO table as shown in Table 1

Table 1. IPO design of customer information management function module

System name: Endowment insurance management system	Designer: XX	
Module name: Customer information	Date: August 13, 2013	
Upper call module: customer management	Callable module: nothing	
input	Handle	output
1.Input query keywords to query customer information 2.Add new customer information 3.Modify the original customer information 4. delete the specified customer information	1.According to the query keywords by the customer, the relevant data records are searched in the database 2.The client information input interface is added to the customer information adding interface, and the database is submitted to the insurance business management database after the data 3.In modifying the customer information interface, the editor needs to modify the customer information field, and then submit the form to store the database 4.When deleting the specified customer information, the user only needs to select the deleted customer record, and click delete function to implement it	1.All customer details in accordance with customer query keywords 2.Data identification of the success or failure of adding, modifying and deleting customer information 3.According to the query key entered by the user, the relevant data records are searched in the database

2.4. Database design

The structure of insurance business management system design and Implementation Based on database design adopted E-R model entity relationship design, definition and complete the entity data through the database logic design, physical design through clear scope and value of each attribute, and then according to the loading test to complete the final design result. In the design and implementation of insurance business management system based on BS architecture, five different object entities are mainly used. The relationships among these entities can be represented by model diagrams, such as Figure 4.

2.5. System security design

Network security design [5]: the design of the system to consider the use of encryption technology, access control technology and physical verification means for the network communication equipment and the server is encrypted, for access control, prevent vandalism and very user login system, steal information through the network.

Database security design: the database is stored in data warehouse, and implementation of insurance business management system design based on architecture, mainly used as the application server data storage, and through the application of database security level for the three layer data access system provides more reliable support, installation of vulnerability scanning and anti-virus software in the corresponding the database server data backup, regularly check the corresponding, can better ensure the security of the database.

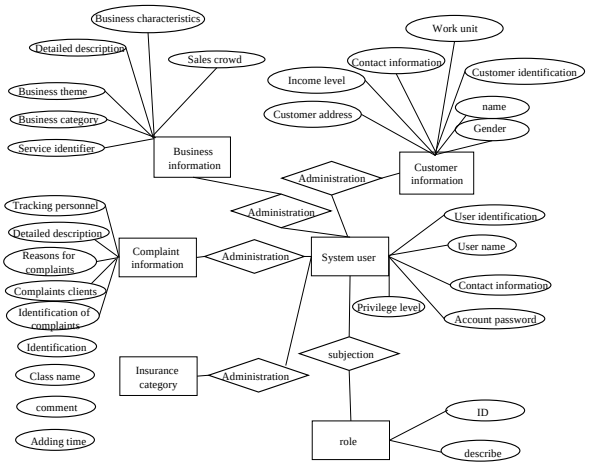

Figure 4. E-R model diagram of insurance management system database

3. TEST OF ENDOWMENT INSURANCE SYSTEM BASED ON WHITE BOX METHOD

White box testing is also called structural testing, transparent box testing, logic driven testing or code-based testing. In the test of insurance business management system based on BS architecture, white box testing is used mainly.

3.1. The basic principle of white box testing

According to the directed graph between modules, the importance of the module can be defined. The importance of a module is defined as the importance of a module.

$$im(x)=\frac{C(X)}{\sum_{x} C(X)} \quad (1)$$

In the formula, $C(X)$ is the number of paths that arrive from the top node and pass through the X[6].

The McCabe metric in the module: McCabe considers that the complexity of the program is determined by the number of loops in the control flow graph corresponding to the program, and the more the number of loops, the more complicated the program is. And the loop cardinality in the program can be given below.

Definition: the cardinality of a strongly connected graph is equal to the number of linearly independent loops in a graph, which can be calculated by formula 2

$$V(G)=e\cdot n+l \quad (2)$$

In the formula, e is the number of edges in G, N is the number of nodes in G [7].

Variable self-instance (Ad), the formula is:

$$Ad=AL-VdL \quad (3)$$

In the formula, AL is the place where the absolute variables of time and space are located, VdL is a recently defined row.

Definition: complexity of variable relation (Vm), the formula is:

$$Vm=\alpha\times Tm+\beta\times|Ad| \quad (4)$$

In the formula, Tm is aggregation deficiency, Ad is the variable self-distance

With the above definition, the calculation formula of variable metric complexity can be given now:

$$MVm=\sum Vm_i \quad \backslash \quad (5)$$

In the formula, Vm_i is the complexity of the variable relation of the i element in $Dset$.

Without considering other factors, the more complex the system is, the higher the defect density will be.

3.2. White box testing process

The endowment insurance management system based on BS as a white box, using the process tree transformation and map the unconstrained edges covering theorem combined with the proposed white box testing process model based on tree, through the cycle calculation process tree is not selected in the path contains no restriction of the number of edges are not covered, choose the best test path. Until the unconstrained edges are covered, selected to achieve the best coverage path of the white box testing. Specific procedures such as Figure 5:

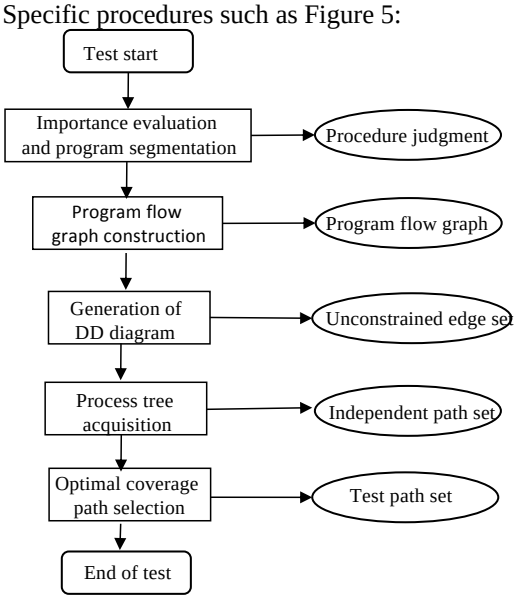

Figure 5. Test process chart

In white box testing, it is not in the software as an available internal structure of the box, the internal structure is studied logic instead of the box, to test the specific process and logic structure details, test results and determine whether the software expected results, through the white box testing method can determine the application to meet the requirements of the business management of insurance enterprise endowment insurance management system BS framework can be better based on.

4. CONCLUSION

By using the framework of BS technology combined with the application of software architecture, improve the access efficiency of data storage, but also reduce the cost of the system resource, not only improve the response efficiency of data operation, but also reduce the pressure of the server and client data processing, which laid the foundation for the improvement of system performance.

REFERENCE

[1]Liu Jie. Talking about the development of personal account information management system of basic endowment insurance. Labour World, 2001, (01): 39-40.

[2]Yu Liqun. Problems and suggestions on the overall management system of the endowment insurance for the people. Times Finance, 2008, (05):160.

[3]Liao Xu. Research on SAP development technology based on BS architecture. China Strategic Emerging Industry, 2017, (20):133-134.

[4]Si Yu. Design and implementation of endowment insurance information management system in Weifang. University of Electronic Science and technology of China, 2014.

[5]Gao Miao. Design of security architecture for tobacco enterprise information network system. Science and Technology of West China, 2010, 9(13): 30-32.

[6]Allen Haley, Stuart Zweben. Development and application of a white box approach to integration testing. Journal of Systems and Software, 2004, 4(4): 309-316.

[7]A reliability assessment tool for distributed software development environment based on java and J/Link. European Journal of Operational Research, 2006, 175(1): 435-445.

The Impact of Climate Change on National Vulnerability

*Liyan Dong[1, 2], ChenShuai Liu[1, 3], Liuye Zhang[1, 4], Aimin Yang[3, *]*
[1]Engineering Computing and Simulation Innovation Lab, North China University of Science and Technology, Tangshan 063210, Hebei, China
[2]College of Metallurgy and Energy, North China University of Science and Technology, Tangshan 063210, Hebei, China
[3]College of Science, North China University of Science and Technology, Tangshan 063210, Hebei, China
[4]College of Mechanical Engineering, North China University of Science and Technology, Tangshan 063210, Hebei, China
**E-mail: 43698059@qq.com*

Abstract: Climate change not only has effects on ecological environment, but also greatly changes humans' life style, which even, due to the weakening and collapse of social and government structures, causes the emergency of fragile states. According to the World Vulnerability Index Table, selecting Senegal to analyze the vulnerability thermal map in 2012, and get the vulnerability mutation node and mutation characteristics. Through the maximum membership function in fuzzy mathematics, define the transitional period of national vulnerability as [0.423, 0.531].
Keywords: National vulnerability; Hierarchical fuzzy evaluation; IAHP; climate change; sensitivity analysis

1. INTRODUCTION

Climate change refers to the change of climate status in a long period of time, such as climate averaging, climate change rate, etc. Its characterization properties are mainly the changes of temperature and precipitation. Changes in climate directly or indirectly change human lifestyles, increase national vulnerability and even lead to the weakening and collapse of social and governmental structures. Vulnerable countries have increased the vulnerability of a country's population to climate shocks such as natural disasters, reduced arable land, unpredictable weather and rising temperatures. Unsustainable environmental practices, immigration and resource shortages that prevail in developing countries may further exacerbate ineffective governance [1-3].

2. SIGNAL ACQUISITION

2.1. Verify the accuracy

To determining the accuracy of the model, we chose Senegal in 2012 for the fuzzy analysis. Through numerical simulations of average food production, the average freshwater person, the number of refugees in the country and total GDP in Senegal in 2012, we get a fuzzy comprehensive matrix of target levels (social, political, economic and cohesive) targeting Senegal [2].

$$A = \begin{pmatrix} 0.012 & 0.0054 & 0.5616 \\ 0.236 & 0.0321 & 0.1108 \\ 0.1290 & 0.0646 & 0.0146 \\ 0.0874 & 0.0236 & 0.0354 \end{pmatrix} \quad (1)$$

Then we use the weight vector B of the quasi-target layer to the target obtained by the AHP in the original model to carry out weight analysis on the ambiguity in the fuzzy comprehensive matrix A. Then we use MATLAB to calculate and finally determine the fuzzy vector C of Senegal's national vulnerability in 2012[3], among them,

$$C = [0.0134 \quad 0.5536 \quad 0.0321] \quad (2)$$

Finally, basing on the principle of maximum ambiguity given, it is clear that Senegal was a vulnerable country in 2012.This result is consistent with the results of the country's fragility Temperature heat picture given by the FFP. The 2012 Temperature heat picture is shown in Figure 1.

2.2. Verify fragile stability

In order to verify the stability of the model, we selected Senegal from 2000 to 2012 to carry out fuzzy analysis to conduct numerical simulation of Senegal's indicators of average grain yield, per capita fresh water volume, domestic refugees and total GDP in 2012.The first guideline layer Aim at the fuzzy comprehensive matrix of the target level (social, political, economic and cohesive).

Then we use the weight vector B of the quasi-target layer to the target obtained by AHP in the original model to carry on the weight analysis to the fuzzy degree in the fuzzy comprehensive matrix and finally get the fuzzy vector C of Senegal's national vulnerability from 2000 to 2008 [4]. We find that Senegal's assessment of 2000-2008 has been more vulnerable. Use MATLAB to draw the tendency of vulnerable membership over time.

Figure 1 shows that Senegal has been in a more vulnerable state for the period 2000-2008, and the results of our model calculations are about the same as the actual results.

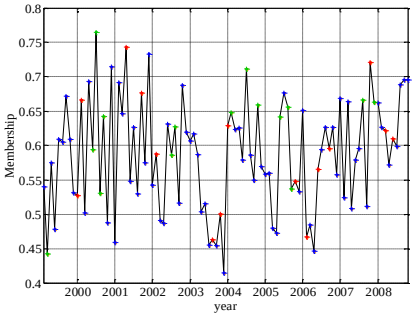

Figure 1. Vulnerable of the degree of membership

2.3. Climate change Mechanisms affecting national vulnerability [5]

The concrete process of studying the effects of climate change on countries becoming more vulnerable and finding a clear turning point in their fragile changes. We do a further analysis of Senegal. By observing its 2013 Vulnerable Country Index, it was found to be more vulnerable than in 2012. To better compare the changes in its vulnerability, we made its 2013 thermogram of vulnerability as shown in Figure 2.

To study the characteristics of climate change, we judge by comparing the average temperature in Senegal in 2012 and 2013. As shown in Figure 2.

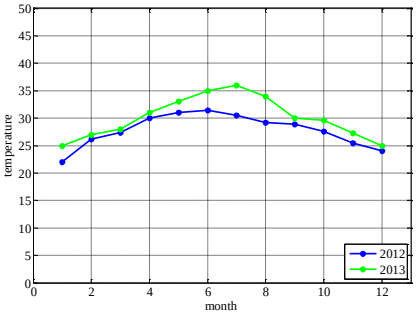

Figure 2. Comparison of temperature changes

As we can see from Figure 2, the monthly average temperature in Senegal in 2013 was significantly higher than its 2012 average monthly temperature due to the increase of global warming and the large-scale of the country between 2012 and 2013 The rate of desertification increases during the gathering of trees [6].

Then we analyze the change of temperature caused by its vulnerability index. We first judge its impact on public services. As can be seen from Figure 2, on the whole, the level of public services that the Senegalese government can provide to its people shows a downward trend in 2013. Among them, the decline trend from March to April 2013 is the most obvious. In this case, it is similar to the temperature-public service model that we established earlier [7]. The reason for the downtrend is analyzed partly by the fact that tourism, as one of the country's major economic sources, has been hit by the domestic election, leaving many tourists unwilling to choose Senegal to avoid getting involved and partly because of the government's main concern At this point of the presidential election, rather than on the basic livelihood of the people.

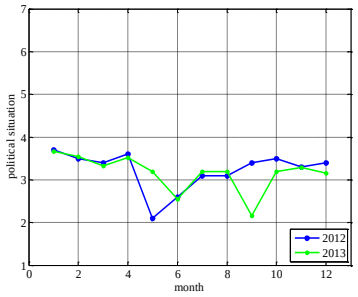

Figure 3. Comparison of public service levels

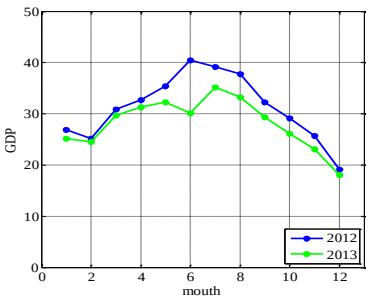

Figure 4. Monthly GDP comparison chart

Then we analyze its monthly total GDP output. As we can see in Figure 3, the overall trend of monthly GDP in 2012 and monthly GDP in 2012 is declining. Separate analysis of 2013, its GDP from February to June showed a slight upward trend, combined with the then Senegal national conditions analysis shows that its growth is due to the short-term impact of cutting trees, while in July to December due to a large number of The severe natural disasters caused by the felling of trees led to a sharp decline in its GDP. And since the temperature is now above normal temperatures, the fruits produced in the country are rapidly decaying and the sales volume has dropped dramatically [8, 9].

Next, we analyze the fresh water content. From Figure 4, we can see that the fresh water content in 2013 is also declining relative to the fresh water content in 2012. One of them is the increase of water content due to the temperature increase, which makes the national freshwater resources, the second reason is that due to the gradual decrease of rainfall caused by the rainy season, many internal rivers in the country have been cut off or dried up more severely. The third reason is that their seawater desalination capacity is relatively poor. Although their sea area is relatively vast [9], However, due to the backward purification equipment and the scale and dispersion of purification, many freshwater purification plants are facing the phenomenon of bankruptcy. Eventually leading to the domestic freshwater resources cannot meet the needs of the people in the country far. Aggravate the country's vulnerability.

Now let's analyze the grain production in Senegal. From Figure 5 and Figure 6, we can see that the

grain output of each year will first decrease and then rise. The reason is that Senegal is in the northern hemisphere and the harvest season is September and October. Therefore, almost every year Food production all showed a slight upward trend during this period. However, since its domestic food cannot be self-sufficient, it is generally analyzed that it needs to maintain its basic livelihood by importing food. On the other hand, through the above analysis, we know that the fresh water content is decreasing year by year, while the temperature is rising. Both of these basic factors have a large impact on food production. In the meantime, given the large share of agricultural population in Senegal, as temperatures rise, countries that are already fragile in the case of freshwater have become more vulnerable.

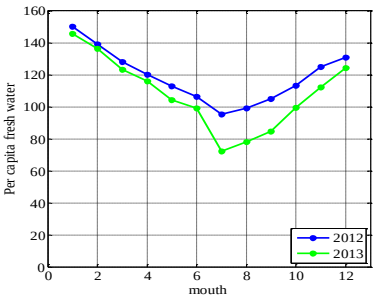

Figure 5. Freshwater content comparison chart

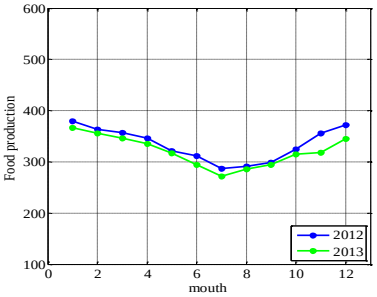

Figure 6. Comparison of food production

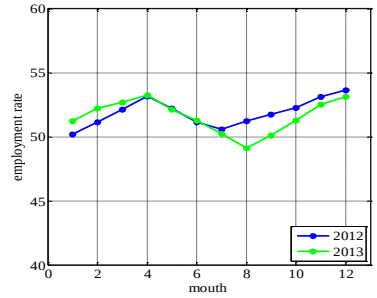

Figure 7. Comparison of employment rates

Then we analyze again the employment rate in Senegalese. By comparison (Figure 7), during January to April, the employment rate in 2013 was significantly higher than the 2012 employment rate, and employment in 2013 after April Gradually lower than the 2012 rate of employment. In April 2013, the number of refugees in Senegal apparently started to rise, partly because of frequent domestic unrest and, on the other hand, famine that led many families to leave their homes. The comparison of the number of refugees is shown in Figure 8.

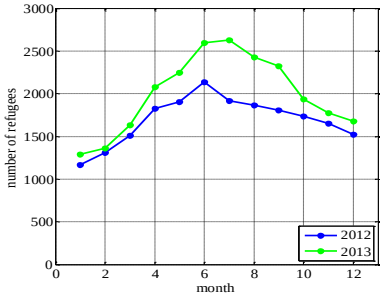

Figure 8. Comparisons of Refugees

Finally, we analyze the two factors of energy and politics. Comparing Figure 9 and Figure 10, we can see that in terms of energy use, the utilization of energy resources in China increased from 2013 to 2012 and showed an overall upward trend. In political terms, high-frequency demonstrations took place in Senegalese in 2012 and 2013.

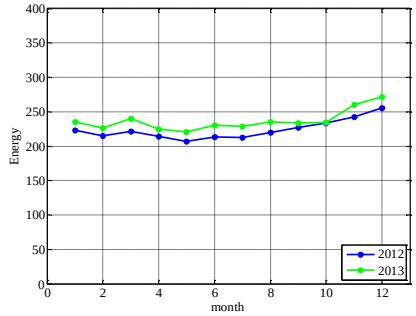

Figure 9. Energy use comparison chart

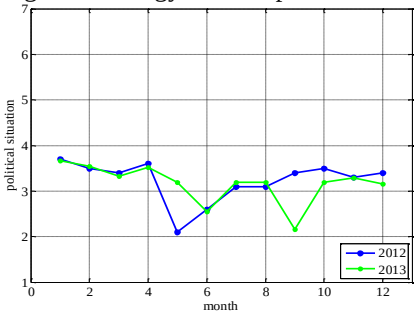

Figure 10. Political situation comparison chart

According to the changing trends of the indicators in the Yemeni countries at the level of one year, it can be seen that in the process of crossing to the vulnerable countries, they are affected by various indicators. Therefore, interventions should be taken to minimize the impact of natural conditions Under, the span is the country of vulnerability.

Because of the Senegalese mutation from 2012 to 2013, the national vulnerability range can be determined by using the maximum membership function in fuzzy mathematics to define the country's stable state range [0, 0.423] and the country in the more vulnerable state range Is [0.423, 0.531], the country is in a fragile state interval [0.531, 1].Therefore, the turning point of the

national vulnerability from stability to vulnerability is [0.423, 0.531].

REFERENCES

[1]Krakowka, A.R., Heimel, N., and Galgano, F. Modeling Environmenal Security in Sub-Sharan Africa – ProQuest. The Geographical Bulletin, 2012, 53(1): 21-38.

[2]Schwartz, P. and Randall, D. An Abrupt Climate Change Scenario and Its Implications for United States National Security, October 2003.

[3]Nick Brooks and W. Neil Adger. Country level risk measures of climate-related natural disasters and implications for adaptation to climate change", January 2003:4-9

[4]Li Zhong Han, Jin Quan Zhang, Yun Yang. Comprehensive Fuzzy Assessment on the Life-Cycle Environment Impact of Bridges. Applied Mechanics and Materials, 2014, 3013(522).

[5]Theisen, O.M., Gleditsch, N.P., and Buhaug, H. Is climate change a driver of armed conflict Climate Change, 2013, 117 (3): 613-625.

[6]M. Stiehm, M. Brede, D. Quosdorf, H. Martin, A. Leder. A Sensitivity Analysis of Stent Design Parameters using CFD. Biomedical Engineering / Biomedizinische Technik, 2013.

[7]Sulaimon Olanrewaju Adebiyi, Emmanuel Olateju Oyatoye, Owolabi Lateef Kuye. An Analytic Hierarchy Process Analysis: Application to Subscriber Retention Decisions in the Nigerian Mobile Telecommunications. International Journal of Management and Economics, 2015, 48(1).

[8]Luyuan Chen, Xinyi Zhou, Fuyuan Xiao, Yong Deng, Sankaran Mahadevan. Evidential Analytic Hierarchy Process Dependence Assessment Methodology in Human Reliability Analysis. Nuclear Engineering and Technology, 2017, 49(1).

[9]Marie Ivanco, Gene Hou, Jennifer Michaeli. Sensitivity analysis method to address user disparities in the analytic hierarchy process. Expert Systems with Applications, 2017, 90.

Environmental Cost Assessment Based on Invest Model Optimization

Yashuai An[1], Shuai Wang[2], Yuliang Guo[2,]*
[1] Hebei University of Engineering, Handan City 056000, Hebei, China
[2] College of Science and Letters, Hebei University of Engineering, Handan 056000, Hebei, China
**Email: 2472801760@qq.com*

Abstract: Based on the InVEST model, we firstly propose the impact factors of the ecosystem service system, namely land use change, vegetation damage, soil erosion and biodiversity. And we establish the criteria for economic loss to measure the impact of each factor on ecosystem services. And then we obtain the weights of each factor to perform logistic regression analysis. Secondly, we use the LELAM model to monetize the economic loss assessment factor and obtain the actual environmental costs. Based on the real benefit of the land use project = project benefit - environmental cost model, we conduct a comprehensive assessment for the true cost of the land use project. Secondly, based on the model established above, we carry out cost assessment for specific examples. Example 1: Estimating the environmental cost of a section of highway construction. First, according to the economic loss standard, we determine the weight of the economic loss assessment factor, bring the data into the ecosystem service evaluation model and obtain the environmental cost of 2, 0205, 600 Dollar for the two years; Example 2: We perform an environmental cost assessment for all land use projects in Sichuan Province for 10 Dollar. The model seeks the final environmental cost of 300 billion Dollar. Finally, based on the genetic algorithm, we optimize the above model to obtain the real benefits of the two examples of land use projects are 1.065 billion yuan and 11.365 trillion Dollar, respectively. By the query data, we conclude that the error is less than 4% to verify the effectiveness of the model.

Keywords: Environmental cost; InVEST model; Logistic regression; LELAM model; Genetic optimization

1. INTRODUCTION

Classical economic theories often ignore the impact of their decisions on the biosphere or assume unlimited resources or capabilities to meet the needs of their economic construction, and even pursue economic construction as a result of environmental damage. The current environmental situation is grim. The biosphere provides many natural conditions for human life to maintain a healthy and sustainable environment, which is called ecosystem services. However, whenever humans change ecosystems, we may limit or remove ecosystem services. As they accumulate, they will directly affect biodiversity and cause environmental degradation, which in turn will result in environmental costs.

In recent years, with the deepening of sustainable development research, it is increasingly recognized that human sustainable development must be based on the protection of the Earth's life support system to maintain the sustainability of the biosphere and maintain the sustainability of ecosystem services. The sustainable development of human society depends fundamentally on the sustainability of ecosystems and their services. Therefore, it is necessary to study the economic value of ecosystem services and incorporate them into the economic accounting system of land use projects in order to promote rational decision-making of natural capital development, avoid short-term economic behaviors that damage ecosystem services, and contribute to the protection of ecosystems. Ultimately, it is conducive to the sustainable development of human beings themselves. The theory and method of quantitative evaluation of ecosystem services and economic value of natural capital have become an important content and focus of sustainable development assessment research at home and abroad. Become the frontier of environmental economics and ecological economics research in current ecology and resource economics [1-5].

2. MODEL ESTABLISHMENT AND SOLUTION

2.1. Model establishment

2.1.1 Identification and screening of environmental impact economic loss assessment factors

We need to establish an environmental impact economic loss assessment model. First, we need to identify and predict environmental impact factors. Project environmental impact factor screening is a reasonable ranking of environmental impact factors.

Evaluate project selection

From the current situation of global environmental assessment, different projects have different degrees of environmental economic losses. Therefore, when we do environmental economic loss assessment, we must first screen the project. We divide the project into four categories, as Table 1:

In summary, first determine the area where the project construction may have an impact based on the boundary of the assessment scope. According to the requirements of assessment depth and breadth, further determine the scope of economic impact assessment

of environmental impact in the target area.

Table 1. Classification of land development projects

Project type	Environmental impact characteristics	Assessment requirements
S1 classes	little or no effect on external environment and economic loss	No separate environmental and economic loss assessment is required
S2 classes	Produce favorable and adverse effect to loss of external environment economy	A brief assessment of environmental and economic losses shall not be taken as the focus of the assessment
S3 classes	Beneficial impact on the external environment and economy	Detailed assessment of their environmental and economic losses
S4 classes	Have serious adverse effect on external economic loss, or have considerable number of immigration projects	Detailed assessment of environmental economic losses is the focus of ecological assessment model

Determination of Environmental Impact Economic Loss Assessment Factors.

We introduce the InVEST model. (Integrated Valuation of Ecosystem Services and Trade-offs) referred to as InVEST, which is for our effective natural resource management and decision making. The InVEST model can quantify ecosystem service functions and present them in the form of graphs, which are ideal for analyzing ecosystem services and land use change factors. The InVEST model is used to help land-use project planners and managers provide a means of assessing the value of multiple natural resources [3-10].

The InVEST model is used to assess the value of multiple ecosystem services across the globe, and we use scenario analysis to predict the evolution of ecosystem service function values over time.

We use the InVEST model to quantitatively estimate ecosystem services for each differentiated region.

The design of InVEST is divided into 4 levels: 0 layer, 1 layer, 2 layers and 3 layers.

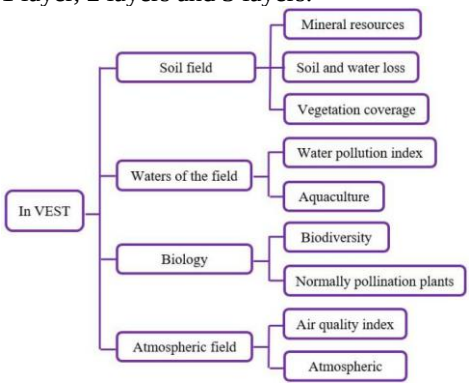

Figure 1. InVEST structure factor analysis diagram

We can predict and estimate the degree of land development based on specific projects in the real world. Through our research, we can use the InVEST model to quantify various ecosystem service functions such as biodiversity, air quality damage, plant crop pollination, loss of soil resources, and water purification.

We make reasonable improvements to make it suitable for a variety of ecosystem service function assessment modules. It mainly includes four modules: biological, water, soil and air. In each module, we separately perform factor analysis of the evaluation project, as shown Figure 1.

Based on the above InVEST model, we have established the following environmental economic loss assessment system. Environmental economic loss assessment is a quantification of the status quo and impact of environmental quality damage, using monetization technology to assess the economic losses caused by environmental impacts, and to serve project construction decision-making and regional social development assessment services.

Analysis of Environmental Impact Economic Loss Assessment Factors

Different types of land use space allocation

Based on our above model we derive the weights of the various environmental cost impact factors:

Based on the proportion of each impact factor, we use Logistic regression to further estimate the analysis of spatial land conversion, and estimate the ecological environment cost under the land project.

With different types and scenarios of land use spatial allocation, we use the optimized InVEST model and carry out monetization processing. The ecological assessment model we established is affected by different driving factors in the spatial distribution position. It includes two major categories: natural environment elements and socio-economic factors. We conduct a comprehensive assessment based on the factors affecting land use change in global projects. We choose soil organic matter content, annual precipitation, and air quality index as natural driving factors; per capita GDP and population density as social and economic drivers. We use the above factors to conduct logistic regression analysis of the probability of land use space conversion. Logistic regression is used to calculate the probability of the project's damage to the ecological environment:

$$\log(\frac{p_i}{1-p_i}) = \beta_0 + \beta_1 X_{1i} + \beta_2 X_{2i} + \ldots + \beta_n X_{ni} \quad (1)$$

Logistic regression was performed on the probability of occurrence of the six types of land use types and the respective driving factors. We use the stepwise regression method to estimate the environmental cost, and automatically remove the weaker driving factors in the model. The resulting regression coefficient

is the probability of the space conversion of the land use type. In the calculation of the fit of the logistic regression, we use the ROC method to test. When the ROC value is between 0.5 and 1.0, the probability distribution of the regression result is consistent with the real distribution.

We imported the searched data into SPSS for logistic regression analysis. The final regression results and ROC test are shown in Table 1. The weak influence factors for each type of land use type logistic regression are also different. We performed specific clustering in the modeling process. Based on logistic regression analysis and ROC testing, we summarize the ROC test values for each factor in different land types. As shown in the table below.

Through logistic regression, we derive the weight of the impact of land development projects on various types of land.

Establishment of Indicator System

In the assessment of environmental economic losses, the key is to determine the content and scope of its assessment. Based on the classification of environmental economic evaluation projects, we selected a land use plan for Sichuan Province as a large-scale national project. According to the natural ecological environment impact characteristics and environmental economic loss assessment conditions and requirements of Sichuan Province's land use planning, we have divided the Sichuan Province land planning environmental economic loss assessment system into three levels [3], as shown Figure 2.

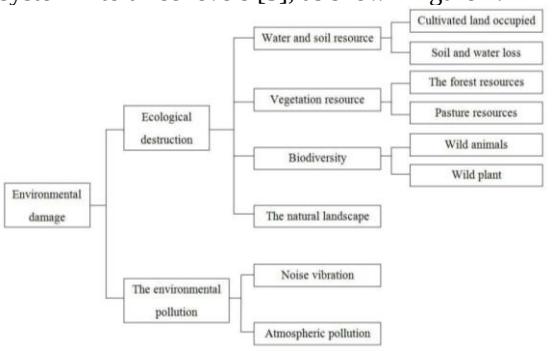

Figure 2. Sichuan Province land use planning environmental impact economic loss assessment system

Establishment of an Evaluation Procedure

We need to conduct an environmental economic loss assessment, and we should study the resources, environment and socio-economic profile of the region in which the assessment is conducted.

The focus is on assessing the impact of environmental damage on the resources, social, and cultural and economic development of the region. Focus on analyzing the adverse changes caused by the assessment.

By establishing an indicator system for analysis and evaluation, we analyze and classify the evaluation indicators, determine the indicator parameters and evaluation methods for each indicator, and monetary ally estimate the economic losses caused by each indicator, and finally calculate through comprehensive calculation. Estimate the economic loss caused by the environmental damage of the assessment object.

Based on the above-mentioned established land use planning environmental economic loss assessment indicators in Sichuan Province, by determining the indicator parameters and evaluation methods that are appropriate for each indicator, Monetization valuation of various economic losses caused by the negative environmental impacts caused by it. Finally, through comprehensive calculation, the economic loss value caused by the environmental damage of land use planning in Sichuan Province is obtained and incorporated into the economic evaluation of the project.

2.2. Assessment of economic loss of ecological damage to land resources

2.2.1. Land resource destruction economic loss composition

In the land use, there is an ecological loss of land occupation, the land use mode has changed, and the land value has been lost. This part of the value loss is called environmental loss and effective ecological loss. After the transformation of land use mode, the ecosystem services of the land disappeared. This is called environmental loss, and the economic and social benefits of land are lost. This is called effective ecological loss.

In the process of constructing the project land, another part of the land is ecologically lost. This part of the ecological loss is environmental damage. Occupation of land in land use, ecosystem services of land resources do not exist, and the ecological service function of land resources is lost. There is also a recovery fee. The composition of the economic loss of land resource ecological damage is shown in Figure 3.

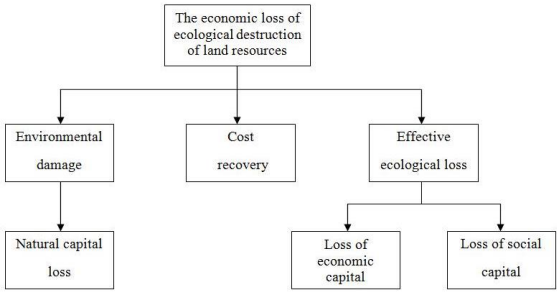

Figure 3. Composition of economic loss of land resource ecological damage

2.2.2. Calculation of economic losses caused by land resources destruction land resource damage economic loss calculation

Based on the above analysis, we can conclude that the effective ecological loss of land use resources (leaves) in land use is equal to the sum of economic capital losses and social capital losses of land resources.

$$Y_e = -(K+S) = -[\sum_{j=i}^{m} Z_j K_e(j) + \sum_{j=i}^{m} Z_j S_e(j)](2)$$

Note: Negative sign indicates loss,in the formula:Zj is the area occupied by the j-th land type for a certain type of construction project; Ke(j)is the unit value of the economic capital of the jth class ecosystem; Se(j)is the unit value of the social capital of the jth class land ecosystem.

The environmental loss of land resources occupied by a certain type of construction project in land use is equal to the loss of natural capital of land resources.

$$-N_e = -[\sum_{j=1}^{m} Z_j N_e(j)](3)$$

In the formula: Ne(j) is the unit value of the natural capital of the j-type land ecosystem; Zj is the same as above.

The land occupied by the construction project is basically occupied permanently, so it is necessary to reopen a piece of land to compensate the occupied land. The cost of restoration involved here includes the cost of occupying another land, the cost of soil improvement, replanting, fertilization, watering, de-worming, cultivation, fire prevention and management. The recovery cost of land resources occupied by a certain type of construction project in land use (indicated by De).

$$D_e = \sum_{j=1}^{m} D(j) Z_j (4)$$

In the formula: D(j)is the unit land restoration cost of the category j land ecosystem; Zj is the same as above.

The total ecological loss He of the land occupied by a certain type of construction project is equal to the sum of the effective ecological loss, environmental loss and recovery cost of the land.

$$H_e = (-N_e) + D_e + Y_e = (-K) + (-S) + (-N_e) - D_e (5)$$

$$H_e = -\sum_{j=1}^{m} Z_j K_e(j) - \sum_{j=1}^{m} Z_j S_e(j) - \sum_{j=1}^{m} Z_j N_e(j) - \sum_{j=1}^{m} Z_j D\ (j)(6)$$

$$= \sum_{j=1}^{m} \{-Z_j K_e(j) + [-Z_j S_e(j)] + [-Z_j N_e(j)] - Z_j D(j)\}(7)$$

The negative sign is removed, and only the numerical value indicates the amount of ecological loss, so the above formula becomes:

$$H_e = \sum_{j=1}^{m} \{Z_j K_e(j) + Z_j S_e(j) + Z_j N_e(j) + Z_j D(j)\}(8)$$

$$\sum_{I=1}^{N} X_I(j) = Z_j K_e(j) + Z_j S_e(j) + Z_j N_e(j) + Z_j D(j)(9)$$

In the formula: A indicates the types of ecological losses caused by occupation of land resources in land use, namely economic capital loss, social capital loss, natural capital loss, and recovery costs.

2.2.3. Building a LELAM model

The land ecological loss assessment (LELAM) model is an ecological damage economic loss assessment model that occupies land use land resources [6].

Assume that in the land, the ecological loss of a certain type of construction project land at a certain point is composed of the ecological loss of m land types, then the ecological loss hI of the first part of the m land type is:

$$h_I = X_I(1) + X_I(2) + ... + X_I(j) + X_I(m)(10)$$

In the formula: hI is the ecological loss of Part I of m land types; XI(j) is the ecological loss of Part A of j species;I=1, 2 , …, N, j=l, 2, …, m.

At a certain point in time, the total ecological loss He of the M land types is:

$$H_e = \sum_{I=1}^{N} h_I = \sum_{I=1}^{N} \sum_{j=1}^{m} X_I(j)(11)$$

$$So, H_e = \sum_{I=1}^{N} X_I(1) + \sum_{I=1}^{N} X_I(2) + ... + \sum_{I=1}^{N} X_I(m)(12)$$

2.3. Model solution

The model is solved by an example. We do case studies by using the eco-efficiency costs of land use development projects in Sichuan Province.

2.3.1. Natural environment and socio-economic generalization

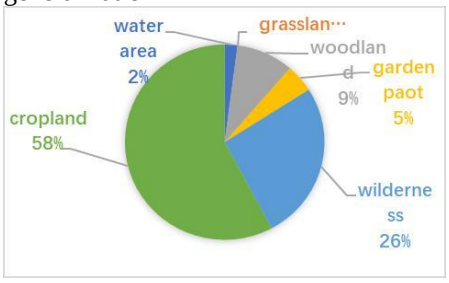

Figure 4. Land use project change rate after 2001

The natural characteristics of Sichuan Province are diverse, and basically include various ecological service functions around the world. It is conducive to the rationalization of the model of the environmental degradation cost of global land development.

The topography and geomorphology form the characteristics of gully vertical and horizontal and various types of landforms. There are many kinds of soils in Sichuan Province, and the distribution is complex, mainly purple soil, followed by yellow soil; Wanzhou District is a subtropical monsoon humid zone with four distinct climates. The average annual temperature is 17.7 °C, and the highest annual average temperature is 19.0 °C. 1243 mm [8].

The rate of change of land use projects after 2001 is shown in Figure 4.

2.3.2. Evaluation of land use conversion in Sichuan province using remote sensing technology

Economic loss assessment of occupational land ecological damage in the process of urbanization in

Sichuan Province.

We use TM data and OLI remote sensing images for data analysis to study the impact of land use projects in the Sichuan region on landscape class flowers. When selecting the influence of remote sensing, in order to avoid the influence of disturbance factors such as seasonal factors and clouds. When selecting remote sensing areas, we should select the remote sensing data with good vegetation growth in June 2010 and January 2019. Remote sensing images are shown in Figures 5-6.

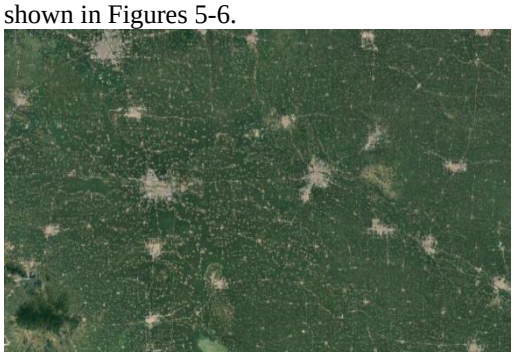

Figure 5. Schematic diagram of Sichuan remote sensing in 2010

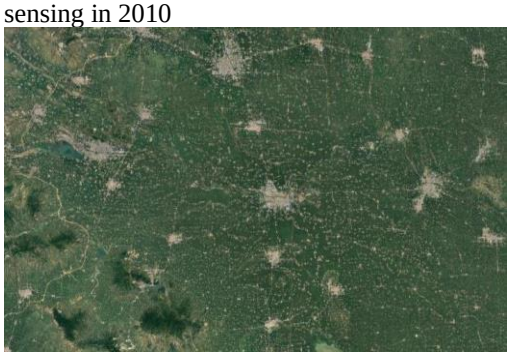

Figure 6. Schematic diagram of Sichuan remote sensing in 2019

The above picture shows the remote sensing images of Sichuan Province in 2010 and 2019. By comparison, it has been found that its topography, waters and vegetation have undergone tremendous changes. First, the land use increased from 10.21% to 60.87%; the coverage of forest grassland decreased from 50.634% to 13.231%; the waters changed little but the water content decreased by nearly 50%. Among them, urban planning, roads and railways are the main land use projects. By searching for the use of land resources for two years, they are substituted into the ecosystem service evaluation model to obtain environmental costs for two years.

We have occupied 724, 737 mu of various types of land in the process of urbanization in Sichuan Province from 2010 to 2019. The most occupied land is cultivated land, accounting for 57.81% of the total land area, followed by occupation of unused land. 26.22% of the area, as shown in Figure 4. In 2010, the urbanization of Sichuan Province has expanded on a large scale, and the urban area has increased by 306.6 square kilometers. It has established a large-scale development in the form of encroaching on a large amount of cultivated land.

Sichuan's total environmental losses are recorded as N=496 million US dollars

Sichuan's total environmental losses are recorded as N=496 million US dollars

N □ N1 □ N 2 □ N3 □ 2.8489 □ 0.8612 □ 0.706 □ 4.396(One hundred million U.S. dollars)

The total effective ecological loss in Sichuan Province is recorded as

Y=3.30599.2 (billion USD)

Y □ Y1 □ Y2 □ Y3 □ 1.78023 □ 0.71546 □ 0.81023 □ 3.30592(billion USD)

The total ecosystem restoration cost of Sichuan Province is recorded as

D=1.32077 billion US dollars

D □ D1 □ D2 □ D3 □ 0.70626 □ 0.28504 □ 0.3294 □1.32077 (billion USD)

(One hundred million U.S. dollars) (One hundred million U.S. dollars)

2.4. Model role analysis

Firstly, the ecological service system evaluation model we established has effectively solved the problem of estimating the value of environmental costs. When planning the land use project, we bring the data into the model pair by predicting the area and type of land resource utilization. The environmental cost of the project is estimated. Then based on the real benefit of the land use project = project benefit - environmental cost model, we can get the real project benefit. Through our query of the network data, we found that if the environmental cost exceeds 3% of the total cost, the environmental cost of the project is too high. And the impact on the environment is too large.

3. CONCLUSION

Therefore, when planning the project, the land use project planner can use our model to evaluate the actual benefits of the project, and then improve the plan according to the proportion of environmental cost to reduce the environmental cost and reduce the impact of the project on the environment. For the management personnel, the company's projects and plans can be properly arranged according to the environmental costs, and the direction of the company can be controlled more rationally to avoid project risks.

REFERENCES

[1]Liu Zifeng. The economic loss caused by land occupation in Liu Zifeng's urbanization process. Chongqing University, 2003.

[2]Liu Gengyuan, Yang Qing. Ecosystem Service Value Non-monetary Quantity Accoun ting: Theoretical Framework and Methodology. China Environmental Management, 2018, 10 (04): 10-20.

[3]Xu Lingyun, Ding Ling. Water quality risk assessment of the Heishui River Basin based on the INVEST model. Pearl River, 2019, (01): 146-152.

[4]Yuan Xianqiang. Dynamic change of land use

landscape pattern and ecological envi ronment assessment in Yingkou City based on remote sensing. Liaoning Normal University, 2017.
[5]Su Qing. Railway Green Line Selection Environmental Impact Economic Impact Asses sment. Central South University, 2009.
[6]Costanza R. the Value of the Worlds Ecosystem Service sand Natural Capital. Nat ure. 1997, 387: 253-260
[7]Dai Yongli, Shi Dezhen. Research on road environment cost monetization model. Environmental Science, 2012, 38 (02): 69-72.
[8]Yang Yuanyuan, De Wei, Fu Hua. Research framework for ecosystem service function value evaluation based on InVEST model. Journal of Capital Normal University (Natural Science Edition), 2012, 33(03): 41-47.
[9]Qi Wei. Comprehensive evaluation of township ecological environment based on CPS GA-BP neural network. Nanjing Normal University, 2016.
[10]Zhang Zhiqiang, Xu Zhongmin, Cheng Guodong. Evaluation of ecosystem service value and natural capital value. Journal of Ecology, 2001, (11): 1918-1926.

Change-E-III Soft Landing Track Design and Control Strategy

Yu Bi[1,2], Hanying Li[1], Ruishan Li[1,], Aimin Yang[3]*
[1] Mathematical Modeling Innovation Lab, North China University of Science and Technology, Tangshan 063210, Hebei, China
[2] North China University of Science and Technology, Tangshan 063210, Hebei, China
[3] College of Science, North China University of Science and Technology, Tangshan 063210, Hebei, China
**E-mail: 1002533393@qq.com*

Abstract: The moon is the closest celestial body to the earth. Chang 'E III launched by China has successfully achieved a soft landing on the surface of the moon. How to achieve a soft landing has become the focus of attention. First, according to Kepler's law, the speed relationship between the nearest moon and the far moon point is obtained, and the process of Chang 'E III from the far moon point to the near moon point is analyzed. The speed is obtained from the law of mechanical energy conservation. Finally, the space spherical coordinate system of the moon is established, and the position in the lunar fixed coordinate system is obtained by combining the number of orbital roots. The position of the recent moon point can be obtained by the transformation of the coordinate system(*19.51°W, 43.82°N*), and the altitude is 15km., The location of the far moon is(*160.49°E, 43.82°S*) and the altitude is 100km. A lunar inertial coordinate system is established. For the plane of landing trajectory, the trajectory equation is obtained by fitting the landing orbit at the deceleration stage as a standard parabola. Since the control law is the same, the main deceleration section is used to replace the fast adjustment phase. The elevation map of the rough obstacle avoidance and fine obstacle avoidance section was used to obtain the best safe landing site. During the slow speed drop phase, do uniform deceleration until the speed is reduced to zero. For the optimal control strategy, the state equation of soft-landing orbit is simplified, then the terminal constraints of soft-landing orbit are dealt with by the multiplication sub method, the joint choke gradient method and the constraint operator are introduced to optimize the iterative solution of soft-landing orbit. For error analysis, because the shape of the moon is 1/963.7256, the moon is approximated as a circular sphere. In the lunar fixed coordinate system, the radius of the moon is uniformly used as the average radius; When the Chang 'E III detector flies around the moon, Chang' E III moves in the gravitational field in the center of the moon, ignoring various photodynamic factors; The various types of speeds sought are all relative speeds. The scope is limited to the two-body system category, regardless of whether the detector orbits with the moon. Then the sensitivity analysis is carried out, the parameters in the model are analyzed one by one, and the changes in a certain range are simulated and the results are compared.

Keywords: kepler's law; orbital optimization; image processing; multiplication

1. INTRODUCTION

Chang 'E III successfully launched and reached the lunar orbit. The mass of Chang 'E III is 2.4 T, and the main deceleration engine can produce adjustable thrust from 1500N to 7500N, and the specific impulse is 2940m/s, which satisfies the control requirements for speed adjustment. The four sides are equipped with small attitude adjustment engines. After the thrust direction is given, various attitude adjustment controls can be automatically implemented. The scheduled landing point of Chang 'E III in Hongwan District is 19.51 W, 44.12 N, and the altitude is -2641m. In the case of high-speed flight, Chang 'E III must ensure the accurate realization of a soft landing in the scheduled area of the moon [1-4]. The focus is on designing a landing orbit and an optimal control strategy. For the landing track design, the basic requirements are the following three points: the landing preparation track is 15km in the near month and 100km in the far month; From the landing orbit from the recent month to the landing point, the soft landing process can be divided into six stages, and the state of each stage at the key point should be satisfied [5-7]. And the fuel consumption during the soft-landing process is minimized.

2. THE POSITION OF THE NEAREST AND DISTANT MOON AND THE CORRESPONDING SPEED

According to Kepler's second law, the product of the rate of Chang 'E III at a certain point and the distance from that point to the center of the moon is a fixed value. When the longitude is one degree, the actual ground distance is: $2\pi R_c / 360$ .When the Latitude is one degree, the actual ground distance is: $\pi R_j / 90$.

2.1. Recent Moon, Far Moon Speed

According to Kepler's second law and the law of mechanical energy conservation:

$$V_A^2 = \frac{2GMR_B}{R_A(R_B + R_A)} \tag{1}$$

It is known that the distance from the moon to the surface of the moon is R_1 = 15km, the distance from the far moon to the surface of the moon is R_2 = 100km, and the average radius of the moon is R= 1737.013 km, so there is: $R_A = R_1 + R$, $R_B = R_2 + R$, Substituting to formula(1) yields: $V_A = 1.6925 km/s$, Similarly, the far month speed can be: $V_B = 1.6529 km/s$. The speed direction of Chang 'E III at the near and far moon points is along the track tangent direction.

2.2. Location of Recent and Distant Months

The spherical surface of three-dimensional space can be used to define the space spherical coordinate system on the moon, describing the position of the near and far moon points and the position of the satellite on the moon. Show in Figure 1.

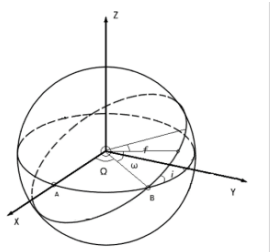

Figure 1. Space spherical coordinate system of the Moon

By Kaipulefangcheng:

$$E = M_1 + e\sin E \tag{2}$$

$$M_1 = n(1-t) \tag{3}$$

Find the relationship between *E* and *f*:

$$r_0 = a(1-e\cos E) \tag{4}$$

$$f = \cos^{-1}\left[\frac{1-\frac{a(1-e^2)}{r_0}}{e}\right] \tag{5}$$

From the coordinates of the satellite in the elliptical orbital plane, the coordinates of the satellite in the space spherical coordinate system of the moon can be obtained.

$$n^2 a^3 = \mu \tag{6}$$

It is known that the T moment satellite is near the moon, and the formula(3) can be used to find the time of the satellite at the recent month M_0.

From formulas(4) and(5) can be derived:

$$\begin{cases} x' = a(\cos E - e) \\ y' = a\sqrt{1-e^2}\sin E \end{cases} \tag{7}$$

Assuming that Chang 'E III moves in the gravitational field in the center of the moon and ignores various photodynamic factors, the moon is regarded as a circular sphere at this time. Then the position of Chang' E III in the lunar fixed coordinate system is:

$$\begin{bmatrix} x \\ y \\ z \end{bmatrix} = \frac{a(1-e^2)}{1+e\cos f}\begin{bmatrix} \cos\Omega\cos(\omega+f)-\sin\Omega\sin(\omega+f)\cos i \\ \sin\Omega\cos(\omega+f)+\cos\Omega\sin(\omega+f)\cos i \\ \sin(\omega+f)\sin i \end{bmatrix} \tag{8}$$

In the calculation of Chang 'E III elliptical orbit, this article introduces a kind of *Walker* [1]. It is proposed to eliminate singular improved orbital roots. The number of orbital roots in this group will only produce singularity when the orbital angle *i=180°*, but the probability of occurrence in the Chang 'E III transfer orbit can be ignored. Its basic form is:

$$p = a(1-e^2) \tag{9}$$

$$f = e\cos(\omega+\Omega) \tag{10}$$

When Chang 'E III is at the point of the month, the number of orbital roots is: *i=90°*, the right ascension of the ascending node B *=353.9°*, M_1*=0°*, *f=0*, *Ω=37.9°*, *ω=52.1°*

The position of Chang 'E III in the fixed coordinate system is:

$$\begin{cases} x = 1.0358e+06 \\ y = 1.3480e+06 \\ z = 1.7520e+06 \end{cases}$$

From the definition of the latitude and longitude of the moon, it can be found that the position of the recent moon point is(*19.51°W,43.82°N*), the altitude is 15km, and the same is found: the location of the far moon point is(*160.49°E,43.82°S*), elevation is 100km.

3. EXPRESSION AND OPTIMAL CONTROL STRATEGY OF LANDING ORBIT

The plane of landing trajectory is taken out separately as the $x'oy'$ coordinate system. The landing orbit of the main deceleration stage can be fitted as part of the standard parabola, and the expression of its running trajectory can be considered.

From the near monthly point coordinates (15,0) and the end point coordinates (37,3) of the main deceleration phase, the expression of the winner's deceleration phase landing orbit is:

$$x^2 = -19.67y + 15 \tag{11}$$

3.1. Landing Prep Track

At this stage, the main engine of Chang 'E III was shut down and was affected by the gravity of the moon and flew in an elliptical orbit.

3.2. Establishment of Soft-Landing Dynamics Model for Landing Orbit in Main Deceleration Stage

At this stage, the parabola was reduced from 15km in recent months to 3km from the lunar surface, and the relative speed dropped from 1.7 km/s to 57m/s.

The inertial coordinate system of the lunar center and the Chang 'E III orbital coordinate system are established, as shown in Figures 2-3, respectively.

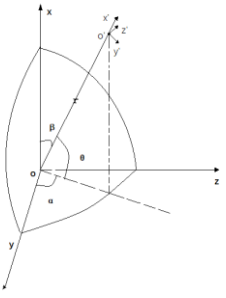

Figure 2. Moon surface inertial coordinate system

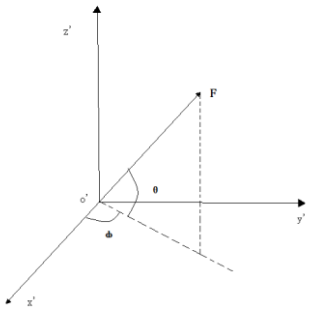

Figure 3. Chang 'E 3 orbital coordinate system

Influential factors such as non-ball items of lunar gravity, solar and lunar gravitational perturbation, etc. can be ignored [4] and at the same time, the influence of Coriolis force and traction caused by the rotation of the moon can also be ignored[5] And A soft landing mass cardio dynamics equation is established for the main deceleration section:

$$\begin{cases} \dot{u} = \dfrac{F}{m}\cos\theta\cos\varphi - \dfrac{uv}{r} + \dfrac{v^2}{r\tan\beta} \\ \dot{v} = \dfrac{F}{m}\cos\Theta\cos\varphi - \dfrac{vw}{r} - \dfrac{uv}{r\tan\beta} \\ \dot{w} = \dfrac{F}{m}\sin\Theta - \dfrac{\mu_1}{r^2} + \dfrac{(u^2+v^2)}{r} \\ \dot{r} = w \\ \dot{\alpha} = \dfrac{v}{r\sin\beta} \\ \dot{\beta} = \dfrac{u}{r} \\ \dot{m} = -\dfrac{F}{v_e g_E} \end{cases} \tag{12}$$

From the characteristics of the moon and soft landing process, the terminal constraints of soft landing orbit are dealt with by the multiplication submethod, and then the joint choke gradient method is used to solve the soft landing orbit.

The optimization of the Chang 'E III soft landing orbit can be converted into a nonlinear optimal control strategy problem with control constraints and terminal constraints, that is, within the time $[t_0, t_f]$, the optimal control function *u(t)* is determined to satisfy the differential equation:

$$\dot{x} = f(x(t), u(t), t) \tag{13}$$

Introduce the costate variable $\lambda(t)$ to form the Hamilton function[4]

$$H = L(x,u,t) + \lambda^r f \tag{14}$$

The equations of motion for the soft landing of Chang 'E III are:

$$\dot{x} = f(x(t), u(t), t) \tag{15}$$

In this paper, we use the multiplication submethod to deal with the terminal constraints of orbital optimal control, namely[6]

$$\phi(x(t_f), t_f) = \frac{\sigma}{2}\sum_{j=1}^{m}\psi_j^2(x(t_f), t_f) - \sum_{j=1}^{m} v_j \psi_j(x(t_j), t_j) \tag{16}$$

The terminal time of the soft landing orbit is free, so each time the integral orbital state equation is integrated, the terminal time t_f must be determined [7] and take the time when a terminal condition reaches satisfaction as terminal time t_f.

The simulation curve is shown in Figure 4.

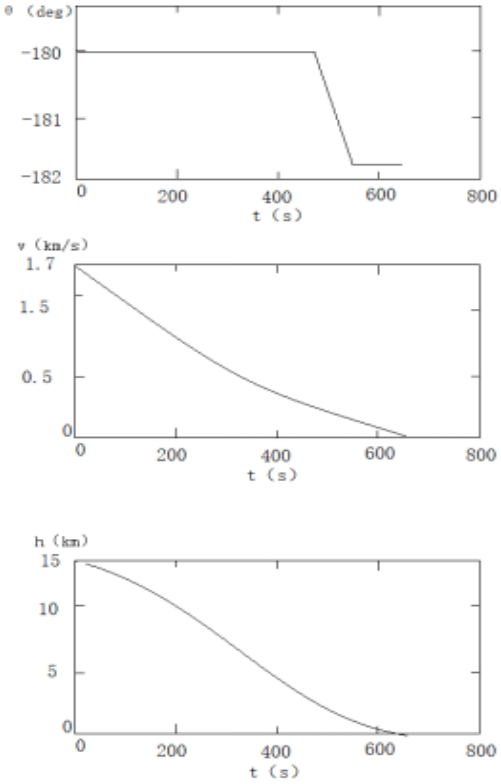

Figure 4. Simulation graph

It can be seen from the thrust angle of attack curve that the control quantity changes smoothly, without mutation, easy to control, and satisfies the control quantity constraints. The speed change curve and height change curve of the lander are smooth and converge well to the terminal constraints.

3.3. Quick Adjustment Phase

The main requirement at this stage is to adjust the attitude of the aircraft using a small attitude adjustment engine, and the horizontal speed is reduced to 0m/s, so that the engine thrust direction of the winner is downward.

$$F_2 t_2 = m_2 u_1 \tag{17}$$

3.4. Crude Barrier Avoidance Phase

The main purpose of this stage is to avoid large craters, so it is first necessary to determine the location of the crater. Find a three-dimensional map (as shown in Figure 5) and a grayscale enhancement map(as shown in Figure 6) at 2400m from the surface of the moon. Grayscale can be used to measure the level of terrain.

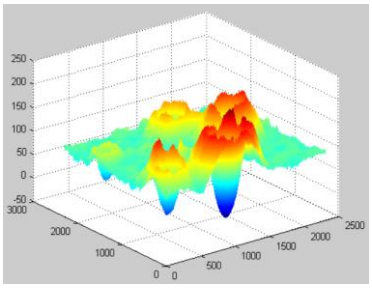

Figure 5. Three-dimensional map at 2400m

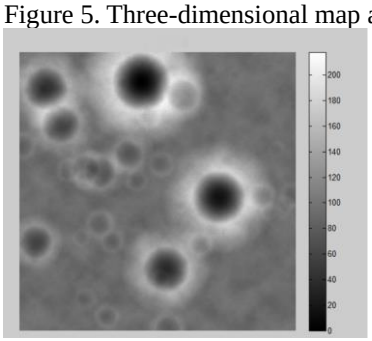

Figure 6. Grayscale enhancement

Through observation, the crater distribution area in the area can be drawn in the grayscale map, which is not suitable for landing area, and the estimated landing area can be found. In order to obtain the exact point of existence of the crater, Figure 7 can be obtained by using Matlab and the altitude of the crater can be obtained from Figure 8.

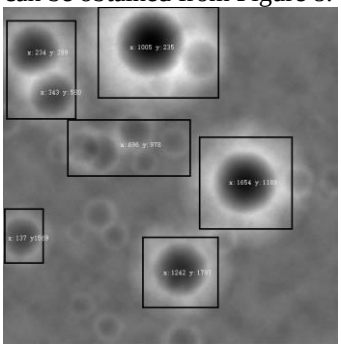

Figure 7. Grayscale enhancement of coarse barrier avoidance

3.5. Fine Obstacle Avoidance Phase

By determining the crater distribution, the displacement of the landing trajectory is analyzed, and the optimal control strategy is found.

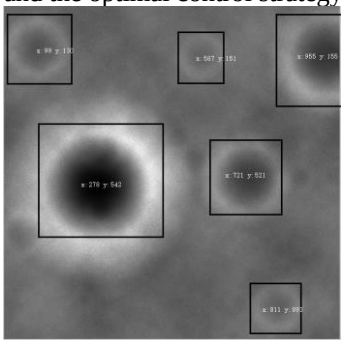

Figure 8. Grayscale enhancement of fine barrier avoidance

4. ERROR ANALYSIS

For the transfer orbit of Chang ‘E III, there are two main types of errors, one is the system error; The second is to assume the estimation error and Jisuanwucha.

In the second type of error, because the shape of the moon is 1/963.7256, the moon is approximated as a circular sphere, and the radius of the moon in the lunar fixed coordinate system is uniformly used as the average radius; Chang ‘E III moves in the gravitational field in the center of the moon, ignoring the influence of various photodynamic factors; The various types of speeds sought are all relative speeds, regardless of whether the detector orbits with the moon.

Assume that the mechanical model used to calculate Chang ‘E III’s operation is: $\dot{X} = F(X,t)$

The mechanical model of the landing preparation orbit is: $\dot{X} = \bar{F}(X,t) = F(X,t) - \Delta F(X,t)$

Among them, for the mechanical model error, that is, a class of errors, as long as it is small enough, the error caused by the landing preparation orbit of Chang ‘E III is negligible.

5. SENSITIVITY ANALYSIS

This paper mainly analyzes the sensitivity of the parameter specific impulse ve, and focuses on the main deceleration stage. The results are as follows:

Table 1. Table of relations between specific impulse and time

v_e(m/s)	t(s)
2939.97	615
2939.98	617
2939.99	619
2940.01	623
2940.02	625

From the Table 1, it can be seen that for each increase or decrease of a percentage, the range of time t changes is within 2s, about 0.03 %, and it can be concluded that it is less sensitive than Chong ve.

REFERENCES

[1]Walker M.J.H, Ireland B, Owens J. A Set of Modified Equinoctial Orbit Elements. Celestial Mechanics, 1985, 36(1):409-419.

[2]Walker M.J.H. A set of modified equinoctial orbit elements. Celestial Mechanics, 1986, 38(4):391-392.

[3]Beauty Curtis. Orbital mechanics. Beijing: Science Press, 2009, 25-59.

[4]Cai Y.F. Research on the guidance control method of lunar probe soft landing. Northwestern Institute of Technology, 2006.

[5]Ceng Y. Spacecraft flight mechanics. Northwestern Industrial University Press, 1993.

[6]Wang M.G, Yuan jianping, Luo jianjun. RLV re-entry trajectory airborne rapid optimization. Astronautical Journal, 2005, 26(3): 253-256.

[7]Tang Q. Moon soft landing orbit rapid optimization. Computer Simulation, 2007, 24(12): 24-27.

Analysis of The Use of College Campus Loans

Xuebing Chen[1,2], Yi Yang[3], Xiaoqing Meng[1,4], Aimin Yang[1,2,]*
[1] Engineering Computing and Simulation Innovation Lab, Tangshan, 063210, Hebei, China
[2] College of Science, North China University of Science and Technology, Tangshan, 063210, Hebei, China
[3]Agriculture and Forestry Economic Management College, Henan University of Animal Husbandry and Economy, Zhengzhou, 450000, Henan, China
[4] College management, North China University of Science and Technology, Tangshan, 063210, Hebei, China
**Email: aiminyang@qq.com*

Abstract: China's Internet finance has developed rapidly, with more and more campus loans for college students as loans, and some negative impacts. Through the investigation of the use of campus loans in colleges and universities, the reasons for students using campus loans are analyzed, and corresponding countermeasures are given. Combined with the survey data, logit regression is used to explore the reasons why students use campus loans. It is concluded that men are more likely to use campus loans than women, and the subjective attitude towards campus loans also affects students' attitudes toward using campus loans. Some related suggestions are given by describing the statistics.
Keywords: logit regression; questionnaire analysis; campus loan; description statistics

1. INTRODUCTION

The growing development of Internet finance in China has led to the formation and development of a large number of online loan companies. Only when there is demand, there is a market. Based on the effective support of the Internet platform, the online loan company has effectively solved the urgent need for funds for the shortage of funds in the market [1]. At present, Internet finance exists in different forms, but with the help of the Internet platform, the idle funds in the market are loaned to the capital demanders at a certain loan interest rate. In recent years, in the concentration of many online loan clouds, campus loans with college students as the mainstay have mushroomed and developed. [2-3]

Campus loans, which are campus network loans, are a platform for borrowing to help students solve economic difficulties and start a business. However, in recent years, news of college students who have been burdened with huge amounts of money due to loans to the campus have been repeatedly exposed, and incidents of suicide due to absenteeism have also occurred from time to time [4]. For a time, campus lending has become one of the hot topics of sensational campus and society [5]. This survey mainly hopes to understand the main problems of the existing regulatory measures of campus loans through the status of campus loans of college students and the recognition and evaluation of relevant regulatory measures, and propose targeted improvement measures according to relevant theories. Regulate the college students' campus loan ideas.

2. CAUSE ANALYSIS

With "personal basic information" (gender, grade, living expenses, emergency money selection), "attitude on campus loans", "use around the people" as independent variables, "campus loan use" as a dependent variable, study students choose campus. The reason for the loan is to establish a logistic regression model.

2.1. Selection of Variables

The dependent variable of the model is whether the student surveyed uses campus loans. It is a dichotomous variable. Its two levels are "used" and "never used", which are coded as 1 and 0 respectively, and select the students to be investigated. The six variables of "grade", "gender", "living expenses", "whether to choose online lending platform borrowing when urgently using money", "use of surrounding people" and "attitude to campus loans" are added to the model. The five variables are all discrete variables, so they are all converted into virtual variables introduced into the model, and the forward selection method is used for logistic regression, as Table 1.

Table 1. variable assignment table

Variable name	Assignment
Campus loan use	1: used 0: Never used
Grade (x1)	1: Freshman 2: Sophomore 3: Junior 4: Senior
Gender (x2)	1: male 0: Female
Living expenses (x3)	1: Less than 1,000 yuan 2: 1000-1500 yuan 3:1500-2000 yuan 4: More than 2,000 yuan
Choose online lending platform to borrow when you are in a hurry (x4)	1: selected 0: not selected
Attitude towards campus lending (x5)	1: Benefits outweigh the disadvantages 0: Do more harm than good
Surroundings use (x6)	1: Yes 2: No

2.2. Result Analysis

Table 2. Overall situation of the significance test of the regression equation

Omnibus test of model coefficients

	χ^2	Df	Sig.
step	5.527	1	0.019
block	45.421	3	0.000
model	45.421	3	0.000

Table 2 shows the overall situation of the significance test of the regression equation. It can be seen from the table that the likelihood ratio chi-square statistic is 5.527, and the p-value is less than the significance level of 0.05, so the null hypothesis should be rejected. of.

Table 3. Hosmer-Lemeshow results

Step	χ^2	Df	Sig.
3	1.974	5	0.853

Table 3 shows the Hosmer-Lemeshow test value of 1.974, with an accompanying probability of p=0.853>0.05, which did not reach a significant level, and the overall regression model had a good fit, indicating that the independent variable had a significant effect on the dependent variable.

Table 4. Regression coefficients for each variable

variable	B	S.E. statistic	Wald statistic	Df	P-value	Exp(B)
x2	0.922	0.395	5.446	1	0.020	2.515
x4	1.896	0.403	22.151	1	0.000	6.659
x5	1.512	0.424	12.732	1	0.000	4.534
constant	-1.779	0.484	13.519	1	0.000	0.169

As can be seen from Table 4, only the gender (x2), the choice of online lending platform lending (x4) and the attitude towards campus lending (x5) entered the equation, and the P values were all less than 0.05, and the coefficient was significant. Therefore, these three variables are important predictors selected by the respondents. Explain whether the students surveyed use campus loans and gender, whether they choose online loan platform when they use money urgently, and their attitude towards campus loans. Let the probability of the student using the campus loan be p, and write the logistic regression model as:

$$\log itP = 0.922x_2 + 1.896x_4 + 1.512x_5 - 1.779 \quad (1)$$

So, you can see:

①Men and women increased the logitP by an average of 0.922 times.

② When the money is used urgently, the online loan platform is selected to increase the logitP by an average of 1.896 times compared with the unselected students.

③Students who feel that campus loans have more advantages than disadvantages make the logitP increase by an average of 1.512 times than those who believe that campus credits are more than good.

From this, we can draw the following conclusions: From the perspective of gender, men are more likely than women to choose campus loans, and they are more likely to choose campus loans. When they use money urgently, they are more likely to use campus loans, and feel that the benefits of campus loans outweigh the disadvantages. May use campus loans.

3. PREVENTIVEP MEASURES

3.1. School Campus Loan Prevention Method

According to the survey, 134 students surveyed believe that the school activities (scenario dramas, etc.) are better, accounting for 81.2% of the total respondents, followed by 78.1%. The surveyed students believe that the school holds a special lecture in a better way; the number of individuals who think that individual talks and seminars are better, accounting for 38.7% and 41.2% respectively; the number of people who think the theme class is better is the least, accounting for the total survey 20.6% of the person, as Figure 1.

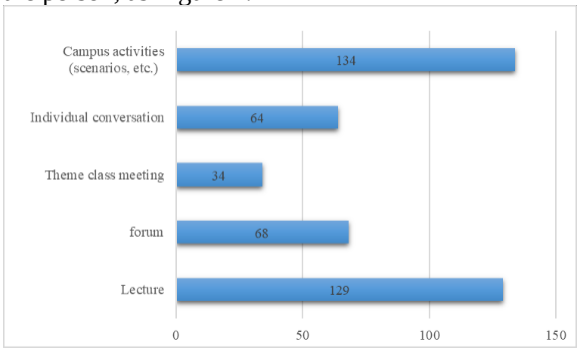

Figure 1. School measures to prevent campus loan risk

3.2. Students Avoiding Campus Loan Risk Methods

According to the survey, 90.3% of respondents chose to replace safer platforms (such as ant flower buds, Jingdong white bars, etc.); 81.2% of respondents chose to enhance Personal awareness of prevention; 63.6% of respondents chose to cultivate rational consumption concepts, and about 40% of respondents chose to learn financial management knowledge, establish scientific consumption concepts, deepen consumption awareness, and eliminate campus loans, accounting for a small proportion, as Figure 2.

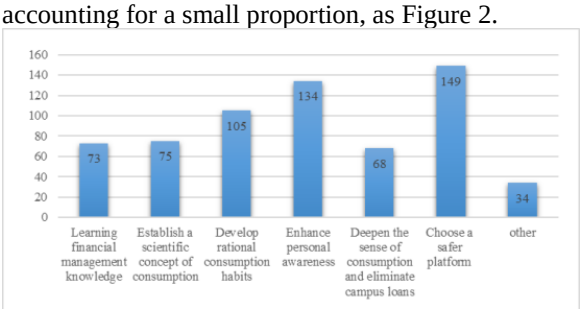

Figure 2. Students avoiding campus loan risk measures

Among the questions of sexuality, the ranking of "supervising and controlling the relevant departments" is the highest, with an average order of 1.56, so the respondents believe that this measure is the most important; the second is "students learn to manage their own finances, rational consumption" and "net The lending platform raises the threshold for review and improves the industry climate, with an average

order of 2.46 and 2.15; the average ranking of parents and school measures is lower, at 4.46 and 4.37 respectively, as Figure 3.

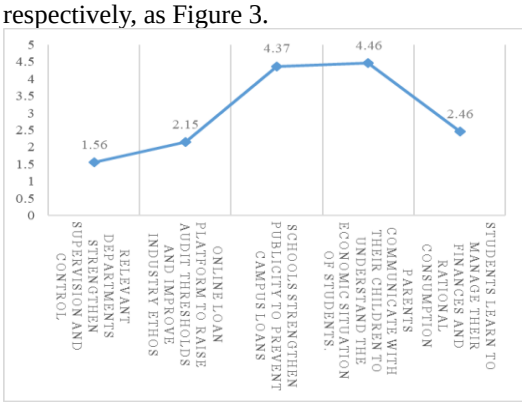

Figure 3. Ranking of the importance of preventing campus credit risk measures

4. CONCLUSION

(1) Men are more likely to use campus loans than women. When they use money, they are more likely to use campus loans. The attitude towards campus loans is also an important factor affecting students' use of campus loans.

(2) When studying the reasons for students using campus loans, it was found that men and women increased the logitP by an average of 0.922 times compared with women. When the money was used urgently, the online loan platform was selected to increase the logitP by an average of 1.896 times compared with the unselected students. Students are more likely to increase logitP by an average of 1.512 times compared to students who believe that campus credits are greater than profit.

(3) The school organizes campus activities, and the special lectures are welcomed by the students. The theme class meeting is not feasible.

When studying the school's measures to prevent campus loan risk, about 80% of the students surveyed thought that organizing campus activities and conducting special lectures were better. Among the 165 valid questionnaires, only 34 people thought that individual conversations were more effective, accounting for 20.6%, and it is more troublesome to implement, so the feasibility is not high. It is recommended that schools can regularly carry out college activities on campus credit risk prevention and control, or lectures on related topics, and strengthen the promotion of campus loan risk protection measures.

(4) More than 80% of respondents believe that the "choose a safer platform" and "enhance personal awareness" measures can avoid the risk of campus loans.

In the study of students' measures to avoid campus loan risk, 90.3% of the students believe that "choose a safer platform (such as ant flower bud, Jingdong white strip, etc.)" can better avoid campus loan risk measures; 81.2% of students It is considered that "enhancing personal prevention awareness" can better avoid the risk of campus loans. Only 41.1% of the students chose to "deepen the sense of consumption and eliminate the campus loan", indicating that the feasibility of eliminating the campus loan is low. Therefore, students can use a safer loan platform when they are in a state of emergency, and enhance their awareness of financial management in their daily lives.

(5) The relevant departments should strengthen supervision and the platform should raise the threshold for review.

In the study of effective measures to avoid campus loan risk measures, it is found that the relevant departments have the highest ranking and the highest importance. The state has already introduced relevant policies, but there are some problems in supervision. There is a phenomenon of "714 high-altitude" in the online loan platform, so the relevant departments Strengthening supervision of campus loans can effectively reduce the risk of campus loans; secondly, the platform itself has made a difference. The current online lending platform is to attract users and promote misleading advertising information such as "0 interest rate, 7 days interest-free", resulting in Vicious competition, the platform should raise the threshold for review, reduce the bad debt rate, to increase revenue rather than raise interest rates at a glance; students should also learn to manage their own finances, to achieve rational consumption, the high consumption of most students is Because of the comparison psychology and herd mentality, contemporary college students should learn financial management knowledge and achieve rational consumption in order to fundamentally prevent the risk of campus loans.

REFERENCES

[1]Zhao L. On the prevention and rectification of campus loans. Journal of Liaoning Teachers College (Social Science Edition), 2018, (2): 133-134.

[2]Gu H.L. Eliminating the "Campus Lending" Trap to Build a Harmonious Campus in Colleges and Universities. Industry and Technology Forum, 2016, 15(19): 264-265.

[3]Li W, Yuan Q, Zheng W, et al. Investigation and research on the status quo and influencing factors of "campus loan". Journal of North China University of Technology(Social Science Edition), 2018, 18(1): 11-14 .

[4]Mo C.C. The Harm, Causes and Avoiding Strategies of College Campus Loan Chaos. Journal of Shenyang University (Social Science Edition), 2018, (1).

[5]Zheng C.M, Jia S.S. Comparison of domestic and international campus loan platforms and regulation analysis. Finance and Economics: Academic Edition, 2016, (17).

Shadow Market Segmentation Based On K-means Clustering

Xuebing Chen[1,2,], Yi Yang[3], Xinjia Yang4, Yang Han[1,2]*
[1] *Engineering Computing and Simulation Innovation Lab, Tangshan 063210, Hebei, China*
[2] *College of Science, North China University of Science and Technology, Tangshan, 063210, Hebei, China*
[3] *Agriculture and Forestry Economic Management College, Henan University of Animal Husbandry and Economy, Zhengzhou, 450000, Henan, China*
[4] *Zhengzhou University of Light Industry, College of Electrical Information Engineering, Zhengzhou, 450000, Henan, China*
**Email: xuebingcheng@qq.com*

Abstract: Shadow play is one of the oldest dramas in China. It is a must for Chinese folk art. The research on the market of shadow culture derivatives has far-reaching significance for the development of shadow play. Through a questionnaire survey, this paper investigates the residents' willingness to purchase shadow-shadow derivatives in some cities in Tangshan City, Hebei Province, and their sensitivity to the price of derivatives. Finally, based on the questionnaire data, the K-means clustering method was used to segment the respondents, and finally the four types of consumers, price-sensitive, shadow-like, price-sensitive and insignificant, were given. The characteristics of the four types of consumers. At the end of the article, we present some development suggestions for the shadow film derivatives market.
Keywords: k-means clustering; chinese shadow play; derivative market

1. INTRODUCTION

The shadow play also called "shadow drama" "light shadow drama" "tu ying xi" is a silhouette of a character made of light or animal skin or cardboard to perform a story [1]. The repertoire and the aria are influenced by the local opera, and the artist is manipulating. Singing and matching music [2]. Tangshan Phi Phi is also called "Le Ting Ying" and "Zhangzhou Shadow". It is popular in Tangshan, Hebei, Chengde, Langfang and other cities and counties in the three northeastern provinces. It has a major influence in Chinese shadow play. Status. However, with the acceleration of the modernization process, the audience of Shadow Play has plummeted and the crisis of survival has intensified.

"Derivatives" refers to things derived from native things [3]. Art derivatives are art peripheral products developed on the basis of original works of art [4,5]. Shadow Derivatives refers to products that are used by all the elements related to the shadow play to produce economic benefits in all aspects of life [5]. Nowadays, the shadow derivative has been extended to all aspects of people's daily life such as toys, handicrafts, souvenirs, daily necessities, clothing, home, audio and video, books, online games, food and beverage.

In addition, due to the long time-consuming production of Tangshan Shadows, the sensitivity of manuals is extremely high, and many of them are passed on to the children, and the family inheritance of the children is not passed down. It is necessary to protect them and develop them.

In recent years, China's enthusiasm for the protection of intangible cultural heritage has been unprecedentedly high, and the protection of intangible cultural heritage has been increasing. The "One Belt, One Road" interconnection project aims to explore the potential of the regional market, promote investment and consumption, and create Demand and employment. Therefore, the development of the derivatives market is the only way to develop the Tangshan Shadow and even the Chinese shadow market. It is believed that the support of the national policy and the market are welcome, and the development of the shadow film derivatives market has ushered in new opportunities. The shadow culture has shown a good momentum of vigorous development.

2. MARKET SEGMENTATION

Market segmentation is the process by which an enterprise divides the entire market into different consumer groups based on different consumer needs. It plays an extremely important role in the production and marketing of enterprises. It can bring the following aspects to help enterprises: develop optimal marketing strategies, find market opportunities, rationally allocate resources, gain competitive advantage and improve economic efficiency.

Cluster analysis is one of the most commonly used methods in market segmentation. Cluster analysis is the process of dividing an object into several groups, so that the data in the same group has a high degree of similarity, while the data objects in different groups are not similar. Through the K-means clustering method, the villa daily rent purchasers are divided into several different types, and targeted marketing strategies are adopted for different types of villa buyers to improve the company's revenue.

2. DATA PREPROOCESSING

Choose three subdivision variables: price tolerance, quality demand, and the taste of the shadow play. The raw data is processed, and the three variables of price tolerance, quality demand and shadow taste are divided into three grades: low, medium and high. The processing methods are as follows.

2.1. Classification of Price Tolerance

For the Q13 four-priced shadow crafts in the questionnaire, if the respondent answers “positive choice”, it is recorded as 4 points; if the respondent answers “possible choice”, it is recorded as 3 points; if it is investigated If the respondent replies "may not choose", it is recorded as 2 points; if the respondent answers "definitely not selected", it is recorded as 1 point. Because the price of each craft is different, the weights of different options are different. The weight ratio is 1:2:3:4. The scores of each respondent are weighted and averaged. The formula is as follows:

$$\overline{F} = 0.1F_1 + 0.2F_2 + 0.3F_3 + 0.4F_4 \quad (1)$$

If the average score is greater than 3.2, it is defined as the consumer with high price ability, and the consumer is recorded as 3; if the average score is greater than or equal to 2 and less than or equal to 3.2, it is defined as the consumer with the price ability to accept the general. Such consumers are recorded as 2; if the average score is less than 2, they are defined as consumers with low price ability, and such consumers are recorded as 1. In this way, all respondents are divided into three grades of high, average and low preference for the shadow design elements.

2.2. Classification of the Quality Requirements of Respondents

If the survey selects five or more of the options in Questionnaire Q14, it is defined as a consumer with high quality requirements, and marks such consumers as 3; if selected, the option in Questionnaire Q14 is selected. Three or four or one are defined as consumers with average quality requirements, and such consumers are marked as 2; if they are selected by surveying two of the options in Questionnaire Q14, they are defined as Consumers with low shadow quality requirements and mark such consumers as 1.

(3) Classification of the taste of the respondents

If the survey selects three or more of the options in Questionnaire Q15, it is defined as a consumer with a high taste, and marks such a consumer as 3; if the survey selects one of the options in Questionnaire Q15 Or two, which are defined as consumers with a taste of taste, and mark such consumers as 2; if the “not interested” option in the option in Questionnaire Q15 is selected, it is defined as low taste. Consumers and mark such consumers as 1.

In theory, each aspect can divide consumers into three categories, so the market is divided into 27 parts:

Integrate and analyze these twenty-seven categories. According to the actual meaning, we can divide all consumers into four categories:

Type 1 consumers: price-sensitive. For this type of consumer, they value the price more than the quality. Only the price is within the range they are willing to consume. The group is usually a group of students or a group with lower incomes.

The second type of consumer: the shadow element preference type. This type of consumer does not value the price of the shadow derivative, they value the quality of the derivative, and the experience and experience brought to them during the consumption process.

The third category of consumers: early adopters. Tangshan Pi Ying as a national intangible cultural heritage, is a traditional industry, but due to the lack of development in recent years, the narrow spread of the status quo, leading many consumers, especially young consumers, to contact the shadow culture less. For them, the most important thing is the freshness of the shadow culture.

The fourth category of consumers: irrelevant type. In addition to the 1, 2, 3 and 3 categories of consumers, there are some consumers are not very valued for the price and quality of the shadow derivative, and there is no sense of freshness. For this part of the consumer, no matter how much energy the company puts into satisfying the needs of such customers, they will not (or will definitely) go to the villa for daily rental consumption. Therefore, if companies invest too much energy in such consumers, they will not increase their turnover.

These four classifications are determined based on theoretical knowledge plus actual conditions and will serve as the basis for determining the K value in the next K-Means cluster.

3. K-MEANS CLUSTERING

3.1. Output Result

Table 1 shows the results of one-way ANOVA between various types of samples formed after rapid cluster analysis. For the price bearing capacity, its sum of squares between groups is 84.620, the sum of squares in the group is 0.310, the F statistic is 72.704, and the correlation probability of F statistic is 0.00 less than the significance level of 0.05, so for the price bearing capacity, 4 types There are significant differences between consumers. There is also the same conclusion about quality demand and taste. Therefore, the K-means clustering analysis classified into four categories is successful, and the clustering analysis is very effective.

Table 1. One-way ANOVA results between various samples

	Clustering		Eror		F	Sig.
	Mean square	Df	Mean square	Df		
Price bearing capacity	84.620	3	0.310	806	272.704	.000
Quality demand	98.892	3	0.326	806	303.383	.000
Taste of taste	104.949	3	0.287	806	365.313	.000

Table 2. Number of samples included in each of the four categories

Cluster	Number of samples
1	376
2	169
3	111
4	154

Table 2 lists the number of samples for each of the four classes. Among them, there are 376 in the first category, 169 in the second category, 111 in the third category, and 154 in the fourth category.

3.2. Result Analysis

Table 3. Specific differences in the four categories

Case cluster number		Price bearing ability score	Quality demand score	Taste of taste
1	N	376	376	376
	mean	2.45	2.69	1.52
	median	3.00	3.00	1.00
	Std.	0.651	0.641	0.628
2	N	169	169	169
	mean	1.53	2.34	2.72
	median	2.00	2.00	3.00
	Std.	0.47	0.663	0.449
3	N	111	111	111
	mean	1.18	1.36	1.45
	median	1.00	1.00	1.00
	Std.	0.386	0.441	0.362
4	N	154	154	154
	mean	2.64	1.10	1.42
	median	2.00	1.00	1.00
	Std.	0.496	0.297	0.481

Table 3 shows the specific differences in price tolerance, quality demand and early taste of the four categories 1, 2, 3 and 4. It can be seen that the first type of consumer quality demand average score is the highest among the four types of consumers, so it is the quality demand type consumer; the second type of consumers have higher average scores of taste and quality demand scores. However, the price tolerance is low, which is the early adopter; the third category of consumers has a score of less than 1.5, the price tolerance is lower, and the price is sensitive; the fourth type of consumer has higher price tolerance. However, the skin taste and the price tolerance are lower, which is an irrelevant consumer.

In summary, respondents are divided into four categories, including quality demand consumers, early adopters, price sensitive consumers, and insignificant consumers. Among them, quality demand consumers (like design products with shadow elements) accounted for 376 people, accounting for 46.4% of the total number of surveys; taste consumers (like fresh shadow form) were 169, accounting for 20.8 of the total number of surveys. %; price-sensitive consumers (not interested in anything) were 111, accounting for 13.7% of the total number of surveys; unimportant consumers (like the shadow itself) were 154, accounting for 19% of the total number of surveys.

4. CONCLUSION.

Nearly half of the respondents are quality consumers, and early adopters and price-sensitive consumers each account for 20%.

Segmenting the shadow market, the respondents are divided into four categories of consumers, including quality demand consumers, early adopters, price sensitive consumers and insignificant consumers. Among them, 376 are quality demand consumers, accounting for 46.4% of the total number of surveyed; 169 are early adopters, accounting for 20.8% of the total survey; and 111 are price sensitive consumers, accounting for 13.7% of the total surveyed. The number of insignificant consumers was 154, accounting for 19% of the total number of people surveyed. Quality demand consumers are mainly middle-income residents; early-stage consumers are mainly young people; price-sensitive ones are mainly students and young people who have just entered the society; and irrelevant consumers have no obvious trend.

REFERENCES

[1]Research on the Protection of the Shadows of Dongdong Road from the Perspective of Intellectual Property. Northwest Normal University, 2016.

[2]Xue H.P. On the Development of Shadow Play and the Inheritance of New Ways. Journal of Chongqing University of Science and Technology (Social Science Edition), 2008, (11):169-170.

[3]Yang J.Y. Reflections on the Decline of Shadow Plays. Art Education, 2006, (5):14-15.

[4]Pan C.X, Zhou Y.B. From Shadow Art to Interactive Media Design. Decoration, 2003, (11): 26-27.

[5]Wei S. Development Status and Countermeasures of Luoshan Shadow Play in Henan Province. Journal of Kaifeng College of Education, 2018, (8): 254-255.

Intelligent Processing of Flame Spectrum Big Data in Converter Steelmaking Furnace Mouth

Shuaijie Shan[1,2], Xueyong Jia[1,2], Yuying Wu[1,3], Donghao Jin[1,3], Yue Ying[1], Caijun Zhang[4,]*
[1] Engineering Computing and Simulation Innovation Lab, Tangshan, 063000, Hebei, China
[2] College of Electrical Engineering, North China University of Science and Technology, Tangshan, 063210, Hebei, China
[3] College of Metallurgy and Energy, North China University of Science and Technology, Tangshan, 063210, Hebei, China
[4] North China University of Science and Technology, Tangshan, 063210, Hebei, China
**E-mail: ncst_ssj_bg@163.com*

Abstract: With the increasing demand for smart manufacturing and green production in the steel industry, the realization of automated smelting of small and medium-sized converter plants has become a restrictive link in the progress of China's steel industry. Based on the artificial experience to determine the flame of the furnace mouth, this study intends to construct a sample set for steelmaking end point prediction by extracting the flame spectrum characteristics of the furnace mouth. First, a light intensity value of 2048 wavelengths of the mouth flame were collected using a USB 4000 grating spectrometer. Secondly, the main features of the flame spectrum information are extracted as the input of the sample set by combining the least squares band fitting and wavelet analysis. Then use the self-developed Steeling Making software to reverse the carbon content, temperature value, oxygen consumption and other indicators in the steelmaking process as the output of the sample set. Finally, the sample set corresponding to the input and output synchronization of the intelligent steelmaking key prediction model is constructed.
Keyword: spectral big data; intelligent smelting; feature extraction; sample set

1. INTRODUCTION

In order to improve the level of automatic smelting of steel mills, the requirements of society for capacity and green production in the steel industry are realized. Many scholars at home and abroad have developed dynamic control methods for rich and powerful control, flue gas analysis dynamic control, and sub-gun + flue gas analysis in the automatic smelting of large and medium-sized converters, but due to the high cost [1-3]. And the dependence of flue gas analysis on static models is higher [4], which limits the application of these three methods in small and medium-sized converter plants.

Steelmaking is the process of converting molten iron into molten steel. This process involves many complicated processes, including reducing carbon content, increasing molten steel temperature, and removing impurities [5-6]. The accurate control of molten steel temperature guarantees the subsequent steel rolling process such as refining and continuous casting. The most important indicators for the performance of steel grades are the key carbon and phosphorus content of molten steel [7]. Zhang X et al. used the end bath temperature, iron oxide content, limestone quality, tapping temperature, and alkalinity of slag as sample input sets to predict the tapping time and the composition of molten steel during tapping [8]. Dahiya K et al. used the amount of molten iron, oxygen blowing and auxiliary additive quality as sample input sets to predict the molten pool temperature and molten steel carbon content, which provided an idea for intelligent steelmaking [9]. The Jadon S is combined with the heat balance furnace gas analysis method to predict the carbon content of the blowing end point by denoising attenuation [10]. Ravishankara A R et al. studied a gas based on infrared test furnace, which measures the carbon and sulfur content in molten steel by measuring the change of infrared energy attenuation, and then realizes the prediction of steelmaking end point [11].

Domestic scholars continue to develop new testing methods to study the flame information of the mouth. Tian Lu et al. [12] collected the flame intensity and image information of the converter mouth in real time, and can predict the carbon content and temperature of the molten pool. He Taozhen et al [13]. designed a system for real-time online judgment and control of converter end-point temperature and carbon mass fraction by analyzing the flame intensity and image information of the converter mouth. Wang Rulun et al. [14] and others flame analysis technology based on photoelectric technology, machine vision and metallurgy principle, real-time collection of furnace flame intensity and image information, the melting pool carbon content and temperature forecast. Xu Benhong [15-20] analyzed the characteristic line intensity of various elements by the spectrum emitted by the molten steel during the oxygen blowing process, and found that the intensity of the characteristic line is related to the content of oxygen in the molten steel.

In summary, on the small and medium-sized

converters, based on the optical information at different times of the converter smelting process, and further extracting spectral features, optimization algorithms, forecasting molten steel temperature and carbon content. It is an automatic steelmaking control method with low cost, accuracy, reliability, high efficiency and stability.

2. GENERATION OF SPECTRAL DATA

In the steelmaking process, steel mills mainly judge the color, shape and changing trend of the flame at the furnace mouth. The essence of the steel mill is the change of the flame spectrum radiation, and the shape change can reflect the light intensity change to some extent. The data of this project is acquired by the USB4000 grating spectrometer to collect information such as the spectral radiation intensity of the furnace flame. The intensity value corresponding to 2048 wavelengths is collected each time. The computer setting is collected every 0.5s, the furnace flame wavelength range is 340.535-1027.963nm, and the light intensity range is 340.535-50000. The step size of the wavelength is 0.285 nm, and the converter is smelted for 15 minutes as a cycle. During this period, 1800 data is collected, and each group of data has a light intensity value of 2048. A total of 3.69×106 spectral intensity values were generated for the entire cycle.

3. SPECTRAL DATA COLLECTION

The core component in spectral data acquisition is the spectrometer. In this study, the spectrometer USB4000 micro-grating spectrometer developed by Ocean Optics was selected. It has the hardware foundation of small size, light weight and direct connection with computer, and has a powerful electronic system. It is convenient to connect with the telescope detection system, and the data can be read by using the driver. In addition, it detects wavelengths ranging from 200 to 1150 nm, and has a low failure rate. It can be adapted to the complex environment of the smelting site. After testing, the full spectrum intensity of the furnace flame can be obtained relatively completely.

The trend of the intensity of each band in the process of converter steelmaking is shown in Figure 1. The distribution of light intensity at each wavelength before, during the middle and late stages of steelmaking can be roughly the same as the theory. Since the steelmaking process is controlled by open loop, there are a series of uncertain factors in the smelting process, so the light intensity distribution is uneven in the later stage of smelting. This study uses data mining algorithms and intelligent algorithms to mine spectral big data, aiming to provide a feasible pre-processed sample set for key intelligent judgment of steelmaking.

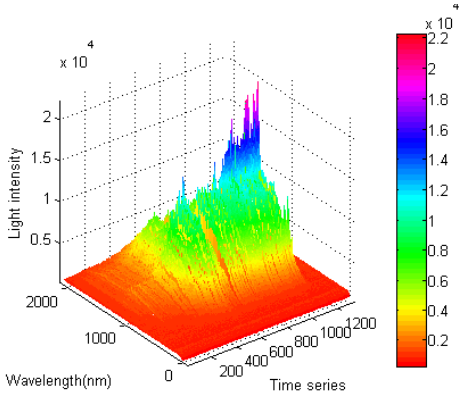

Figure 1. Time series diagram of all optical spectrum intensity

4. THEORETICAL ANALYSIS

4.1. Least Squares Fitting Algorithm

The general method of polynomial fitting can be summarized as the following steps [16-18]:

(1) Draw a rough graph of the function from the known data - a scatter plot to determine the number n of fitting polynomials.

Draw a scatter plot based on the given data and construct a polynomial function class of the scatter plot to solve the $p_n(x)=\sum_{i=0}^{m} a_k x^k$ so that:

$$I=\sum_{i=0}^{m}[p_n(x_i)-y_i]^2=\sum_{i=0}^{m}(\sum_{k=0}^{n}a_k x_i^k-y_i)^2=\min \quad (1)$$

At this time, the fitting function is obtained as a polynomial, and the $p_n(x)$ satisfying the formula (1) is a least squares fitting function, and the power of n is determined.

(2) List calculation $\sum_{i=0}^{m} x_i^j (j=0,1,2,\ldots,n)$ and $\sum_{i=0}^{m} x_i^j y_i (j=0,1,2,\ldots,n)$.

It can be known from equation (1) that a_k is a multivariate function, so the solution of the minimum value can be transformed into the extremum of the $I=I(a_0,a_1,\ldots,a_n)$, and the necessary conditions for solving the extremum of the multivariate function are obtained:

$$\sum_{k=0}^{n}(\sum_{i=0}^{m}x_i^{j+k})a_k=\sum_{i=0}^{m}x_i^j y_i, \qquad j=0,1,\ldots,2n \quad (2)$$

(3) Write the normal equations $a_0,a_1,\ldots,a_n$ and find out.

From the normal equation (2), the equations are listed, and then the $a_0,a_1,\ldots,a_n$ is solved.

$$\begin{bmatrix} m+1 & \sum_{i=0}^{m} x_i & \cdots & \sum_{i=0}^{m} x_i^n \\ \sum_{i=0}^{m} x_i & \sum_{i=0}^{m} x_i^2 & \cdots & \sum_{i=0}^{m} x_i^{n+1} \\ \vdots & \vdots & & \vdots \\ \sum_{i=0}^{m} x_i^n & \sum_{i=0}^{m} x_i^{n+1} & \cdots & \sum_{i=0}^{m} x_i^{2n} \end{bmatrix} \begin{bmatrix} a_0 \\ a_1 \\ \vdots \\ a_n \end{bmatrix} = \begin{bmatrix} \sum_{i=0}^{m} y_i \\ \sum_{i=0}^{m} x_i y_j \\ \vdots \\ \sum_{i=0}^{m} x_i^n y_j \end{bmatrix} \tag{3}$$

Judging from the necessary and sufficient conditions of the symmetric positive definite matrix, the coefficient matrix of equation (3) is a symmetric positive definite matrix.

(4) Write the fitting polynomial. Solving $a_k,(k=0,1,\ldots,n)$ from equation (3), so that the polynomial $p_n(x)=\sum_{i=0}^{m} a_k x^k$ can be obtained.

4.2. Wavelet Analysis

Wavelet analysis is a time-frequency local analysis method with variable window size and variable time window and frequency window. It has high frequency resolution and low time resolution in the low frequency band and strong adaptability [19,20].

Compared with the Fourier transform, the wavelet transform replaces the trigonometric function with a wavelet basis, that is, a wavelet function $\psi(t)$ that satisfies certain conditions. $\psi(t)$ is transformed and translated to get a family of functions:

$$\psi_{a,b}(t)=|a|^{-\frac{1}{2}}\psi(\frac{t-b}{a}) \quad a,b\in R, a\neq 0 \tag{4}$$

Among them, $\psi_{a,b}(t)$ is called continuous wavelet, a is the scale factor, and b is the time factor. For $f(t)\in L^2(R)$, the continuous wavelet transform is:

$$W_f(a,b)=|a|^{-\frac{1}{2}}\int_{t=-\infty}^{\infty} f(t)\overline{\psi}(\frac{t-b}{a})dt \tag{5}$$

Among them, $W_f(a,b)$ is the wavelet transform coefficient of $f(t)$.

5. SAMPLE SET CONSTRUCTION

The main research roadmap for this project is as follows Figure 2.

5.1. Spectral Stabilization Feature Extraction based on Least Squares Fitting Algorithm

The spectrometer obtains the full spectrum information of the furnace mouth every 0.5s, corresponding to the light intensity value of 2048 wavelengths. In this study, a set of full spectrum information is recorded from the time of the tapping of the converter, and a set of full spectrum information is recorded at the time of the completion of a furnace. The image about the wave is shown in Figure 3.

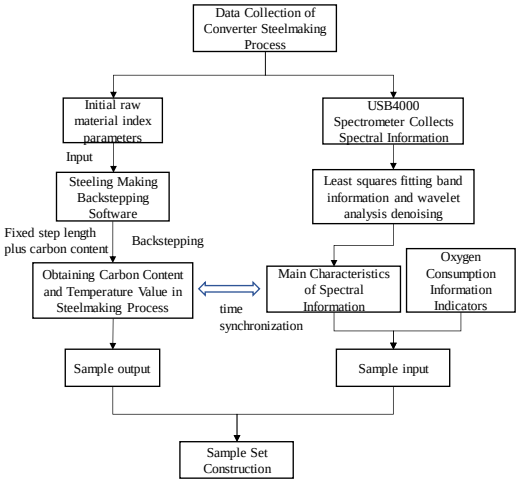

Figure 2. Research route

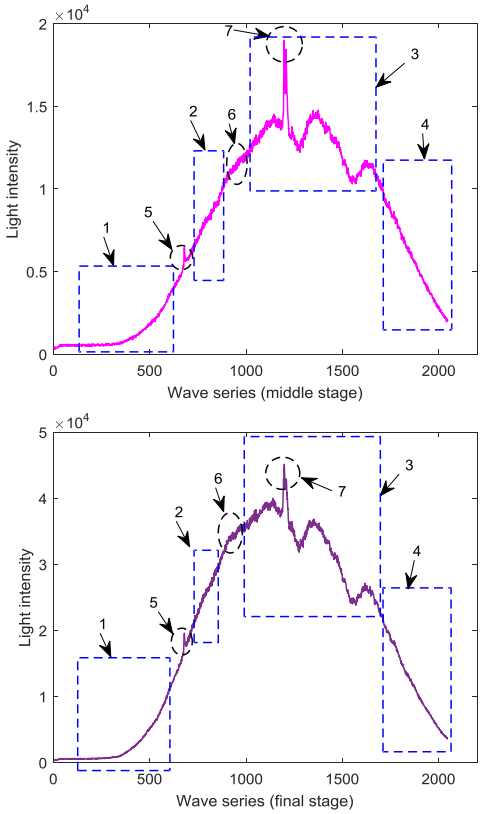

Figure 3. Variation trend of light intensity in wavelength sequence

As shown in Figure 2, the abscissa is the wavelength value and the ordinate is the light intensity value. From the figure, you can get three relatively smooth areas, one data messy area, and three characteristic areas. The smooth region bands are band 1-[230,650], band 2-[770,960], band 4-[1730,2048]; The data in the messy area band is band 3-[1080, 1680]; The characteristic region bands are band 5-[650,750], band 6-[960,1060], band 7-[1250,1300]. The three smooth bands contain more than the general information of the full band. Do a least squares fit to get:

$$f(\lambda)=\begin{cases} a_1\lambda^2+b_1\lambda+c_1, & \lambda_{11}\le\lambda\le\lambda_{12} \\ a_2\lambda^2+b_2\lambda+c_2, & \lambda_{21}\le\lambda\le\lambda_{22} \\ a_3\lambda^2+b_3\lambda+c_3, & \lambda_{31}\le\lambda\le\lambda_{32} \end{cases} \quad (6)$$

5.2. Spectral Instability Feature Extraction based on Wavelet Analysis

The characteristics of the spectral information in Figure 2 can be obtained. The full-band spectral intensity of the tapping steel has not only stable characteristics, but also three peaks, which are unstable characteristics, and the peak appears in a fixed wavelength band. Therefore, it is judged that there are some links between the three unstable characteristics and the carbon content of molten steel and the temperature of molten steel. The instability characteristics of the full-band 2048 wavelengths are located by wavelet analysis, and the processing results are shown in Figure 4.

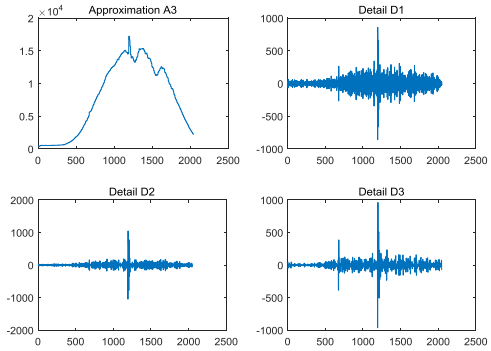

Figure 4. Wavelet reconstruction 3 layers approximate 1, 2, 3 layer detail map

It can be seen from Fig. 4 that the original signal from the three-layer decomposition reconstruction in wavelet denoising can be clearly observed. In the full-band spectrum of the furnace flame, the light intensity corresponding to different wavelengths has large fluctuations, and the full-band light intensity value has 3 smooth areas and 3 unstable areas. Finally, the original signal of the 3-layer reconstruction is obtained with err=1.4552e-11, and the reconstruction degree is higher.

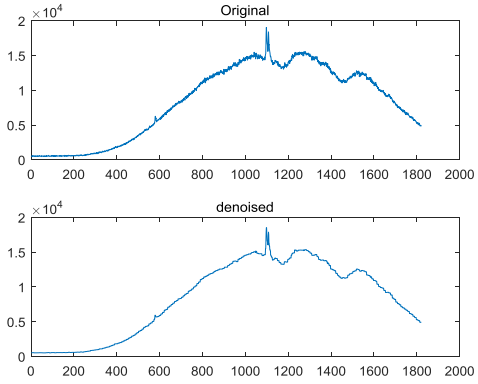

Figure 5. Three-layer approximation signal and original signal

Wavelet analysis is used to identify individuals or groups containing noise from the signal, and then reconstruct the modified component signal. From Figure 5 above, it can be concluded that the continuous approximation is taken from the signal with increasing high frequency information. The noise becomes less and less, and the 3-layer approximation becomes cleaner with the original signal, which helps to stabilize the feature extraction.

Combine certain thresholds, discard some high-frequency information, and not lose too many of the sharp features in the original signal. Finally, the unstable feature regions of the spectral information are extracted by threshold limits and Threshold-ed coefficients as shown in Figure 6.

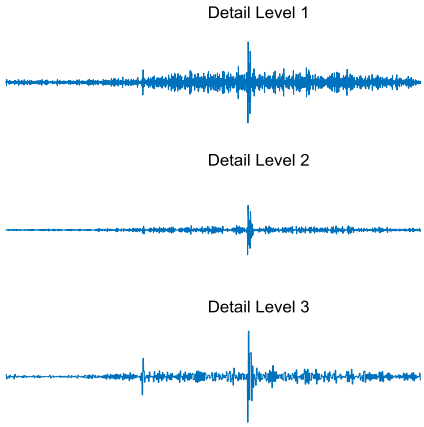

Figure 6. Three-layer approximation signal detail analysis

As can be seen from Figure 5, most of the noise occurs in the middle of the spectral signal, and can be clearly obtained from the fluctuations in the figure. And further formalize the three unstable feature points mentioned above, which are obtained by the three sharpest fluctuations in Figure 6.

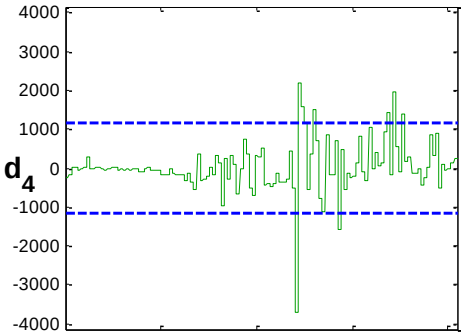

Figure 7. Wavelet 1-D analytic results

It can be seen from Figure 7 that there are seven unstable characteristics (feature peaks) of the spectral information, and the interval setting conditions are as follows: Feature peak 1- [820,851], Feature peak 2-[918,936], Feature peak 3-[990,1008], Feature peak 4-[1083,1126], Feature peak 5-[1183,1312], Feature peak 6-[1389,1496], Feature peak 7-[1676,1774]. In order to better characterize the unstable characteristics of the spectral information, in order to better

characterize the unstable characteristics of the spectral information, the integral area of the characteristic peak wavelength region is replaced by the wavelet feature.

5.3. Sample Set Construction

Under the condition of time synchronization, the oxygen consumption index and the main features of the spectral information collected during the smelting process, as well as the stable and unstable characteristics of the spectral information extracted by the wavelet analysis are taken as sample inputs. The control targets (carbon content, temperature values) collected during the steelmaking process are used as sample outputs to establish a sample set that is synchronized with the input and output.

The sample set construction principle is as follows:

STEP1. Run the SM software. Open SM.exe;

STEP2. Enter the raw material data (the amount of molten iron, etc.) corresponding to the heat;

STEP3. Open the adjustment ratio button and adjust the steel smelting parameter value until the cumulative oxygen consumption at the end point is calculated;

STEP4. By changing the carbon content in the area, the temperature value corresponding to the carbon content and the cumulative oxygen consumption are gradually reversed.

STEP5. Record the data according to Table 1.

On the basis of the data in Table 1, the least square method is used to construct the functional relationship between the carbon content and the cumulative oxygen consumption ratio as a function of the cumulative oxygen consumption ratio. A sample set corresponding to the cumulative oxygen consumption, cumulative oxygen consumption ratio, spectral information characteristic value, carbon content and Kelvin temperature value in the process of 70% to 100% steelmaking progress can be obtained.

Table 1. Data reversal table of steelmaking process based on SM software

Cumulative oxygen consumption ratio	Cumulative oxygen consumption
100%	Q_end
Q_1 / Q_end	Q_1
Q_2 / Q_end	Q_2
Q_3 / Q_end	Q_3
⋮	
Q_n-1 / Q_end	Q_n-1
70%	Q_n
Carbon content	**Temperature value**
C_end	T_end
C_end + 1 * 0.01	T_1
C_end + 2 * 0.01	T_2
C_end + 3 * 0.01	T_3
⋮	
C_end + (n-1) * 0.01	T_n-1
C_end + n * 0.01	T_n

6. CONCLUSION

The spectral information of the furnace mouth flame during the converter steelmaking process reflects the dynamic trend of carbon content and temperature value to some extent. The stable and unstable characteristics of the furnace flame spectral information extracted by the sub-band least squares fitting algorithm and the wavelet analysis algorithm can reflect the full spectrum information well. Seven main characteristics and unstable characteristics were extracted from the main features of the flame spectrum information of the steelmaking furnace mouth, and the oxygen consumption index collected during the steelmaking process was used as the sample input. The control target index (carbon content, temperature value) collected during the steelmaking process is taken as the sample output, and the sample set corresponding to the input and output synchronization is constructed to provide a theoretical basis for realizing the automatic steelmaking technology of the converter.

ACKNOWLEDGMENT

The research work was supported by the project grant of Innovation and Entrepreneurship Training Program of North China University of Science and Technology. Project number: X2018092. Project Information: 2018 North China University of Science and Technology Students Innovation and Entrepreneurship Training Program Project, Project No. 2018092.

REFERENCES

[1]Wang X F, Tang F P, Lin Y, et al. Development of novel RH degassing process with powder injection through snorkel nozzles. Ironmaking & Steelmaking, 2014, 41(9):694-698.

[2]Zhu B, Liu Q, Zhao D, et al. Effect of Nozzle Blockage on Circulation Flow Rate in Up-Snorkel during the RH Degasser Process. Steel Research International, 2016, 87(2):136-145.

[3]Liu H, Wu Q, Wang B, et al. BOF steelmaking endpoint real-time recognition based on flame multi-scale color difference histogram features weighted fusion method//Control Conference. IEEE, 2016.

[4]Zhao Y, Kong J, Yang J, et al. TCO Endpoint Control System for Converter Steelmaking// International Conference on Electrical & Electronics Engineering. 2011, 399-402.

[5]Al-Yaseen W.L, Othman Z.A, Nazri M.Z.A. Multi-level hybrid support vector machine and extreme learning machine based on modified K-means for intrusion detection system. Expert Systems with Applications, 2017, 67:296-303.

[6]Hagenauer J, Helbich M. A comparative study of machine learning classifiers for modeling travel mode choice. Expert Systems with Applications, 2017, 78:273-282.

[7]Turgeman L, May J,H, Sciulli R. Insights from a machine learning model for predicting the hospital Length of Stay (LOS) at the time of admission. Expert

Systems with Applications, 2017, 78:376-385.
[8]Zhang X. Application of Static and Dynamic Model for Automatic Steelmaking in Jinan Iron and Steel Co. Angang Technology, 2007.
[9]Dahiya K, Chauhan V.K, Sharma A. Online Support Vector Machine Based on Minimum Euclidean Distance//Proceedings of International Conference on Computer Vision and Image Processing. Springer Singapore, 2017.
[10]Jadon S. Code clones detection using machine learning technique: Support vector machine// International Conference on Computing, Communication and Automation. IEEE, 2017.
[11]Ravishankara A.R, Portmann R.W. Nitrous Oxide (N2O): The Dominant Ozone-Depleting Substance Emitted in the 21st Century. Science, 2009, 326(5949):123-5.
[12]Tian L. Converter end point prediction technology based on furnace flame analysis. The Chinese Society for Metals, Baosteel Group Coporation. Proceedings of the 10th China Iron and Steel Annual Conference and the 6th Baosteel Academic Annual Conference. The Chinese Society for Metals, Baosteel Group Coporation: 2015, 5.
[13]He T.W, Tian L, Wen H.B, Liu Z.M, Feng Z.J, Zhou C.B. Endpoint Prediction System for Converter Steelmaking Based on Furnace Flame Information. China Metallurgy, 2013, 23(02): 40-43.
[14]Wang R.L, Liu Z.M, Tian L. Application of Furnace Flame Information in End Point Control of Converter Steelmaking. Shanxi Metallurgy, 2012, 35(05): 25-27.
[15]Xu B.H. Hyperspectral mapping and verification based on spectral feature extraction parameters. China University of Geosciences (Beijing), 2016.
[16]Yu L, Hong Y.S, Yan L, et al. Hyperspectral estimation of soil organic matter content based on partial least squares regression. Transactions of the Chinese Society of Agricultural Engineering, 2015, 31(14): 103-109.
[17]Huang J.P, Li W, Li Q.Y, et al. A least squares inverse time migration method based on plane wave static coding. Chinese Journal of Geophysics, 2015, 58(6): 2046.
[18]Wang L.Y, Xu G.B. Post-test Estimation of Weighted Total Least Squares Adjustment Stochastic Model. Journal of Wuhan University·Information Science Edition, 2016, 41(2): 255-261.
[19]Li Y, Bai Y, Li C. PM10 Concentration Prediction Model Based on Wavelet Analysis and BP Neural Network. Environmental Monitoring Management and Technology, 2016: 24-28.
[20]Zhang L.F, Wang F, Yu L.B, et al. Experimental study on reducing the lower limit of measurement of tunable semiconductor laser absorption spectroscopy by wavelet analysis. Spectroscopy And Spectral Analysis, 2016, 36(06): 1794-1798.

Big Data Driven Blast Furnace Temperature Intelligent Prediction

Xueyong Jia[1,2], Jiahao Wang[1,3], Xiaojian Feng[4,]*
[1] Engineering Computing and Simulation Innovation Lab, North China University of Science and Technology, Tangshan 063210, Hebei, China
[2] College of Electrical Engineering, North China University of Science and Technology, Tangshan 063210, Hebei, China
[3] College of Science, North China University of Science and Technology, Tangshan 063210, Hebei, China
[4] Department of Discipline Construction, North China University of Science and Technology, Tangshan 063210, Hebei, China
**E-mail: 1845528549@qq.com*

Abstract: A non-linear time series prediction model based on nonlinear time series for RBF neural networks is proposed, which overcomes the problem that a single neural network is easy to fall into local minimum values and slow network training in nonlinear time series prediction. The key to the construction of RBF neural network is to select the center. The dynamic k-means clustering algorithm adopts the method of adjusting the cluster center to make the selection of the network center more precise. In this paper, the structural principle of RBF neural network is briefly described. Then the dynamic K-means algorithm is applied to the center selection of RBF neural network, and finally the simulation experiment is carried out. The simulation results show the practicability and effectiveness of the algorithm.
Keywords: RBF neural network; k-means; nonlinear time series; prediction

1. INTRODUCTION

Steel is one of the most important raw materials in modern society. Blast Furnace Ironmaking plays an important role in China's economic development. In the blast furnace production, maintaining a reasonable furnace temperature is one of the necessary conditions for production development. Due to the complexity of the blast furnace ironmaking process and the difficulty in measurement, it is difficult to directly measure the furnace temperature. Therefore, the silicon content of the blast furnace hot metal (generally called chemical heat) is used to indirectly reflect the temperature change in the furnace. The hot state of the blast furnace hearth. In reality, the way to detect the silicon content of molten iron mainly includes the on-site observation of iron and the monitoring of iron water quality. The method of direct observation has the accuracy and the iron water quality monitoring has a certain hysteresis, which cannot meet the real-time and accurate response to the production of blast furnace temperature and molten iron quality. The establishment of mathematical models for prediction has become an important means of predictive control of silicon content in molten iron.

In response to the structural problem of Radial Basis Function (RBF) neural network, Qiao Junfei et al. proposed a structural dynamic optimization design method, using Sensitivity analy (SA) to analyze hidden layer neurons. The effect of output weighting on the output of the neural network solves the problem that the RBF neural network has too large or too small RBF neural network structure [1]. Wei Min et al. used the gradient descent method and optimization method to derive the dynamic optimal learning rate of RBF neural network and applied it to the network learning algorithm. The prediction effect of RBF neural network with dynamic optimal learning rate is better than the traditional fixed learning rate. The RBF neural network has a faster convergence rate [2-8].

The prediction of silicon content in blast furnace hot metal belongs to time series forecasting problem. The main methods are traditional AR-MAX model and neural network method. The neural network expert system model is used to predict the silicon content of molten iron, which has strong nonlinear mapping ability. At present, BP neural network is used to predict the silicon content of blast furnace hot metal. However, in the BP learning algorithm, the network weight mainly depends on the first derivative information of the criterion function, and its convergence speed is relatively slow. At the same time, it may converge to a local minimum. The RBF neural network not only has strong nonlinear mapping ability, but also has the characteristics of fast convergence and global optimization. To this end, this paper uses the RBF neural network model to predict the silicon content of molten iron for the stick-square problem of blast furnace temperature. By using the dynamic K-means algorithm to optimize the RBF network center, a nonlinear time series prediction model based on RBF neural network is established. The model has high nonlinear mapping and parallel processing capability. The radial basis network (RBF) has excellent characteristics such as adaptive determination of network structure and output independent of initial weight. It can approximate any

continuous nonlinear function and can process the system. The inherently difficult to analyze law, the theory proves that the RBF network in the forward network is the optimal network of the full mapping function, and the effect is good in practice.

2. THEORETICAL KNOWLEDGE

RBF neural network is a kind of feedforward neural network with excellent performance. RBF network can approximate arbitrary nonlinear functions with arbitrary precision and has global approximation ability, which fundamentally solves the local optimal problem of BP network and has a compact topology. The structural parameters can be separated and learned, and the convergence speed is fast. The RBF network and fuzzy logic can achieve a good complementarity and improve the learning generalization ability of the neural network [3-5].

2.1. RBF Neural Network Algorithm

The neural network is a neural network model proposed by Moody and Darken. It simulates the neural network structure of local adjustment and mutual coverage in the human brain. It has a strong biological background and the ability to approximate any nonlinear function. The RBF neural network structure has three layers: the input layer, the RBF layer, and the output layer. The structure is shown in Figure 1. Each layer has a completely different function. The input layer consists of a number of source points (sensing units) that connect the network to the external environment; the second layer is the only hidden layer in the network. Its role is to perform a nonlinear transformation from the input space to the hidden layer space. The action function (base function) in the hidden layer node will locally respond to the input signal, that is, when the input signal is close to the central range of the basis function, the hidden layer node will produce a larger output, thus seeing this A network has local approximation capabilities. The output layer is linear, which provides a response to the active mode (signal) acting on the input layer [6-8].

The hidden layer function uses a Gaussian function:

$$G_i(r) = \exp\left(\frac{-r^2}{2\sigma_i^2}\right) \tag{1}$$

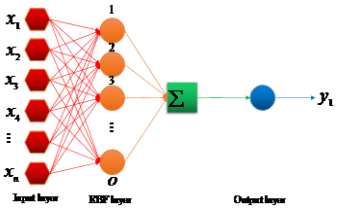

Figure 1. RBF neural network structure

2.2. Dynamic K-means Clustering Algorithm for RBF Network Center

The role of the dynamic K-means clustering algorithm in the selection of the RBF network center is to adjust the clustering center to make the selection of the network center more accurate [7-8]. Its calculation process can be briefly described as follows.

First, let the number of categories be 0 (the first input forces a category mode to be created to support the input). Later, each time a new input vector is encountered, the distance between it and any of the assigned category patterns is calculated. If the P th input vector is specified as $X^{(p)}$ and the j rd cluster center is C_j, the Euclidean distance d can be expressed as:

$$d = \left\| X^{(p)} - C_j \right\| = \left[\sum_{i=1}^{M} (X_i^{(p)} - C_{ji})^2 \right]^{\frac{1}{2}} \tag{2}$$

Where M is the dimension of the input vector.

Let the distance between input vector $X^{(p)}$ and all assigned pattern categories be known, and the nearest center to the input vector is C_k, where T is the number of known subcategories.

After determining the center closest to the input vector, k is determined, and thus d_0 is determined. First compare it to the distance limit of ρ, there are two cases:

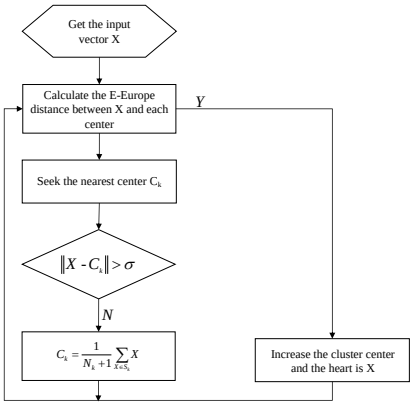

Figure 2. Dynamic clustering method

(1) When $d_0 < \rho$, the input vector $X^{(p)}$ is within the allowable error range when the input vector belongs to the k category. That is, if S_k is used to represent a set of all input vectors corresponding to the K th center, then $X^{(p)} \in S_k$. At this time, the idea of the k-means clustering method can be introduced, and the center update is performed by obtaining the average of all member vectors. which is:

$$C_k = \frac{1}{N_{S_k} + 1} \sum_{X \in S_k} X \tag{3}$$

Where N_{S_k} represents the number of input vectors to which the Kth cluster center is paired.

When $d_0 > \rho$, the input vector $X^{(p)}$ is within the allowable error range and thus cannot be assigned to the category. At this point, a new cluster center should be assigned centered on $X^{(p)}$, and the flow chart of the algorithm is shown in Figure 2.

(3) The above process uses the method of dynamic

clustering to find the center C_j of the network in real time. After determining the network center, the corresponding radius σ_i can be equal to the average distance between the training samples belonging to the class, namely:

$$\sigma_i = \frac{1}{T} \sum_{X^{(p)} \in S_j} (X^{(p)} - C_j)^T (X^{(p)} - C_j) \quad (4)$$

Algorithm design

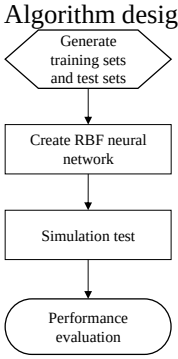

Figure 3. Model building process

Step 1. Determine the input layer and output layer of the RBF neural network according to the actual situation.

Step 2. Use the dynamic k-means mean algorithm to find the center and width of the RBF network.

Step 3. Use the negative gradient algorithm to find the weights.

Step 4. The flow chart for selecting the training sample and the test sample for the test model is as follows Figure 3.

2.3. Nonlinear Time Series Prediction Model based on RBF Neural Network

Nonlinear time series prediction model based on NAR model:

$$y_t = f(x_{t-1}, x_{t-2,} \cdots x_{t-p}) + e_t \quad (5)$$

Where: $E(e_t \mid x_{t-1}, \cdots) = 0$, and e_t have a finite variance of σ^2.

Then the minimum variance prediction is:

$$\hat{x}_t = \hat{f}(x_{t-1}, \cdots, x_{t-p}) \quad (6)$$

Using the RBF neural network to approximate function $\hat{f}$ is a one-step prediction:

$$\hat{x}_t = NN_\Phi(x_{t-1}, \cdots x_{t-p}) \quad (7)$$

The same reason can get two-step prediction:

$$\hat{x}_{t+1} = NN_\Phi(x_{t-1}, \cdots x_{t-p}) \quad (8)$$

By using the time series, the accuracy of one-step prediction is 0.59372, and the accuracy of two-step prediction is 0.57823. The simulation results are satisfactory, and the prediction results are highly accurate.

3. RESULTS SIMULATION

This paper selects 1000 sets of data to predict the furnace temperature using the improved RBF neural network model.

The last 500 sets of data were selected for prediction. The use of the graph clearly shows the magnitude of the error between the actual value and the real. The data is predicted from 900-975. It can be seen that this data can be very good to show that the predicted value is very similar to the real value, and satisfactory results can be obtained.

4. CONCLUSION

(1) The RBF neural network prediction model has the characteristics of simple structure and high prediction accuracy, and has obtained satisfactory results in predicting silicon content.

(2) Using the dynamic k-means algorithm to find the RBF network center, the selection of the network center is more accurate, and the prediction results are more accurate.

(3) The RBF neural network does not have the minimum problem of local minimum problem. The growth structure learning algorithm automatically constructs a near-optimal network, which fundamentally solves the over-fitting problem and improves the generalization ability of the network.

ACKNOWLEDGMENT

The research work was supported by the project grant of Innovation and Entrepreneurship Training Program of North China University of Science and Technology. Project number: X2018093.

REFERENCES

[1]Qiao J.F, Han H.G. Structural Dynamic Optimization Design of RBF Neural Networks. Journal of Automation, 2010, 36(06):865-872.

[2]Wei M, Yu L.A. RBF neural network with optimal learning rate and its application. Journal of Management Science, 2012, 15(04): 50-57.

[3]Krakowka A.R, Heimel N, Galgano F. Modeling Environmenal Security in Sub-Sharan Africa-Pro Quest. The Geographical Bulletin, 2012, 53(1): 21-38.

[4]Chen H.Y. A Nonlinear Time Series Prediction Model Based on Improved RBF Neural Network. Journal of Hunan University of Engineering, 2015, 25(01):41-43+47.

[5]Wu K.J, Wang T.J. Chaotic time series prediction based on RBF neural network optimization. Computer Engineering, 2013, 39(10):208-211+216.

[6]Wu C.G, Zhu S.Z, Wang B.H, Guan Y.H. POD-RBF neural network for nonlinear time series prediction. Small microcomputer system, 2013, 34(08):1848-1851.

[6]Guo L.P, Yu J.N, Zhang J.G, Qi Y.G, Zhang X.D. Nonlinear time series prediction based on genetic algorithm based on RBF neural network. Journal of Hebei Normal University, 2011, 35(03):244-247.

[6]Zhang D.Q, Ning X.X, Liu X.N. On-line prediction of nonlinear time series based on RBF neural network. Control Theory and Applications, 2009, 26(02):151-155.

Determination of Seat Volume Based on Grey Prediction

Zongchen Fan[1,], Chaoqun Ma[1,2], Mengxiao Li[1,2], Jian Xiao[1,2]*
[1] Mathematical Modeling Innovation Lab, North China University of Science and Technology, Tangshan, 063210, Hebei, China
[2] North China University of Science and Technology, Tangshan, 063210, Hebei, China
**E-mail: Zongchen_fan@163.com*

Abstract: With the progress of the times and the development of science and technology, the concept of sustainable development and the concept of scientific development have become an indispensable part of life. At the same time, the campus that shoulders the heavy responsibility of education, scientific research, and social services is also a major resource. Therefore, it is very important to build a conservation-oriented campus. In view of the irrational problems in the allocation of seats in the campus construction of North China University of Science and Technology, the relevant model process was established to evaluate and predict. Using grey predictions to predict the number of students in the school in the next three years, and to get the total number of students in the school, combined with the current number of seats in the school, the total number of seats per student in the school from 2019 to 2021 is 3.19, respectively. 2.98, 2.75, and thus the seat waste rate is 0.357, 0.313, 0.254. Finally, according to the seat waste rate, the school should make recommendations for the school, should take the seat waste rate as the upper limit, combined with the actual situation to close a certain proportion of classrooms, thereby reducing waste of resources and promoting the development of a conservation-oriented campus.

Keywords: grey forecast; seat volume; saving campus

1. PROBLEM RAISED

Forecast the changes in the number of seats in the next three years and give corresponding rewards and punishments to a certain aspect of the construction of a conservation-oriented campus based on the results obtained [1-5].

2. ESTABLISHMENT OF PREDICTIVE MODELS

2.1. Prediction of Seat Volume in the Next Three Years

Supposing sequentially$X^{(0)}$have observation value for n,generate new sequences by accumulating $X^{(1)} = \{X^{(1)}(1), X^{(1)}(2), \dots, X^{(1)}(n)\}$,then the corresponding differential equation of the GM(1,1) model is:

$$\frac{dX^0}{dt} + aX^0 = \mu \quad (1)$$

Among them: called the development gray number is α ; called the endogenous control number is μ.

Set α as the parameter vector to be estimated, which can be solved by the least squares method. Predict the model by solving the differential equation:

$$x_{k+1}^{(1)} = \left[x^{(0)}(1) - \frac{\mu}{\alpha}\right] e^{-ek} + \frac{\mu}{\alpha}, k = 1,2, \dots, n \quad (2)$$

2.2. Establishment of Grey Prediction Model

Because the analytic hierarchy process cannot accurately express the change relationship of the future seat volume, it has a certain impact on the accuracy of the test results, as Table 1. Therefore, the GM(1,1) model in the grey forecast is used to predict the number of people reporting 2019, 2020, and 2021 in the next three years. Find out the number of students reported by the University of Science and Technology in 2015, 2016, 2017, and 2018. The following Table 1 shows the following [6-10].

Table 1. Number of people reported in 2014-2018

Year of enrollment / year	2014	2015	2016	2017	2018
Admission number / person	5716	5612	6674	6944	7406

(1) The GM(1,1) model is used to predict the number of people reported in the three years of 2019, 2020, and 2021. The prediction formula is:

$$\mathrm{P} = (1 - e^{-0.1017})(x^{(0)}(1) - \frac{4895.9397}{-0.1017}) \quad (3)$$

(2) According to the formula, the results are 7822, 8659, and 9587 respectively. Considering that most of the students are in the four-year system, according to the number of people reported in recent years, the formula (10) is used to calculate the total number of students in the next three years, which are 28846, 30831, and 33474, respectively.

$$P_z = \sum_{a=1}^{4} P_a \quad (4)$$

(3) According to the predicted total number of students in the three years, the actual per capita seats in the year are calculated by formula (11) to be 3.19, 2.98, 2.76.

$$Z_s = S/P_z \quad (5)$$

2.3. Determination of the Per Capita Seat Waste Rate

Based on model building and actual analysis, Find the per capita reasonable seat occupancy and per capita actual seat occupancy in 2018 and 2019Therefore, according to formula (6), the per capita seat waste rate is calculated to be 0.406 and 0.357 respectively.

$$\mathrm{D} = \frac{Z_2 - Z_3}{Z_2} * 100\% \quad (6)$$

According to the data obtained from the gray forecast, the per capita seat waste rate in 2020 and 2021 is predicted to be 0.313 and 0.254.

2.4. Determination of Rewards and Punishments in Energy Conservation

The school establishes relevant classrooms and self-study rooms, and regulates students' self-study attitudes. This is used as a comprehensive assessment at the end of the period.

Privately occupy the classroom and study room, minus 5 points.

Privately occupy the classroom, study room and lock the door, prohibit others from entering, deduct 10 points.

Self-study littering, minus 2 points, and carry out sanitary labor.

Influencing others to self-study, minus 2 points.

Self-study littering and affecting others' self-study, minus 5 points, and carrying out sanitary labor.

Take up more than one seat and subtract 2 points.

1 months of self-study performance, plus 2 points, can be accumulated.

Excellent self-study in 8.1 semesters, plus 15 points, other points are not cumulative.

Students can be educated on multiple violations of relevant content.

3. RESULT ANALYSIS

According to the data obtained by the gray forecast, the per capita seat waste rate in 2020 and 2021 is predicted to be 0.313 and 0.254 [11]. It can be seen from the calculation results that there is a problem of seat waste in our school, which may cause waste of resources in power, manpower and material resources. It is also foreseeable that in the next few years, due to the expansion of enrollment in schools, the seat waste rate will decrease year by year, but there is still waste. Based on the above results, it is recommended that the school can reduce the seat waste rate to achieve energy saving purposes by combining the actual situation with the seat waste rate as the upper limit and closing the classroom according to a certain percentage.

REFERENCES

[1]Feng L.Y, Ming M.M. Research on the Evaluating Campus Evaluation Index System Based on Analytic Hierarchy Process (AHP)—Taking Inner Mongolia University of Finance and Economics as an Example. Journal of Kunming Metallurgy College, 2013, (04):22-25.

[2]Wang W. Research on determining the weight of influencing factors of contact network segment quality evaluation based on analytic hierarchy process. China Railway, 2019, (04):60-64.

[3]Luo D, Wei B.L. A Unified Processing Method and Application of a Class of Discrete Grey Prediction Models. Systems Engineering-Theory & Practice, 2019, 39(02): 451-462.

[4]Tong M.Y. Grey modeling method and its application in prediction. Chongqing University, 2016.

[5]Xie M. Multi-attribute grey decision-making method based on analytic hierarchy process and its application. Mathematics in Practice and Theory, 2018, 48(20):107-113.

[6]Lei M.Y, Mu Z.H, Lei J.C. Progress and Prospects of Economical Campus Construction at Present. China New Communications, 2019, 21(05): 167.

[7]Shi H.P, Yu Y.Y, Dong X.C. Research on the Construction of Economical Campus and the Cultivation of Young Talents. University Logistics Research, 2018, (02): 19-21.

[8]Chen Z.X. Logistics Management and Innovation of Colleges and Universities under the Background of Economical Campus. Journal of Kunming Metallurgy College, 2017, 33(02):8-13.

[9]Yu W.J. Research on the Construction of Economical Campus. China Collective Economy, 2017, (06): 127-128.

[10]Yin S, Yan X.L. Progress and Prospects of China's Economical Campus Construction. Construction Technology, 2016, (12):10-12.

[11]Wang Q, Chen K. Data mining and analysis of energy-saving campus building energy consumption. Modern Economic Information, 2015, (24): 8

.

Optimization Model of Trajectory Design and Control Strategies for Aircraft' Soft-landing

Yujie Jiang[1,2,], Ruonan Wu[1,2], Jing Wang[1,2], Xiaoqiang Guo[1,3]*
[1] Engineering Computing and Simulation Innovation Lab, Tangshan, 063000, Hebei, China
[2] College of Economics, North China University of Science and Technology, Tangshan, 063210, Hebei, China
[3] College of Science, North China University of Science and Technology, Tangshan, 063210, Hebei, China
**E-mail: 2310905017@qq.com*

Abstract: Soft-landing is a key problem for lunar exploration. Based on the braking and soft-landing of the moonlight of Chang'e-3, the optimal control problem of soft-landing is transformed into a linear constrained quadratic regulation problem based on rendezvous and docking idea. The soft-landing control is realized by the position of the aircraft relative to the landing point and state feedback. The corresponding coordinate system is established with the predetermined landing point as the origin of coordinate, and the nonlinear kinematics model of the aircraft is obtained. After reasonable approximation, and considering the fuel optimization, control thrust and state constraints, the optimal state feedback controller design method is given by using the linear constrained quadratic regulation theory.
Keywords: two body problem; trajectory design; kepler motion; optimal control

1. INTRODUCTION

The moon is rich in material resources, containing all the elements in the earth's crust and most of the mineral deposits. Through the study of the origin and evolution of the moon, it will provide a basis for the establishment of the lunar base after the space station, so the lunar exploration has an important historical reason and research significance. The braking and soft-landing of the moonflight are one of the most critical technical aspects in the lunar exploration program [1-3]. During the lunar landing flight, the trajectory is mainly divided into three parts: the earth escape stage, coast arc stage, and lunar capture stage. The coast arc stage refers to this part from the near-earth orbit to the near-moon orbit. The main braking problem is to consider the orbit design [4-6] and the orbital control problem [7-8] of the aircraft. The lunar capture section mainly refers to the soft-landing part of the aircraft. The braking mode is mainly divided into three types: gravity-turn braking method, nominal orbit braking method and explicit braking method.

2. SOFT-LANDING DYNAMICS MODEL OF AIRCRAFT BASED ON TWO BODY PROBLEM

Figure 1 shows the whole process of the lunar landing aircraft from ground to soft-landing on the moon. Firstly, the aircraft is carried by a rocket and sent from the ground to a predetermined earth parking orbit. After entering orbit, the aircraft detects its attitude, speed and position, determines the working status of each part, and then establishes communication with the ground. When the time is right, the thrust engine drives the aircraft off the earth parking orbit and into the moon transitional orbit, as shown in ②in figure 1. In order to reduce fuel consumption, the engine will stop working and flow to the moon at its own speed and gravity. During this period, two attitude adjustments and two to three orbit corrections are needed. The main purpose of orbit correction is to make the aircraft have accurate flight direction at the entry point of the transitional orbit between the earth and the moon, and to ensure that the aircraft enters the parking orbit on the moon. After entering the lunar parking orbit, the lunar landing aircraft will redetect its speed, position and attitude data, and calculate the optimal Horman orbital point to complete the orbit change task. When the time phase point arrives, the engine is pushed back and decelerated, and the aircraft is orbited into the near-moon orbit. The braking and control for a soft landing is implemented at the approach point of the lunar transfer orbit, that is, ⑥in the Figure 1.

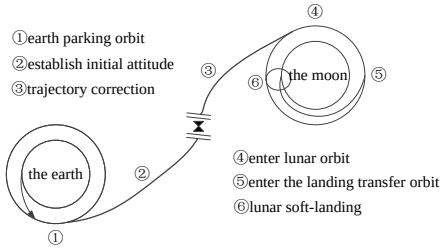

Figure 1. The diagram of the whole flight process of lunar landing

In order to accurately analyze the state of the aircraft during flight, three classical physics formulas are firstly introduced:

①Formula of universal gravitation $F = \frac{GMm}{r^2}$

②Kepler ' s second law$vr\ sin\ \theta = k$

The motion of Chang'e-3 around the moon can be approximately regarded as the motion of planets in the solar system around the sun, which satisfies the applicable conditions of the above two formulas.

③Formulas for calculating work $W = Fs \cdot cos\ \theta$

After Chang'e-3 entered the elliptical orbit around the moon, it was in the conservative field where the moon was located. Because there is no atmosphere on the moon, the atmospheric drag is not considered in the

dynamic model of Chang'e-3. The soft-landing time from orbit altitude of about 15 km to lunar surface is short, usually within ten minutes. Therefore, the gravitational perturbation of the sun and the earth to the moon can be neglected, and only the motion rules under the "two-body model" of the moon and Chang 'e-3 need to be studied. In order to more intuitively represent the Chang 'e-3 landing preparation orbit, the schematic diagram is as follows:

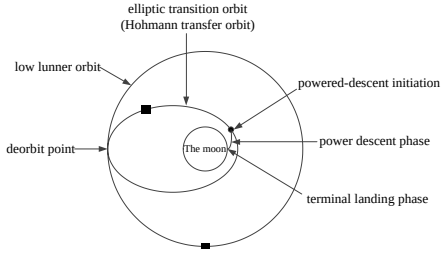

Figure 2. The diagram of landing preparation trajectory of Chang'e-3

According to Figure 2, the speed of Chang'e-3 at perilune and apolune in the elliptical orbit is angular to the vector diameter, which can be obtained from Kepler's second law:

$$k = v_1 r_1 \sin 90^\circ \quad (1)$$

$$k = v_2 r_2 \sin 90^\circ \quad (2)$$

Combine formula (1) and (2),

$$v_1 r_1 = v_2 r_2 \quad (3)$$

Taking the infinity as the zero potential energy point in the gravitational field of the moon, the potential energy $-\frac{GMm}{r}$ of Chang'e-3 at any point in the elliptical orbit has the kinetic energy of $\frac{1}{2}mv^2$, so the total energy can be expressed as $E = \frac{1}{2}mv^2 - \frac{GMm}{r}$

Then the total energy of Chang'e-3 at the near and far moon points is respectively: $E_1 = \frac{1}{2}m{v_1}^2 - \frac{GMm}{r_1}$

$$E_2 = \frac{1}{2}m{v_2}^2 - \frac{GMm}{r_2}$$

According to question, the total energy of the Chang'e-3 in the landing orbit is conserved, thus it can be obtained that $E_1 = E_2$,that is

$$\frac{1}{2}m{v_1}^2 - \frac{GMm}{r_1} = \frac{1}{2}m{v_2}^2 - \frac{GMm}{r_2} \quad (4)$$

Since the average radius, equatorial average radius and polar radius of the moon are 1737.013km, 1737.646km and 1735.843km respectively, and the shape oblateness of the moon is 1/963.7256. The moon is regarded as a sphere and its average radius 1737.013km is taken as the radius of the sphere.

The distance from the near and far moon points to the surface of the moon is much smaller than the average radius of the moon, so the average radius of the moon cannot be ignored. The perilunar to the center of the moon is equal to the sum of the distance from the perilunar to the surface of the moon and the mean radius of the moon. So,

$$r_1 = 15 + 1737.013 = 1752.013km \quad (5)$$

The same can be

$$r_2 = 100 + 1737.013 = 1837.013km \quad (6)$$

Combine fomular (3)、(4)、(5) and (6), substitute G、M, we can conclude that

$$v_1 = \sqrt{\frac{2GMr_2}{r_1(r_1+r_2)}} = 1.6927km \cdot s^{-1} \quad (7)$$

Substitute equation (7) into equation (3), we can conclude that

$$v_2 = \frac{r_1}{r_2}v_1 = 1.6144km \cdot s^{-1} \quad (8)$$

The basic requirements of Chang'e-3 landing orbit design: the preparation orbit for landing is the orbit near the moon and the orbit far away from the moon; The landing orbit is from the near moon point to the landing site, and the soft landing process is divided into six stages: landing preparation orbit, main deceleration, attitude adjustment, obstacle avoidance stage, fine obstacle avoidance, and slow decline stage. Minimize fuel consumption during soft-landing.

Because Chang'e-3's landing site is $(19.51°W, 44.12°N)$, leaning toward the very low part. According to the data, the longitude and latitude of Chang'e-3 are basically unchanged. According to astronomical knowledge, we can see that the plane of the landing orbit is perpendicular to the equatorial plane of the moon, parallel to the longitude plane $44.12°N$, and the landing orbit is from low latitude to high latitude. Make the schematic diagram as follows Figure 3:

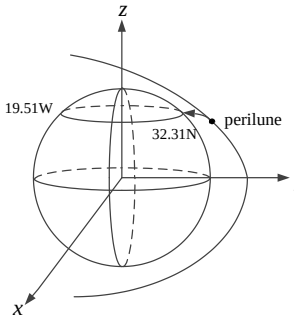

Figure 3. The diagram of landing orbit

Chang'e-3 began to decline at the perilune. The strength and direction of the initiative force of Chang'e-3 have been changing all the time. Therefore, we calculate the kinetic energy change by calculating the external work of the initiative force, which can omit the calculation process and simplify the calculation. In this process, gravity does positive work and Chang'e-3 does negative work. The whole process of descent is T.The work did by combined external force equals to the change of kinetic energy:

According to the kinetic energy theorem:

$$mg_0 \times (h_0 - H(T)) - \int_0^T (F(t) \times v(t))dt = \frac{1}{2}m \times (v_T^2 - v_1^2) \quad (9)$$

The horizontal displacement of the time period T:

$$x(T) = \int_0^T (\cos\theta(t) \times v(t))\,dt \quad (10)$$

In the model hypothesis, we assume that Chang'e-3 always moves in a plane perpendicular to the lunar equator during the descent process. We can get the conversion relationship between distance and latitude

through relevant geographical knowledge:

$$p = \frac{360}{2\pi R} = 30.301 \text{ kilometer per degree}$$

Where P is the horizontal distance changed by the change of latitude by $1°$.

According to the law of conservation of energy, it can be known that:

$$\frac{1}{2}mv_1^2 + mg_0r_1 = \frac{1}{2}mv_2^2 + mg_0r_2 \quad (11)$$

Because the engine thrust is mainly used to reduce the aircraft lateral velocity, and overcome the radial velocity caused by the moon's gravity. Assuming that the Chang'e-3 can through regulating mechanism made itself by constant force in vertical direction in the process of movement direction downward, horizontal direction also subjected to constant force, and its direction is in contrast to the horizontal velocity, with initial speed of 1.6927km/s. Therefore, the parabolic descent process can be decomposed into the motion of uniform acceleration in the vertical direction and uniform deceleration in the horizontal direction. Chang'e-3 is basically located above target in $3km$. Therefore, the horizontal velocity approximately to 0, and 57m/s was its vertical velocity, as Figure 4.

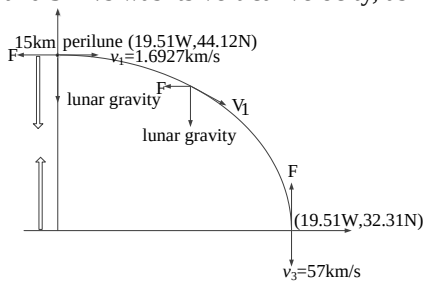

Figure 4. Force analysis of Chang'e-3 in the landing orbit

Among them,

$$h_1 = \frac{v_3}{2}t_1$$

$$v_3 = 0.057km \cdot s^{-1}, h_1 = 12km$$

We can conclude that

$$t_1 = 421.02s$$

Converted to latitude:

$$\frac{357.89}{30.301} \times 1° = 11.81°$$

According to the location of the landing site $(19.51°W, 44.12°N)$, from figure 2, Chang'e-3 is moving from south to north, so the position of the perilune is $(19.51°W, 32.31°N)$ with an altitude of 15 km.

Since the near and far moon points are the two endpoints of the long half axis of the elliptical orbit respectively, and the line between the two points passes through the center of the moon (figure 5), it can be known from symmetry that the position of the far moon point is $(160.49°E, 32.31°S)$ and the height is 100 km.

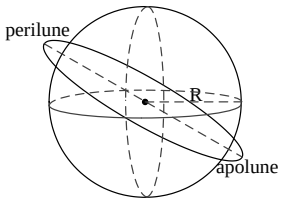

Figure 5. The diagram of relative position of near and far moon

3. TRAJECTORY DESIGN AND OPTIMAL CONTROL STRATEGIES

According to the momentum theorem,

$$\begin{cases} F_g t = m_1 u_1 + \Delta m \cdot v_e - m_0 v_0 \\ m_1 = m_0 - \Delta m \end{cases}$$

Solving the equation:

$$F_g t = \Delta m(v_e - v_1) + m_0(v_1 - v_0) \quad (12)$$

It can be seen from the formula $F_g t = \Delta m(v_e - v_1) + m_0(v_1 - v_0)$, the shorter the braking time, the more fuel is saved. So the minimum fuel consumption is the optimization goal.

As shown in Figure 5, for the kinetic problem of known displacement and initial velocity, the first acceleration and then deceleration is the most time-saving, that is, the most fuel-saving. This picture is a velocity time image that illustrates how the known displacement and the initial and final speeds minimize the amount of exercise time used. Two of the shaded parts are equal in area.

Such problems are involved in the rapid attitude adjustment, obstacle avoidance stage, fine obstacle avoidance, and slow decline stage. In order to visually show the process of the soft landing of the Chang'e-3, the dynamic model of each stage is analyzed below, and the schematic diagram is as follows Figure 6.

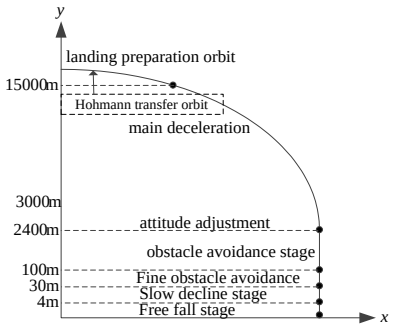

Figure 6. The diagram of Chang'e-3 landing path

The Chang'e-3 aircraft entered the soft-landing orbit from the perilune, and the landing preparation orbit was in the same plane as the soft-landing orbit. According to this, the soft-landing orbit is on the plane passing through the landing point and the moon center. In reality, the plane that satisfies this condition is not unique. However, in order to express this process more simply and clearly, the soft-landing orbital plane can be constrained to the plane of the polar axis (north and south poles) of the moon, that is, the plane where the landing point and the polar axis are located as the plane of the soft-landing orbit. Based on this, a plane coordinate system is established, as shown in Figure 7.

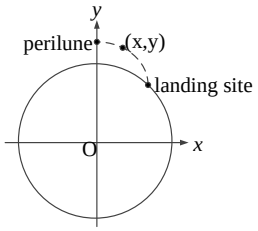

Figure 7. The diagram of planar coordinate systems of soft-landing orbit

The rectangular coordinate system is based on the moon center, with the straight line pointing to the near moon point as the axis, the vertical direction as the axis, and the positive direction pointing to the south. In this coordinate system, the soft-landing process of the Chang'e-3 can be subdivided into six phases, the main deceleration stage, rapid attitude adjustment, coarse obstacle avoidance phase, precision obstacle avoidance phase, slow phase, and free fall stage. The stress state and change of each stage are basically the same. Therefore, the general force analysis model of Chang'e-3 is given here, and then the optimal control strategy of each stage is discussed separately.

Assume that the main engine thrust component of the Chang'e-3 soft-landing process is $u_x(t)$ and $u_y(t)$, and the initial conditions of the position and velocity of each stage are$\big(x(t_0), y(t_0), v_x(t_0), v_y(t_0)\big)$, and the termination condition is$\big(x(t_e), y(t_e), v_x(t_e), v_y(t_e)\big)$, then the force of the Chang'e-3 during the landing process is as shown in Figure 8 .

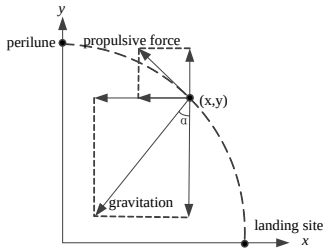

Figure 8. The force diagram of Chang'e-3 landing process

Based on this, the equation of motion of the Chang'e-3 was established:

$$\frac{d^2x}{dt^2} = \frac{GM}{x^2+y^2} sin\,\alpha\,(t) + \frac{u_x(t)}{m(t)}$$
$$\frac{d^2y}{dt^2} = \frac{GM}{x^2+y^2} cos\,\alpha\,(t) + \frac{u_y(t)}{m(t)}$$

Where,$\alpha(t) = arctan\frac{x(t)}{y(t)}$, and by the Chang'e-3 main engine specific impulse definition,

$$\frac{dm}{dt} = \frac{\sqrt{u_x^2(t)+u_y^2(t)}}{v_e}$$

v_e is the specific impulse of the engine, the goal of optimal control is the fuel economy, that is

$$min\,z = \int_{t_0}^{t_f} \frac{\sqrt{u_x^2(t)+u_y^2(t)}}{v_e} dt$$

Taking into account the constraints of the state of each stage, the problem can be reduced to the following optimization model:

$$\begin{cases} z = \int_t^{t_f} \frac{\sqrt{u_x t + u_y t}}{v_e} dt \\ st. \frac{dx}{dt} = \frac{GM}{x+y}\alpha t + \frac{u_x t}{mt} \\ \frac{dy}{dt} = \frac{GM}{x+y}\alpha t + \frac{u_y t}{mt} \\ \frac{dm}{dt} = \frac{\sqrt{u_x t + u_y t}}{v_e} \end{cases} \tag{13}$$

$$m(t_0) = m_0, x(t_0) = x_0, y(t_0) = y_0, \frac{dx}{dt}(t_0) = v_{x_0}, \frac{dy}{dt}(t_0) = v_{y_0}$$
$$m(t_f) = m_f, x(f) = x_f,$$
$$y(t_f) = y_f, \frac{dx}{dt}(t_f) = v_{x_f}, \frac{dy}{dt}(t_f) = v_{y_f}$$

It is noted that the optimal control problem for different stages is mainly the difference between the corresponding initial state and the terminating state constraint, and the basic model is similar.

(1) The motion model of the Chang'e-3 in the vertical direction

For the dynamics model of the rapid attitude adjustment, coarse obstacle avoidance phase, precision obstacle avoidance phase, and slow phase, the model analysis shows that to minimize fuel consumption, the time spent in each phase should be minimized, so we take the lead. So we take the strategy of turning off the engine first to let it fall freely and then slow down.

Acceleration phase:

$$\begin{cases} y = v_0 t_1 + \frac{1}{2} g t_1^2 \\ g = \frac{GM}{R^2} \end{cases} \tag{14}$$

Deceleration phase:

$$\begin{cases} \frac{dy}{dt} = v \\ \frac{dv}{dt} = -\left(\frac{F}{m} - \frac{GM}{R^2}\right) \\ \frac{dm}{dt} = -\frac{F}{v_e} \end{cases} \tag{15}$$

(2) The movement model of the Chang'e-3 in the horizontal direction

In the rapid attitude adjustment, coarse obstacle avoidance phase, precision obstacle avoidance phase, and slow phase, the translational motion is the same. They all adopt the motion mode of accelerating first and then decelerating. The position of the most suitable landing is determined by analyzing the digital elevation model and the horizontal distance from the Chang'e-3 is calculated. Assuming the distance is S, the horizontal thrust is F' , and the following differential equations are listed:

$$\begin{cases} \frac{ds}{dt} = v \\ \frac{dv'}{dt} = \frac{F'}{m} \\ \frac{dm}{dt} = \frac{F}{v_e} \end{cases} \tag{16}$$

For a more intuitive view of the landscape near the lunar landing site, a three-dimensional view of the lunar surface is shown Figure 9:

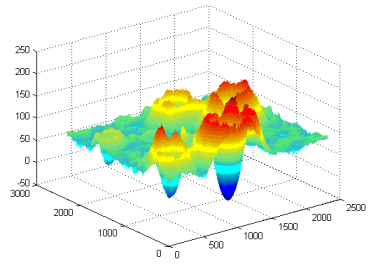

Figure 9. The stereogram at $2400m$ above ground

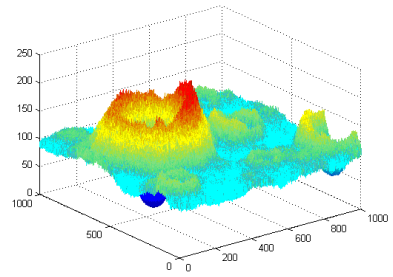

Figure 10. The stereogram at $100m$ from the ground

In order to determine the landing position of Chang'e-3, the digital elevation maps at $2400m$ and $100m$ from the lunar surface can be used to make contour maps as shown in Figures 10-11.

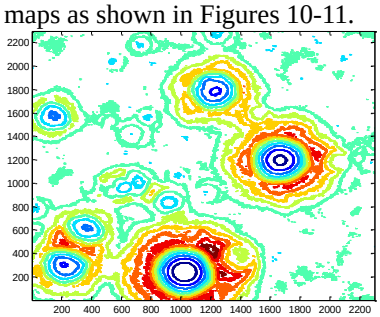

Figure 11. The contour plot at $2400m$ altitude

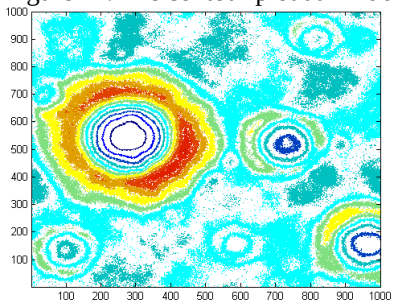

Figure 12. The contour plot at $100m$ altitude

The red and yellow parts of the contour map indicate areas with high altitude, the blue and green parts indicate that the lower area is also placed, and the white elevation is between green and yellow. Chang'e-3 is located directly above the contour plot. The narrow spacing of the contour lines reflects the large fluctuation of the terrain, which is not suitable for the landing of the Chang'e-3. In the case of considering the shortest distance and reducing the energy consumption, in the contour map taken at 2400m, roughly select the area near (1150,1150) for selection, and the contour plot of the shot at 100 meters, select (550,300) landing nearby.

4. CONCLUSION

This paper is a combination of theoretical derivation and data processing analysis. Firstly, under the premise of reasonable assumptions, the landing problem of Chang'e-3 is transformed into a "two body problem" and a corresponding dynamic model is established. Using the knowledge of classical physics celestial problems, a simple mathematical model was established by using Kepler's second law and the law of conservation of energy. The speed and position of the near-month and far-moon points of the Chang'e-3 in the orbit were determined. Then, the strategy of optimum design and control is completed with the idea of stages. Combining with the control requirements of each stage, the knowledge of physical dynamics is used to solve the problem. Taking the minimum fuel consumption as the optimization objective, the ordinary differential equations of each stage are established, and the total time consumption and fuel consumption weight of Chang'e-3 soft-landing process are obtained by solving the equations.

Finally, through error analysis and sensitivity analysis of landing point accuracy and orbit stability, the practical feasibility of the orbit was verified, and the requirements of fuel saving and safe landing of Chang'e-3 were realized, which laid a foundation for the historical return stage of lunar exploration and the realization of manned landing on the moon in China.

REFERENCE

[1]Cheng R.K. Lunar Terminal Braking, Lunar Missions and Exploration. New York Wiley, 1964, 308-355.

[2]He Y, Luo Q, Liu J.H, Trajectory design and Control Strategies of Chang'e-3 Soft-landing Orbit. silicon valley, 2014, 33(23):14-19.

[3]Zhu D.Y. The tenth National Postgraduate Mathematical Modeling Competition. Practice and Cognition of Mathematics, 2014, 44(14):1-70.

[4]Tang Q. Fast optimization of trajectory for lunar soft landing. computer simulation, 2007, (12):24-27.

[5]Liu X.W. Attitude control of the soft landings terminal phase for lunar lander. Harbin Institute of Technology, 2007.

[6]Wang J, Li J.F, Cui N.G, Liu H. On initial point selection of the continued-propulsion soft-landing trajectorie. Engineering Mechanics, 2003, (06): 145-148.

[7]Guo Z. A study on the optimal low-thrust orbit maneuver of lunar satellite. Acta Astronomica Sinica, 2000.

[8]Li T, Yang D, Cui H.T. One method of calculating cislunar transfer trajecotry. Journal of Astronautics, 2003.

Characteristics and Causes of Ozone Concentration in Beijing

Hao Qin, Xinyan Dong, Hanying Li*
College of Science, North China University of Science and Technology, Tangshan, 063210, Hebei, China
**E-mail: qh981124@163.com*

Abstract: Photochemical smog pollution is an important environmental issue affecting air quality in Beijing. Using the National Population and Health Science Data Sharing Service platform to provide Beijing's 2015-2016 ozone and temperature, precipitation and positive relative humidity and other meteorological data, the hourly measurement data, the basic characteristics of ozone concentration in Beijing, and the combination of meteorology. The factors are correlated with ozone meteorology and a quantitative calculation model is given. Through the analysis of the characteristics and causes of ozone concentration in Beijing, it is expected to provide reference for the prevention and control of ozone pollution in North China.

Keywords: Beijing; ozone; spearman correlation; meteorological factor

1. INTRODUCTION

Ozone (O_3) plays an important role in global and regional atmospheric environmental changes. It not only has an important impact on the geothermal radiation budget system, but also has significant environmental effects. As a secondary pollutant, near-surface ozone not only causes direct or indirect damage to vegetation crops and ecological environment, but also causes certain harm to human health by affecting the human respiratory system [1-4]. Therefore, it is of great practical significance to study the synergy between meteorological elements and related sensitive diseases.

Ozone near the ground is mainly derived from photochemical smog [5], but local ozone concentration will be significantly affected by meteorological factors [6-8]. Experts believe that ozone pollution incidents generally occur under conditions of high temperature, strong radiation, and relatively low temperature. Due to many factors, the meteorological conditions and photochemical pollution in different regions are different, and there may even be large differences. Liu et al. believe that the concentration of VOC in Beijing affects the ozone concentration in summer. In the weather with small wind or static wind, high temperature and high humidity, ozone is likely to exceed the standard [9]. This is caused by the influence of meteorological factors on the surface ozone concentration. Less low cloud cover, suitable relative humidity, strong solar radiation, small ground wind speed and specific wind direction will lead to the emergence of high concentration ozone. Among them, ultraviolet radiation and temperature are important factors affecting ozone concentration. In Deng Xuejiao and Yang Jie's research, it is also clear that terrestrial ultraviolet radiation has a significant impact on the photochemical reaction of ozone generation [10]. High temperature brings strong ultraviolet radiation, which promotes the photochemical reaction and increases the concentration of ozone.

Through the above research and analysis, we can find that meteorological factors such as temperature, ultraviolet radiation, wind speed, relative humidity, cloud and fog have an important effect on the near-surface O_3 concentration, but in different cases, the dominant factors are not the same. Guided by various meteorological causes, the ground O_3 gradually accumulates, causing the concentration to rise. Based on the time-lapse data from 2015 to 2016 in Beijing, this study explores the causes and health effects of gas pollutants and meteorological conditions from multiple time granularities, and establishes quantitative models for meteorological and environmental data. In order to provide reference for the prevention and control of ozone pollution in North China.

2. ANALYSIS OF OZONE CONCENTRATION CHARACTERISTICS IN BEIJING

The daily maximum 8h average ozone concentration of Beijing in the three years of the year, month and day was analyzed. From the special trend of ozone concentration trend and its concentration change, the basic concentration of Beijing 2016-2017 was obtained.

2.1. Basic Situation of Ozone Pollution

Statistics on the maximum 8h average concentration frequency of ozone day from January 2016 to December 2016 in Beijing, and plot the frequency distribution in Figure 1.

As can be seen from the above figure, the average 8h average concentration of ozone in Beijing in 2016 is $60 \sim 120 \mu g / m^3$, with an average of $93.41 \mu g / m^3$. The maximum daily concentration of 8h is greater than $200 \mu g / m^3$, which occurs for 35 days, mainly distributed from August to November, up to $284.25 \mu g / m^3$. The average concentration is less than 20 and occurs for 43 days, mainly distributed from January to April, with a minimum of $9.32 \mu g / m^3$.

According to the above analysis, the ozone concentration is related to the season month, and the concentration is highest between May and July of the year. This is because the temperature is higher during this period, the solar radiation is enhanced, the precipitation is less, and the photochemical reaction is become more which causes the ozone concentration to approach the peak and stays at a higher range.

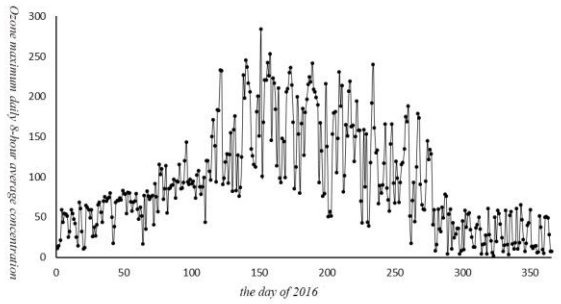

Figure 1. Beijing 2016 average concentration frequency distribution graph

2.2. Analysis of the Characteristics of Ozone Monthly Concentration Change

The average value of ozone pollution concentration in Beijing from 2015 to 2016 was statistically analyzed, and the monthly mean value curve was plotted as shown in Figure 2.

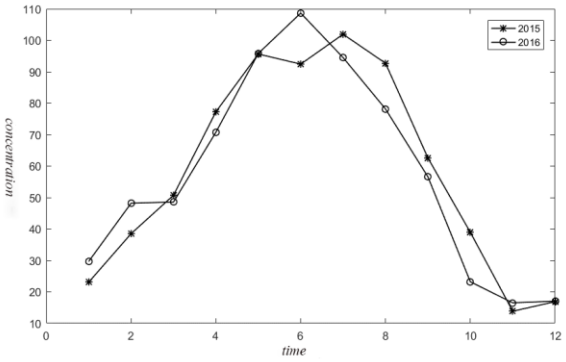

Figure 2. O_3 pollution monthly mean concentration change graph

It can be seen from Figure 2 that from the change of ozone concentration in the year from 2015 to 2016 in Beijing, the concentration of the ozone is first increased to a certain peak and then decreased. The average concentration of ozone in 2015 is $58.08\mu g/m^3$ at 7 The peak of the month is $101\mu g/m^3$, and during the period from May to August, the monthly concentration of ozone continues to peak. The average monthly concentration of ozone in 2016 is $57.5\mu g/m^3$, peaking in June, and the monthly concentration is at a higher value during the period from May to 7. Overall, Beijing's ozone concentration changes in 2016 are more volatile. In the second half of 2016, the ozone concentration has a downward trend. In 2016, the ozone concentration decreased compared with 2015, indicating that Beijing has continuously improved the city through various methods and measures. The ozone concentration improves the environmental quality.

2.3. Analysis of the Variation Characteristics of Daily Ozone Concentration

The two days with the highest daily average concentration in 2015 and 2016 were selected for statistical analysis, and the daily concentration curve was drawn.

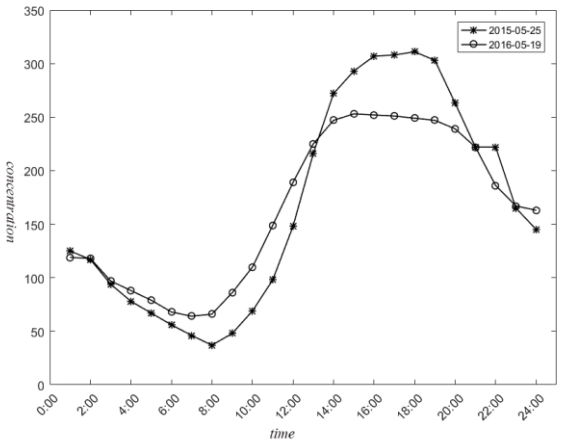

Figure 3. O_3 Pollution day concentration change graph

By analyzing the above Figure 3, the hourly average value of ozone starts to rise at 8:00 am and peaks between 14:00 and 19:00 in the afternoon, starting from 20:00 in the evening to 8:00 in the next day, and between 7:00 and 9:00 in the morning. When the valley value is reached, the daily variation of ozone concentration is remarkable. From 8:00 in the morning, with the increase of temperature, the increase of solar radiation, various exhaust emissions and other factors, the ozone concentration gradually increased; the temperature reached the peak in the afternoon, the solar radiation increased, which promoted the photochemical reaction of the gas to generate ozone; The solar radiation is weakened, and the photochemical reaction is reduced, resulting in a slow increase in ozone concentration. At the same time, the reducing agent such as NO reacts reversibly with ozone, and continuously consumes ozone, causing its concentration to fall to the valley before sunrise; The increase in ultraviolet radiation and the near-surface ozone concentration have started a new round of upward trend. Compare the two days with the highest concentration on two days. It can be found that the peak ozone concentration in 2016 is lower than that in 2015, and the ozone concentration changes with the increase of solar radiation and temperature in the afternoon, indicating that the ozone prevention work in Beijing has achieved good results.

3. OZONE METEOROLOGICAL ANALYSIS

Based on the above analysis of the characteristics of ozone concentration in Beijing, in order to more clearly understand the specific reasons for the change of ozone concentration with time, the cause of ozone

meteorology is analyzed in combination with the climate factors of Beijing from 2016 to 2017.

3.1. Correlation Analysis between Temperature and Ozone Concentration

The Spearman correlation analysis was performed by selecting the monthly average temperature and the monthly average ozone concentration in 2016-2017. The results are shown in Figure 4.

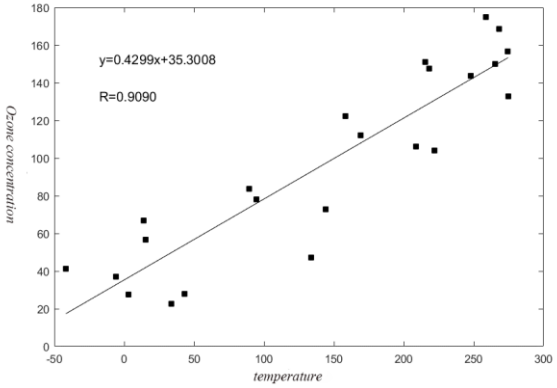

Figure 4. Temperature-ozone spearman correlation analysis graph

It can be seen from the above figure that the temperature is linear with the ozone concentration. The correlation coefficient between temperature and concentration is calculated as R=0.9151, that is, the temperature has a positive correlation with the ozone concentration, and the temperature is one of the influencing factors of the ozone concentration increase. By observing the trend of the linear equation, as the temperature increases, the solar radiation continues to increase, the photochemical reaction proceeds, the ozone concentration shows an increasing trend, and the growth law of the ozone concentration under the influence of temperature can be obtained. The equation is as follows:

$$y=0.4335x+34.7426 \quad (1)$$

The monthly average ozone concentration change trend is the same as the temperature change trend, and has other environmental influence factors. Therefore, in order to better reflect the strong correlation between temperature change and ozone concentration change, the average daily temperature and temperature in July with the highest monthly average temperature in 2016 were selected. The trend curve is shown in Figure 5.

As can be seen from the analysis in Figure 5, the maximum concentration of ozone on the 8h day has the same trend as the average daily temperature. The temperature decreases in the middle of July, the solar radiation decreases, and the ozone concentration decreases. At around the end of July, the temperature rose, the solar radiation gradually strengthened, and the ozone concentration peaked. All day, the curves of the two are close to the same, showing a good positive correlation. As the temperature rises, the UV radiation is strengthened, the photochemical reaction rate is increased, and the decomposition of oxygen molecules in the atmosphere is enhanced, resulting in an increase in ozone concentration.

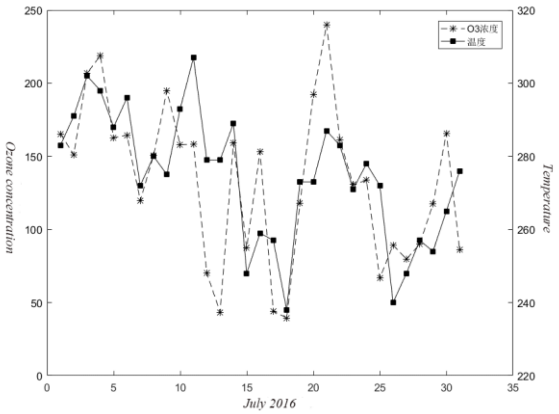

Figure 5. Temperature-ozone trend graph

The comprehensive monthly average temperature trend and the correlation between daily average and ozone concentration show that the ozone meteorological cause has a strong correlation with the temperature change, and the ozone concentration will increase when the temperature is high.

3.2. Correlation Analysis between Precipitation and Ozone Concentration

Combined with the physical properties of ozone, ozone has a certain water solubility. Therefore, according to the trend of precipitation in Beijing in 2016 and the trend of ozone concentration, we can get the 2016 precipitation and ozone concentration as Spearman. Correlation analysis chart shown in Figure 6.

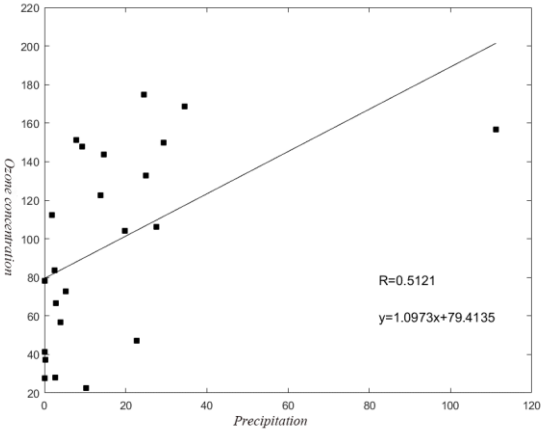

Figure 6. Precipitation-ozone spearman correlation analysis graph

It can be seen from Figure 6 that the concentration of ozone in precipitation is different from that in non-precipitation, and the correlation coefficient between precipitation and its concentration is R=0.5121, indicating that the correlation between the trend of precipitation and the trend of ozone concentration is medium, both of which are positive. Correlation, that is, as the amount of precipitation increases, the ozone concentration increases. The linear function equations of the two can be obtained

by linear fitting:

$$y = 1.0973x + 79.4135 \quad (2)$$

According to the literature, Beijing's climate is typical of warm temperate semi-humid continental monsoon climate, summer is hot and rainy, winter is cold and dry, spring and autumn are short. Therefore, the above analysis shows that the relationship between precipitation and ozone is uncertain. The correlation between precipitation and ozone concentration in this region in July 2016 is selected.

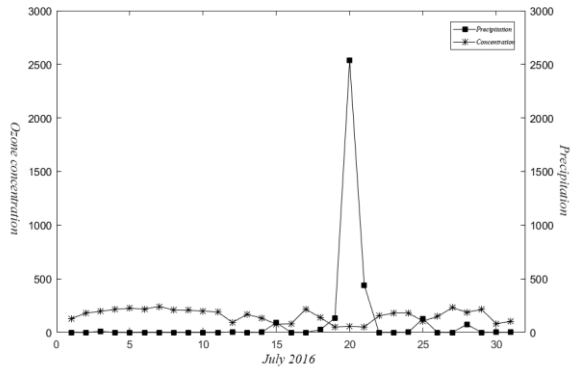

Figure 7. Precipitation-ozone trend graph

Combined with the above Figure 7, the precipitation in this area has been in the state of no precipitation or small precipitation in July, but the precipitation increased sharply on the 20th, reaching a peak of 2596mm. At this time, the ozone concentration is close to the valley value, and the ozone concentration has been in stable fluctuation. The state and concentration have remained below $500\mu g/m^3$, and it is known that the area has experienced heavy rainfall on the 20th, but the impact on ozone is small. From the analysis of precipitation and ozone concentration in July, it is known that as the precipitation increases, the ozone concentration decreases, and the whole has a significant negative correlation.

From the above analysis, it can be seen that the correlation analysis between precipitation and ozone concentration shows that there is a positive correlation between precipitation and ozone concentration analysis in 2016, and the correlation is moderate; however, in July, the average daily concentration trend analysis shows that There is a strong negative correlation between precipitation and ozone concentration. Combined with the reasons for the change of ozone concentration caused by many factors, combined with the above results and literature review, the possible reasons are as follows: (1) Due to the influence of various meteorological factors on ozone concentration, the promotion of ozone by other factors (such as temperature) is greater than that of precipitation. The inhibition of ozone.

(2) Different levels of precipitation have different purification effects. The moderate rain has the best effect on the wet removal of ozone, followed by the magnitude of heavy rain. The micro-precipitation and light rain not only have no effect but also increase the concentration.

In combination with the designated rainfall level of the China Meteorological Administration, only the correlation between the rainfall and the moderate rainfall and the ozone concentration can be obtained:

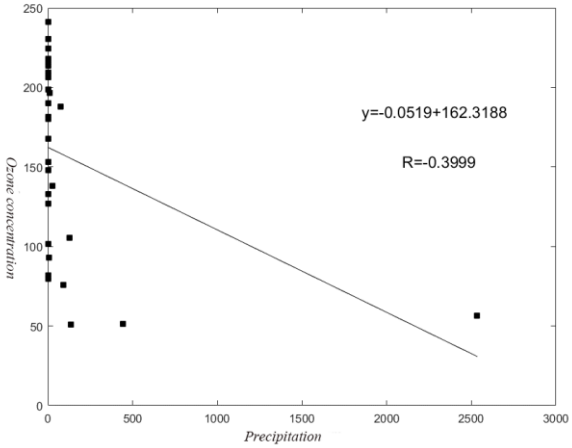

Figure 8. Precipitation-ozone correlation analysis graph

It can be seen from the above Figure 8 that the correlation coefficient between precipitation and ozone concentration is R=-0.3999, and the ozone concentration decreases with the increase of precipitation. The two are negatively correlated, and the function expression of precipitation and ozone concentration can be obtained.

$$y = -0.0519x + 162.3188 \quad (3)$$

From this, it can be proved that the precipitation is negatively correlated with the concentration of ozone, that is, the precipitation increases and the ozone concentration decreases. Based on the above research, it can be concluded that when the precipitation is large, the change trend of precipitation is negatively correlated with the trend of ozone concentration.

(3) Correlation analysis between positive relative humidity and ozone concentration

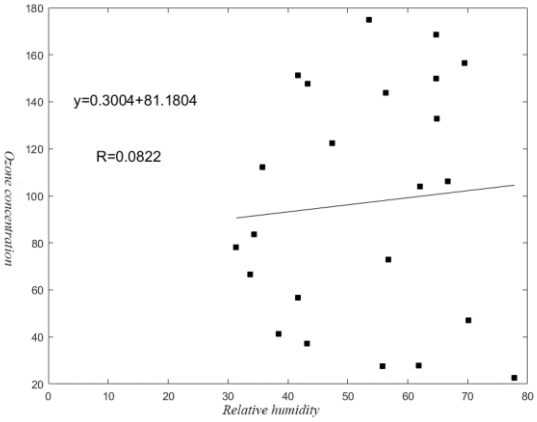

Figure 9. Positive relative humidity-ozone Spearman correlation analysis

In addition to temperature and precipitation, positive relative humidity in the air can also affect changes in

ozone concentration. Spearman correlation analysis was performed by selecting the relative humidity and ozone concentration in 2016, as shown in Figure 9.

It can be seen from Figure 9 that the correlation coefficient between relative humidity and ozone concentration is $R = 0.0822$, the correlation coefficient approaches 0, and the correlation intensity is almost zero. There is almost no linear relationship between the two, and the change of relative humidity hardly affects the change of ozone concentration. Neglecting the effects of minor changes can be considered as relative humidity is not related to ozone concentration.

4. CONCLUSION

The three-grain changes in the annual, monthly and daily ozone concentrations of Beijing 2015-2016 were studied separately, and the changes in ozone concentration were significantly seasonal. It can be obtained from the annual average concentration analysis. During the summer period from May to July, the solar radiation is higher and the temperature is higher. At this time, the concentration of ozone is continuously accumulated. The reason for the analysis is that high temperature promotes the occurrence of photochemical reactions in the atmosphere, and precursors such as CO, NO, and NO_2 undergo chemical reactions under ultraviolet radiation, and oxygen molecules in the air are also decomposed together to increase the concentration of ozone. After the monthly concentration and daily concentration statistics of ozone concentration, the overall trend of the concentration can be increased first and then decreased and peaked during the month of July. The concentration gradually rises from 8 o'clock in the day due to the gradual increase of solar radiation. Between 14 and 19, the peak is reached due to the continuous accumulation of concentration. At night, the ozone concentration decreases due to the temperature drop and the consumption of reducing agent.

In addition, the causes of ozone were analyzed in combination with temperature, precipitation and positive relative humidity. The trend of temperature change is linearly positively correlated with the trend of ozone concentration. The trend of precipitation under moderate rain is positively correlated with the trend of ozone concentration. The trend of precipitation above moderate rain is linearly negatively correlated with ozone concentration.

ACKNOWLEDGMENT

North China University of Science and Technology College (X2018053).

REFERENCES

[1]Liu S.K, Cai S, Chen Y, et al. The effect of pollutional haze on pulmonary function. Thorac Dis, 2016, 8(1): E41-E56.

[2]Zychowski K.E, Lucas S.N, Sanchez B, et al. Hypoxia-induced pulmonary arterial hypertension augments lung injury and airway reactivity caused by ozone exposure. Toxicol Appl Pharm, 2016, 305(6): 40-45.

[3]Hu H, Ha S.D, Xu X.H. Ozone and hypertensive disorders of pregnancy in Florida: Identifying critical windows of exposure. Environ Res, 2017, 153: 120-125.

[4]Di Q, Wang Y, Zanobetti A, et al. Air pollution and mortality in the medicare population. N Engl J Med, 2017, 376(26): 2513-2522.

[5]Meng X.P, Gao Y. Electric Systems Analysis. Beijing: Higher Education Press, 2004, 3-21.

[6]Sillman S. The relation between ozone, NOx and hydrocarbons in urban and polluted rural environments. Atmospheric Environment, 1999, 33(12): 1821-1845.

[7]Hidy G.M. Ozone process insights from field experiments part I: overview. Atmospheric Environment, 2000, 34(12):2001-2022.

[8]Solomon P, Cowling E, Hidy G, et al. Companrison of scientific findings from major ozone field studies in North America and Europe. Atmospheric Environment, 2000, 34(12):1885-1920.

[9]Wu K, Kang P, Wang Z.S. Ozone temporal variation and its meteorological factors over Chengdu City. Acta Scientiae Circumstantiate, 2017, 37(11): 4241-4252.

[10]Wang L, Liu R.Y, Han G.R. Study on the relationship between surface ozone concentrations and meteorological conditions in Nanjing, China. Acta Scientiae Circumstantiate, 2018, 38(04): 1285-1296.

Application of MAS-CA Model in Studying the Evolution of World Language Distribution

Siyuan Ren[1], Jiahe Yan[2], Duo Wang[3], Xiaoqiang Guo[1,]*
[1] College of Science, North China University of Science and Technology, Tangshan, 063210, Hebei, China
[2] College of Metallurgy and Energy, North China University of Science and Technology, Tangshan, 063210, Hebei, China
[3] Mechanical college, North China University of Science and Technology, Tangshan, 063210, Hebei, China
**E-mail: 7298754267@qq.com*

Abstract: In order to study the evolution of global language over time, it is considered that the cellular automaton model has the natural advantages of integrating with GIS / RS technology systems in data and analysis models, and a good vision of real simulation effects that hope to achieve space-time interaction. By establishing the MAS-CA model, we have achieved quantitative research and analysis of language development trends. Under the full consideration of political policy, regional influence, immigration and assimilation, economic globalization, cultural considerations and other influencing factors, this paper transforms the above factors into simple principles and synergies through three sub-cellular automata and two-layer attributes. The work agent is in effect. To validate our theory, we simulated models of various distributions over time, with the help of Matlab. Based on the predicted trends, some of the GIS mentioned above data and impact simulation results clearly show us the distribution of various language speakers. According to the CA model combined with data documents, language development is more sensitive to immigration than other factors, so it is more sensitive to geographic distribution. These languages change at a lower rate over the same period of time. The MAS-CA model fully reflects the essence of the complex science of "simple subsystem interactions with complex structures", its "bottom-up" research method, powerful cooperation and complex computing power, and inherent parallel computing power and space-time. Dynamics makes it ideal for system modeling with complex spatiotemporal features.

Keywords: MAS-CA model; global language distribution evolution; factors affecting language growth and decline; mathematical modeling

1. INTRODUCTION

There are many languages in the world that are influenced by many complex factors. In the context of global economics, the analysis believes that the factors affecting the development of language and distribution include political strategy and school language education, regional factors (local and immigration), the impact of globalization, economic globalization, globalization of communication, Seven aspects of cultural soft power and comprehensive national strength [1-3].

In the context of the rapid development of the Internet and the development of economic globalization, we build a MAS-CA model by analyzing a large amount of data to simulate the evolution of global language distribution over time. According to the multi-agent system (MAS) and cellular automata theory, various influencing factors and the respective attributes of these languages can be set as the attribute set and rules of the Agent, and then based on the combination of the GIS system (using grayscale grid images) The cellular automata is set up to construct a variety of agents and various influencing factors of the simulation system that can dynamically describe the interaction between them, so as to realize the dynamic simulation and prediction of the evolution of the number of people using the global language [4,5].

2. MAS-CA MODEL COMPOSITION

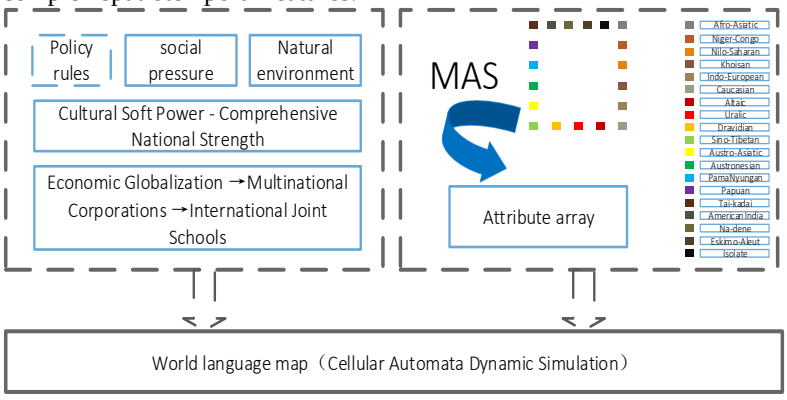

Figure 1. Framework of global language population distribution model based on MAS

According to the data from GIS, a global language dynamic distribution model based on multi-agent will be buit here. It consists of a comprehensive environment, a multi-agent system, and a regional population density of 3 parts. Among them, the integrated environment is mainly used to consider the impact factor, which consists of two layers and three cellular automata, which are the policy rule layer and the natural geographic layer; the three cellular automata are cultural soft power-comprehensive country Power Cellular Automata, Economic Globalization - Multinational Corporations - International Union School Cellular Network Automaton and Positional Pressure Cellular Automata; in a multi-agent system, each agent program array stores behavior, location information, and so on The attributes of the agent; the regional population density of each language includes demographic data and corresponding density data from around the world. The model framework can be seen in Figure 1, and the agent is affected by the influencing factors and acts on these factors.

3. ESTABLISHMENT OF MAS-CA MODEL MODEL

The experimental area covers the entire world. The data used includes nearly 20 years of remote sensing images, texts and political quotas, and the national soft power rankings of national cultural languages. The statistics are mainly from the China Institute of Statistics, China Statistical Yearbook and the National Bureau of Statistics report US Bureau of Statistics, combined with Matlab and Arc-Object to build the system and apply it. In order to increase the speed of the system, all spatial data is evenly converted into 100 meters in ArcGIS 10.2 * 100m grid raster data.

3.1. Integrated Environment

Languages used and promoted by the government in a country or school, social pressure, immigration and immigration, globalization of international business relationships and rapid development of the Internet, including increasing global tourism and social media, these factors intersect. The resulting integrated environment has a huge impact on language development trends. The integrated environment consists of two layers of integrated environment layer and three cellular automata, which capture the 5 * 5 windows through the mobile, each layer interacts with the agent, applies the mobile window to all data layers, and the data is stored in the corresponding intelligence. In the array of attributes of the body, consider all the influencing factors for comprehensive evaluation.

3.1.1. Integrated environment layer attribute design

(1) Policy planning layers

The language promoted by the government is one of the most important issues in a country when considering the language used in the school. National policy planning plays an important role in the evolution of language development and the distribution of the number of people using language. The role of language guides the evolution of national language and thus affects the development of world language. In order to simulate the distribution of users of various languages over time, the policy plans of some major countries involving the top ten languages are supplemented and the corresponding areas are designated as overlays.

(2) Natural environment layer

Since ancient times, people have been demanding the natural environment of the living area. They do not consider the language development in the ocean, namely the Arctic Circle, the Antarctic Circle, the desert and the plateau. To this end, we regard mountain woodland as the public 6 green space and water body as natural environmental factors, and use the exponential distance attenuation function to reflect the state of the natural environment.

$$E_{ij} = c_1 e^{-\delta_1 D_{river}} + c_2 \sum_{i=1}^{n} \frac{G - belt}{4r^2} \quad (1)$$

Where: Eij That the state of the natural environment; Driver Indicates the vertical distance to the body of water; δ1: Said water body space attenuation coefficient; r: Said neighborhood radius; G-belt: said the number of green spaces in the neighborhood; c1,c2: said that the weight coefficient, set to equal.

3.1.2. Integrated environment cellular automaton

Cellular Automata, consists of four parts: cell, cell space, neighbors and rules, fully embodying the essence of complex science. "Complex structures come from the interaction of simple subsystems. Its "bottom-up" research Methods, powerful complex computing power, inherent parallel computing power and spatiotemporal dynamics make it an ideal feature for simulating systems with complex time and space. The corresponding cell state is the state language system involved in the corresponding language. The conversion rules and determinations can simulate the dynamic development of the world language in the time interval. The three cellular automata involved in this paper are constructed as follows:

3.1.3. Cultural soft power-comprehensive national strength cellular automaton

(1) Cultural soft power assessment part

The CA of cultural soft power mainly considers the factors of cultural migration and group assimilation. After consulting a large amount of literature research data, the corresponding test formula can be obtained from the existing hard index system of cultural soft power: Cultural Soft Power = the efficiency of the political system and the degree of domestic recognition [overseas] [art diplomacy (impact of values + international image and international reputation + Outreach of sports and international competitions + Performance and effectiveness) + (cultural innovation ability + strategic decision level + policy effectiveness) (scientific strength + education level + talent pool or human capital + international

cultural products and cultural heritage impact + national ethical standards)]. Using English letters instead of the above, you can get a simplified cultural soft power evaluation formula:

$$P_e = S_p\left[D(V+I+P+S)+(C_e+S_I+P_y)(T+E+H_e+C_I+M)\right] \quad (2)$$

Despite the fact that all indicators or indicators in the formula require another formula or calculation method. However, by roughly comparing and roughly measuring each indicator, we can get the cultural soft power data of major countries or regions and their approximate ranking order from front to back: UK, Germany, USA, France, Canada, Australia, Switzerland, Japan. , Sweden, the Netherlands, Denmark, Italy, Austria, Spain, Finland, New Zealand, Belgium, Norway, Ireland, South Korea, Singapore, Portugal, Brazil, Poland, Greece, Israel, Czech Republic, Turkey, Mexico, China.

(2) Comprehensive national strength assessment section

Comprehensive national strength is the most important basic indicator for measuring a country's national conditions and basic resources. In order to be able to quantify it, this paper divides the national strategic resources into seven resource types and twenty-three indicators, and the weighted sum of these indicators constitutes the comprehensive national strength. These seven resources are:

①Economic resources (GNP or GDP);
②Human capital;
③Capital resources;
④Knowledge and technical resources;
⑤Government resources;
⑥Military power;
⑦International resources.

According to the large amount of data research results of authoritative scholars, we have obtained the empirical formula for calculating the comprehensive national strength, that is, the sum of the corresponding weight and the ranking product.

$$NP = \sum(ai * Ri) \quad (3)$$

The report of the comprehensive national strength factor and its weighting factor table is shown in Table 1.

Table 1. Comprehensive national strength factor and its weight coefficient

Comprehensive national strength	Weight coefficient
Economic power	0.35
Science and technology	0.20
Military force	0.10
Social development level	0.10
Ecological power	0.10
Government regulation and control	0.08
Diplomacy	0.07
total	1.00

According to the report of the Institute of Modern Studies, the China International Relations and Strategy Research Group's data statistics report, the Chinese Academy of Sciences' Sustainable Development Research Institute of Chinese Academy of Sciences' Sustainable Development Strategy Research Group released the 2003 China Sustainable Development Strategy Report, comparing and ranking the 13 largest countries in the world. Comprehensive national strength. According to the statistical methods and calculation methods of the report, each country has different weights in different periods and ranks differently. Table 2 shows the results of the integrated country rankings in 1990. In 1995, three different periods were reported in 13 countries and 2000.

For language, the influence of comprehensive national strength and soft power on language development each account for a certain proportion. Therefore, it is necessary to give it the right to operate, and the parameter value is determined by parameter estimation.

Table 2. Thirteen countries comprehensive national empowerment program sort

country	1990	1995	2000
Australia	10	9	9
Brazil	11	11	11
Canada	3	3	3
China	9	8	7
France	5	5	5
Germany	4	4	4
India	12	12	12
Italy	8	10	10
Japan	2	2	2
Russia	6	7	8
South Africa	13	13	13
United Kingdom	7	6	6
United States	1	1	1

3.1.4. Multinational corporations-international joint schools cellular automata

The model requires four kinds of input data, all data must have the same data format, the same number of rows and columns, the same projection and the same size, data are grid representation.

3.1.5. Location pressure cellular automata

(1) Slope

Terrain is the most basic condition for urban development. Flat and wide urban areas or suburbs are more suitable for establishing and building large multinational companies and international cooperative schools. The slope level must be a percentage of the slope value (not the degree slope value), ranging from 0 to 100. The slope usually comes from the Digital Elevation Model (DEM). The cell below the threshold is "live-1"; the cell that exceeds the threshold is "Death-0"

(2) Transportation

Using the binary taxonomy, a cell with a value of 0 indicates that entering a non-urban area is "death 0" due to inconvenient traffic, and considering any cell 11 greater than 0 as an easily accessible urban area, the Cell status is " Live-1". Identify urban areas

primarily through digital city maps and aerial photographs, threshold remote sensing images or population density distribution.

3.1.6. Multinational corporations & international joint schools

Following a binary taxonomy, cells with a value of zero represent multinational companies or international co-op schools that do not have a language in their area, with a cell status of "death-0" and any cells greater than 0 are considered local Language of multinational companies or international joint schools, cell status is "live-1".

In the development of single-core countries, assuming that the social pressure in the region is getting closer to the development center, a simple distance factor is used to express the overall pressure. However, with the development of single-core countries and the increasing population of large cities, employment pressure will certainly increase, which will promote the learning and development of second and third languages. Therefore, as the population of the region grows, cell pressure will increase:

$$P_{ij}^{\ t} = d_1 e^{-\eta_1 D_{heart}} + d_2 \sum_{i=1}^{n} \frac{Pop}{4r^2} \tag{4}$$

When t is said, the pressure in the department of the Agent (the main language) indicates the distance between the centers of the attenuation indices. It also indicates that the pressure development center distance and the population-induced pressure increase weight coefficient density are respectively. r represents the radius of the neighborhood, Pop represents the person near the number, and is set to be equal. The simulation of the sub-battery displays the distribution of the number of users as a second language and a third language in a particular region of the country.

3.1.7. Cellular automaton rules

(1) At the current time, if the number of cells N alive around one cell is 3.

Then the next time the cell is live.

(2) At the current moment, if the number of cells N alive around one cell is 2.

Then the next life and death of the cell state remains unchanged.

(3) In other cases, the cell is dead (ie, the cell turns to death if it originally lived, but remains unchanged if it had previously died).

Using Matlab language to represent the above three alternative rules as shown in equation (5)

$$X = (X \,\&\, (N == 2)) \| (N == 3) \tag{5}$$

3.2. Multi-Agent Comprehensive Decision Rules

Multi-agent, a smart individual who is active in the cell. This model attempts to abstract and properly describe agents, simulating agents in various languages to detect and react to social environmental information, and social environmental information affects behavior. According to the historical statistical yearbook and GIS data, we set the initial attributes of each major language agent, and add the primary language domain of the main language agent, describe the attribute factions of historical language development and the convenience of mutual learning between different factions. Array to save.

(1) In a self-organizing Esperanto distribution system, the development of language distribution is an interactive process with the surrounding environment. In the process, past agents experience agents that act in the future through interaction with the environment. The agent search f or the appropriate development environment can be relocated according to its own requirements and actual conditions. Population density and comprehensive assessment coordinates within and around the area of 31,521 square kilometers.

$$E_{ij}^{\ t} = \Phi(r_{ij}^{\ t}) = \Phi[w(F_{ijk}^{\ t}, W_k)] \tag{6}$$

r_{ij}^{t} :is to assess the suitability of the overall environment of population living at the moment, is the comprehensive evaluation of the impact factor k;

W_k:is the weight of each impact factor, w is a joint function to calculate the development of each impact factor; Φ :is the agent's action function. Can be simplified as

$$F_{ij}^{\ t} = b_1 S_{ij} + b_2 T_{ij}^{\ t} + b_3 E_{ij}^{\ t} - b_4 P_{ij}^{\ t} \tag{7}$$

Where: S_{ij}, T_{ij}, E_{ij}, P_{ij} respectively, service facilities, traffic accessibility, natural environment and location pressure factors; b_1, b_2, b_3, b_4, reflect the weight of each impact factor.

The average of Esperanto data over the past five years was brought into the model to reconstruct the 2005 world population distribution. Since each language has its own evaluation preferences, this method is used to obtain the simulation results and actual results of the data matrix in the subjective preference weight MCE of the impact factor. The entropy method is used to correct the weights of various influencing factors. Entropy is a theoretical measure of "uncertainty" in information. The larger the amount of information, the smaller the uncertainty, the smaller the entropy, and the more stable the weight impact factor.

Updating the data of three cellular automata, combined with updated GIS information and policy information, can simulate the evolution of the agent over time.

(2) The growth and demise of agents

The integrated social environment affects the cellular automaton in its own attribute array in 19 languages). In the simulation, 1. Based on the natural growth rate of the population, it increases the number of agents and provides them with initial attributes. According to the mortality rate of deaths, the population population system is randomly assigned to the intelligent population system, and then the regional population density model system that is fed back to the intelligent body language is eliminated, and the

corresponding population is reduced. 2. Influence Set the above social environment rules to determine if the agent is growing or dying.

(3) Renewing the Cultural Soft Power-Integrated State Cellular Automata and the International Joint Schools Cellular Automata (Cellular Automata), with updated GIS and policy information to simulate the evolution of agents' Development and evolution.

4. CONCLUSION

According to the CA model and combining with the data documents, language development is more sensitive to immigration than other factors, thus the geographic distributions of these languages change over this same period of time. But its speed is a little slower than the condition, as Table 3.

Table 3. Distribution of world languages by area of origin

Area	Living languages		Number of speakers			
	Count	*Percent*	*Total*	*Percent*	*Mean*	*Median*
Africa	2144	30.2	887310542	13.4	413858	29000
Americas	1061	14.9	50704628	0.8	47789	1110
Asia	2294	32.3	3981523335	59.9	1735625	12000
Europe	287	4.0	1716625664	25.88	5981274	36400
Pacific	1313	18.5	6873346	0.1	5235	970
Totals	7099	100.0	6643037515	100.0	935771	7000

Model the distribution of various language speakers over time.

The model is ideal for system modeling with complex spatiotemporal features. The corresponding cell state is the state language system involved in the corresponding language. According to some conversion rules and time inte to determine rval, we can simulate the dynamic distribution of the world language; in order to simulate th over time, we use the MAS-CA model to simulate different global languages to use the world language as a proxy to formulate corresponding attribute rules.

REFERENCES

[1]He M.S. Based on the development trend of English language to explore the compatibility of English vocabulary. Essay hundred (new language), 2016 (08): 197-198.

[2]Ke C.Q, Ouyang X.Y. Cellular Automata Models of Urban Spatial Simulation Research Progress. Journal of Nanjing University (Natural Science), 2006, (01).

[3]Jia H.T. China's Comprehensive Assessment of National Strength and World Ranking: Theory, Reality and Evaluation Formula. Journal of Nanjing University of Science and Technology (Social Science), 2012, 25(05): 116.

[4]Ligtenberg A, Bregt A.K, Lammeren R. Multi-actor-based land use modeling: spatial planning using agents. Landscape and Urban Planning. 2001.

[5]Jing N. Prediction of urban population distribution based on multi-agent and GIS. Graduate School of the Chinese Academy of Sciences (Guangzhou Institute of Geochemistry), 2007.

Fuzzy Clustering Analysis based on Performance-To-Price Ratio of Different Mobile Electronic Products

Yuqi Wei[1,2,], Fanyan Kong[1,2], Hanyu Yang[1,2], Xu Zhou[1,2]*
[1]Engineering Computing and Simulation Innovation Lab, North China University of Science and Technology, Tangshan, 063210, Hebei, China
[2] North China University of Science and Technology, Tangshan, 063210, Hebei, China
**E-mail: m13290559330@163.com*

Abstract: With the acceleration of the process of social information data, high-tech products have become a hot spot of consumption, and mobile phones are also one of its representatives. College students have more and more demand for mobile phones, various types of mobile phones appear in the market, and their performance is gradually strengthened. The appearance is gradually beautified, and the college students are gradually hesitant to buy the mobile phone. Therefore, we first randomly investigated the popularity of the mobile phone brand and the requirements for the choice of mobile phone among 100 college students, and concluded that most of the students are more concerned about the price. And Xiao mi, Hua wei, Apple and OPPO, VIVO are more popular with college students, so we look for seven domestic mobile phone brands. Collect the function parameters and price data, list the data table, and then perform standard data, establish the standardization matrix, fuzzy similarity relationship, fuzzy equivalent matrix, and finally fuzzy cluster analysis. The mobile phones with high cost performance ratio are Xiao mi 9, Hua wei P10, Mei lan note5, OPPO R11P, which provides college students with a better choice direction for mobile phones.

Keywords: fuzzy cluster analysis; description analysis; market research; classification

1. INTRODUCTION

First of all, it is known that there are many parameter types of mobile phones in the domestic market, in which more representative parameters are selected to introduce, CPU types, RAM, front and rear pixels, main screen resolution, battery capacity, the size of the main screen affects the purchase of consumers. This time, we sent out 100 questionnaires, 100 recovered and 100 valid questionnaires, which were investigated for North China University students of Science and Technology. And combined with second-hand data online search and other measures, to formulate a reasonable scientific investigation

Figure 1 shows that college students are more popular with Xiao mi, Apple, Hua wei, OPPO and other brands, while Jin li, Nubian and other series of mobile phones are not popular. So we investigated the 100 people's requirements for buying mobile phones.

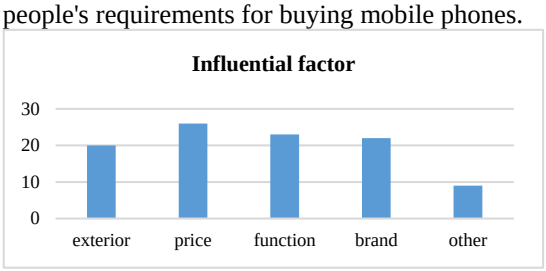

Figure 1. Factors affecting the purchase of mobile phones

It is known that most college students are more concerned about the price of mobile phones because of economic reasons, and some of the respondents are more concerned about appearance, brand and function, so we can see that if college students can buy mobile phones according to their performance-to-price ratio, That will bring great convenience, so this paper analyzes several domestic mobile phones. Fuzzy clustering analysis is to construct fuzzy matrix according to the attributes of the research object itself, and on this basis, the classification relationship is determined according to a certain degree of membership. In order to explain the method of fuzzy clustering analysis, we study the data parameters of official website search, and select seven different types of parameters to carry on the research [1-5]. Analysis Make a table of seven parameter values for each type of phone.

$$X' = \begin{bmatrix} X'_{11} & X'_{12} & \cdots & X'_{1m} \\ X'_{21} & X'_{22} & \cdots & X'_{2m} \\ \cdots & \cdots & \cdots & \cdots \\ X'_{n-1,1} & X'_{n-1,2} & \cdots & X'_{n-1,m} \\ X'_{n1} & X'_{n2} & \cdots & X'_{nn} \end{bmatrix} \quad (1)$$

There are n factors to be classified, each of which is characterized by m sample indicators, then the data matrix can be expressed as follows:

Because the dimensions and orders of magnitude of m indexes are different, using the original data directly to calculate, it is possible to highlight the effect of some particularly large characteristic indexes of order of magnitude on classification, and to reduce or even reject the effect of some characteristics of smaller

order of magnitude [6]. As a result, as long as an indicator changes the unit, it will also change the classification results. Therefore, it is necessary to deal with the original data dimensionless, so that each index value is unified with a common data characteristic range. The mean value and standard deviation, maximum value, minimum value, mean value and standard deviation of each parameter are calculated by SPSS.

There are many methods for standardization of sample data, such as standard deviation standardization method, maximum normalization method, extreme deviation standardization method and mean normalization method. This time, the standard deviation standardization method is adopted, and its model is as follows:

$$X_{ij} = \frac{x_{ij}' - \overline{x}_j'}{S_j} \quad (2)$$

Similarity relation R is a fuzzy measure method to measure the similarity between samples, and it is a fuzzy similarity matrix.

$$R = \begin{bmatrix} r_{11} & r_{12} & \cdot & r_{1n} \\ r_{21} & r_{22} & \cdot & r_{2n} \\ \cdot & \cdot & \cdot & \cdot \\ r_{n1} & r_{n2} & \cdot & r_{nn} \end{bmatrix} \quad (3)$$

We use the distance formula method, and its mathematical model is as follows:

$$r_{ij} = 1 - c\sqrt{\sum_{k=1}^{m}(x_{ik} - x_{jk})^2} \quad (4)$$

Where: C is capable of making $0 \le r_{ij} \le 1$ A constant of, i, j=1, 2, ...n.

Table 1. Fuzzy similarity relation matrix

	1	2	3	4	5	6	7
1	1	0.423	0.4665	0.4647	0.4822	0.624	0.4744
2	0.423	1	0.7933	0.1688	0.1759	0.5086	0.3919
3	0.4665	0.7933	1	0.0102	0.2619	0.2201	0.635
4	0.4647	0.1688	0.0102	1	0.3406	0.2315	0.1534
5	0.4822	0.1759	0.2619	0.3406	1	0.1939	0.4202
6	0.624	0.5086	0.2201	0.2314	0.1939	1	0.3928
7	0.4744	0.3919	0.635	0.1534	0.4202	0.0383	1

In general, the fuzzy similarity relation matrix only satisfies reflexivity and symmetry, however, in order to cluster R, it must be fuzzy equivalence relation, which not only satisfies transitivity, but also needs to be modified. The method of transformation is to multiply R by itself $R \circ R = R^2$ $R^2 \circ R^2 = R^4$.

Table 2. Fuzzy equivalence relation matrix

	1	2	3	4	5	6	7
1	1	0.6826	0.6826	0.4616	0.521	0.4605	0.7303
2	0.6826	1	0.8011	0.4616	0.521	0.4605	0.6826
3	0.6826	0.8011	1	0.4616	0.521	0.4605	0.6826
4	0.4616	0.4616	0.4616	1	0.4616	0.4605	0.4616
5	0.521	0.521	0.521	0.4616	1	0.4605	0.521
6	0.4605	0.4605	0.4605	0.4605	0.4605	1	0.4605
7	0.7303	0.6826	0.6826	0.4616	0.521	0.4605	1

To get different $\lambda(0 \le \lambda \le 1)$ Horizontal intercept array. In this study, we selected the $\lambda = 0.6$ The lower intercept array.

Table 3. Intercept matrices of fuzzy equivalent matrices

1	1	1	0	0	0	1
1	1	1	0	0	0	1
1	1	1	0	0	0	1
0	0	0	1	0	0	0
0	0	0	0	1	0	0
0	0	0	0	0	1	0
1	1	1	0	0	0	1

As can be seen from table 6, when $\lambda = 0.6$ Mobile phone brands can be divided into four categories, {1, 2, 3, 7}, {4}, {5}, {6}.Therefore, we can see that Xiaomi 9, Huawei p10, Mei lan note5, OPPO R11P performance-price ratio is similar, these four brands are domestic hot brands, and are liked by the majority of consumers, so our analysis is reasonable and scientific.

2. CONCLUSIONS

The advantages of fuzzy clustering analysis method: the advantage of cluster analysis model is intuitionistic and the conclusion form is concise. Disadvantages: when the sample size is large, it is difficult to obtain the clustering conclusion. According to the market research, we analyze that the biggest hindrance to the choice of mobile phone for college students is the price problem. For college students, they have no source of income and can only live with their parents' money, so the performance-price ratio is very important to college students. We used cluster analysis method to analyze several kinds of domestic mobile phones. Finally, we divided them into four categories: Xiao mi 6, Hua wei p10, Mei lan note5, OPPO R11P, which have high performance price, Nu bi ya z17, one plus five.

Although the configuration parameters of Jinli s10 are also good, the price is too high and the performance price is a little lower, so if you want to buy it A mobile phone with a high cost-effective value can be selected in Xiao mi 9, Hua wei p10, and the Mei lan note5, OPPO R11P. It can also be seen from FIG.1 that the college students are fonder of the four brands, so the rationality of the fuzzy clustering analysis is verified.

REFERENCES

[1]Chen W.Y, Song Y.Q, Bai H.J, et al. Parallel spectral clustering in distributed systems. IEEE Transactions on Pattern Analysis and Machine Intelligence, 2010, 33(3).

[2]Li J, Cheng J.L, A new algorithm of fuzzy clustering based on feature weighting. High-tech wave, Electronics. 2006 (01).

[3]Kwong S, Liu H.Y. Fuzzy cluster analysis of urban housing construction in China. Journal of Tsinghua University (Natural Science Edition). 1989, (05).

[4]Uykan Z, Güzeliş C, Celebi M.E, et al..Analysis of input-output clustering for determining centers of RBFN. IEEE Transactions on Neural Networks, 2008, 11(4).

[5]Xu A.P, Xu W.P. Fuzzy clustering research based on self-organized competition neural network technology. Computer engineering and science. 2006, (11).

[6]Zhang Y, Song W.Y. Fuzzy cluster analysis method in graduate enrollment. Zeng Literature and Art, Journal of Beijing normal University (Natural Science Edition). 2001, (04).

Physical Balance Characteristics and Balanced Risk Assessment of the Elderly

Xiaocan Zhong[1,2,], Zhikang Tian[2], Yang Liu[2], Lu Liu[1,3]*
[1] *Engineering Computing and Simulation Innovation Lab, Tangshan, 063001, Hebei, China*
[2] *North China University of Science and Technology, Tangshan, 063231, Hebei, China*
[3] *College of Science, North China University of Science and Technology, Tangshan, 063210, Hebei, China*
**E-mail: 2710096401@qq.com*

Abstract: Falling injuries caused by physical imbalance among the elderly are a common problem among the elderly at present. How to effectively prevent physical imbalance is an urgent problem in kinematics and clinical rehabilitation. Therefore, it is of practical significance to select the appropriate feature extraction model and to make an objective evaluation of the elderly's physical balance ability, combining with the elderly's sports characteristics and risk assessment methods. Firstly, a gait parameter model based on gait analysis is established, in order to study the body sway of the elderly when walking, a human motion balance model based on the comparative analysis method was established. Secondly, on the basis of the body balance assessment system about the body balance assessment report, a balance model for the elderly based on the center of gravity shift under the frame sequence distribution is established. By solving the model and analyzing the pictures drawn, the paper draws a conclusion, and finds out the relevant knowledge from the references, so as to put forward some reasonable suggestions for the elderly with weak balance ability.
Keywords: feature extraction; method of moment synthesis; risk assessment for balance; walking ability

1. INTRODUCTION

The center of gravity refers to the action point of gravity, while the center of gravity refers to the action point of gravity in all parts of the human body. In the process of human body stationary or gait movement, its own gravity plays an important role. At rest, the tester maintains his balance by slightly swinging the center of mass of the human body and keeping it in the support plane; during gait movement, the projection of the center of mass of the subjects meets the ZMS condition [1]. In addition, Cartesian coordinate system is widely used in space research.

2. MODEL OF HUMAN BODY CENTER OF GRAVITY

Its three axes x, y and z are orthogonal to each other. Any vector in the Cartesian coordinate system is composed of components in the three directions of x, y and z. Assuming that the coordinates of any small part in the main parts of the human body are x_i,y_i and z_i, the coordinates of the organs'center of gravity are x_c,$y_c$and z_c.According to the resultant moment theorem in mechanics, the moment of three parts is taken respectively. The human body is simplified into 14 rigid bodies, namely the head, torso, left upper arm, right upper arm, left forearm, right forearm, left hand, right hand, left thigh, right thigh, left calf, right calf, left foot, right foot. Let the coordinates of the rigid body be $x_i,\ y_i, z_i,(i = 1,2,\cdots,14)$and the weight of the human body is x, y, z [2,3]. According to the mechanics of the combined torque theorem, the 14 rigid bodies are taken separately, as shown in Figure 1:

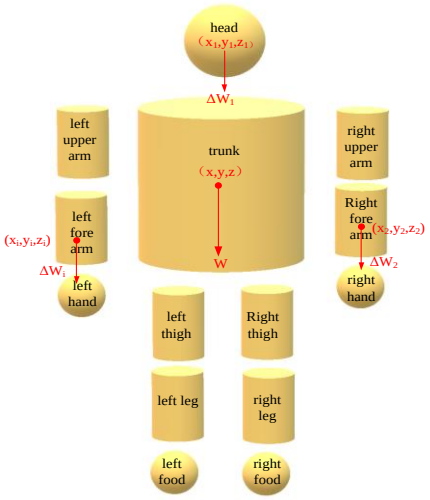

Figure 1. Schematic diagram of each rigid body

Momenting in the x direction, there is

$$W \cdot x_c = \Delta W_1 x_1 + \Delta W_2 x_2 + \cdots + \Delta W_n x_n = \sum \Delta W_i x_i \quad (1)$$

Then take the moment in the y direction, there is

$$W \cdot y_c = \Delta W_1 y_1 + \Delta W_2 y_2 + \cdots + \Delta W_n y_n = \sum \Delta W_i y_i \quad (2)$$

Similarly, the z direction can be used to take the moment.

$$W \cdot z_c = \Delta W_1 z_1 + \Delta W_2 z_2 + \cdots + \Delta W_n z_n = \sum \Delta W_i z_i \quad (3)$$

From the above three formulas, the coordinate formula of the body weight in three different directions can be obtained.

$$\begin{cases} x_c = \frac{\sum \Delta W_i x_i}{W} \\ y_c = \frac{\sum \Delta W_i y_i}{W} \\ z_c = \frac{\sum \Delta W_i z_i}{W} \end{cases} \quad (4)$$

Among them, $W_i$is the gravity received by each part.

Assume that the organ density distribution of each part of the human body is uniform, so the inertia parameter $\lambda_i$of the Bravin Fischer human body model can be calculated into the formula $W = \lambda_i \cdot W_i$, and the relative weight of each link is as shown in the Table 1.

Table 1. Bravin's Fischer Human Body Model Inertia Parameter Table

link	relative weght of each link N
head	0.0706
trunk	0.4270
left upper arm	0.0336
right upper arm	0.0336
left form arm	0.0228
right form arm	0.0228
...	...

W is the total gravity that the human body receives, and its size can be calculated by $W = m \cdot g$,g = $9.8\text{N} \cdot kg^{-1}$.The variance of Wujinzhan is 907.7472, which is larger than that of Chenfue 217.3785. Therefore, it is known that people who are easy to fall are unstable in body swing and their balance ability declines during free walking, which leads to excessive and uncoordinated left and right swing during walking.

3. THE ELDERLY BALANCE ABILITY ASSESSMENT MEDEL

The evaluation indicators of human balance can be described in many ways. Through various research results, it is known that human balance is mainly affected by vestibular organs, proprioceptive sensory system and nerve central system, such as the changes of limbs in motion, body swaying, swaying, etc. or by their own emotions, age and environment [4-8]. Influences of other factors. From the physiological point of view, the balance ability of the human body is mainly related to the human body's proprioceptive ability, vision, age and height physiological conditions, as Table 2.

Table 2. Evaluation index parameters

evaluation index	definition
Trajectory area	Area of projection trajectory map of human body gravity center
Long total trajectory of shaking	Total Track Length of Center of Gravity Swing in Test Time
Vacillation shift	The distance from the center of gravity projection coordinate to its average position
Mean variance of trajectory	Mean square deviation of instantaneous coordinates of barycenter projection from its average position
Average shaking angle	Mean value of instantaneous angle of center of gravity deviating from human body center line in test time

According to the actual data provided by the appendix, the paper simulates and calculates the influencing factors of human balance force through comparative analysis. In addition, advice is also needed for older people with poor balance. On the basis of the body balance assessment report from Question 1 and the body balance assessment system from Question 2, an elderly balance model based on the center of gravity shift under the frame sequence distribution is established [5].

When the human body is in a static state, the center of gravity of the human body has a certain degree of slight swing, and its swing range is always in the support plane. The swing process of the center of gravity shows the change of the trunk posture. In this paper, the real-time change of the trunk posture is obtained by a triaxial accelerometer fixed in the heart pit of the chest cavity of the subject. When the human body is in the process of gait movement, the position and direction of the subject's body are constantly changing, usually showing periodic characteristics.

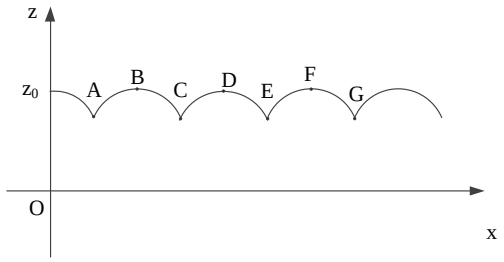

Figure 2. Graph of center of gravity displacement from side view

In Figure 2, the direction of X axis represents the direction of human walking, the direction of Z axis represents the height of the center of gravity, A, C, E and G represent the lowest point of the center of gravity, when the left and right feet start and fall alternately in the course of walking, and B, D and F represent the highest point of the center of gravity, when a leg and the ground are vertical instants. Assuming that point A is the state where the left foot falls while the right foot rises, as it moves, the left leg gradually reaches the vertical position, then continues to move, and then goes to the state before the left foot. In this process, the position of the center of gravity changes from low to high to low. From the previous analysis, it is known that the trajectory of the center of gravity between A, B and C is centered on the left foot. A section of upward convex arc whose radius is the distance from the center of the heart and left heel to the center of gravity; Similarly, the trajectory between C, D and E is an upward convex arc whose radius is the distance from the center of the right foot to the center of gravity; the trajectory between E, F and G is also an upward convex arc whose center is the left foot and the distance from the center of the left heel to the center of gravity[6].

Based on the above analysis, we can make it clear that the trajectory of the center of gravity of the human

body is a spatial curve in the course of walking. Assuming that people move along a straight line, and the characteristics of each cycle are the same, according to this characteristic, we can try to establish a mathematical model for it.

4. ANALYSIS OF VARIANCEMODEL OF HOMEOSTASIS

In the past statistical analysis, variance analysis has become a widely used means of data analysis because of its effectiveness and accuracy. Based on this, we can take walking speed as the impact of gait symmetry and regularity as the research target, and use one-way ANOVA model to analyze variance. One-way ANOVA model is as follows:

$$Y_i = \sigma + \mu_i + \varepsilon_{in} \quad (5)$$

Among them, σ represents the mean value of gait indicators, μ_i represents the additional effect of gait symmetry and regularity indicators in $i(i = 1,,2,\cdots,n)$class, ε_{in} is random error obeying normal distribution, andn is joint number.

In the process of human gait movement, human dynamic balance ability plays a fundamental role. In reference [7], it can be known that dynamic balance refers to the ability of the human body to adjust and maintain this posture automatically under different walking speeds, different road conditions or disturbances. Among them, Zero Moment Point (ZMP) is widely used in relevant professional field, as Figure 3.

Figure 3. Dynamic changes of human walking

The zero-moment point was first proposed by Vukobratovic et al. in the late 1970s, which can be understood as an equivalent point of zero resultant moment in the support surface. When the human body is in gait motion, under the influence of inertia, the ground projection of the center of gravity has the possibility of escaping from the support surface, but as long as the ZMP point remains in the support surface, the human body can maintain dynamic balance. The ZMP formula is as follows:

$$\mathrm{ZMP} = \frac{\sum[m_i\bar{x}_l(\bar{y}_l{}'+g)-m_i\bar{y}_l\bar{x}_l{}'+L_{z,i}]}{\sum m_i(\bar{y}_l{}'+g)} \quad (6)$$

In the formula,$\bar{x}_i$、$\bar{y}_i$、$\bar{x}_i{}'$、$\bar{y}_i{}'$enotes the position and acceleration of the center of gravity on limb i, respectively. $L_{z,i}$ is the differential of the angular momentum of each limb in the vertical direction with respect to time, that is, the rate of angular momentum change. ZMP is a rule that human gait movement must obey. It can be calculated by the main joint parts and get its score. The higher the score, the stronger the balance ability, and vice versa, the weaker the balance ability.

5. MODEL SENSITIVITY VERIFICATION

Sensitivity analysis is to ensure that the predicted value of the model does not deviate from the expected value. If the difference is too large, it means that it needs to be improved. In addition, it can ensure that the model and the assumptions are fully coordinated. Based on this, sensitivity analysis is carried out and the results are as follows Table 3:

Table 3. Changes in two factors under different conditions

conditions	$\alpha_i$increase10%	$\alpha_i$decrease10%
β_i	-0.118	0.139
conditions	$\beta_i$increase10%	$\beta_i$decrease10%
α_i	-0.103	0.124

It can be seen from the above table that the sensitivity order of these two factors is $\alpha_i < \beta_i$, which indicates thatβ_i has a significant effect on the balance of the elderly. Therefore, we can draw a conclusion that the model is more accurate.

6. EVALUATION

According to the literature on human balance ability, the balance ability of the elderly is not only closely related to their age, but also includes changes in muscle strength, decreased joint flexibility, visual impairment, vestibular dysfunction, and decreased sense of vibration [8]. Exercise can delay the decline of balance. Research shows that long-term and continuous practice of Taijiquan, Taiji flexibility ball, strong walking and mountain climbing can help prevent the decline of standing ability on one foot, and can prevent the decline of balance function to a certain extent. These sports have a certain effect on maintaining and improving the balance function of the upright posture of the elderly. Therefore, it is suggested that the elderly should actively participate in these projects which are of great help to the balance ability of the human body, so as to reduce the probability of falls of the elderly to a certain extent.

REFERENCES

[1]Wang B.M. Research on the evaluation of human balance ability and the predicitin effect of fall risk based on the balancer. Northeast Normal University, 2018.

[2]Kawanabe K, Kawashima A, Sashimoto I, et al. Effect of whole-body vibration exercise and muscle strengthening, balance, and walking exercises on walking ability in the elderly. Keio J Med, 2007, 56(1): 28.

[3]Huang P, Zhong M.H, Chen B, Qian N.D. Three-dimensional gait analysis in normal young adults: temporal, kinematic and mechanical parameters. Tissue Engineering Research in China, 2015, 19(24): 3882-3888.

[4]Xie Y.X, Bai W, Zhang Y. Research Status and Trend of Lower Limb Rehabilitation Training Robot. China Medical Device Information, 2010, 16(02): 5-8+56.

[5]Giaquinto S, Galli M, Nolfe G. A polynomial function of gait performance. Funct Neurol. 2007,

22(1): 43-46.
[6]Zhang Z.H. Study on the Body Balance Ability and Fall Risk of the Elderly in China. Summary of Papers of the 20th National Academic Exchange Conference on Sports Biomechanics. Sports Biomechanics Branch of Chinese Sports Science Society, 2018, 3.
[7]Xiang J, Xu F.Y. Research Progress of Gait Analysis in Clinical Rehabilitation. Modern medicine and health, 2014, 30(22): 3411-3413.
[8]Shan R.S, Huang G.Z, Zeng Q, Huang X.H. Effects of gait triggered functional electrical stimulation on temporal-spatial parameters of gait in foot drop patients after stroke. Chinese Journal of Rehabilitation Medicine, 2013, 28(06): 558-563.

Groundwater Numerical Simulation and Environmental Capacity Analysis of Petroleum Industry Based on Modflow

Cancan Zhang
School of Water Resources and Environment, Hebei Geo University, Hebei, 050031, China
E-mail:1587969536@qq.com

Abstract: With the integrated development of the Beijing-Tianjin-Hebeiregion,the petroleum industry in coastal cities has gradually increased. Langfang is an important base for the petroleum industry in North China, and its petroleum base is abundant. However, "running and leaking" in the exploitation of the petroleum industry poses a serious threat to groundwater pollution. Taking a gas station in Langfang as an example, this paper uses GMS software to establish a three-dimensional visual hydrogeological model, and through the MT3DMS solute transport module, to determine the damage caused to the groundwater caused by the leakage of oil in the process of utilization. The results show that under normal conditions, due to the poor diffusion ability of groundwater aquifers in the study area, the impact on surrounding groundwater will continue to affect for a certain period of time, and the environmental capacity of petroleum will gradually decrease from northeast to southwest.

Keywords: numerical simulation; groundwater; pollutant transport; environmental capacity

1. INTRODUCTION

Petroleum industry is the main supplier of energy and it plays an important role in the development of national economy [1-3]. Petroleum and its processed products not only bring many conveniences to people's life, but also cause certain pollution to the surrounding groundwater [4-6]. The leakage of oil industry under accident scenario is the main form of groundwater pollution. Numerical simulation can be used to accurately predict the possible pollution scope and degree of surrounding groundwater caused by oil tank leakage and the environmental capacity of groundwater oil, providing theoretical basis for groundwater pollution prevention and control [7-9].

2. EXAMPLES OF GROUNDWATER ENVIRONMENTAL PROTECTION

MODFLOW is a set of three-dimensional finite difference numerical simulation software specially developed by the United States geological survey in the 1980s for groundwater flow in pore media [10]. It is widely used to simulate the effects of well flow, rivers, drainage, evaporation, and recharge on heterogeneous and complex boundary condition flow systems. MT3DMS is a three-dimensional solute transport model simulating convection, dispersion and chemical reactions in groundwater systems. In the simulation calculation, MT3DMS should be used together with MODFLOW [11].

2.1. General Situation of the Study Area

The study area is located in the south of Langfang city, bordering Tianjin in the east, Bazhou in the west, Cangzhou in the south and Langfang in the north. The terrain of the region is low and flat, with the ground elevation generally ranging from 5 to 7m and the ground slope less than 1/10000. It is located in the low plain of Hebei plain in China.

The surface is formed by the alluvial accumulation of Yongdingriver, and the main landform types are gentle hills, slopes and depressions formed by the alluvial accumulation. The small landform types include gentle hills, sloping lands, low flat lands and shallow depressions, as well as local dune residues such as river sand beach [12].

2.2. Hydrogeological Conditions

The direction of groundwater flow field in the study area is from northwest to southeast. The area is located in the alluvial plain, with hydraulic gradient less than 1/1000.Its runoff is slow and the water quality is poor, mostly salt water.Shallow groundwater is Ⅰand Ⅱwater group, which is diving and micro artesian water. Its buried depth is within 130-160m, and its aquifer thickness is 20-50m. Its lithology is mainly medium fine sand and coarse sand, with a unit inflow of 10-15m^3/ h·m, and the groundwater type is HCO_3-MgCa water.Deep groundwater is Ⅲ and Ⅳ water group, and the lithology is fine sand, medium sand and coarse sand with gravel. Itsunit water inflow is 15-30m^3 / h·m,and its buried depth is 310-550m. The aquifer is 75-175m thick with a unit inflow of 5-30m^3/ h·m, and the groundwater type is HCO_3-Na water. The study is given priority to with shallow waterwhich is supplied mainly by precipitation, and it is consumed by evaporation. It is dominated by salt water, so it is undrinkable and unirrigated. Due to insufficient exploitation and utilization at present, groundwater dynamics are mostly in a natural state. Therefore, the equilibrium elements of shallow groundwater mainly include atmospheric rainfall infiltration recharge, lateral boundary recharge, evaporation discharge and lateral runoff discharge [13].

According to the pumping test study [14-15], the permeability coefficient range in the study area is 5-10m/d. According to the test of porosity, the porosity of mucky clay is 0.12. Its porosity of silty clay is 0.18, and the porosity of floury soil is 0.21. Its longitudinal dispersion is 6.2.

2.3. Numerical Simulation

2.3.1. Flow model

Three dimensional groundwater flow system can be described by the definite solution of the following differential equation:

$$\begin{cases} \frac{\partial}{\partial x}\left(k_{xx}\frac{\partial H}{\partial x}\right)+\frac{\partial}{\partial y}\left(k_{yy}\frac{\partial H}{\partial y}\right)+\frac{\partial}{\partial z}\left(k_{zz}\frac{\partial H}{\partial z}\right)+\mathrm{w}=0,(x,y,z)\in\Omega \\ H(x,y,z)=H_1,\ (x,y,z)\in S_1 \\ K\frac{\partial H}{\partial n}|S_2=\mathrm{q(x,y,z)},\ (\mathrm{x,y,z})\in S_2 \end{cases} \quad (1)$$

Where, Ω stands forGroundwater seepage area;

*H*1 stands for designated water level,m;

*S*1 stands for boundary of the first kind;

*S*2 stands for boundary of the second kind;

*K*xx, *K*yy, *K*zz stand for Permeability coefficients in the x, y, and z principal directions, m/d;

W stands for Source sink term, and it includes evaporation, rainfall infiltration supply and well drainage, m3/d;

q(*x*,*y*,*z*) stands for the flow at different locations on the boundary, m3/d;

$\frac{\partial H}{\partial n}$standsfor the component of the hydraulic gradient on the boundary normal.

2.3.2. Water quality model

Three-dimensional mathematical model of water quality uses theconvection-dispersion equation to describe the migration of pollutants in three-dimensional groundwater flow.The mathematical model of NAPLs migration dissolved in groundwater can be expressed as follows:

$$\frac{\partial C}{\partial t}=\frac{\partial}{\partial x}\left(D_{xx}\frac{\partial C}{\partial x}\right)+\frac{\partial}{\partial y}\left(D_{yy}\frac{\partial C}{\partial y}\right)+\frac{\partial}{\partial z}\left(D_{zz}\frac{\partial C}{\partial z}\right)-\frac{\partial(\mu_x c)}{\partial x}-\frac{\partial(\mu_y c)}{\partial y}-\frac{\partial(\mu_z c)}{\partial z}+f$$

$$\mathrm{C}(x,y,z,0)=C_0(x,y,z)(x,y,z)\in\Omega\ ,t=0 \quad (2)$$

Where, the first three on the right stand for dispersion items, and the next three terms stand for convection items. *f stands for* an increment of solute produced by a chemical reaction or adsorption; *Dxx*; *Dyy*; *Dzz*stand for dispersion coefficients in the x, y and z directions; *μx*; *μy*; *μz*stand for the actual flow velocity in the x, y, and z directions; C stands for the solute concentration, mg/L; Ω stands for the region of the seepage of the solute; C_0 stands for the initial concentration, mg/L.

Based on the numerical model of groundwater seepage which has been identified and tested, couple pollutant transport equation. Then the solute transport model of groundwater can be obtained [16-17].

2.4. Predicted Results

This project adopts double-layer oil tank for oil storage. The outer wall of oil tank is reinforced with glass fiber reinforced plastics, and the inner wall of oil tank is made of steel. Tank tank adopts concrete structure. Under normal operation, there will be no oil product leakage, which may be caused by emergencies and accidents such as geological collapse, old equipment corrosion, etc. This project is aimed at the prediction of groundwater environmental impact under the accident state.The accident status of similar projects is set as shown in table

Table 1. Oil tank leakage accident scene setting

Storage tank	Number of tanks	The material of tank	The volume of a tank	Degree of filling	Reserves	Leakage	The proportion
Diesel fuel tank	2	Double steel	30m^3/ tank	90%	45.36t	45.36kg/d	0.1%
The petrol tank	2	Double steel	30m^3/ tank	90%	39.96t	39.96kg/d	0.1%

MT3DMS software was used to simulate and calculate the migration distance, overrun range and influence range of petroleum in different time periods. The scope of petroleum exceeding the standard shall refer to the requirements in *Sanitary standards for drinking water*(GB 5649-2006), and the lower limit of petroleum detection shall refer to the lower limit of conventional instrument detection. Details are shown in table 2.

Table 2. List of evaluation factors and evaluation criteria

The evaluation factors	Petroleum
Quality standard (mg/L)	0.3
Detection range (mg/L)	0.01

In all the following simulated predictions, the black line indicates that the oil concentration exceeds the water quality standard limit (Excess range), and color slants red to indicate exceed bid more serious. The range within the red line indicates that the pollutant concentration can be detected (the influence range). Numerical simulation and prediction of groundwater pollution are carried out for the pollution point sources in gas stations in different production periods according to the set pollution source intensity. The results of groundwater environmental pollution are shown in figure 1-4 and table 3.

Table 3. Groundwater oil pollution prediction result chart

Time(d)	Maximum superbid distance(m)	Scope of pollution (m^2)	Maximum concentration of pollution halo(mg/L)	Maximum depth of contamination (m)
100	18	956	0.002	5
1000	126	7442	0.010	12

2000	228	16272	0.024	16
3650	391	30506	0.028	20

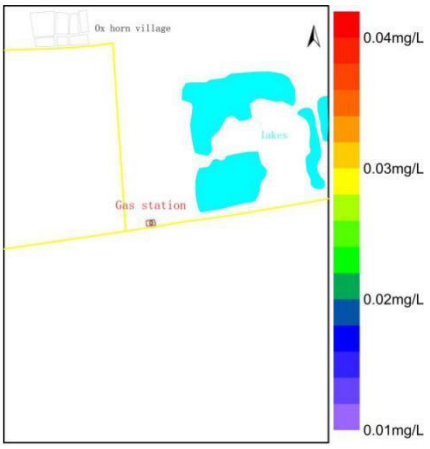

Figure 1. Pollution halo at 100d of leakage

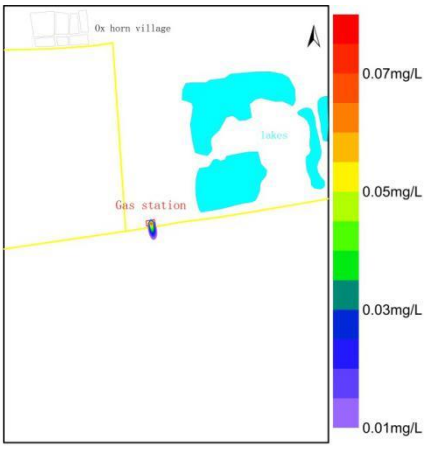

Figure 2. Pollution halo at 1000d of leakage

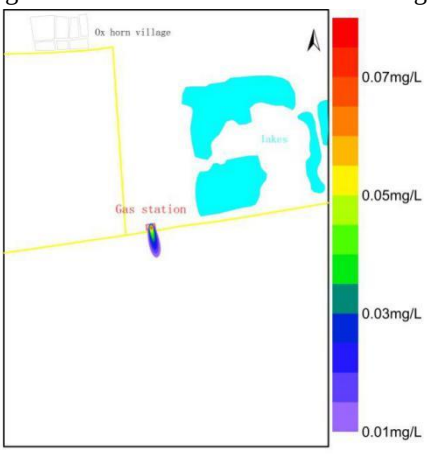

Figure 3. Pollution halo at 2000d of leakage

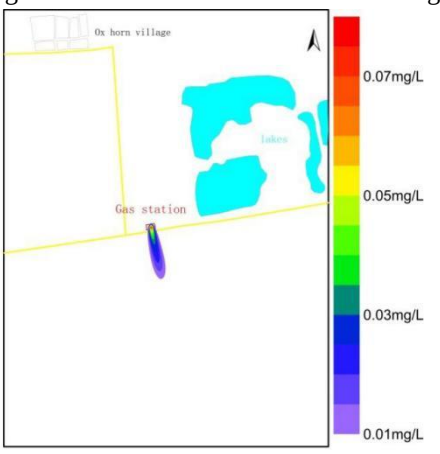

Figure 4. Pollution halo at 3650d of leakage

3. ENVIRONMENTAL CAPACITY OF GROUNDWATER

3.1. The Research Methods

When the groundwater environmental capacity is studied, it can be divided into several research units by regular grid on the plane, and the units are considered to be fully mixed. Groundwater environmental capacity is divided into dilution capacity, self-purification capacity and migration capacity.

3.1.1. Dilution of environmental capacity

When the concentration of groundwater pollutants is lower than the target water quality, only the remaining holding space from the existing water quality state to the target water quality state is considered, and the pollutants caused by degradation of pollutants due to physical, chemical and biological effects and the flow of groundwater are not considered.The amount of pollutants that can be tolerated to achieve water quality objectives by dilution.

Dilution environmental capacity can be calculated by formula (3):

$$Q_d = \frac{10^{-3}}{T}\sum_{i=1}^{n}\left(C_s^i - C_0^i\right)V_i \quad (3)$$

Where, Qd stands for the total dilution capacity of regional groundwater, kg/d; T stands for a defined period of time, d; i=1，2，⋯，n，n stands for total number of cells; Vistands forvolume of groundwater of uniti, m3; Cis stands for the target concentration of the pollutant given in unit, mg/L; Ci0 stands for the background value or initial concentration of the pollutant in the groundwater of unit i, mg/L; 10-3 stands for unit conversion coefficient.

The volume of groundwater can be calculated according to formula (4) :

$$V_i = \mu_i(h_i - b_i)s_i \quad (4)$$

Where, ui stands for the effective porosity of the aquifer in cell i; hi stands for the elevation of the diving level of unit i, m; bi stands for elevation of aquifer floor of unit i, m; si stands for the area of unit i, m2.

In the calculation, it should be noted that the aquifer is composed of different lithology, so the volume of groundwater should be calculated according to different lithology thickness and water supply degree.

3.1.2. Self-purification capacity

It is assumed that the self-purification of groundwater

basically conforms to the first order irreversible reaction equation. In the case of small reaction rate constant (generally not greater than 10-2), the self-purification environmental capacity can be calculated according to formula (5):

$$Q_p = 10^{-3} \sum_{i=1}^{n} K_i C_0^i V_i \quad (5)$$

Where, Qp stands for self-cleaning environmental capacity, kg/d; ki stands for the degradation rate constant of the pollutant in unit i, d-1,and the rest of the signs are the same.

3.1.3. The migration amount

The migration amount is mainly composed of pollutants taken out by artificial groundwater extraction and pollutants taken out by groundwater runoff, which can be calculated according to formula (6) :

$$Q_t = \sum_{i=1}^{n} (C_s^i P_i + C_s^i Q_{out}) \quad (6)$$

Where, Qt stands for the amount of groundwater migration in the calculation unit, kg/d; Pi stands for amount of groundwater mining in zone i, 103m3/d; i =1, 2,⋯,n, n stands for the total number of area; Cis stands for the concentration of a pollutant in a region where the outflow is located; Qout stands for the discharge of groundwater from this unit, 103m3/d, and it includes lateral discharge and overflow to the lower confined aquifer.

3.1.4. Regional groundwater environment

It can be calculated according to formula (7):

$$Q_T = Q_d + Q_p + Q_t \quad (7)$$

Where, QT stands for total environmental capacity of regional groundwater.

3.2. Determination of Parameters

3.2.1. Determination of parameters of dilution capacity

In the calculation of dilution capacity, the service life of groundwater T should be determined. Considering that groundwater should be utilized for as long as possible, so T = 10a=3650d in this study. In this study, by measuring the porosity and combining the lithology of the study area, the value of effective pore u was finally determined to be 0.12.

When calculating the self-purification capacity, the degradation rate constant of the control factor needs to be determined. In this study, the value of oil degradation rate constant k1 =0.00513d⋯.

3.2.2. Determination of parameters of migration amount

It is necessary to calculate artificial exploitation and lateral runoff of groundwater in the study area.Since no groundwater is mined, only the lateral runoff of groundwater in the study area is considered. The lateral runoff of groundwater in the study area was 120.2m3/d.

3.3. Environmental Capacity of Groundwater

The calculation of the environmental capacity of groundwater should first determine the water quality standards for groundwater. Since there is no oil quality index in the national "groundwater environmental quality standard (GB 3838-88)", this paper refers to the "surface water environmental quality standard (GB 3838-2002)". The standard limit of pollutant concentration is subject to the class III standard of "quality of surface water environment gb3838-2002", and the oil limit is determined as 0.05m /L.

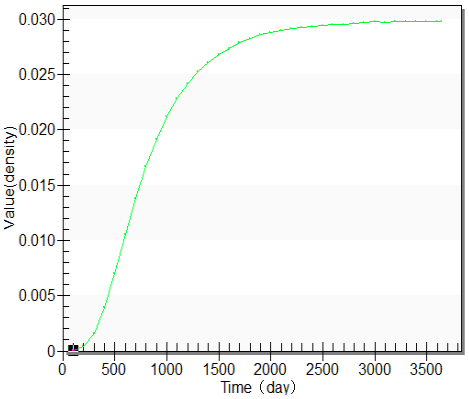

Figure 5. Under abnormal conditions, the concentration of petroleum pollution changes at the downstream boundary of petrol stations

The determination of environmental capacity of petroleum pollutants in groundwater is based on the threshold that the maximum concentration of petroleum pollutants in groundwater does not exceed 0.05mg/L. According to the calculation formula of groundwater environmental capacity, the dilution capacity, self-purification capacity and migration amount of petroleum pollutants in each unit are calculated, and the environmental capacity of petroleum pollutants in groundwater can be obtained by adding them together.

GMS and ARCGIS software are used for simulation to obtain the groundwater environmental capacity map of oil pollutants in the study area, and it isshown in figure 6.

According to figure 6, the minimum and maximum environmentalcapacity of petroleum groundwater inthe study area are 3.50g/d and 13.5g/d respectively.The oil environmental capacity in the gas station increases gradually from northwest to southeast.

It can be seen from the calculation results that the oil environmental capacity at the pollution point source set in the research area is 8.7g/d. The leakage amount at the pollution point source of the gas

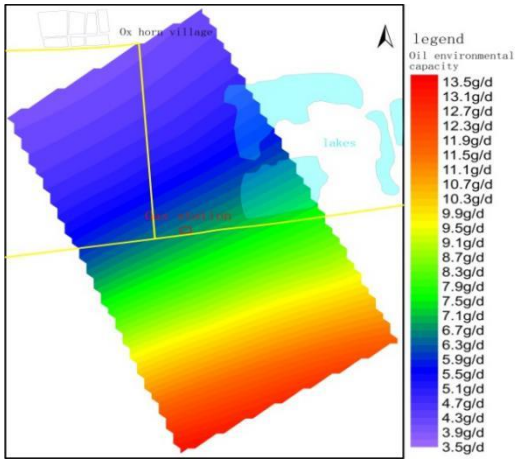

Figure 6. Environmental capacity distribution map of petroleum in groundwater of petrolstations

station has exceeded the scope of the groundwater petroleum environmental capacity, which has caused pollution to the groundwater environment. Therefore, reasonable and effective prevention measures can be put forward according to the groundwater petroleum environmental capacity to control the infiltration amount of petroleum pollutants in the groundwater.

4. CONCLUSION

(1) In view of the fact that after the occurrence of various leakage conditions, the pollutants will continue to spread around with the convection and dispersion of groundwater. Therefore, it is recommended to set up tracking monitoring wells in the areas affected by pollutants to monitor the concentration of pollutants in the aquifer in real time. In this way, we can detect pollution incidents early and take corresponding measures to deal with them in time.

(2) According to the predicted results, under the action of hydrodynamic conditions, pollutants are mainly transported from northwest to southeast near the gas station.

(3) Considering the most unfavorable situation (in the case of leakage of diesel and gasoline storage tanks), it can be seen from the predicted results that the scope of excessive limits of petroleum in the groundwater did not exceed the scope of the gas station site after the leakage accident.

(4) From the overall evaluation results, the project will not have a great impact on groundwater under the condition of effective anti-seepage measures and perfect monitoring system. In case of an accident, the emergency plan should be activated immediately. As long as the groundwater pollution is treated timely, it can be controlled within the scope of the gas station site.

(5) For the contaminated groundwater or soil, physical treatment, chemical treatment, biological treatment and comprehensive treatment can be adopted to control the pollution and restore the site according to the types and characteristics of pollutants.

REFERENCES

[1]Yang S.Q, Shi H.B, Yang J.Z, Shen R.K. Study on the effect of brackish water irrigation on groundwater environment in arid areas. Chinese journal of water resources, 2007, 05: 565-574.

[2]Ren G.J, Yang L.S, Ren X.G, Hu C.L. Visual Modflow application in groundwater environmental impact assessment. Journal of China environmental management cadre institute, 2015, 2503: 83-86.

[3]Zhang Y.S, Jia H.F. Environmental simulation and scenario analysis of groundwater in typical plain areas of Beijing. Journal of Tsinghua university (natural science edition), 2008, 09: 1436-1440.

[4]Zeng W, Yu Y, Miu W, Gao C. Prediction of groundwater environment of apharmaceutical factory based on Visual Modflow. Industrial water and wastewater, 2008, 4901:74-78.

[5] Zhang F, Yin Z, He J.B, Zhang L. Visual MODFLOW in environmental impact assessment of underground water in coal mine construction-a case study of anjiazhuang coal mine, lingtai county, gansuprovince. Gansu geology, 2018, 2701: 70-78.

[6]Hou T. Prediction of groundwater pollution in a simple landfill based on modflow. Groundwater, 2008, 4003: 80-81.

[7]Wang Y.H, Yang S.B, Liu R.Y. Prediction and evaluation of groundwater environmental impact in a power plant based on Visual Modflow. Pollution control technology, 2008, 3103: 13-18.

[8]Mo X.Y, Ma W.D, Li H, Zhang L. Environmental impact assessment of tailings pond groundwater based on modflow-nwt. Environmental monitoring management and technology, 2018, 3004: 32-36.

[9]Yang G.Y. Environmental impact assessment of groundwater in hongqigou red mud reservoir based on MODFLOW. Shanxi architecture, 2014, 4423: 191-192.

[10]Li Y.Z, Yao Y, Pang L, Luo W. Heavy metal pollution assessment of soil and groundwater in southwest mining area based on Visual Modflow. Guangdong agricultural science, 2013, 4017: 168-169+184+3.

[11]Liang C, Zhou A.Q, Guo K, Peng J.S. Numerical simulation of groundwater environmental impact of a domestic waste landfill based on GMS. Resources, environment and engineering, 2016, 3006: 872-875.

[12]Li Y, Yu Y, Gao C. Study on groundwater environment prediction of a chemical plant based on Visual Modflow. Green technology, 2017, 18: 88-92+95.

[13]Hu Y,Yang Z.Y, Zhao J, Yan D.H. Environmental impact assessment of groundwater in typical safe landfills. People's Yellow River, 2014, 3608: 79-82.

[14]Liang J.P, Du P.F, Li Y.Z. Prediction of groundwater flow field changes based on Visual Modflow. Environmental engineering, 2014, 32, S1: 267-270+304.

[15]Zhang Y, Long J.W, Cheng Y.R, Zhao L, Deng

C.G. Prediction of groundwater pollution in a chemical industrial park based on Visual Modflow. Groundwater, 2016, 3802: 88-90.
[16]Liu J.G, Xu G.Z, Ma X.L, Lei J.M, Wu H. Comparative study on the application of different simulation software in groundwater eia. Environmental science and technology, 2008, 41, S1: 359-362.
[17]Sun J. Prediction of effects of zinc ions on shallow groundwater quality. Journal of hunan institute of technology, 2012, 1205: 14-15.

Research on Information-Based Teaching Practice of Road and Bridge Engineering Measurement Course

Guizhen Wang
School of Architecture and Engineering, Chongqing Vocational Institute of Engineering (cqvie), Chongqing, 402260, China
E-mail: suiyueruge4321@163.com

Abstract: Measurement is a technology that emphasizes both theory and practice. A reform idea of the road and bridge engineering measurement information teaching practice has been put forward, aiming at solving the problems that the traditional measurement teaching over-emphasizing theory, the students' low enthusiasm for learning, low training efficiency, and the single assessment mode. This idea, based on the retention of students' after-school training, introduced a variety of modern information based technology and information resources, optimized teaching methods, coordinated the various elements of the teaching process, and guided students to transform from the passive learning mode of listening, remembering, remembering and practicing to active inquiry learning, thereby improving the learning efficiency.
Keywords: information based teaching; road and bridge engineering; measurement course

1. INTRODUCTION

Engineering measurement, a typical course which integrates theory and practice, is a sufficient theory and emphasis on the characteristics of skill and practice. It is the basic compulsory course of many majors of the department of water conservancy and hydropower engineering, such as water conservancy and construction engineering, construction engineering technology, construction engineering supervision, architectural decoration engineering technology and water supply and drainage engineering technology [1].

Although the tasks and techniques of the special measurement course vary according to the needs of each major, the instrument and the basic principles and basic measurement methods are the same. Thus, the Department of Water Conservancy and Architectural Engineering has carried out a teaching reform through collective research, dividing the original engineering surveying courses into two parts, the basic course of Engineering surveying，which is the common part of each major, and the professional engineering survey, which developed into a separate course integrating the theory and practice and would be carried out in two weeks [2].

The basic part of engineering surveying aims at strengthening the students' basic training so that they can master the operation methods and basic usage of leveling instrument, theodolite, steel ruler, total station instrument and RTK (real-time dynamic). The proper use of information-based teaching methods can enable students to experience and learn knowledge in various ways, which would be a big help to build a flipped classroom, where students can review, and think at any time, and improve constantly [3].

2. CHARACTERISTICS OF INFORMATION-BASED TEACHING OF ROAD AND BRIDGE ENGINEERING SURVEY

Supported by information technology and applied with modern teaching methods, information-based Teaching is an activity guided by modern teaching concept. It is a comprehensive process of interaction, integration and practice. The wide application of modern information technology, such as network platform, multimedia and distance education, can accelerate the process of education reform and development. The measurement technology of road and bridge engineering is also developing towards information, intellectualization and networking [4-5].

Specifically, in terms of teaching software and hardware in the course of road and Bridge Engineering survey, many kinds of modern information technology and information resources are used, such as network learning platform, live broadcasting vehicle system, simulation software, and Wechat communication platform [6-7].

By optimizing teaching methods and arranging all elements of teaching process, students are guided to change from passive acceptance learning mode of "listening, memorizing, reciting and practicing" to active inquiry learning mode, which would definitely improve classroom efficiency.

The student's dominant position was fully considerate not only in-class, but also pre-class andafter-class by providing students with online communication learning platform, creating an independent inquiry learning space and a lively and interesting learning environment.

2.1. Analysis of Course Information-based Teaching Design

It is necessary to carry out design analysis, which is the premise of Information-based design， before

carrying out the course Information-based teaching design. The analysis of Information-based teaching course design includes the analysis of learning conditions of the students, analysis of the teaching goals, analysis of the teaching contents and analysis of the teaching methods.

2.2. Analysis of Learning Conditions of the Students

Students paly many roles in the information based teaching classroom, they are not only the ones who need the knowledge construction, knowledge absorption and internalization, but also the protagonist of information-based classroom, the communicator of teachers 'emotions, the collaborator and collaborator of peer learning. Their learning conditions, such as the basic knowledge of subject and mastery of information technology, autonomous learning ability, application ability of information technology and team cooperation abilities all directly affect all aspects of information-based teaching design.

Therefore, in the analysis of students' learning conditions, it is necessary to analyze students' original knowledge, skill level, information ability, cognitive ability, physical and mental emotions, etc. In the information-based teaching of highway and bridge engineering courses in Higher Vocational colleges, the importance of learning situation analysis is particularly important for the reason that, with the reform of college entrance examination system, the types and structures of students in higher vocational colleges are diversified, and their professional foundations and learning abilities vary greatly.

Taking Wuhan Vocational College of Communications as an example, there are four different sources of students majoring in road and bridge engineering: general college entrance examination enrollment, technical college entrance examination students, single enrollment students, and "3 + 2" high school and vocational education convergence training students.

Among them, technical college entrance examination students, single enrollment students and "3 + 2" students have learned the basic operation of "Engineering Survey" before entering higher vocational education, and their measurement skills have reached a certain level, while the general college entrance examination enrollment students in the "Engineering Survey" learning is completely a zero start. Their learning bases are totally different.

2.3. Analysis of the Teaching Goals

The analysis of teaching goals determines the general direction of information-based teaching design. The selection and design of teaching content, strategy, methods, situations and learning evaluation should be based on teaching goals.

For road and bridge Engineering courses, the analysis of teaching goals mainly includes knowledge goals, technical goals and professional accomplishment goals.

Taking the course of Engineering Survey as an example, its knowledge goal is to enable students to master basic measuring principles and methods of elevation, angle, distance, coordinates, and the basic processes and methods of control survey, mapping, construction lofting, etc; its technical goal is to enable students to master the use of total station, level, GPS and other measuring instruments, and to have the ability to solve practical measurement problems in engineering construction; its professional accomplishment is to train the students to become the surveyors and mappers who can go down, stay, endure hardships and be energetic. In addition, for different students, different stages and different contents, a detailed analysis of teaching goals is still needed.

2.4. Analysis of the Teaching Contents

By analyzing of teaching content in the course of information-based teaching design, the teaching content would be integrated and optimized, the teaching knowledge and skills would be organized and the key and difficult points of teaching would be distinguished.

Taking the course "Engineering Survey" as an example, the teaching content of "Engineering Survey" is mainly divided into basic knowledge of Engineering survey, basic survey skills, special survey skills and comprehensive survey skills.

The basic knowledge of engineering surveying mainly includes the basic concepts of Engineering surveying, the basic principles of point location determination and the working principles of surveying, etc; the basic measurement skills include leveling, angle measurement, distance measurement, coordinate measurement, etc; the special surveying skills include control surveying, mapping drawing and construction lofting and the comprehensive survey skills include road engineering survey, bridge and culvert engineering survey, tunnel engineering survey, pipeline engineering survey, etc.

For the course, the point is to improve the comprehensive measurement skills by studying basic measurement skills and the training of special measurement skills. The difficulty lies in improving the comprehensive measurement skills.

Besides, in each teaching project, the teaching content of each sub-project is needed to be analyzed to get more detailed teaching content and specify the teaching difficulties.

2.5. Analysis of the Teaching Methods

Traditional teaching methods mainly includes teaching, conversation, discussion, guidance, demonstration, visiting, exercises, experiments and practice assignments, they all have their own advantages and disadvantages.

In the information-based teaching design, the teaching methods that effectively achieve teaching goals should be selected according to the results of students' learning condition analysis, teaching goal analysis

and teaching content analysis, the characteristics of students and teaching content, the accumulation of curriculum information resources, and the current status of the school information hardware and the construction of information-based teaching platform.

It is particularly necessary to summarize the difficult problems of traditional teaching methods, which can be easily solved by information technology.According to the student's learning condition analysis, the theories of students are generally weak in the courses. It is important to lay emphasis on the training of students' practical ability and vocational skills to cultivate high-quality technical and skilled talents. In the course of road and bridge engineering, the method of obtaining direct experience in the form of intuition, or the method of forming skills and skills in the form of practical training should be adopted more often.

For example, in the teaching of Engineering Survey, adopting the traditional teaching method has resulted in the separation of theory and practice, the separation of internal and external work, the virtual software and data, which leads to teachers' poor teaching and students' poor learning. The information resources are becoming rich and intuitive, the informational methods are more convenient and fast, and the information technology is mature and popularized, which makes it possible to make full use of the information resources and information technology to arrange various teaching sections, apply project teaching method, demonstrate teaching method and simulate training teaching method.

3. THE TEACHING DESIGN OF THE INFORMATION BASED COURSE

3.1. Situational Design of Information Based Teaching

Constructivism holds that learning is always associated with a certain social and cultural background (i.e. context), which means that learners can assimilate or adapt to the new knowledge they have learned by using the relevant experience in their original cognitive structure. By assimilation and adaptation, the learners can construct new knowledge. Therefore, situational design is the first link of information-based instructional design. In the situational design of course information based teaching, it is necessary to collect and accumulate a large number of course-related information materials.

On the basis of making fully use of information resources and information technology, such as text, image, audio, video, artificial intelligence, three-dimensional modeling, to design and create situations to arouse students 'interest, stimulate students' associations, and complete the purpose of "assimilation" and "adaptation" of knowledge. The methods of creating situation in information-based teaching mainly include creating problem situation, story situation, simulation situation and collaboration situation. Several methods could be synthetically applied in the design of information-based teaching situation. For example, several questions such as "Where will maps be used in life?" "What information can we get from Baidu Map?" "How did Baidu Map and Gaode Map in the middle of mobile phone come into being?" could be proposed in the teaching design of "Surveying and Mapping of Large Scale Topographic Maps" in Engineering Survey. By asking these questions to guide students to open their mobile map to display traffic and tourism maps of various cities, and so on, to enable students to have a strong interest in the process of map generation in the surroundings of the map. In the "coordinate lofting", a fast shot built from wasteland to high-rise buildings, and virtual construction scene could be designed. And students can play different roles, such as surveying director, instrument operator, ruler, data recorder and so on. Students can experience different roles in the simulated environment of construction site.

3.2. Design of the Implementation Process of Information-Based Teaching

The implementation process design of information-based teaching is the decomposition of teaching steps and the time allocation of each link. It is an important link of information-based teaching design. It is a script for teachers 'directors and students' actors to complete information-based classroom teaching together, which directly affects the effect of information-based teaching.

The curriculums of road and bridge engineering have the characteristics of practicability of knowledge, pertinence of occupation, multi-level objectives, dynamic updating of curriculum content and so on. Therefore, in the process design of information-based teaching of road and Bridge Engineering courses, we can adopt the project-based process design based on working process. Driven by tasks and interacted with teachers and students in teaching, the process takes students as the center of learning process, so that students can independently acquire information, make, implement and evaluate plans. In the process of doing their own practical tasks they can master professional knowledge and improve professional skills.

For example, in the teaching design of "Surveying and Mapping of Large Scale Topographic Maps" in Engineering Survey,map a topographic in the form of task-driven, and the teaching process are designed as: Course Introduction, Audiovisual Experience, Synchronized Operation, Skills Training, Assessment Interactive, Communication, Summary and Homework. Each process is allocated with time, so that students can master the mapping process of large-scale topographic maps and improve the mapping ability.

The following advice should be paid attention to in the process design of information-based teaching of road and Bridge Engineering courses: In the process of teaching design of information-based teaching of road and Bridge Engineering courses, the students

must be taken as the center, teachers should be taken as guides. Teachers should teach students in the process of practicing, and students should learn in the process of practicing. The teaching and learning should be integrated, and the interaction between teachers and students should be reflected; the implementation process design of information-based teaching is different from normal classroom design. It is an extension of classroom design, including the preparation of information materials before class and feedback after class; the teaching process design of course information based teaching implementation process is not the design of a course, but the teaching process design of a course. In this process design, it is necessary to integrate all knowledge points so that students can master knowledge and skills in the process of systematization and achieve teaching goals; the design of the implementation process of information-based teaching cannot remain unchanged. It needs to be flexibly adjusted according to the different teaching objectives, teaching contents and teaching goals.

3.3. Evaluation Design of Information Based Teaching

Teaching evaluation is the feedback of teaching effect, and its design directly reflects the teaching effect.According to the teaching evaluation, teachers can summarize the advantages and disadvantages of the teaching design and methods, understand students 'learning status, so as to teach students in accordance with their aptitude and optimize teaching design; students can see their own learning growth track, to improve their learning enthusiasm, summarize their learning experience and reflect on their own shortcomings.

In the design of information-based teaching evaluation, data statistics tools can be used to automate statistics to generate information such as scores and student feedback, so as to make teaching evaluation more intuitive, reduce workload and improve efficiency; internet plus information technology can be used to ensure the timeliness and multifaceted nature of evaluation, such as using micro-blog, WeChat, QQ and other information communication methods to make teaching evaluation.For example, in the large-scale topographic map surveying and mapping of Engineering Survey, according to the principle of "emphasizing results and more on process", the evaluation mechanism of "emphasizing process and emphasizing practical effect" is designed. The evaluation among groups, members, students, teachers and students is realized by checking storage, assessment forms and QQ evaluation and other methods. Students' topographic maps were evaluated by experts outside school and peers of enterprises through micro-blog and forums.

The following points should be paid attention to in the design of information-based teaching evaluation of road and Bridge Engineering courses: Information-based teaching evaluation should be student-centered, the results should be emphasis, but process is more important. Students 'participation, interest and attitude, and improve students' thinking ability should be lay heavy emphasis; information-based teaching evaluation needs to track students' development, systematically record students' skill, practical ability and professional accomplishment, and dynamically adjust teaching evaluation methods according to students' current ability; the evaluation of information-based teaching should be carried out in an all-round, multi-level and diversified way, and the aspects of students, teachers, parents, schools, society and other subjects and levels should be considered comprehensively; after the evaluation of information-based teaching, specific suggestions for improvement and feedback each subject must be put forward in a scientific, appropriate and constructive way, and form a development-oriented evaluation mechanism of information-based teaching.

3.4. Application and Practice of Information-Based Teaching

Twenty-five scenarios were designed, 17 micro-classes were made, and 12 evaluation forms for the course Engineering Survey were designed based on the result of the analysis of learning conditions and the decomposed teaching goals of Engineering Survey. The analysis of learning conditions result analyzed three different types of students, namely, the single-enrollment province of road and Bridge Engineering specialty, the unified enrollment of general college entrance examination and the technical college entrance examination. And the result of decomposed teaching goals of Engineering Survey is obtained by decomposing the knowledge target, skill target, the knowledge and skill of the course teaching of project systematization and professional accomplishment target of the course teaching goals of Engineering Survey, distinguishing the key and difficult points of teaching, and adopting flexible teaching methods.

Sixty class hours of the information-based teaching design of were designed by using the comprehensive application of audio-visual perception, synchronous learning, task-driven, simulation training and other means, making full use of network, communication, multimedia and other information technology methods, such as pictures, video, audio, documents, data, charts and data, and using task-driven to arrange all aspects of the teaching process.

Three teachers of engineering surveying specialty in Wuhan Vocational College of Communications have compiled teaching plans and implemented information-based classroom teaching according to the information-based teaching design scheme. This teaching scheme guides students learn from easy to hard, from perception to rationality in the way of "learning by doing, doing by learning, combining

work with study, learning to do “, so that students gradually master engineering measurement skills, the key and difficult points of learning, thus achieving teaching goals. And this teaching design has gradually formed the characteristics of “information teaching integration, paying equal attention to both skills and qualities”.

As a result, students generally find it interesting and easy to learn, while teachers find it easy to teach, and the efficiency is much higher. The results of the teaching evaluation of Engineering Survey rank in the front rank of the whole school.

4. A CASE OF INFORMATION-BASED TEACHING REFORM: TAKING HORIZONTAL ANGLE MEASUREMENT AS AN EXAMPLE

4.1. Establishment of Wechat Group and Network Learning Platform

In view of the characteristics of the popularity of Wechat among college students, the Wechat Communication Group of this course was established by the teachers before the beginning of the course, so that students can join the Wechat Group, and, excellent graduates in the measurement posts and surveying instructors inside and outside the school are invited to join the group at the same time.Before class teachers arrange discussion topics in the Wechat Group. Students can consult the information on the Internet and start the Wechat discussion. Relevant questions can be promptly instructed and answered by the seniors or teachers.

Establishing professional network learning platform, so that students loaded the road and bridge engineering technology network learning platform before class, and entered the road and bridge engineering survey course to preview the content of horizontal angle measurement unit, study training instruction andfamiliarize with measurement norms. The platform also uploaded small software related to measurement for students to download to mobile phones to use, to enhance students’ interest in learning.

4.2. Introducing Live Broadcasting System and Simulating Software

With the information-based teaching reform, the teaching hardware conditions have been improved. The live broadcast system has been introduced into the classroom. This system can display the operation details of measuring instruments in an all-round way by magnifying demonstration and changing angle. After the teacher has explanation, the students will go to the stage to operate the system, and the teacher will guide the other students in the class.Under the guidance of the teacher, while learning and practicing, they can quickly grasp the operation steps, operation essentials and matters needing attention of theodolite. On the other hand, the conditions of teaching software and the quality of making electronic courseware were improved.

For the measurement principles which are difficult to understand, teachers can use animation and video to create situations to help students digest and understand. In the past, due to their unfamiliar with the instruments, students often spent a lot of time exploring the operation, which causes the low efficiency. In order to solve this problem, the three-dimensional simulation software of road and bridge measurement was introduced, and the learning and training mode is simulated first and then practiced. The three-dimensional simulation software for measurement includes virtual simulation training module and virtual operation testing module. Students can conduct three-dimensional simulation training in computer room. In the training module, students conduct measurement simulation training in the simulation environment. In the training process, the system designs the corresponding theoretical knowledge examination tests, by doing these tests, students ‘understanding of the operation process would be constantly strengthened, and the operation errors would be reminded to correct. Under the test module, the students need to simulate the measurement tasks correctly within the specified time, and the system automatically counts the results of the simulation operation. The field practice can be carried out only after the results are qualified. Teachers adjust team members according to feedback data in time to balance the strength of each group. Through the operation of the software, the students subtly transfer the points of attention and key points of the angle measurement, which lays a foundation for the practice of operating the instrument. The system simulates the road and bridge construction site environment and embeds engineering survey norms, which is helpful to cultivate students ‘safety consciousness, normative consciousness and quality consciousness.

4.3. Team Division of Labor and Implementation of Tasks

Students enter the after-class training process after passing the simulated examination. Taking the horizontal angle measurement as an example, the students would carry out the angle measurement according to the designated points. In order to improve students’ autonomous learning ability and cultivate the sense of teamwork, the division of tasks was determined by the students through group discussion according to the training tasks.

After measuring an angle, the role rotation is carried out and the angle is measured again, and the precision analysis is carried out by looking up the norms to cultivate the normative consciousness. In task implementation, students can use online learning platform to re-learn, record and calculate angles through electronic handbook, and upload the results to online teaching platform. After class, in order to cultivate the students’ ability of continuous learning, teachers assigned different difficult assignments on the network learning platform to enhance the ability of students at different levels.Students can exchange

questions on the problems they encounter through the online learning platform to consolidate their learning achievements. From the training effect, compared with the previous classes that did not carry out information-based teaching, the average time for students to complete their first task was reduced from 55 minutes to 32 minutes, the error rate of students' operation was reduced from 36% to 20%, and the average score of skill test was increased from 73 to 81.

4.4. Assessment of Courses in Different Stages

This course was assessed in three stages. With the help of professional network teaching platform, the total scores of simulation training evaluation, field practice evaluation and online test evaluation are evaluated by 30%, 40% and 30% weights respectively.

The results were recorded automatically by teaching platform. Each student's learning situation and evaluate the teaching effect was analyzed by teachers in schools and business instructors, so that they can provide targeted counseling in the later stage for the students. Students can analyze their weaknesses and find out the direction they need to work hard by checking their test scores at all stages.

5. CONCLUSION

In summary, with the support of information based technology and information resources such as web-based learning platform, Wechat communication learning group, live broadcasting information system, measurement simulation software and so on, the teaching methods and arrangements of teaching process were optimized by teachers so that students can break through the limitation of classroom time, which means they can review and consolidate at any time, and the space limitation,which is to say students can perform the measuring instrument operation for outdoor construction environment in doors with simulated system. Students can practice in learn and learn by practicing. This information-based teaching reform has solved the problems of traditional teaching such as difficult to guide students, not accessible to practicing, easy to make errors and the potential instrument damage. By using the information based technology, the sources of the course are all on the internet, the content is much more interesting, the software learned was much more intelligence and the learning evaluations are much more dynamic.

REFERENCE

[1]Wang X.F. Discussion on teaching research of electric power engineering construction survey course. Guangdong vocational and technical education and research, 2018(06): 72-74.

[2]Zheng H. Reform of practical teaching mode of engineering surveying under the information condition. Research and practice of innovation and entrepreneurship theory, 2014, 1(08): 89-90.

[3]Lin K. Practical research on informatization teaching of engineering surveying technology. Wind of science and technology, 2018, (03): 44.

[4]Shen W.L, Zhang K.C. Information-based teaching design of architectural engineering surveying course in higher vocational colleges-taking "level 3 and level 4 surveying" as an example. Western quality-oriented education, 2017, 3(22): 200-201.

[5]Liu L.L, Zhou L. Construction of effective evaluation system of information-based teaching in higher vocational colleges-taking engineering survey as an example. Information technology and informatization, 2017, (10): 77-80.

[6]Lu Y.F, Tan Q.F, Gu H, Lian Y. Informatization teaching design of practical training course of architectural engineering survey in higher vocational colleges. Journal of anhui water resources and hydropower vocational and technical college, 2016, 16(04): 59-61.

[7]Sun S, Wu L.Y, Ye W. Research on teaching design of vocational college curriculum informatization-taking the course of "road and bridge engineering detection technology" as an example. Journal of zhenjiang technical college, 2016, 29(04): 101-103.

Research on Security Processing Method of Data Time Transfer Process

Yuejuan Jing, Han Peng, Xiaoyin Wang*
Xi'Aeronautical University, Xi'an, Shanxi, 710077
**Email: jingyuejuan-1981@163.com*

Abstract: As an independent global satellite navigation system, Beidou satellite navigation system plays an important role in positioning and traffic management. However, when time is transmitted, the security of data is difficult to be effectively guaranteed, which seriously affects the reliability of the transmission process. Therefore, continuous improvement of the security processing of the data time transfer process is of great significance to ensure the safe and efficient transmission of data. Based on this, a data processing method based on Beidou satellite navigation system is proposed. The high-precision GNSS time transfer method is used as a reference to design the data time transfer mode; the data security processing scheme is designed to realize the data time transfer process security process. The experimental results show that the processing method greatly improves the data transmission efficiency and data security, and has high application advantages.
Keywords: beidou satellite navigation system; time transfer; data security; processing

1. INTRODUCTION

The rapid development of social economy has enabled people to apply more resources to the field of science and technology for technological innovation and development, so the level of advanced technology in various fields has been significantly improved. As one of the high-tech industries, Beidou satellite navigation technology has its own perfect industrial chain, so it is also widely used in many industries, especially in the fields of transportation and electronic positioning. In the face of the increasing market demand brought by its wider application range, it is constantly seeking to improve and develop itself. How to ensure satellite data security has become one of the core issues of general concern in this field [1]. On the one hand, only by effectively ensuring data security can users be protected. Once the security of data information is illegally violated, not only the user's personal information may be leaked, but the navigation system may be misled, providing incorrect data information, causing serious accidents such as aircraft and other vehicles leaving the route. On the other hand, only by effectively ensuring data security can the user's needs be met. The security of data is the basis for the smooth operation of the system. Only when the security of data is guaranteed can the user be provided with safe and reliable services [2]. Therefore, a method based on the data transmission process of Beidou satellite navigation system is studied to improve the secure transmission of data.

2. DATA TIME TRANSFER PROCESS SECURITY PROCESSING METHOD

2.1. Choice of Time Delivery Method

Time transfer refers to the time offset between time users who have used two or more participating comparisons using time comparison techniques. The way of time transmission is roughly divided into three types, namely, carrying clock, wired transmission and wireless transmission [3]. Because the GNSS time transfer method has the advantage of high precision, it is more suitable for the time transfer requirement of the Beidou satellite navigation system [4]. Therefore, the GNSS time transfer method is selected as a reference for the overall design of the method. The general structure of GNSS time transfer mode is shown in Figure 1.

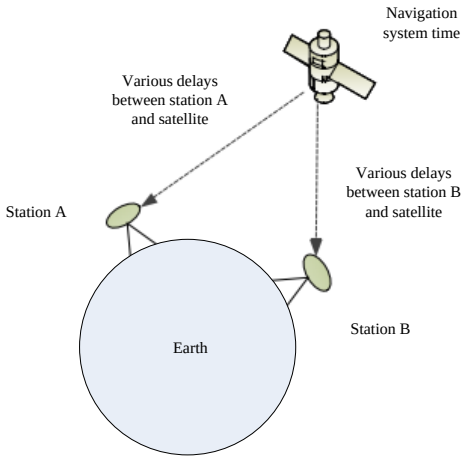

Figure 1. Schematic diagram of GNSS time transfer structure

2.2. Safe Handling Method Design

Based on the above GNSS time transfer, the data transmitted in the time transfer is safely processed. The specific design ideas are shown in Figure 2.

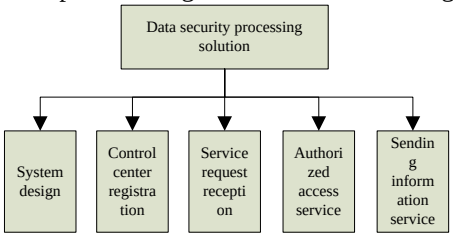

Figure 2. Safety management ideas

Analyze many factors that may threaten data security in time delivery, and proceed from various aspects to process data security to form a data processing solution. The awareness of data security protection during system design and the independence of each link are strengthened; In order to ensure the safe operation of the system, various components such as chips are required to be registered in the control center; The service request shall be sent when the relevant service is performed, and the control center shall verify the service request to determine whether it meets the requirements; The authorized access is verified to prevent illegal users from entering the system and interfere with the normal operation of the system, thus forming related hidden dangers; In order to ensure the security and reliability of data transmission, relevant key information should be sent to the control center to perform identity and request verification when performing related request services [5]. Through the above method, the data security processing scheme design is completed.

3. EXPERIMENT AND RESULT ANALYSIS

In order to verify the effectiveness of the data processing method based on the Beidou satellite navigation system, the following experiment was designed to verify its application effect. In order to fully embody the application advantages of the method, the method and the traditional data security processing method are used to carry out the data information transmission test under the same interference condition, and the interference degree, the statistical data transmission efficiency and the data security degree are continuously increased during the experiment. Record these two indicators and observe the experimental results.

3.1. Experimental Environment Settings

In order to ensure the accuracy and effectiveness of the experimental results, the experimental parameters are strictly controlled. Since the purpose of the experiment is to test the effectiveness of the data processing method based on the Beidou satellite navigation system, it is necessary to control the variables of the operating system environment and the intensity of the interference data transmission to prevent it from interfering with the accuracy of the experimental results. . The experiment was carried out in the GX-Developer V7.0 and GX-Simulator6.0 simulation environments. The system hardware environment settings are shown in Table 1.

Table 1. Experimental environment settings

Related configuration	Configuration parameter
CPU	PIII 2_500 or higher
RAM	2G(Recommended 4G or higher)
Operating system	Windows 7 and higher
JDK	JDK 1.6
WEB server	Apache Tomcat
Database	Oracle 11g
Browser	Firefox 49
Network protocol	TCP/IP

3.2. Verification Process

During the experiment, different data security processing methods were used to conduct data information transmission test under the established system environment, and a contrast test was set up. Through the experimental time change to increase the degree of signal interference, the data transmission efficiency and data security of the two methods are tested, and the two indicators are recorded and a comparison chart is drawn. Data transmission efficiency and data security test results are shown in Figures 3 and 4 respectively.

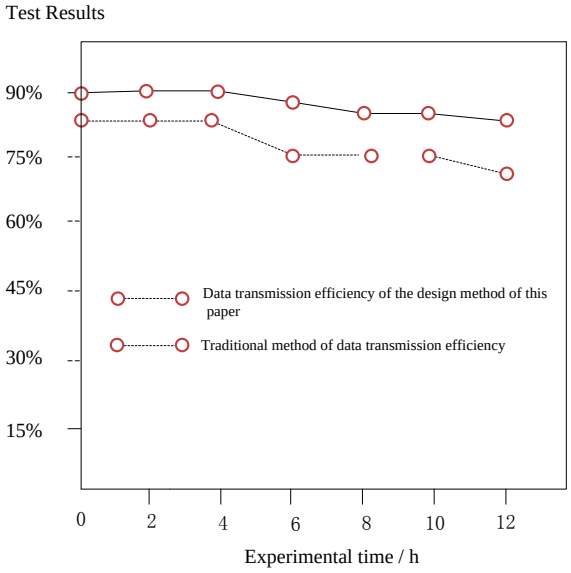

Figure 3. Data transmission efficiency comparison result graph

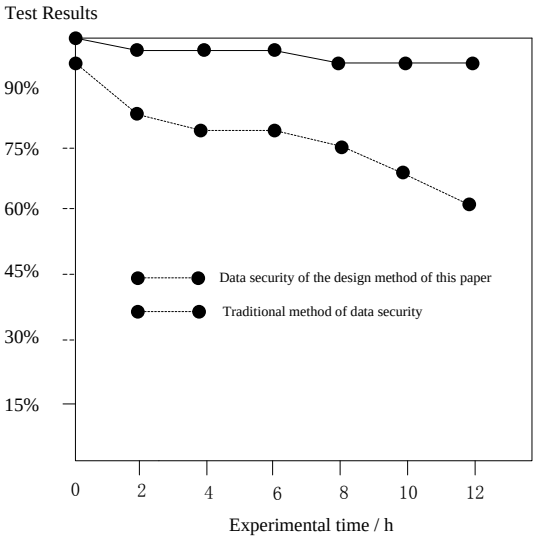

Figure 4. Data security comparison result graph

Analysis of Figure 3 and Figure 4 shows that the data processing method based on the Beidou satellite navigation system has a clear advantage in terms of data transmission efficiency and data security. The

data transmission efficiency is analyzed. The data transmission efficiency of the method is always between 90% and 80%, and the average data transmission efficiency can reach 85%. The data transmission efficiency using the traditional method is significantly larger than the method, and its data transmission The efficiency dropped from 85% to 70% and the average transmission efficiency was 77.5%. Therefore, compared with the traditional method, the data processing method based on the Beidou satellite navigation system can improve the data transmission efficiency by 7.5%.

The data security degree is analyzed and the data security degree based on the data processing method of Beidou satellite navigation system is always 96%-100%, and it is hardly affected by the increased degree of interference. The average data security can reach 98%; while the data security using the traditional method has dropped from 95% to 60%, indicating that in the case of serious interference, the traditional method is difficult to resist external interference, and the average data security is only 77.5%. Therefore, compared with the traditional method, this method can improve the data security by 20.5%.

In summary, the data processing method based on the Beidou satellite navigation system can improve the data transmission efficiency by 7.5% and improve the data security by 20.5%, which is extremely effective.

4. CONCLUSION

Based on the selection of time transfer method and data security processing, the data processing method based on Beidou satellite navigation system is designed. The comparison of experiments shows that the method improves data transmission efficiency and data security. Effectiveness, able to support the secure transmission of data.

ACKNOWLEDGEMENT

School-level research fund project Project No. 2017KY0206; Shaanxi Provincial Key Research and Development Project, Project No. 2018GY-028.

REFERENCES

[1]Li Z.B, Li W.L, Wei Z.Z, et al. Research and implementation of key module of data security processing mechanism in software defined network. Journal of Computer Applications, 2018, 38(7): 1929-1935.

[2]Ju A.K, Guo Y.B, Zhu T.M. Security Situational Awareness and Early Warning Architecture of Big Data Network Based on Open Source Tool Set. Journal of Computer Science, 2017, 44(5): 125-131.

[3]Wang J.R, Ma P, Wang W. Application of Composite Quantile Regression Based on Genetic Algorithm in Settlement Data Processing. Industrial Safety and Environmental Protection, 2017, 43(3): 52-55.

[4]Ma Y.Y, Shi Y.Y, Zhang H, et al. Security Data Feature Processing Method Based on Cultural Gene Algorithm and Least Squares Support Vector Machine. Computer Science, 2017, 44(3): 237-241.

[5]Wang L, Li L.W, Shi J.W, et al. Research on data transmission and security control operation method of data interaction between EMS and DMS. Power System Protection and Control, 2018, 46(10):75-80.

Application of Sensing Technology in Automatic Control System of Agricultural Machinery

Yanguo Guo
Guangxi Science & Technology Normal University, Laibin, 546199, China
E-mail: gf123vv@163.com

Abstract: In recent years, the level of agricultural machinery automation technology has been continuously improved, and the automation requirements for agricultural machinery automatic control systems are also constantly improving. The effective application of sensing technology to the automatic control system of agricultural machinery can effectively improve the planting efficiency of agriculture, promote the rapid development of agricultural machinery automation technology in China, and escort the development of agriculture. Therefore, the article first explores the development of sensor technology and the impact on the automatic control system of agricultural machinery, focusing on the specific application of sensor technology in the automatic control system of agricultural machinery.
Keywords: sensing technology; agricultural machinery automatic control system; application

1. INTRODUCTION

With the current rapid development of China's agricultural development, the machinery and equipment used in agriculture is accelerating the development of automation, and this is also an important manifestation of the current modernization of the agricultural industry. As a very key component in the mechatronics system, the main function of the sensor is to obtain important information in all aspects quickly and accurately [1]. This provides a powerful way for the automation of agricultural machinery in China and the identification of machinery. The support of information and data is the basis for an important level of improvement in the development of agricultural machinery. If the sensor is not used effectively in agricultural machinery, it will seriously affect the accuracy of agricultural machinery work, and at the same time affect the information processing and monitoring in agricultural production. Therefore, in actual agricultural production processes, the use of sensors can affect the overall performance of agricultural machinery.

2. OVERVIEW OF THE AUTOMATIC CONTROL OF THE SPECIFIC CONTROL IN THE TRACTOR

Tractor has a wide range of applications in the agricultural production process [2]. The rotation of the agricultural machinery in the tractor and the connection between the various constructions need to be strengthened, and the direction of rotation of the agricultural machinery also needs to be controlled. However, since the sensing system in the roll angle of the tractor mainly measures the tractor roll angle, the tractor and the agricultural implement need to maintain the same inclination in the field work, and it is necessary to combine the horizontal in the automatic control process. Rolling angles enhance control decisions and promote good working practices in agricultural machinery control. Figure 1 is a control structure diagram.

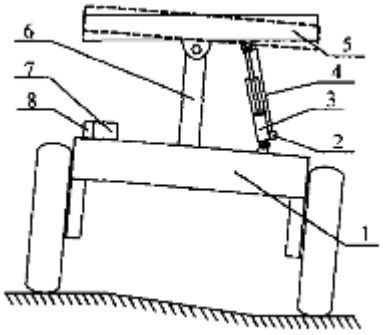

Figure 1. Control structure diagram (1. Tractor; 2. Displacement sensor; 3. Hydraulic cylinder; 4. Wire rope; 5. Agricultural machinery; 6. Rotating mechanism; 7. Rolling angle sensing system; 8. Automatic leveling controller)

3. SENSOR APPLICATION IN AGRICULTURAL AUTOMATION EQUIPMENT

3.1. Digital Sensor Positioning

In the process of agricultural machinery production, the high-precision GPS positioning system is relatively complicated. This technology requires a lot of capital investment, and this technology cannot be effectively implemented in some small-scale agricultural operations; For GPS positioning systems with low technical content, the specific positioning accuracy during the working process is very low, and it is not suitable for use in some small-scale farmland cultivation. In response to this situation, the most effective way in the agricultural labor process is to automate the agricultural machinery. The use of sensors can improve the overall working efficiency of

the machinery, which requires the use of data sensor technology. The main working principle of the digital sensor is digital compensation, which is constructed by a reasonable physical model and with the establishment of the corresponding mathematical model to ensure the accuracy of the digital compensation. In the actual work, a relatively simple and effective compensation information software can be drawn for the digital model, and the digital error generated by the microprocessor chip is compensated and corrected. After the A/D transition signal is converted by the analog output signal of the mechanical sensor, in the microprocessor that enters the next stage, the obvious problem at this time is that it is doped with some pulse type. The influence of noise, so the degree of such noise must be reduced, thus effectively achieving a true zero drift and avoiding the error phenomenon as much as possible [3].

3.2. Application of Sensing Technology in Agricultural Machinery Chassis

Sensor technologies such as pressure sensors, digital sensors, and photoelectric sensors have been widely used in agricultural machinery automatic control systems. These sensors have played an important role in agricultural machinery automatic control systems. At present, the number of sensors used in agricultural machinery used by people is about 20, and these sensors are respectively placed in various parts of agricultural machinery, which is the main part to improve the performance of agricultural machinery automatic control system. If there is no sensor technology in agricultural machinery. Application, equivalent to the loss of sensory organs in agricultural machinery, represents the importance of applying sensor technology in agricultural machinery automation control systems.

3.3. Application of GPS Positioning Technology

The GPS positioning system itself is a system that requires very high precision. In the research and development process, it requires a lot of cost, but for some small-scale farm operations, it is impossible to complete its accuracy requirements, so GPS Positioning technology cannot be applied to farmland with a small area. In the process of agricultural production, agricultural machinery work will be affected by environmental factors, eliminating this situation, and designing GPS positioning technology to high-precision mode, which requires effective and more accurate digital compensation for GPS positioning system. . In the agricultural machinery operation, the digital model can automatically draw relatively simple and effective compensatory information software, and then use the generated digital error to perform effective compensation and correct correction after the chip is micro-processed. Digital compensation can draw a relatively high precision digital model through a more reasonable physical model and related mathematical models. The reliability index of the digital model thus obtained is also very high, and the numbers obtained by other methods of the calculation system can be effectively supplemented and the error values can be corrected in time. When the agricultural machinery automatic control system receives the analog output signal from the sensor, it will change the A/D that appears in it, and the converted signal enters another microprocessor for the next step, and after this The microprocessor technology is subject to some noise-like noise, which minimizes this noise and achieves ideal zero drift and avoids numerical errors.

3.4. Application of Moisture Detection Technology

When choosing the seeds of a plant, pay attention to the water content of the grain itself. The moisture content of the grain determines the growth of the plant, so it is important to check the moisture of the grain. The way to detect moisture mainly includes capacitive and resistive. The former mainly uses the cylindrical electrode to calculate the water content in the grain. This technology is not affected by the grain density. When the latter detects the water content of the grain, the result is related to the temperature of the grain itself and the measured pressure value, and it is necessary to add a heat sensitivity during the detection process to improve the detection accuracy.

3.5. Digital Sensor Implementation Positioning

Agricultural machinery also needs to have high precision for positioning. The GPS positioning method has certain complexity. If this positioning method is used in the agricultural production process, not only a large amount of construction funds are needed, but also it is difficult to use in some small farmland applications. Promotion, and positioning in the GPS system is also difficult to achieve good precision, in order to better improve the accuracy of agricultural machinery positioning, digital sensors are used in the agricultural production process in a certain place. In the digital sensor, its main working principle: digital compensation, through the digital compensation method can reasonably establish the corresponding physical model and related mathematical models, and combined with the data information to draw a very accurate and reliable digital model, and thus more Improve the accuracy of digital compensation. The sensing system implemented in the roll angle of the tractor is mainly installed with three different axes, wherein the corresponding sinusoidal motion can be set for the platform in each function turntable, but the other two lock it in the non-moving state. . Combined with the tractor hoeing in the field, the frequency obtained by the sinusoidal motion is 0.5, 0.75, 1.0 and 2 (unit: Hertz), and the specific amplitude values can be selected as: 2/4/6/8 and 10, The practical use of agricultural machinery is mainly to draw a simple figure with reference to the digital model, as shown in Figure 2. The software combined with the compensation calculation and the microprocessor

correct the error, which allows the sensor to obtain an effective output of good analog information.

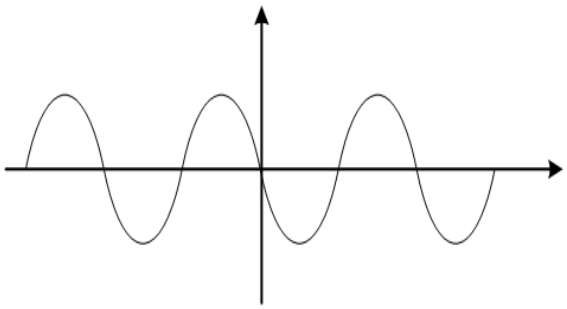

Figure 2. Digital model diagram

4. CONCLUSION

The automatic control system of agricultural machinery is the product of the development of science and technology technology and the inevitable trend of agricultural development in the future. Therefore, it is necessary to strengthen the application degree of sensor technology in the automatic control system of agricultural machinery, improve the agricultural production efficiency of agricultural machinery and equipment, and improve the overall agricultural machinery. The operation performance helps agricultural machinery to better maintain high-efficiency agricultural performance in agricultural fields with poor farming environment and promote the development of agricultural automatic mechanization in China.

REFERENCES

[1]Zhu Y.B. Practice Analysis of Application of Sensing Technology in Automatic Control System of Agricultural Machinery. South China Agriculture, 2017, 11(23): 98-100.

[2]Ayi X, Li T.Y. Simulink Simulation Design and Implementation of Pseudo-code Phase Modulation System. Journal of Xinjiang Normal University (Natural Science Edition), 2013, (04): 39-42.

[3]Wang X.Y. On the Importance of Sensors in Agricultural Machinery. Agricultural technology and equipment, 2016, (04): 21-22,25.

Research Status of Mask Projection Stereo Lithography Apparatus and Selective Laser Sintering

Wenbo Xu, Xuewen Zong*
Mechanical Engineering Department, Henan Institute of Technology, Xinxiang, 453003, China
**E-mail: 798264342@qq.com*

Abstract: The classification and development of Stereo Lithography Apparatus and Selective Laser Sintering are introduced, the working principle of these two forming methods is explained in detail. The advantages and problems of mask projection process are pointed out, the factors influencing the quality of sintered parts in Selective Laser Sintering are expounded from different aspects. The development trend of mask projection Stereo Lithography Apparatus and Selective Laser Sintering is summarized.
Keywords: stereo lithography apparatus; mask projection; oxygen inhibition; selective laser sintering

1. INTRODUCTION

The most outstanding advantage of 3D Printing Technology is that it is not limited by part structure. That is to say, it can quickly process parts with arbitrary complex shapes in principle [1]. Compared with the traditional manufacturing method, it can reduce about 60% of the production time and 70% of the manufacturing cost [2]. 3D Printing Technology is suitable for new product development, rapid single and small batch parts manufacturing, complex shape parts manufacturing, mold design and manufacturing, etc. It has great development prospects. Castings suitable for rapid casting are shown in Figure 1.

Figure 1. Castings suitable for rapid casting

3D Printing Technology includes Stereo Lithography Apparatus (SL), Selective Laser Sintering (SLS), Fused Deposition Modeling (FDM), Laminated Object Manufacturing (LOM) and 3Dimensional Printing (3DP). The parts manufactured by these printing methods have different applications because of different raw materials and working principles.

SLA is based on liquid photosensitive resin as raw material. It is controlled by a computer control system that laser beams of specific wavelength and intensity are gathered on the surface of liquid photosensitive resin in the resin tank and cured by scanning irradiation to solidify layer by layer until the solid model is formed. SLA was first proposed by Charles W. Hull in 1984 and applied for a national patent in the United States. The advantages of parts made by SLA process are high surface quality and precision, and can produce parts with great complexity of structure, which are excellent for investment casting.

SLS is an additive manufacturing technology that uses laser as heat source and solidifies powder materials by sintering layer by layer, and eventually adds solid models. There are many kinds of raw materials used in SLS process, such as paraffin, polystyrene, nylon, ceramics, coated sand and even metal powder. The advantages of this process are good mechanical properties of prototype parts, high intensity without design and construction support, wide selection of forming materials, and high utilization rate. On the other hand, the disadvantages of this process are low precision, rough surface and post-processing is necessary.

2. RESEARCH STATUS OF MASK PROJECTION TECHNOLOGY

With the continuous development of SLA technology, John R et al. have increased the manufacturing speed of Z-axis by more than 100 times in recent years by using Continuous Liquid Interface Production (CLIP) of oxygen-inhibiting mechanism. This makes the manufacturing method of mask projection stereo lithography apparatus become a research hotspot [3-4], the working principle of CLIP is shown in the Figure 2.

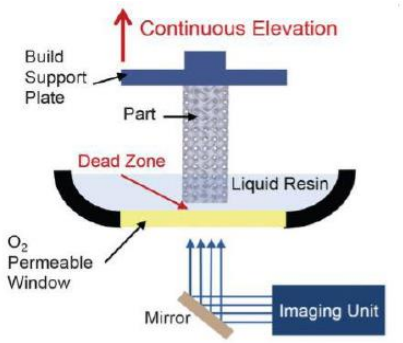

Figure 2. The working principle of CLIP

A variety of manufacturing methods have been created for the prototype manufacturing of parts and the progress of optical devices [5]. Meanwhile, the manufacture of mask plate has gone through many forms. Among them, there are some several typical mask projection SLA technologies, include direct positive mask projection light modeling technology, LCD mask projection rapid prototyping technology, DMD mask projection rapid prototyping technology. The working principle and problems of several mask projection techniques are shown in Table 1. The part prototype made by mask projection technology is shown in Figure 3.

Figure 3. The part prototype made by mask projection technolog

Table 1. Comparison of several typical mask exposure curing technologies

Typical technology	Working principle	Problems
Direct positive mask projection light modeling	According to the mask shape, the phototrigger is sprayed on the surface of the photosensitive resin through an inkjet printer, and then cured by exposure.	The optical resolution of molding machine and the diffusion speed of photo-trigger in resin affect the forming accuracy of this technology.
LCD mask projection rapid prototyping	The manufacture of mask makes good use of the controllability of LCD liquid crystal molecule, and curing the solid with photosensitive resin irradiated by ultraviolet light through the mask. At the same time, the advantages of high resolution of LCD are used to manufacture more micro-parts.	With the increase of service time, the transmittance of liquid crystal to ultraviolet light will gradually decrease. In addition, it is precisely the reason that the switching speed of liquid crystal molecules is not fast enough and the contrast is low, which will cause the edge of the parts to be blurred. These shortcomings also hinder the further development of LCD mask projection technology.
DMD mask projection rapid prototyping	DMD is composed of many aluminium micro-reflectors. It has good reflectivity to ultraviolet light. Compared with LCD mask technology, DMD has obvious advantages and great potential for development.	Precision is high, but the price of DMD components is very expensive.

3. INFLUENCING FACTORS OF SINTERED PARTS QUALITY IN SLS

Sinter Station 2000 prototyping Machine Produced by DTM Company of the United States in 1992 realizes commercialization of SLS process [6-7], the working principle is shown in Figure 4. Influencing factors on sintering quality of sintered parts include material and process, and the quality of sintered parts is mainly measured by intensity and precision. But then again, intensity and precision are contradictory measures. Therefore, while guaranteeing the intensity requirement of sintered parts, the forming precision of sintered parts can be improved as much as possible, especially in large and complex parts.

The influencing factors of materials are mainly determined by the types and proportions of modified materials. For example, for polystyrene (PS) powder in the sintering process, PS sintered parts are one of the most commonly used sintering materials because of their low shrinkage and high forming precision.

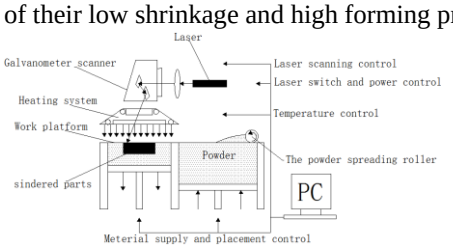

Figure 4. The working principle of SLS

Due to the low strength of PS powder, the failure of the casting prototype is often caused by the insufficient intensity of sintered parts when making large and complex prototype, as we can see from Figure 5. The flawless SLS prototype is shown in Figure 6.

Figure 5. Prototype with defect due to insufficient intensity

Figure 6. The flawless SLS prototype

The influencing factors of process parameters are mainly composed of the following parameters.

(1) Laser power: Laser power determines the laser energy scanning on the powder surface. With the increase of laser power, more energy is absorbed by powder and the intensity of sintered parts is higher. On the one hand, when the laser power is too high, the excess heat will diffuse to the sintered powder on the side surface and bottom of the sintered parts, resulting in poor dimensional precision, large shrinkage, warpage deformation, gasification and even carbonization. On the other hand, when the laser power is low, the melting of the material is insufficient, and the interlaminar adhesion may occur.

(2) Scanning speed: The scanning speed determines the scanning and heating time of the laser beam. When the laser power is constant, the lower the scanning speed, the longer the time of laser heating the powder and the more heat acting on the powder surface, the higher the intensity. On the one hand, when the scanning speed is low, it is difficult to clear powder and the positive deviation is large. On the other hand, when the scanning speed is fast, the melting degree of powder particles is low, which leads to low strength, and makes the size error deviate from the negative direction.

(3) Scanning distance: The scanning distance is related to the laser spot diameter. The size of scanning distance determines the overlap and separation degree of two adjacent laser lines. When the laser power is constant, If the scanning distance is larger, the overlapping parts of the adjacent two scanning lines will be less, and the powders melted will be less and, resulting in the lower intensity of the sintered parts. The smaller the scanning distance is, the smaller the state change of powder particles, the smaller the shrinkage deformation and the better the dimensional precision are.

(4) Single layer thickness: The single layer thickness not only affects the energy absorbed by the layers, but also affects the forming efficiency. The smaller the thickness of single layer, the stronger the downward penetration ability of laser, the better the bonding strength between layers, and the lower the forming efficiency. The larger single layer thickness, the lower the laser energy to reach the bottom powder of each layer, which is not conducive to the bonding between the layers, and the lower the intensity.

(5) Preheating temperature: In order to reduce the temperature difference between the upper and lower surfaces during powder sintering, and to reduce the shrinkage and warpage of sintered parts. We should make the preheating temperature of amorphous polymers generally lower than the glass transition temperature (Tg).

4. CONCLUSION

After decades of development, Stereo Lithography Apparatus has changed from traditional scanning curing to MIP-SLA mask projection technology based on digital micromirror array. With the continuous improvement of Continuous Liquid Interface Production technology, there is a trend that mask projection technology will replace the traditional SLA process. At the same time, due to the continuous production of large-size surface light sources, new mask projection exposure technology will have greater breakthroughs in large-size parts.

Selective Laser Sintering technology needs to make breakthroughs in modeling and simulation. Sintering process is complex and difficult to observe in real time. At the same time, in order to better grasp the sintering process and guide the selection of process parameters, it is necessary to develop computer simulation of sintering process. In the optimization of post-treatment process, although SLS can directly form metal parts, the mechanical and thermal properties of the parts can not meet the requirements of using directly. The performance of sintered parts can be improved obviously after the post-treatment process, but it will have a great impact on the dimensional precision. Therefore, it is necessary to optimize the existing post-treatment process to improve the comprehensive quality. In recent years, there will be more breakthroughs in surface quality, dimensional precision, mechanical properties and manufacture of Large-scale Prototype.

REFERENCES

[1]Salmoria G.V, Lauth V.R, Cardenuto M.R, et al. Characterization of PA12/PBT specimens prepared by selective laser sintering. Optics and Laser Technology, 2017, 98: 92-96.

[2]Klahn C, Leutenecker B, Meboldt M. Design strategies for the process of additive manufacturing. Procedia CIRP. 2015, 36: 230-235.

[3]John R. Tumbleston R, David S, Nikita E, et al. Continuous liquid interface production of 3D objects. Science, 2015, 347(6228): 1349-1352.

[4]Janusziewicz R, Tumbleston J.R, Quintanilla A.L, et al. Layerless fabrication with continuous liquid interface production. Proc Natl Acad Sci USA, 2016, 113(42): 11703.

[5]Lan H.B, Li D.C, Lu B.H. Micro-and nanoscale 3D printing. Scientia Sinica (Technologica), 2015, 45(09): 919-940.

[6]Kumar S. Selective Laser Sintering/Melting. Reference Module in Materials Science and Materials Engineering. 2014, 10: 93-134.

[7]Kwon D , Park E , Ha S , et al. Effect of humidity changes on dimensional stability of 3D printed parts by selective laser sintering[J]. International Journal of Precision Engineering and Manufacturing, 2017, 18(9):1275-1280.

Application of Automatic Control Technology in Machinery

Yongyang Li
Guangdong University of Science & Technology, Dongguan, 523083, China
E-mail:1286735550@qq.com

Abstract: Science and technology are constantly developing and the society is constantly improving. This paper starts with the analysis of the main control methods of automatic control technology, and discusses the application of automatic control technology in machinery. It is expected that the research in this paper will help to promote the improvement of mechanical properties.
Key words: machinery; automatic control technology; control method

1. INTRODUCTION

For each country, agricultural production occupies an extremely important position. The economy and future of a country are determined by its level of mechanization, and directly affect the national economy and people's livelihood. With the further development of science and technology, the automation technology is promoted towards the development of mechanical and electrical cooperation [1]. At the same time, the microprocessors in the past have been replaced by virtual instruments, which is conducive to the exchange and communication of information. In addition, in the context of the information age, people's lives are increasingly inseparable from mechanical information. Based on the current mechanical development, China's machinery industry has begun to apply automatic control technology widely [2]. Through this technology, it can more accurately analyze the quality of agricultural products, and more accurately locate seeding and harvesting, creating a broader development space and more. The possibility.

2. CHARACTERISTICS OF MECHANICAL AUTOMATIC CONTROL TECHNOLOGY

For the development of machinery, the introduction of automatic control technology can effectively improve the operational efficiency of the machine, and ensure that the use of machinery for agricultural production activities to achieve better returns.

(1) Stability Through the application of automatic control technology in the machine, it is ensured that in the process of mechanical work, it can achieve better stability and ensure the efficiency and efficiency of agricultural machinery operation.

(2) Flexible and simple configuration The application of automatic control technology promotes the use of machinery for the corresponding production activities, with more flexible application effects, making the operation of the machine easier [3].

(3) Real-time control In order to ensure the operational efficiency of the machine and improve the efficiency of mechanical control, the real-time control objectives of agricultural machinery can be fully achieved through the application of automatic control technology. In this way, it is ensured that in the conduct of agricultural production work, reasonable control of different machinery can be carried out in real time to ensure that the expected agricultural production targets are achieved.

(4) Autonomous fault diagnosis Through the application of automatic control technology, it is ensured that independent diagnosis and troubleshooting can be achieved for the problems occurring in the mechanical application process during the specific use of the machine. Based on the automatic control technology, the operation and maintenance personnel can be combined with the corresponding fault alarms to find the fault location in the first time and complete the fault investigation quickly and efficiently.

3. AUTOMATIC CONTROL TECHNOLOGY IN THE APPLICATION OF MACHINERY

3.1. PLC Technology

The PLC is an electronic system with programmable functions. The edited program can be directly stored in the memory. The textile machine can automatically complete the production task according to the corresponding code instructions. In textile machinery, PLC technology is mainly used on the flower cleaning machine and the yarn doubling machine, thereby greatly improving the working efficiency of the mechanical equipment.

3.2. Programmable Computer Controller Technology

The programmable controller has been upgraded and upgraded, and a programmable computer controller has been introduced to realize the multi-threading of the operating system, so that the reserve of application software is continuously expanded. The programmable computer controller can meet the various functional requirements of different modules. Different control measures can be used for different modules. The data can be packaged and stored in the CPU to ensure the high efficiency of the operating system and meet the overall control of the project. demand. In short, the programmable computer controller has great advantages, meets the

development standards of the industry, has good development potential, and needs to further improve the technical application in the future development process.

3.3. Space Temperature and Humidity Automatic Control Technology

In the greenhouse vegetable cultivation, farmers can obtain higher profits by planting off-season vegetables. However, because the anti-season vegetables have higher requirements on the temperature and humidity of the planting environment, it is required to supervise the agricultural personnel in the past greenhouse vegetable cultivation [4]. For the growth of crops, in the design of automated vegetable greenhouses, designers need to skillfully apply temperature and humidity sensors to smart vegetable greenhouses, and set multiple temperature and humidity sensors to fixed positions in greenhouses. Collect temperature and humidity information, and send the information to the central computer. The computer will combine the preset thresholds to properly control the humidification, exhaust and other mechanical equipment to ensure that the humidity and temperature in the vegetable greenhouse are in the proper range. Figure 1 inside.

Figure 1. Humidity and temperature automatic controller in vegetable greenhouse

3.4. Application of Automatic Control Technology in Coal Mine Machinery

China is not only a large coal producing country, but also a large coal country. In order to increase the total output of coal, the automatic control technology can be rationally used in coal mining machinery. In the coal mining machinery, the remote automatic control system is widely used, and the system can remotely and automatically control the equipment such as the shearer and the scraper conveyor. 1) Application in the shearer The application of the remote automatic control system in the shearer can realize the real-time positioning and video tracking of the shearer. The remote control center can start and stop the shearer and the running speed. The automatic control is carried out, so that the shearer can automatically increase and accelerate the acceleration and deceleration according to a preset program on the working surface, which not only greatly improves the coal mining efficiency, but also prevents the occurrence of a safety accident. 2) Application of scraper conveyor in scraper conveyor is one of the most important mechanical equipments in coal mine production. Through the application of remote automatic control technology, online monitoring and real-time control of conveyor operation can be carried out.

3.5. Linear Motor Drive Technology

The drive system of the transmission machine is a rotary motor system, and the mechanical structure is relatively restrictive, which makes it difficult to improve its performance. Current researchers need to increase efforts to develop linear motor drive systems. By using the linear motor drive system, the error of the mechanical rotation of the motor table can be reduced. During the rotation of the machine tool, the chain length can also be shortened to achieve the advantage of zero rotation. While ensuring the running speed of the machine, it can also improve the accuracy and rigidity of the operation, reduce the generation of noise, and further prolong the formation of motion. At present, the linear motor drive technology is widely used in the operation of the machine tool. For example, a company using linear motor drive technology for production can improve production efficiency, ensure efficient processing technology, and further improve production performance.

3.6. Full Closed Loop AC Servo Drive Technology

Among many electromechanical power plant products, digital AC servo system technology is widely used. This technology is relatively simple to operate and easy to debug, and can meet the requirements of digitization and precision. Using this technology, the position of the sampling photoelectric encoder is obtained by digital signal, and the control loop of position and speed is formed. The high-speed operation of the processor is used to increase the efficiency of the automatic control system. By driving the high-turning Fourier, the resonance generated by the mechanical operation can be realized. Eliminate. By using closed-loop AC servo drive technology during mechanical operation, the precision control of the machine can be continuously improved, and researchers are constantly introducing a more advanced full-closed AC servo system. The position feedback component is installed in the mechanical motion terminal, which can improve the advanced nature of the full-closed AC servo system. The motor encoder can eliminate the gap problem of the mechanical transmission, reduce the error of the mechanical rotating component, and improve the positioning accuracy. Many automation equipments

are currently undergoing retrofit and upgrade of servo systems and have a wide range of applications.

4. APPLICATION ADVANTAGES

In machinery, automatic control technology has the following application advantages:

(1) Real-time control of the machine. In the machine, the automatic control technology is mainly based on electrical control, and the control effect is achieved by signal transmission. This allows real-time control of the mechanical operation process.

(2) It can improve the overall performance of the machine. When the automatic control technology is applied in the machine, the I/O signal is usually used, so that the internal circuit of the machine can be isolated from the external environment, and the filtering device can effectively suppress the interference, thereby making the machine The overall performance has been further improved.

(3) Self-diagnosis of faults can be realized. Because the machinery needs to work in the field, affected by environmental factors, the machine often has various failures, and the application of automatic control technology can realize the self-diagnosis of mechanical failure. When a fault occurs, the automatic control device or system in the machine will diagnose the fault in the first time, and handle the fault through self-repair. For the fault that cannot be handled, the machine will issue an alarm prompt. This ensures the safety and stability of the operation.

5. CONCLUSION

In summary, with the rapid development of technology, the automatic control technology has become more and more perfect. This technology has been widely used in many fields due to its various advantages. The application of automatic control technology in the field of machinery can greatly improve the operational safety, stability and reliability of mechanical equipment, thereby significantly increasing the related production efficiency.

REFERENCES

[1]Li J, Zhu Q.F, Exploring the Design of Automatic Control System of Robot Arms in Non-structural Environment, 2018, (04): 56-58.

[2]Cao R.H, Discussion on the design of automatic control system for mechanical three-dimensional parking equipment. China Equipment Engineering, 2017, (10): 109-111.

[3]Liu Y.Q, Le G.Q, Analysis of the application of automatic control technology of mechanical equipment under the control of microelectronic sensing signals. Southern Agricultural Machinery, 2018, (03): 43-44.

[4]Fang L.W, Zhang K. Design of automatic control system for mechanical auxiliary equipment based on CAN bus. Science and Technology, 2017, (10): 102-104.

Optimization Analysis of Air Gap Magnetic Field in Electromagnetic Harmonic Movable Tooth Drive System

Yubo Ren, Weidong Bian, Ruile Yan*
School of Mechanical Engineering, Yanshan University, 066004, Qinhuangdao, Hebei, China
E-mail:ryb@ysu.edu.cn

Abstract: The electromagnetic harmonic movable tooth transmission system relies on the deformation of the flexible wheel to promote the transfer power of the movable tooth, and the flexible wheel is deformed under the action of the electromagnetic force. The greater the deformation, the greater the torque that can be transferred. In order to avoid the loss of magnetic density, the strong magnetic material is added into the flexible wheel. It can be seen from the post-processor of Ansys that the transmission efficiency of magnetic density can be increased and the loss can be reduced, thus the transmission performance of the system can be improved.
Keywords: flexible wheel; magnetic field distribution; electromagnetic force; optimization

1. INTRODUCTIONFOREWORD

The schematic diagram of the electromagnetic harmonic movable tooth drive system is shown in Fig. 1 and consists of three basic components:

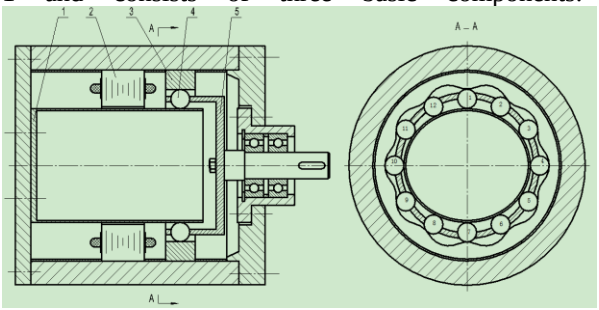

Figure 1. Schematic diagram of electromagnetic harmonic movable tooth drive system (1: flexible wheel; 2: electromagnetic winding; 3: center wheel; 4: movable tooth; 5: movable gear rack)(1) Exciter The exciter consists of an electromagnetic winding and a flexible wheel. The flexible wheel is a cup-shaped metal cylinder with a radius of r and a thickness of t, which is firmly connected with the base. There is an air gap of δ thickness between the flexible wheel and the electromagnetic core winding. The soft wheel will deform under the action of the rotating magnetic field, that is, the magnetic field force sequence will be applied to the corresponding two sectors, and the flexor will deform in the corresponding position, and when the flexure wheel deforms, The movable teeth will be pushed to move along the radial guide groove of the movable rack.

(2) Movable gear It is composed of a movable tooth frame and a set of movable teeth. The movable tooth frame can be a thin-walled cylinder, often connected with the output shaft, and the movable tooth is composed of a movable tooth body (steel ball).

(3) Center wheel The inner tooth shape of the center wheel is the envelope of the tooth profile curve at the outer end of the movable tooth.

Among the three components, the exciter is the active part, the movable gear and the center wheel are fixed arbitrarily, and the other one is the follower.

When the system is connected with three-phase alternating current, the flexible wheel produces periodic radial elastic deformation under the action of electromagnetic winding. Due to the change of radial dimension of the flexible wheel, the radial thrust is generated, forcing the live teeth in contact with the working tooth shape of the center wheel. Moving along the guide slot of the movable gear rack, at the same time, because of the constraint of the living gear rack and the high pair of the central gear profile, during the movement of the tooth profile along the center gear of the inner tooth, the movable tooth rack is rotated at equal angular speed, so the movable tooth is rotated at an equal angular speed. The movable tooth drive has completed the rotational speed transformation motion. The movable teeth in contact with the non-working profile of the center wheel, driven by the radial guide groove of the movable gear rack, return to the starting position of the work sequentially to complete the work. One of its work cycles. Each movable tooth can only push the follower to a certain angle, and the continuous movement of the system is realized by the succeeding work of each movable tooth [1].

According to the transmission principle, the greater the electromagnetic force, the greater the radial deformation of the flexible wheel and the greater the torque output of the system. Therefore, in order to improve the transmission performance of the system, the mathematical model of the magnetic field will be established in this paper, and then the coupled magnetic field will be optimized, thus a large magnetic force is obtained.

2. ANSYS MAGNETIC FIELD ANALYSIS

2.1. Mathematical Description of Magnetic Field

In the analysis of magnetic field with Ansys, if the

change of the magnetic field in axial direction is ignored, it becomes a two-dimensional problem. In the analysis, scalar magnetic potential φ is often introduced. For the nonlinear plane quasi-stable magnetic field, the scalar magnetic potential satisfies the quasi-Poisson equation, and its boundary value problem equation can be expressed as follows:

$$\begin{cases} \Omega: \frac{\partial}{\partial x}(\beta_x \frac{\partial u}{\partial x}) + \frac{\partial}{\partial y}(\beta_y \frac{\partial u}{\partial y}) = -f \\ S_1: u = u_0 \\ S_2: \beta \frac{\partial u}{\partial n} = q \end{cases} \quad (1)$$

In the formula Ω is the electromagnetic field; S_1、S_2 is the boundary of the first and second types of magnetic fields; *x,y,n* is flexor axial, circumferential and radial; u denote magnetic potential φ; β is the magnetic permeability μ or the magnetic reluctivity ν; f current density J_z; u_0 the known magnetic potential values on boundary; q is the intensity of the normal magnetic field on the boundary H_n or tangential magnetic induction intensity B_t.

For harmonic motor, the finite element method can be used to solve the harmonic motor because its magnetic field contains many kinds of media, and the non-linearity of the material is considered for ferromagnetic materials. When the continuation finite element method is used to calculate the electromagnetic field quantity at any point in the element, the calculation of electromagnetic field quantity is [2]:

(1) For scalar potential φ the intensity of the magnetic field H can be obtained, the components are:

$$\begin{cases} H_x = -\frac{\partial \varphi}{\partial x} = -\sum_{i=1}^{N} \frac{\partial N_i}{\partial x} \varphi_i \\ H_y = -\frac{\partial \varphi}{\partial y} = -\sum_{i=1}^{N} \frac{\partial N_i}{\partial y} \varphi_i \end{cases} \quad (2)$$

(2) For vector potential A_z the magnetic induction intensity $\vec{B}$ can be obtained, the components are:

$$\begin{cases} B_x = \frac{\partial A_Z}{\partial y} = \sum_{i=1}^{N} \frac{\partial N_i}{\partial y} A_{Z_i} \\ B_y = -\frac{\partial A_Z}{\partial x} = -\sum_{i=1}^{N} \frac{\partial N_i}{\partial x} A_{Z_i} \end{cases} \quad (3)$$

In the formula the Ni is a generalized shape function, for the triangular elements, the number of terms N is of the extended Ritz interpolation function, which is greater than 3, so the higher order interpolation is realized on the linear element.

2.2. Model Building

Ansys provides two modeling methods from top to bottom and from bottom to top, and users can choose the appropriate modeling mode according to the actual situation. In this paper, the model is on a single plane, the whole model is not complex, its specific parameters are shown in Table 1, the bottom-to-top modeling method can be used. First, a series of key points are drawn, then the appropriate key points are selected to form the desired lines, and then the surface is drawn by the lines. Finally, a suitable model can be constructed by Boolean operation of some columns.

Table 1. Model parameter

Number of phases	Number of pole-pairs	Stator slot number	Stator inner diameter	Stator outer diameter	Flexible wheel inner diameter	Pulley outer diameter
3	1	24	35mm	50mm	34.2mm	34.4mm

The slot shape of the stator selects a common semi-closed slot, the shape of which is shown in Figure 2, and its specific dimensions are as follows: $b_0 = 1.3\text{mm}, b_1 = 2.4\text{mm}, b_2 = 3\text{mm}, h_0 = 0.47\text{mm}, h_1 = 0.48\text{mm}, h_2 = 3.04\text{mm}$.

The finite element model is shown in Figure 3.

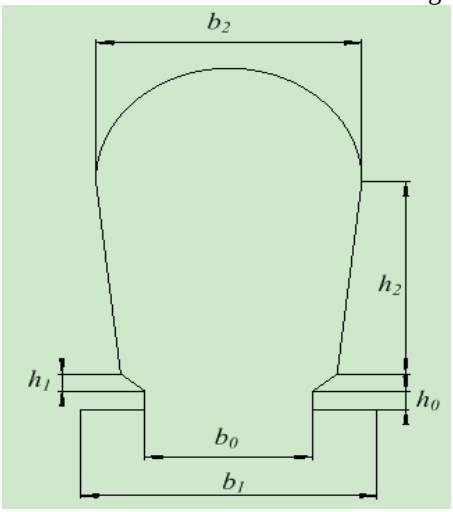

Figure 2. Semi-closed slot

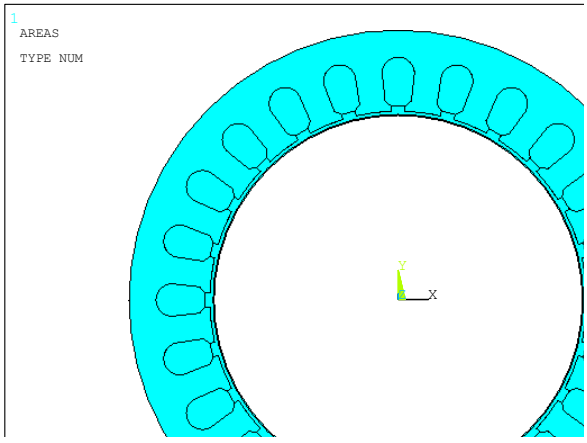

Figure 3. Two-dimensional finite element model

2.3. Grid Division

After the attributes and mesh size settings are complete, you can mesh. There are two types of meshes, free mesh and mapping mesh. In this paper, free mesh is selected, and the result is shown in Figure 4.

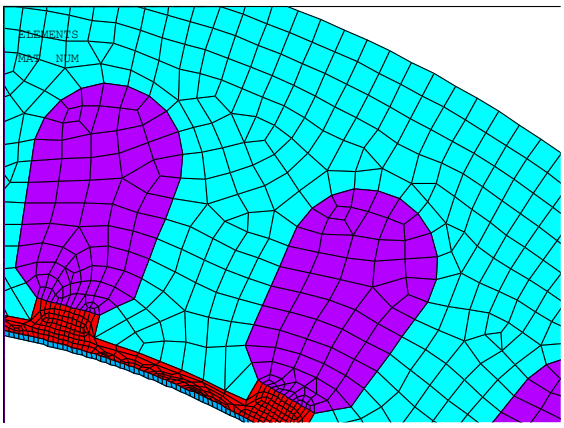

Figure 4. Grid division

2.4. Loading and Solving

After the mesh partition is completed, the finite element model needs to be loaded. Loading consists of two steps, the loading of forces and the loading of boundary conditions. Under the condition of no loading, the loading of magnetic field analysis is divided into current density loading and boundary condition loading. After calculation, the current density is loaded into the winding region. Due to the alternating current, it is necessary to pay attention to the direction of current at all times. The boundary condition is that the magnetic density direction is always parallel to the stator outer boundary.

When the loading is complete, it can be solved. Directly enter the command solve all can and it can be solved. When the solution is done dialog box pops up, the solution is completed.

The post-processor POST1, of the Ansys software allows you to observe and analyze the results of an overall model or a part of a model at a certain point in time for a particular loading and boundary condition. Therefore, using this post-processor, we can observe the magnetic inductance line distribution of the whole model after the power on, as shown in Figure 5 and Figure 6.

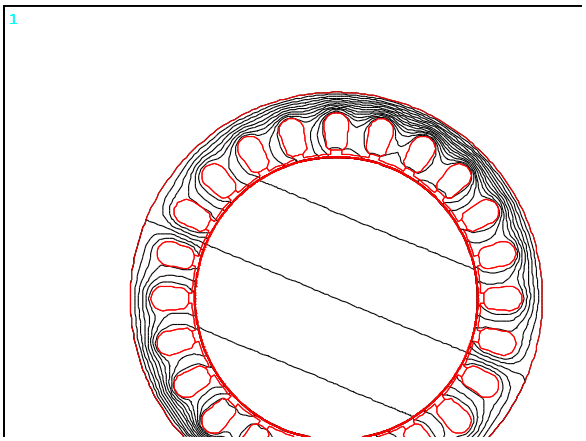

Figure 5. Magnetic density distribution

As can be seen from Figure 5, the whole magnetic field is divided into two poles by the above-mentioned loading, and the magnetic inductance line is a closed curve through the air gap. On the whole, most of the magnetic inductance lines are closed through the magnetic conductivity of the flexors, and the magnetic circuits are concentrated on the flexors, but a very small number of magnetic inductance lines pass through the large air areas inside the flexors to form closure. This can be seen clearly from the three magnetic inductance lines in the middle of the diagram. Figure 6 shows the distribution of electromagnetic forces acting on the whole flexible wheel. It can be seen from the diagram that there is a pair of large electromagnetic forces at the boundary between the poles, while the other parts along the circumferential direction of the flexible wheel are relatively small, which is an uneven distribution of several consecutive segments. Such a force condition is detrimental to the deformation of the flexure wheel.

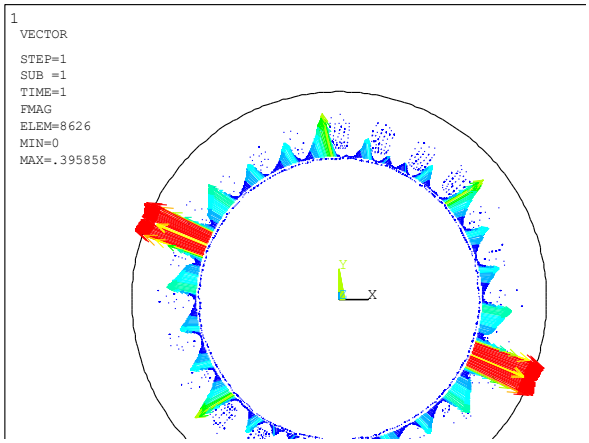

Figure 6. Electromagnetic force distribution

3. MAGNETIC FIELD OPTIMIZATION

The above analysis shows that at this time the system has the problem of small electromagnetic force and less spatial magnetic inductance distribution in the flexor. This is because the flexor is a hollow structure, and the large air area in its interior seriously affects the conduction of magnetic density. Because the value of electromagnetic force is too small, a large amount of energy will be lost on heating, which is not good for the stable operation of the system, but also not conducive to energy conservation and environmental protection. On the premise of this problem, the structure of the system is optimized in this paper.

In order to avoid the problem of large amount of magnetic density loss, the flexible rotor core assembly is added to the flexible wheel to improve the magnetic circuit and increase the air gap magnetic induction intensity. The method adopted in this paper is to form a flexible radial magnetic circuit by the combination of concave and convex interlaced surfaces, which is composed of overlapping pieces of the same elements, thus improving the permeability and weakening the influence of eddy current. The greater the number of links is, the better the flexibility is, and the more additional air gaps are formed on the radial flux closed path. In this paper, 12 links are used for

analysis, as shown in Figure 7.

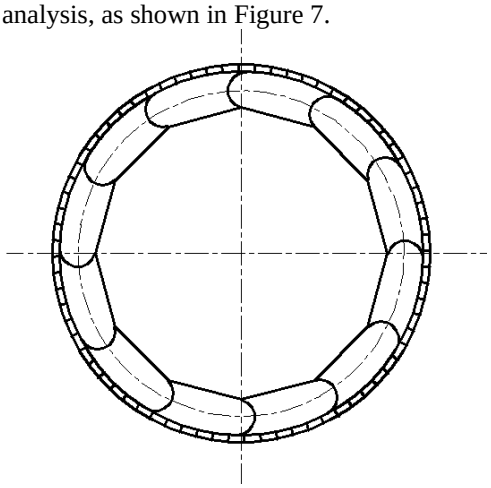

Figure 7. Chain-link flexible core assembly

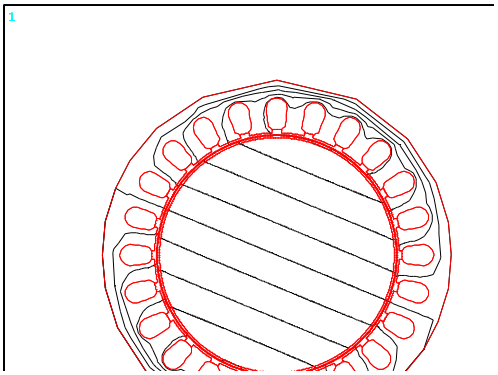

Figure 8. Magnetic field distribution

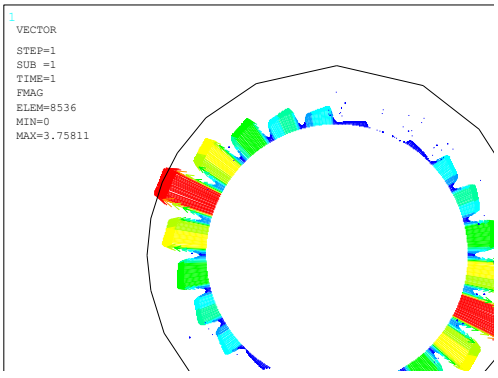

Figure 9. Electromagnetic force distribution

Figure 8 and Figure 9 show the improved distribution of the magnetic inductance line and the flexure wheel force. From the comparison between Figure 8 and Figure 5, it is obvious that the linear density of air gap magnetic inductance increases after optimization, indicating that the value of air gap magnetic density increases at this time. Figure 9 contrasts with figure 6, where the maximum electromagnetic force is $0.395\mathrm{N}\cdot\mathrm{m}$ without optimization, and the maximum electromagnetic force after optimization is $3.76\mathrm{N}\cdot\mathrm{m}$, which can be seen to be nearly 10 times greater than before. And its distribution is more uniform, which improves the performance of the system.

4. CONCLUSIONTHE ENDING

In order to solve the problem that the electromagnetic force of the system is small and the distribution of spatial magnetic inductance lines in the flexor is less, the magnetic field system is optimized in this paper, and flexible core components are added to the inner region of the flexible wheel to improve the magnetic circuit. By means of Ansys analysis, it can be seen that after optimization, the linear density of air gap magnetic induction increases, the air gap magnetic density increases, and the electromagnetic force of the optimized air gap increases obviously. The output torque of the system can be greatly improved.

ACKNOWLEDGEMENT

This paper is supported by National Natural Science Foundation of China. (No. 51875497)

REFERENCE

[1]Ren Y.B, Xu L.Z, Liang Y.L. Analysis of torque characteristics of electromagnetic Harmonic movable Tooth Drive. Mechanical Engineering of China, 2015, 26(15): 2000-2004.

[2]Tang Y.C, Liang Y.P. Analysis and calculation of electromagnetic Field of Motor, Beijing, Mechanical Industry Press, 2010, 11-13.

Design of Fault Diagnosis Module Based on Virtual Instrument and Multi-signal Model for Target Search Combination of Certain Equipment

Yiwei Zhao[1,], Xuanhai Li[1], Qianyu Chen[1], Mingfang Wang[2], Yuhao Dong[3]*
[1]PLA Dalian Naval Academy
[2]Unit 93861
[3]PLA Air Force Engineering University, Xi'an, Shanxi, 710051
**E-mail: 821387717@qq.com*

Abstract: In this paper, virtual instrument technology is proposed to integrate the modular instrument of USB bus and construct the field fault diagnosis equipment based on portable military reinforced computer as the main control platform [1]. Using virtual instrument software to develop fault detection system and embedding fault diagnosis strategy generated by multi-signal model can not only satisfy in-situ detection of equipment signals such as real-time acquisition, signal processing and analysis, but also realize fault diagnosis and isolation.
Keywords: Fault Diagnosis, technical requirements, hardware design

1. INTRODUCTION

A search radar is one of the most important electronic information equipments of a certain type of equipment, which is responsible for the important task of searching and tracking targets. The search radar is a complex equipment which integrates machinery, electronics and electromagnetism. It usually works in high altitude, mountains, islands and other harsh environments. Its components are easily damped and aged. Its combat readiness is directly related to the normal operation and operational effectiveness of a certain type of equipment, which puts forward higher requirements for the field maintenance and guarantee of radar [2]. In order to quickly and accurately detect the signal detection and fault diagnosis of large and complex equipment, and solve the problem that the testing and diagnostic equipment is difficult to solve in the field or in a narrow space, field-level fault diagnosis devices are often used. The field level fault diagnosis device needs to consider the requirements of function, volume and power consumption, especially the internal function module is the key factor in the design, and it is also a difficult problem to solve.

2. DESIGN TECHNICAL INDICATORS OF FAULT DIAGNOSIS DEVICE FOR A SEARCH RADAR

According to the requirement analysis of the test and diagnosis of a search radar, the main technical requirements of the maintenance support auxiliary equipment used at the field level are determined as follows.

Table 1 The main technical requirements

Pulse period	20us
Pulse width	2us
Frequency of carrier signal	30MHZ
Range	0-300V(2V，10V，50V，100V，300V)
Accuracy	±0.30%
Range of frequency	20Hz-1MHz(1KHz，50KHz，200KHz，1MHz，10MHz)
Frequency accuracy	±0.5%
Accuracy of amplitude	±2%
Period of Pulse	20us
Working Temperature Conditions	－15-40℃
Vibration	1.5G(5Hz～200Hz)
Attacking	15g@11ms

Fault detection rate: refers to the ability to detect and find one or more faults in the equipment. Generally defined as the ratio of the number of faults correctly detected by a specified method to the total number of possible faults, it can be expressed as a percentage.

$$FDR = \frac{\lambda_D}{\lambda} \times 100\% \quad (1)$$

Fault isolation rate: Generally defined as the ratio of the number of faults detected and isolated to the total number of possible faults, it can be expressed as a percentage.

$$FIR = \frac{\lambda_L}{\lambda_D} \times 100\% \quad (2)$$

3. HARDWARE DESIGN OF FAULT DIAGNOSIS DEVICE

According to the design requirements and technical indicators of the fault diagnosis device, it can be seen that the main control module, multimeter module, oscilloscope module and signal source generation module are needed, and these modules are the key to the design of the field fault diagnosis device. Because it is easy to carry and use in the field. At the same time, the performance and volume of each module should also be fully considered.

To sum up the above factors, we adopt mature specialized modules in the market to achieve. Because of the high integration requirement of the fault diagnosis device, the portable military reinforced computer is used as the main control platform, and the modular instrument of USB bus is integrated to construct the fault diagnosis device. Among them, the functions and indicators of each module are as follows [3].

(1) Main control module: the whole machine control of the control fault diagnosis device. Intel Atom N270 low power processor, 1.6GHz CPU and 1G memory military hardened computer are used to realize this function. At the same time, the control of oscilloscope module and multimeter module is realized by USB bus.

(2) Oscilloscope module: complete the waveform measurement of the response signal of the test circuit. The Nextkit acquisition card of Panhua Measurement and Control Company is used. It is a USB data interface and can be integrated into the computer. The acquisition board has the function of waveform acquisition, which can be defined by users, and has the function of secondary development.

(3) Multimeter module: complete the measurement of the voltage, current and impedance of the circuit board under test. It is implemented by NI's USB-4065 multimeter module. With the following indicators: channel number: 5; resolution digit: 6.5 bits; maximum DC: 300 V.

(4) Signal Source Module: It mainly generates radar pulse signal, so as to test and diagnose the circuit board. Because the signal source module of this module is very important in radar signal detection, the design is introduced separately.

(5) Power supply module: There are two ways to supply power: one is to change 220V AC current into + 19V DC power through AC-DC adapter, and charge the battery at the same time; the other is to use lithium battery to supply power, using 5000mAh capacity, power up to 65W, efficiency up to 85%. At the same time, the intelligent lithium battery controller is configured to monitor the output current and voltage of the battery. The monitored data is output through bus protocol. It can configure various functions in the battery management configuration tools and configuration software, mainly to adjust the pressure difference between the charge and discharge of the batteries.

4. CONCLUSION

After testing, other performance indicators of the fault diagnosis device can meet the design requirements.

Based on virtual instrument and multi-signal model, the system develops corresponding signal source module [4], oscilloscope module, multimeter module and control module, and realizes the design of field-level fault diagnosis equipment. The experimental results show that the performance index of the system fully meets the design requirements. At present, it has been successfully applied to the on-site maintenance of a search radar and plays an important role in the maintenance and support of the search radar.

REFERENCES

[1]Parag K. Lala, Fellow, IEEE, and Alfred L. Burress, Self-Checking Logic Design for FPGA Implementation, IEEE Transactions on instrumentation and measurement, Vol.52, No. 5, October 2003, pp.1391-1398.

[2]Roman Lysecky, Frank Vahid, A Configurable Logic Architecture for Dynamic Hardware/Software Partitioning, Proceedings of the Design, Automation and testing in Europe Conference and Exhibition (DATE04), 2004, IEEE, pp.01-06.

[3]Vince Hopkin, Bob Kirk, FPGA MIGRATION TO ASICS, Wescon/95, Conference record. Microelectronics Communications Technology Producing Quality. pp. 268-271.

[4]Jemika Malik, Anand Ojha, Design of A Vlsi Fpga Intrgrated Circuit, 2005 IEEE Region 5 and IEEE Denver Section Technical, Professional and Student Development Workshop, 2005, pp.12-15

Combustion Simulation of High-concentration Organic Liquid Wastes

Xiaowen Hao[1,], Zhijun Zhang[2], Zhengyu Wang[2]*
[1] School of New Energy, Harbin Institute of Technology, Weihai, 264209, China
[2] The First Company of China Eighth Engineering Division LTD, Jinan, 250014, China
**E-mail: haoxiaowen@sohu.com*

Abstract: Incinerators are widely used for processing liquid wastes with organic of high concentration. The liquid jet incinerators of L type have the advantages of high combustion efficiency, fast adjustment temperature, relatively low construction cost and maintenance cost dealing with the wastes. However, the combustion reactions of the organic in the incinerator are very complex, and it is very difficult to carry out experimental research. The simulation can be more intuitive to obtain the regulation in the incinerator although the simulation research being far more enough. This manuscript numerically simulated the waste incinerator of a chemical enterprise. The inlet air velocity and the waste mass flow were the main variables in the simulation. By studying the combustion regulation of organic liquid waste in incinerator, the regulations of combustion and flow in the incinerator were obtained. The calculations showed that the increase in inlet air velocity and waste mass flow rate changed the combustion process. The uniformity of flow and temperature distributions have been changed by higher inlet velocity. The efficiency of the waste treatment in the incinerator was very high. The simulation provides the basis for the design of the incinerator.
Keywords: Velocity field, Temperature field, Organic liquid wastes incinerator, Numerical simulation, Combustion.

1. INTRODUCTION

The pharmaceutical, textile, petroleum, chemical and other industries emit a large amount of high-concentration organic liquid wastes every year. The treatment of waste liquids can be biologically and physically chemistry in the industry, which are not up to standard and costly. Microbial methods, magnetic separation methods, and ion exchange methods have been studied [1-3], whose industrial applications have not yet been realized due to various reasons such as immature technology and cost. The use of Incinerator to treat organic liquid wastes is simpler and more efficient than other technologies. It can not only recover heat, reduce treatment costs, but also incinerate harmful substances to achieve comprehensive utilization of waste and protect the environment [4-5]. At present, intensive combustion methods have been widely used in developed countries to treat high-concentration organic liquid wastes [6].

Theoretical analysis, experimental and industrial applications are proceeded for the organic liquid waste incinerators. The study for the incinerators include pyrolysis and combustion kinetics of waste [7-9], design calculation and optimization of incinerator operation [10-13], sulfur dioxide, nitrogen oxides and hydrogen chloride emission control [14-16], and so on. Fluidized bed boilers have the most research, with liquid jet incinerators and rotary kiln incinerators being the least. The liquid jet incinerator has strong adaptability and has obvious advantages such as low construction cost, fast adjustment temperature and relatively low maintenance cost. The liquid jet incinerator can handle complex organic liquid wastes of various components.

The liquid-jet incinerator are available in vertical, horizontal, L and Π types. The L type incinerator has been widely used due to the long residence time of the flue gas and the small area. However, its research is still insufficient. This is mainly due to the turbulent flow in the incinerator, the complex combustion reaction, and the high temperature in the furnace. There are great difficulties in experimental research. However, its research is still insufficient. This is mainly due to the turbulent flow, the complex combustion reaction, and the high temperature in the incinerator. There are great difficulties in experimental research.

A three-dimensional physical model and mathematical model were established for the L type incinerator in this manuscript. The velocity field and temperature field in the liquid waste incinerator were analyzed. The incineration characteristics of the waste liquid in the furnace were analyzed. The effects of incinerator inlet air velocity and waste liquid mass flow on the characteristics of the incinerator were analyzed, too.

2. PHYSICAL MODEL

An L type liquid-jet incinerator with a treatment capacity of 10t/h in a refinery was composed of three parts of the thermal oxidation chambers I, II and III as shown in Fig.1. The thermal oxidation chamber I was vertically arranged, and the tails were arranged horizontally with the chamber II and III [17]. When the device was in operation, the concentrated industrial organic waste liquid was transported

through the waste liquid distributor and uniformly sprayed into the furnace through the mechanical atomizing burner in the upper part of the thermal oxidation chamber I. An auxiliary fuel gas burner and a primary air inlet were vertically disposed at the top of the chamber I. The six mechanical atomizing nozzles were 30° from the central axis of the chamber I. The industrial organic liquid wastes were sprayed into the combustion chamber through the atomizing nozzle to enhance the turbulent mixing and waste liquid incineration efficiency.

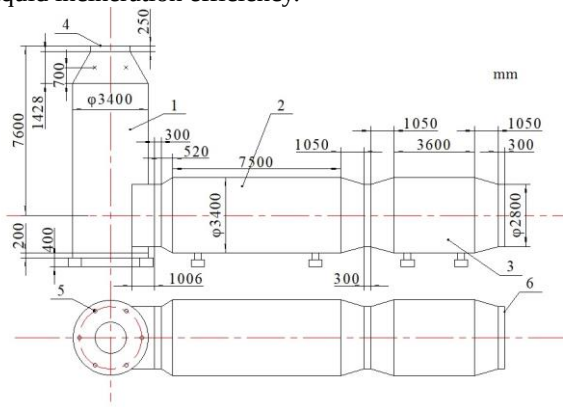

(a) Structure diagram

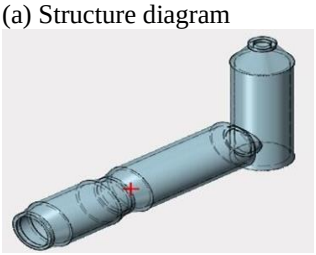

(b) 3-D Model

1. Thermal oxidation chamber I, 2. Thermal oxidation chamber II, 3. Thermal oxidation chamber III,
4. Air inlet, 5. Atomizing nozzle, 6. Flue gas outlet

Figure 1. Structure of the L type liquid-jet incinerator

3. SIMULATION METHOD

3.1. Assumptions of the Simulation Process

The geometry of the incinerator was relatively special, the components of the chemical liquid waste were very complicated, and the combustion process involved many complicated chemical reactions. The physical model and mathematical model must be simplified and assumed In order to obtain stable and realistic calculation results. The following assumptions were used for simulation calculations:

(1) The device was stable in operation. The liquid waste proposed and the primary air injected during operation were constant. The secondary air into the nozzles was ignored. The effect of the auxiliary fuel on the combustion in the incinerator was ignored. The auxiliary fuel is only used for preheating and ignition of the incinerator.

(2) The fluid in the incinerator was assumed to be a fully developed turbulent state.

(3) The liquid wastes were uniformly atomized by the nozzles. The particle size distribution of the wastes conforms to the Rosin-Rammler law. The velocity of the wastes was determined by the nozzle outlet cross-sectional area and the volume flow rate of the liquid waste. The nozzle was simplified to a point where the atomization phase was omitted and the atomized droplets were sprayed into the furnace using a conical jet source.

(4) There is heat dissipation from the incinerator wall.

(5) Since the time scale of the heterogeneous reaction is much larger than the turbulent pulsation time scale, the influence of turbulent pulsation on the heterogeneous reaction is negligible. So it can be assumed that the reactant and product concentration were calculated on a time-averaged basis.

(6) It is difficult to accurately obtain the chemical composition of the liquid waste and its parameters such as the heating value. The simulated liquid used herein was n-Pentane (C_5H_{12}), the molecular weight was 72, the boiling point was 309.1K, the density was 3.4537 kg/Nm^3, and the heat of combustion was 3245 kJ/mol.

3.2. Initial Conditions

The Realizable k-ε model is derived from the experimental phenomena and has a wide range of application and acceptable accuracy, which was selected in flow simulation. The Discrete Random Walk Model (RSM) was selected to track the trajectory of waste combustion particles and the effect of instantaneous turbulent pulsation on the combustion particles of liquid wastes. The Finite Chemical-Rate/Eddy-Dissipation model was used to simulate the waste liquid combustion process. The Discrete Phase Mode (DPM) model was used to simulate the distribution of atomized organic liquid wastes. The effects of droplet gasification and internal heat transfer on heat transfer and mass transfer were considered in the calculation process of the DPM model. The P-1Model model was chosen to simulate the radiation process in the incinerator.

C_5H_{12} was set as discrete phase and was injected into the furnace at a fixed location by the nozzles during the simulation. The air was blown into the incinerator as a continuous phase.

Tab. 1 shows the simulation conditions. There are two conditions. The first one is that the liquid mass flow rate of per nozzle is a constant, which is 0.1 kg/s. The inlet air velocity (air flow) is changed. The second one is that the inlet air velocity is a constant, which is 15m/s. The flow rate of per nozzle is changed.

Table 1. Simulation conditions

Condition number	Mass flow rate of per nozzle (kg/s)	Inlet air velocity (m/s)
1-1	0.1	12.5
1-2		15.0
1-3		17.5
1-4		20.0
1-2	0.1	15.0
2-1	0.2	
2-2	0.3	
2-3	0.4	

The profile of the central section and of the cross-sections A_1-A_2 and B_1-B_2 (the height from the bottom of the thermal oxidation chamber I being 6.4 m and 3.5 m) were analyzed.

4. RESULT AND DISCUSSION

4.1. Inlet Air Velocity on Velocity and Temperature Fields in the Incinerator

4.1.1. Resultant velocity in the incinerator

Fig. 2 shows the resultant velocity distributions in the incinerator. The velocity range of ordinate increases with the increase of inlet velocity. The velocity distributions in the cross-sections A_1-A_2 are affected by the nozzle. And the velocity distributions along the axis are uniform in the chamber I till the turn to the chamber II. The velocity are more ununiform in the chamber II and III with higher inlet velocity. So the baffles are necessary installed in the turn.

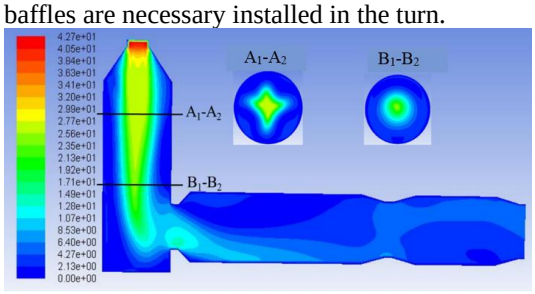

(a) 1-1

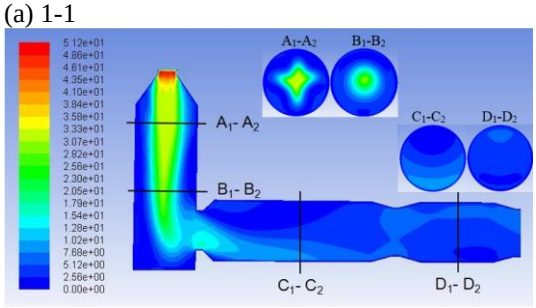

(b) 1-2

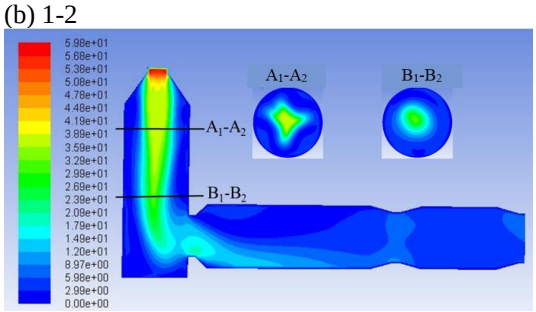

(c) 1-3

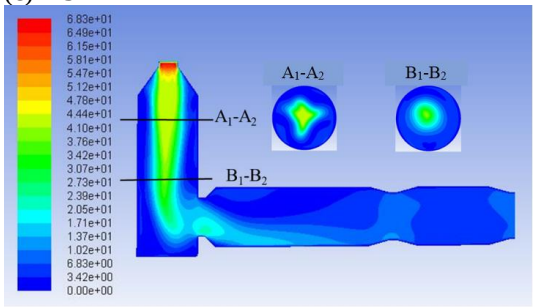

(d) 1-4

Figure 2. Resultant velocity distributions with four inlet velocities, m/s.

4.1.2. Temperature fields in the incinerator

Fig. 3 shows the temperature fields in the incinerator. The velocity distribution affected the temperature distribution. But oxygen was excessive and the residence time was long enough in the simulation. So the C_5H_{12} can be burned with the efficiency higher than 99%.

There is a fierce gas phase combustion reaction in the flame center, so the inner flame temperature is higher than the outer flame. An elongated central combustion zone is formed in the chamber I, and the area of the central combustion zone becomes larger as the inlet air velocity increases. As the waste liquid is exhausted, the high-temperature flue gas gradually diffuses toward the bottom of the chamber I and forms a large high-temperature zone at the lowest part of the chamber I. So there is violently chemical reaction in the lowest part. The flue gas continues to propagate along the chamber II and III, and the temperature slowly decreases in the horizontal section.

The higher the inlet air velocity, the more incompletely burned waste liquid is brought to the lower part of the chamber I. The high temperature flue gas continues to diffuse into the bottom of the chamber I and the chamber II due to the gravity, inertia, and furnace geometry.

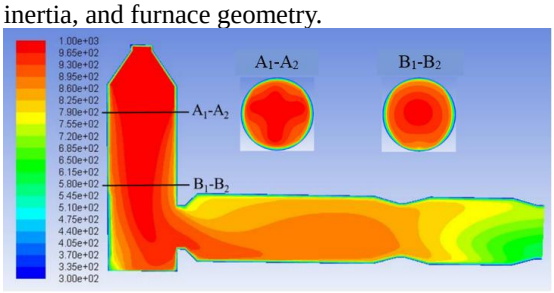

(a) 1-1

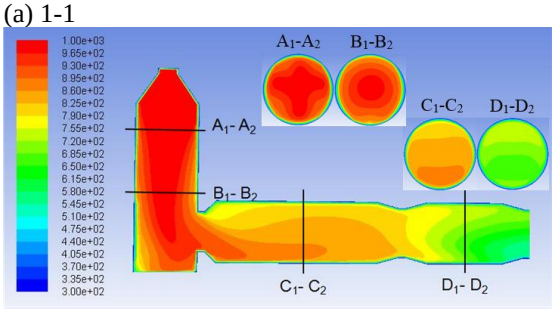

(b) 1-2

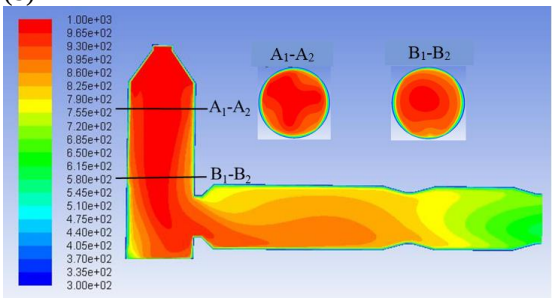

(c) 1-3

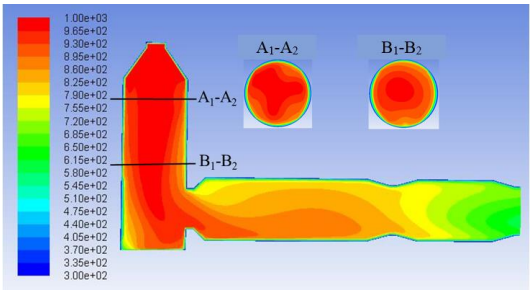

(d) 1-4

Figure 3. Temperature fields with four inlet velocities, K.

4.2. The Mass Flow of the Liquid Waste on Velocity and Temperature Fields in the Incinerator

The mass flow of the liquid waste, which has low impact on the velocity. The greater the mass flow, the more liquid is burned, and the higher the temperature, the faster the velocity.

Fig. 4 shows velocity along the vertical axis in the chamber I. The velocity of the flue gas initially decreases sharply and then flattens, and finally drops sharply from the top to the bottom of the chamber I. This is because the reaction is intense at the top, the temperature of the flue gas rises sharply, the volume of the flue gas increases rapidly. And at the low part, the flue gas gradually flows to the chamber II.

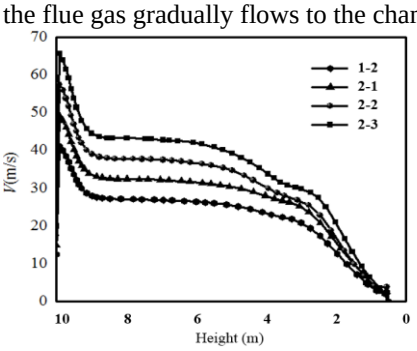

Figure 4. Velocity along the axis in the vertical chamber I.

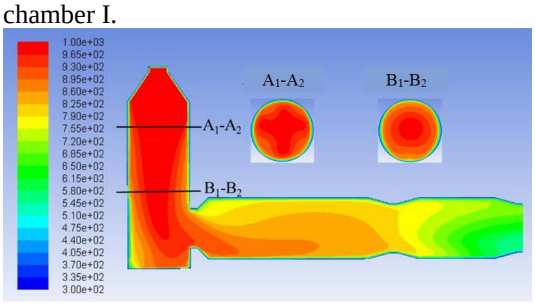

(a) 1-2

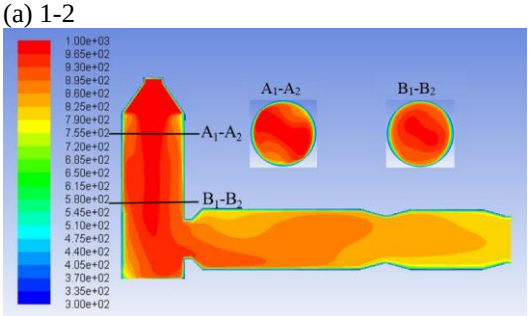

(b) 2-1

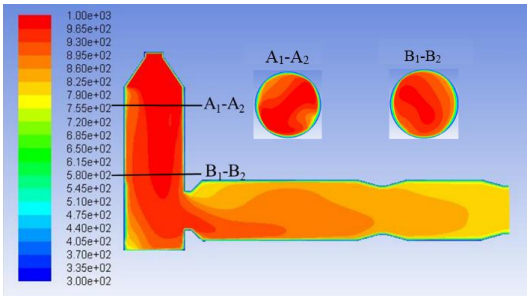

(c) 2-2

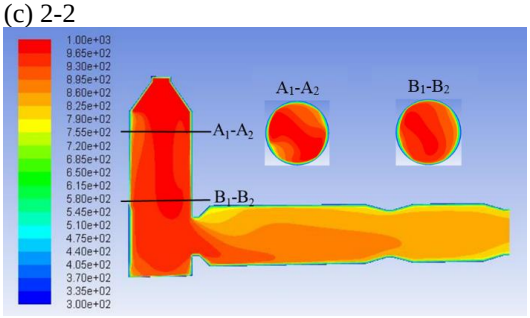

(d) 2-3

Figure 5. Temperature fields with the mass flow varies, K

Fig. 5 shows Temperature fields with the mass flow varies. The central high temperature zone changes from the previous cross shape to the flat shape as the mass flow rate of the waste liquid increasing. The high temperature area spreads to the furnace wall, the area of the main combustion area in vertical section is getting larger and larger with larger mass flow. Temperature in the horizontal section is increased, and the temperature distribution is more uniform with larger mass flow in this section.

5. CONCLUSIONS

An organic liquid waste incinerator of L type was simulated. The regulations of velocity and temperature fields were got with reasonable assumptions.

The inertia of air flow in incinerator is greater and the uniformity is better with the increasing inlet velocity of the primary air in thermal oxidation chamber I. But the velocity are more ununiform in the chamber II and III with higher inlet velocity. An elongated central combustion zone is formed in the chamber I, and the area of the central combustion zone becomes larger as the inlet air velocity increases.

The larger the mass flow rate of liquid waste is, the larger the high temperature combustion area is in the vertical section and horizontal one.

REFERENCES

[1]J. Svoboda, A realistic description of the process of high-gradient magnetic separation, Minerals Engineering, 2001, 14(11): 1493-1503.

[2]J. Lu, Y. Ma, Y. Liu, and M. H. Li, Treatment of hypersaline wastewater by a combined neutralization-precipitation with ABR-SBR technique, Desalination, 2011, 277(1): 321-324.

[3]M. Kazemimoghadam, New nanopore zeolite

membranes for water treatment, Desalination, 2010, 251(1-3): 176-180.
[4]Q. Y. Fang, A. A. B. Musa, Y. Wei, Z. X. Luo, and H. C. Zhou. Numerical Simulation of Multifuel Combustion in a 200 MW Tangentially Fired Utility Boiler, Energy & Fuels, 2012, 26(1): 313-323.
[5]Y. Bai, Y. B. Bao, X. L. Cai, C. H. Chen, and X. C. Ye, Feasibility of disposing waste glyphosate neutralization liquor with cement rotary kiln, Journal of Hazardous Materials, 2014, 278: 500-505.
[6]D. W. Sevon, and D. J. Cooper. Modeling combustion efficiency in a circulating fluid bed liquid incinerator, Chemical Engineering Science, 1991, (46): 2983-2996.
[7]L. F. Calvo, M. Otero, and B. M, Jenkins, Heating process characteristics and kinetics of sewage sludge in different atmospheres, Thermochimica Acta, 2004, 409 (2):127-135.
[8]K. Ehrhardt, A. Ehret, and W. Leuckel, Experimental study on the dependence of burnout on the operation conditions and physical properties in wastewater incineration, Symposium (International) on Combustion, 1998, 27 (1):1293-1299.
[9]C. L. Sun, and J. A. Kozinski, Ignition behavior of pulp and paper combustible wastes, Fuel, 2000, 25(79): 1597-1593.
[10]Zeng L, Pels J and Van H, Direct causticization of kraft black liquor solids with TiO2 in a fluidized bed, Technology, 2015, 14(4): 297-304.
Tappi Journal, 2000, 83(12):53.
[11]D. W. Sevon, and D. J. Copper, Modeling combustion efficiency in a circulating fluid bed liquid incinerator, Chemical Engineering Science, 1991, 46(12): 2983-2996.
[12]R. S. Bie, Y. L. Bao, and L. D. Yang, Thermal calculation method of incineration of organic waste liquid in fluidized bed incinerator, Journal of Harbin Institute of Technology, 1998, 30(1):39-42.
[13]G. Z. Zhu. Study on using cement turning kiln to incinerate hazardous waste along with cement materials, Acta Scientiae Circumstantiae, 2000, 20(6): 810-812.
[14]Zell U, Shamekhi R and Roth P., Waste water combustion in laboratory swirl burners-II. NO formation from dissolved N-compounds, Chemical Engineering Science, 1988, 43(7):1667-1676.
[15]X. Li, K. Zhao, Y. Liu, Experimental Study on the emission of HCl from incineration of chlorinated waste water in fluidized bed, Boiler Technology, 2004, 35(2): 73-75.
[16]J. Nadziakiewicz, and M. Koziol, Co-combustion of sludge with coal, Apply Energy 2003, 13(75): 239-248.
[17]H. C. Yin, L. X. Fu, J. B. Chen, P. Ying, and L. Mu, Numerical investigation of characteristics of combustion process and pollutant emission in waste water incineration, Journal of thermal Science and

Research of Photoelectric Counting for Online Bars

Jianhong Huang[1], Dongdong Zhao[2], Xindong Wang[2], Yidong Xu[2], Zhijie Li[2]
[1]SHANG YANG Machinery Co., Ltd of Zhejiang, Quzhou 324000, China
[2]Key Laboratory of Air-drive Equipment Technology of Zhejing Province Quzhou, Zhejiang 324000, China

Abstract: In this paper, a new type of on-line bar counter is introduced, which uses photoelectric sensor and photoelectric encoder to achieve accurate counting. The bar technology device was manufactured in the laboratory, and the bar counting process was simulated. The results show that the mechanical pretreatment device designed before calculation can sort out the bar in disorderly arrangement on the transmission chain, eliminate the overlap and cross of the bar, and realize the accurate bar counting by the joint calculation of two sensors.
Keywords: Bar counting device; Sensors; Photoelectric counting

1. INTRODUCTION

The automatic counting of threaded steel bar (bar) is an important subject that has not been completely solved in China, and it is also one of the difficult problems that need to be solved urgently in the production practice of steel mills. With the improvement of dimension accuracy and performance prediction accuracy of bar rolling, it is urgent for users and distributors to require steel rolling enterprises to deliver in negative tolerance. Negative tolerance delivery refers to the theoretical weight of bars out of the factory valuation [1-3]. The actual quality of bars is the actual data obtained by electronic metering and weighing, while the theoretical quality is calculated theoretically according to the standard geometric size and number of supports of different specifications of products. The theoretical quality is equal to the standard cross-sectional area of steel with corresponding specifications, the standard length, the steel density and the number of bars [4-5]. The standard geometric dimensions and the density of bars are known by agreement. Therefore, obtaining the accurate number of bars is the key to determine the theoretical quality and realize the packing of the fixed number of bars. According to the requirement of GB1499-1998, the allowable deviation between the actual weight and the theoretical weight of bars is between (+7%-4%), so the benefits brought by the delivery of bars on negative tolerance by enterprises to production enterprises, suppliers and users are obvious. At present, domestic bar manufacturers mainly adopt manual methods. Because the manual counting method has high labor intensity, low accuracy and low production efficiency, it cannot meet the requirements of fierce competition in bar production industry.

2. COMPOSITION OF A NEW ON-LINE BAR COUNTER

Aiming at the problems existing in the field of on-line bar counting, a new mechanical-photoelectric counting system is proposed, which mainly consists of mechanical and photoelectric parts. The following are introduced separately.

1) Mechanical part: The main function is to sort out the disorderly arrangement of bars in the transmission chain, eliminate the overlapping and crossing of bars, prepare for the subsequent counting of electrical components, and divide the bars according to the counting results after counting, so as to realize the function of fixed support and bundling.

The overall working process is as follows: (1) Bar separation pretreatment; (2) Number of lead screw; (3) Bar batch processing. It includes: 1#, 2# transmission chain, plucking claw/combination stop, screw counting device, lifting baffle and 4# transmission chain, as shown in Figure 1.

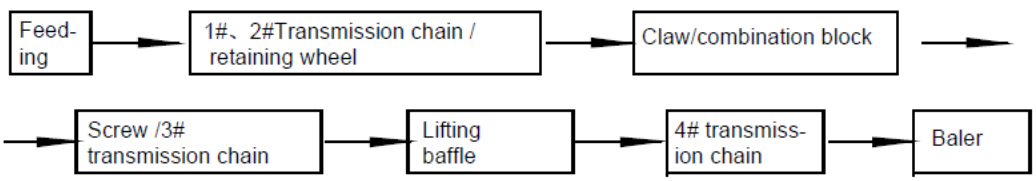

Figure 1. Composition of bar-counting machine

(2) Photoelectric part: This part mainly detects the bar and sends out signals according to the test results. There are many kinds of photoelectric components, including photoresistors, photodiodes, phototransistors, photocontrolled silicon controllers and integrated photosensitive devices [6-7], but they all belong to photosensitive sensors made of photoelectric effects of semiconductors. The core of counting is composed of light emitters and light receivers (see Figure 2). When there is no bar passing

between the light emitting body and the light receiving body, the light receiving body is turned on, and the low level is output by reverse and shaping. When a bar passes through, the bar blocks the light path and the receiver is not conductive, and the high level is output by the director in reverse. By recording the number of times of high level, we achieve the goal of bar bundling count.

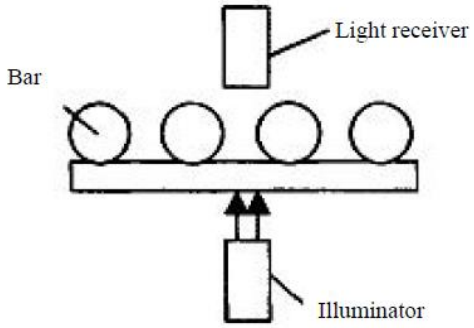

Figure 2. Photoelectric sensor working diagram

3. PHOTOELECTRIC COUNTING PRINCIPLE

The crossover and overlap of bars can be basically eliminated by separating and pretreatment of bars, and the single-row flat laying of bars can be realized, as shown in Figure 3 (a). Therefore, the use of reflective photoelectric sensors with maintenance devices can achieve the purpose of counting. However, the actual situation is more complex. There is still a small amount of bar overlap on the counting screw as shown in Figure 3 (b), which affects the final counting accuracy.

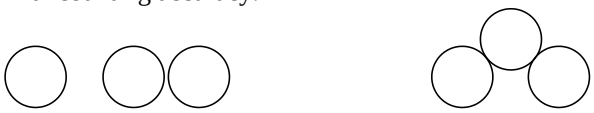

(a) single-layer arrangement of bars (b) overlapping of bars

Figure 3. Conditions of bar steels on counting screw

When the state of Figure 3 (b) appears, the deviation will occur only with the photoelectric sensor, and the more serious the overlap, the greater the deviation. In order to eliminate the decline of counting accuracy caused by this bar state, the photoelectric sensor and photoelectric encoder are used to detect the overlap of counting lead screw. The test results are checked. The principle is described below.

The photoelectric encoder is coaxially mounted with the counter screw. The resolution of the encoder is *N*, the guide of the counter screw is *d*, and the diameter of the bar is *Φ*. When the counting lead screw rotates once a round, it will drive the *d* distance of the bar running. At this time, the encoder just outputs *N* pulses, so each pulse corresponds to the linear displacement $l = d / N$ of the bar running. If the number *m* of output pulses of the photoelectric encoder is measured during the blocking of the counting sensor (i.e. when a bar passes), the distance *L* of the bar passing through the sensor probe (including overlappers) can be accurately measured as follows:

$$L = m \cdot l = \frac{md}{N} \tag{1}$$

The number of bars passed is as follows:

$$n = \frac{L}{\phi} = \frac{md}{N\phi} \tag{2}$$

3. PHOTOELECTRIC COUNTING SIMULATION EXPERIMENTS

3.1. Introduction of experimental device

In order to effectively simulate the status of bar on the counting screw and verify the feasibility of using double sensors to achieve accurate counting of bar, the counting screw is simulated by the experimental car, especially the special overlap of bar on the screw. As shown in Figure 4, the photoelectric encoder and wheel are coaxially mounted. The motor and workshop are driven by synchronous belt. The photoelectric generator fixed on the ground is used for detection. The signals sent by the encoder and photoelectric sensor are processed by PLC. The car is controlled by PLC for speed change, positive and negative rotation and start-stop.The selection of other components is shown in Table 1.The rated speed of the motor $n_N = 1500\text{r/min}$, the diameter of the car wheel $d = 50\text{mm}$, the resolution of the encoder *N* = 1000 ppr, and the transmission ratio of the car to the motor is 14:32. The diameter of the bar is $\phi = 20\text{mm}$ .The relationship between bar diameter and pulse number is as follows:

$$m = \frac{d}{\pi D} \times 1000 = 6.366d \tag{3}$$

In the formula, d is the diameter of bar, mm.

The relationship between car feed speed and motor speed:

$$v = \frac{\pi \times 14 \times 50}{60 \times 32} n = 1.1454n \tag{4}$$

In the formula, n is the speed of the motor, r/min

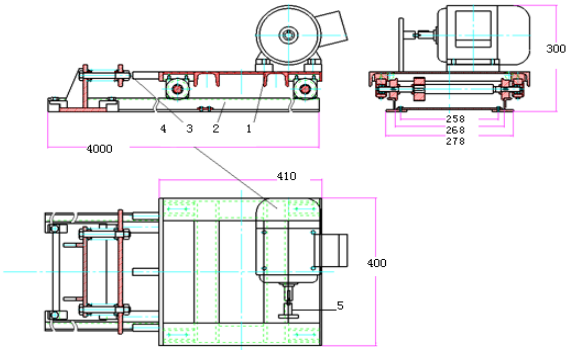

1-frame; 2-parallel track; 3-shock absorber; 4-drive motor; 5-encoder

Figure 4. Experiment dolly

Table 1. List of experiment devices

Name	Model	Main parameter	Details
Photoelectric switch	HJ18-R33DPK	U_N=10-36VDC PNP output mode	Shanghai Juma Electric Co., Ltd.
Encoder	ZKX-6A100BM1-G24F	N=1000 V_H=0.7V_{CC} V_L=0.06V_{CC}	Changchun Yuheng Optics Co., Ltd.
CPU212	6ES7-212-1BB23-0XB8	Digital Quantity:8I/6O	Siemens (China) Co., Ltd.
Extension module	6ES7 232-0HB22-0XA8	Analogs:2AO	
Programming Cable	6ES7 901-3CB30-0XA0	PC/PPI Series	
Frequency converter	AC60-T3-R75G	U_N=380V P_N=0.75kW	Shenzhen Weichuang Electric Co., Ltd.
Asynchronous motor	Y Series	P_N=0.55kW n_N=1500r/min	Wuxi Hadian Motor Co., Ltd.

Table 2. Relation between check object and checking height

Detection height mm	45	65	0~2000	0~2000
Minimum Diameter of Detecting Object mm	1.5	3	5	＞5

3.2. Experimental results and analysis

3.2.1. Study on the detection characteristics of photoelectric sensors

(1) The smallest detection diameter of photoelectric sensor increases with the detection distance and the smallest diameter of detectable object. The reason is due to the divergence of infrared light. When the detection distance is too large, the infrared light divergence will make the spot bigger, and the diameter of the detection object smaller, which will cause the phenomenon of missed detection and false detection. When the detected object is ≥ 5 mm, the detected object can be recognized accurately. The relationship between the detected object and the probe height of the sensor is measured experimentally as shown in Table 2.

(2) The influence of the minimum diameter of the object detected by the sensor on the bar detection

Because of the influence of the ribs of the threaded bars, the spacing of the two threaded bars when they are placed side by side densely is smaller than the minimum detection diameter of the photoelectric sensor. In this regard, the pulse calibration using photoelectric sensors and coders can be distinguished by program checking, as shown in Figure 5.

3.2.2. Effect of different motion speed on bar testing results

The bar counting of the trolley at different moving speeds is set in the experiment. According to the bar counting results under different conditions, the influence of the bar moving speed on the counting results is obtained. The 12 bars are arranged in various forms. The results of test under different conveying speeds are shown in Table 3.

Table 3. Relation between transporting velocity of bar and checking resul

Motor speed r/min	131.0	174.6	281.3	262.0	305.5	350.0
Speed m/s	0.15	0.20	0.25	0.3	0.35	0.4
Number of bars (pcs)	12	12	12	12	12	12
Bar diameter (mm)	20	20	20	20	20	20
The corresponding detection time of a single bar (ms)	133	100	80	67	57	50
Counting results (pcs)	12	12	12	12	12	12

From Table 2, it can be concluded that: Under the existing working conditions, the bar conveying speed has little effect on the test results. The reasons are as follows: The response speed of the counting depends on the response time of the photoelectric sensor and the response speed of the processor. Because the response time of the sensor is less than 1 ms < 100 ms (the maximum detection time of a single bar), and the response speed of the system is faster than that of the sensor, the conveying speed has no effect on the detection results under the existing working conditions.

3.2.3. Counting of bars in different arrangements

Pulse Counting Principle: The photoelectric encoder is coaxially installed with the counting trolley. The actual running speed n of the motor, i is the transmission ratio of the motor to the trolley [5], the diameter D of the trolley wheel, the resolution of the encoder N (the number of pulses output by the encoder in one rotation cycle), and the diameter of the bar ϕ. When the motor rotates for one round, the running distance of the trolley is $d = \frac{n}{60 \cdot i} \pi D$

the number $p = \frac{60i}{n\pi D} \cdot \phi \cdot N$ of pulses corresponding to the diameter ϕ of each bar. When adhesion and overlap occur, the number of coder pulses corresponding to one shielding zone of photoelectric switch is *q (q > p)*, and the corresponding number of bars is identified by $m = \frac{q}{p}$ judgment (In practice, the rolling precision of the bar should be considered).

The experiment was carried out with the threaded steel bar of φ20. The different arrangement of the bar and the analysis results are shown in Figure 5.

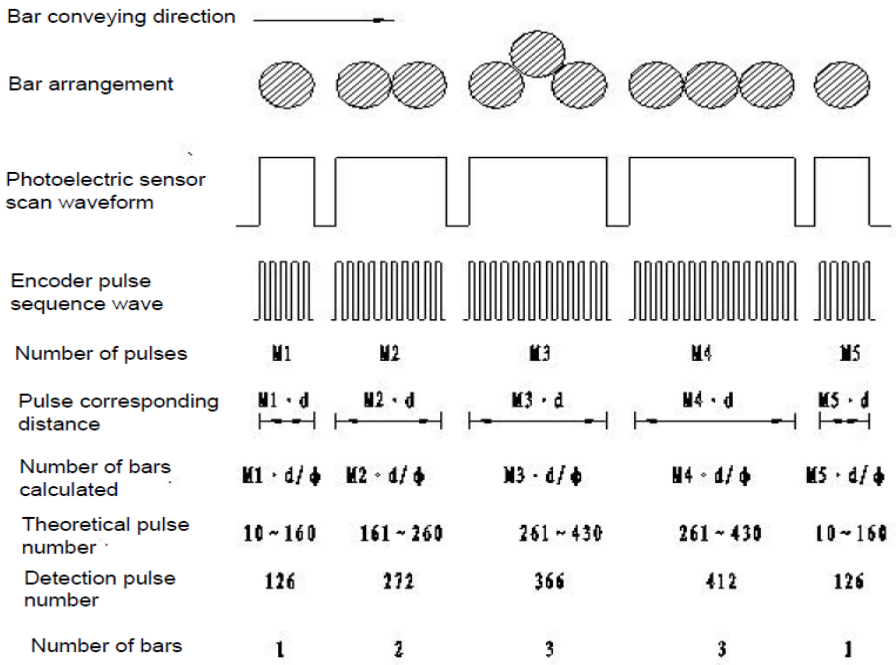

Figure 5. Time sequence of pulse signals in counting process

From Figure 5, it can be seen that the number of bars can be accurately determined by using photoelectric sensor and coder combined detection and operation, so as to achieve the purpose of accurate detection of bars.

4. CONCLUSION

1) The optoelectronic sensor can improve the detection accuracy and reduce the smallest diameter of the detectable object by choosing laser counter-fire sensor. The detection height of the photoelectric sensor should be as small as possible to avoid the problems such as the deterioration of detection accuracy caused by light divergence.

2) The bar conveying speed has no effect on the test results. However, when the transmission speed is too high, the jitter caused by the speed change may cause the wrong detection of the bar.

3) The stacking and crossing of bars can be eliminated by using mechanical pretreatment device, and the counting of special overlapping state of bars on the counting screw can be effectively realized by using photoelectric switch and coder, with the accuracy of 100%.

Acknowledgement: Key Research and Development Program of Zhejiang Science and Technology Department (2017C02027)

REFERENCE

[1]Zhang Jiuquan, Jin Youzhong. A Counting Device for Bar Shapes. Techniquesof Automation& Applications, 2009, 28(07): 92-93.

[2]Mao Qingzhou, Pan Zhimim, Gao Wenwu. Using Iterative Houhg Round Transformand and Connected Area to Count Steel Bars Reliable.Geomatics and Information Science of Wuhan University, 2014, 39(03): 373-378.

[3]An Haisheng, Zhang Weige. Theoretical Weight Delivery and Pbaruct Quality Control of Building Steel. Modern Quality, 2001, (6): 35-36.

[4]Qiu Jiyue, Tang Jiemin. Negative deviation pbaruction optimization. Iron and Steel, 1999, 34 (1): 74-77.

[5]Yu Youwen, Chang Jian, Cheng Jihong. Sensor Principle and Engineering Application. Xi'an University of Electronic Science and Technology Press. 2003, 7.

[6]Song Qiang, Xu Ke, Xu Jinwu, et al. Bar automatic counting technology based on image processing. Iron and Steel, 2004, 39(5): 34-37.

[7]Wang Weiyong, Zhu Yuquan. A Rebar Counting Method Based on Multi-Template Coverage. Computer and Modernization, 2005, (5): 25-27.

Research of Bicycle Automatic Control System by Using LQR Optimal Theory

Yishu Zhang
College of Mechanical Engineering, Xi'an University of Science and Technology, Xi'an, 710054, China
**E-mail: 714720644@.qq.com*

Abstract: The bicycle plant is a typical multi-variable, nonlinear and statically unstable system. In such a rapidly growing and highly automatic society, how to make bicycle automatically work is more and more worthy to be studied. In this paper, the mathematical modeling of the bicycle is firstly established. Based on the as-built model, the automatic controller of the bicycle is designed based on linear quadratic regulator (LQR) optimal theory. In addition, the computer simulation is carried out to verify the validation of the proposed LQR optimal controller, and the bicycle automatic control system presents the satisfactory performance in the existence of uncertain disturbance.
Keywords: Autopilot; Bicycle control; Disturbance; LQR; Optimal control

1. INTRODUCTION

In engineering practice, the proportional, integral and differential (PID) control is the most widely-used regulation method. According to the current error of control system, PID controller can calculate out the control quantity by means of the proportional, integral and differential operations [1]. The history of PID has up to nearly 80 years ago, and it has become one of the main technologies in industrial control because of its obvious advantages, such as simple structure, good stability, reliable work and convenient adjustment. A certain research showed that more than 90% of the controllers employed the PID method for the process control systems in 1989 [2]. However, when the traditional PID controller is applied in the bicycle control system, the satisfactory control effect will not obtained, because the bicycle plant is a typical unstable, multi-variable, nonlinear and strong coupling control plant[3]. Therefore, other better regulation technologies should be studies in the control of bicycle plant.

The linear quadratic regulator (LQR) theory [4] belongs to a state-space design method, and it has the earliest and the most mature development in the modern control theories. Through the optimal LQR theory, the designed state feedback controller can minimize the quadratic objective function, which is an attractive feature of LQR approach. Therefore, the LQR system can possess the good advantage in the comprehensive performance. In other word, we can get the ideal state convergence performance by using smaller control consumption. Particularly speaking, LQR can get the optimal control law in the form of linear state feedback, and it is easy to constitute a closed-loop optimal control, therefore it has been widely applied in many areas and studied in many literatures [5-8]. Moreover, LQR has enough ability to deal with the unstable, multi-variable and coupling systems. In addition, the application of MATLAB software provides the favorable condition for the simulation verification of LQR control scheme. As a result, we will introduce the LQR theory to construct the optimal controller for bicycle system.

The remainder of this paper will be organized as follows. The Section 2 will describe the bicycle plant and then establish a state-space model for this plant. Based on the as-built model in state-space form, the automatic controller will be designed for bicycle system by using LQR theory in Section 3. Section 4 will present the verification and the advantage of the proposed LQR controller by means of computer simulation and scheme comparison. In addition, the corresponding conclusions will be given in Section 5.

2. PROBLEM DESCRIPTION

The bicycle is a typical multi-variable, nonlinear and statically unstable plant, and it is illustrated in Figure 1, where *f* denotes the friction force, *N* denotes the holding force from the ground, and *Mr* denotes the hinge moment. The bicycle has three inputs, which involves the yaw moment to change the yawing direction, the roll moment produced during the deflection of bicycle body, and the hinge moment to provide a push force. Moreover, assume that the bicycle has a symmetrical structure, and its mass-center is placed on the symmetrical plane.

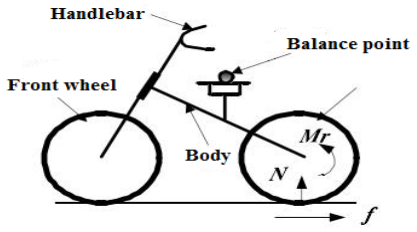

Figure 1. The structure diagram of bicycle plant

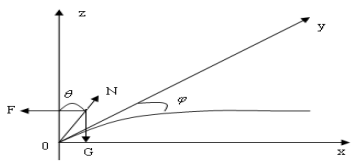

Figure 2. The force diagram of the bicycle

The force diagram of the bicycle is shown as Figure 2, In Figure 2, oxyz denotes the coordinate system of bicycle traveling path, φ denotes the yawing angle, θ denotes the yawing angle, *F* denotes the coupling force in yaw direction, and *G* denotes the force of gravity.

Based on the following simplification principles, the model of the bicycle will be established.

Principle 1. Assume the bicycle is driven in uniform linear motion, and its velocity is 5m/s, which is a usual velocity in practice. The hinge moment provides the push force, which always balances the friction force. Therefore, we ignore the degree of freedom (DOF) with respect to the horizontal hinge moment, and then the bicycle can be simplified into two DOF.

Principle 2. The rolling angle rate of bicycle is coupling with the yawing angle rate. In concrete, the rolling motion can automatically generate the yawing acceleration, meanwhile the yawing motion can also automatically generate the rolling acceleration. Therefore, the bicycle can be further simplified into single DOF, and the yawing direction is chosen in this paper.

Principle 3. The disturbance can be simplified into the initial yawing angle. Moreover, when the bicycle encounters the un-rough roads or the sudden wind, the rolling angle (which can generate the yawing acceleration) or the yawing angle will occur. After balancing, both of them can simplify into the yawing angle with disturbance.

The design goal of bicycle automatic control system is to realize the correction of yawing angle with disturbance, and then to recover the standard yawing direction in a shorter time, which is illustrated by Figure 3.

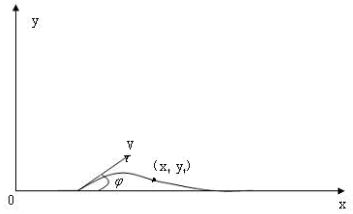

Figure 3. The illustration diagram of the control goal.

From Figure2, we can get the following equation:

$$\begin{cases} N\cos\theta - G = 0 \\ N\sin\theta - F = 0 \end{cases} \tag{1}$$

Based on $\cos\theta \approx 1$ and $\sin\theta \approx \theta$, we can get the linear equation with respect to (1), which is shown in (2).

$$\begin{cases} N - G = 0 \\ N\theta - F = 0 \end{cases} \tag{2}$$

The coupling force between the rolling angle speed and the yawing angle speed is expressed by Eqs. (3)-(4).

$$F = m\frac{v^2}{\rho} \tag{3}$$

$$\rho = \frac{\Delta s}{\Delta\varphi} \approx \frac{v\Delta t}{\dot{\varphi}\Delta t} = \frac{v}{\dot{\varphi}} \tag{4}$$

Where, *v* is the speed of bicycle, *m* is the mass of bicycle, and ρ is the radius of curvature.

According to Eqs. (2)-(4), we can get the following equation:

$$\begin{cases} N = mg \\ N\theta = m\dfrac{v^2}{\rho} = mv\dot{\varphi} \end{cases} \tag{5}$$

According to (5), the simplification equation will be acquired.

$$\dot{\varphi} = \frac{g\theta}{v} \tag{6}$$

The location of bicycle in the coordinate system of traveling path is expressed by:

$$\begin{cases} x = \int_{t_0}^{t_f} v\cos\varphi dt \\ y = \int_{t_0}^{t_f} v\sin\varphi dt \end{cases} \Rightarrow \begin{cases} x \approx \int_{t_0}^{t_f} v dt \\ y \approx \int_{t_0}^{t_f} v\varphi dt \end{cases} \tag{7}$$

With the differential operation on (7), we can get:

$$\begin{cases} \dot{x} = v \\ \dot{y} = v\varphi \end{cases} \Rightarrow \begin{cases} \ddot{x} = 0 \\ \ddot{y} = v\dot{\varphi} \end{cases} \tag{8}$$

According to Eqs. (6) and (8), we can choose the following state variables:

$$\begin{cases} x_1 = y \\ x_2 = \dot{x}_1 = v\varphi \\ \dot{x}_2 = \ddot{x}_1 = v\dot{\varphi} = g\theta \end{cases} \tag{9}$$

Then, we can further get the following differential equation:

$$\begin{cases} \dot{x}_1 = x_2 \\ \dot{x}_2 = g\theta = 10\theta \end{cases} \tag{10}$$

Based on Eq. (10), the state-space model of bicycle can be finally acquired as Eq. (11).

$$\begin{cases} \dot{\mathbf{x}} = \mathbf{A}\mathbf{x} + \mathbf{b}\theta \\ y = \mathbf{C}\mathbf{x} \end{cases} \tag{11}$$

Where, the vectors and matrices are shown as:

$$\mathbf{x} = \begin{bmatrix} x_1 \\ x_2 \end{bmatrix},\ \mathbf{A} = \begin{bmatrix} 0 & 1 \\ 0 & 0 \end{bmatrix},\ \mathbf{b} = \begin{bmatrix} 0 \\ 10 \end{bmatrix},\ \mathbf{C} = \begin{bmatrix} 1 & 0 \\ 0 & 0 \end{bmatrix}$$

The terminal condition is set as:

$$y_{t_f} = 0$$

Until now, the control plant of bicycle has been established in the state-space form, and it will provide a basis for the next controller design.

3. CONTROLLER DESIGN PROCESS

For a class of linear system, just as (11), we can design the feedback control law based on LQR optimal control theory [5], which can minimize the following quadratic performance index:

$$J = \frac{1}{2}\int_0^{\infty}\left(\mathbf{x}^{\mathrm{T}}\mathbf{Q}\mathbf{x} + R\theta^2\right)\mathrm{d}t \qquad (12)$$

where, $\mathbf{Q}$ is generally chosen as a positive definite symmetric matrix, and R is a positive number. From (12), we can see that the performance index is composed by the regulation error term and the control consumption term. As a result, the minimization of this performance index can bring the optimal comprehensive performance of control system.

In this case, the optimal feedback control law can be expressed as:

$$\theta^* = -\mathbf{k}^*\mathbf{x} = -R^{-1}\mathbf{b}^{\mathrm{T}}\mathbf{P}\mathbf{x}\,,\quad \mathbf{k}^* = \begin{bmatrix} k_1^* & k_2^* \end{bmatrix} \qquad (13)$$

where, $\mathbf{k}^*$ represents the optimal feedback vector, and $\mathbf{P}$ is a positive definite symmetric matrix and it satisfies the following Riccati equation:

$$-\mathbf{P}\mathbf{A} - \mathbf{A}^{\mathrm{T}}\mathbf{P} + \mathbf{P}\mathbf{b}R^{-1}\mathbf{b}^{\mathrm{T}}\mathbf{P} - \mathbf{Q} = \mathbf{0}\,. \qquad (14)$$

Aiming at the as-built state space model of bicycle, the automatic controller has been designed, and its output can be calculated according to (13). Furthermore, the computer simulations about this designed controller will be presented in next section.

4. SIMULATION RESULTS

In this section, the proposed LQR automatic controller for bicycle will be verified with different quadratic parameters. Moreover, the effects from the selection of parameters on system performance can be also acquired.

In this simulation, the initial conditions of bicycle are expressed by:

$$\mathrm{x}_1(0) = \mathrm{y}_0 = 0,\ \mathrm{x}_2(0) = \mathrm{v}\varphi_0 = 0.2$$

Moreover, the restricted conditions of bicycle are expressed by:

$$0 \le \theta \le 10^{\circ}\left(=\frac{18}{\pi}\mathrm{rad}\right),\ 0 \le \varphi \le 10^{\circ}\left(=\frac{18}{\pi}\mathrm{rad}\right)$$

In first, the quadratic parameters in (12) are chosen as:

$$\mathbf{Q} = \begin{bmatrix} q_1 & 0 \\ 0 & \dfrac{90}{\pi} \end{bmatrix},\quad q_1 = 10\,,\quad R = \frac{18}{\pi}$$

We can calculate the feedback gain vector in (13), which is $\mathbf{k}^* = \begin{bmatrix} 1.321 & 2.294 \end{bmatrix}$.

The regulation process of the two state variables in system (11) are illustrated by Figure 4.

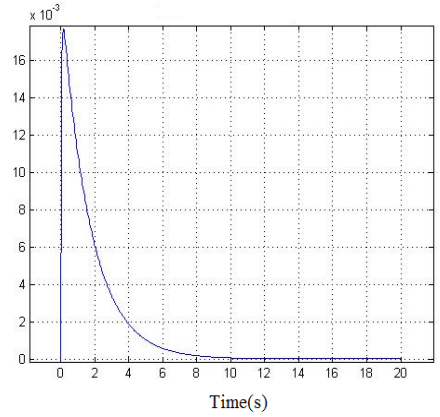

(a) Variable x_1

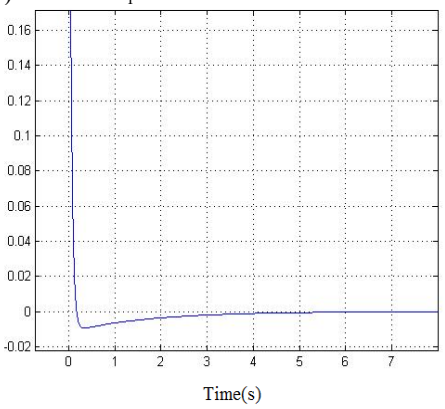

(b) Variable x_2

Figure 4. The regulation curves of state variables with q_1=10, where the unit of variable x_1 is m/s and the unit of variable x_2 is m/s^2

At this time, the quadratic parameters in (12) are re-newly chosen as:

$$\mathbf{Q} = \begin{bmatrix} q_1 & 0 \\ 0 & \dfrac{90}{\pi} \end{bmatrix},\quad q_1 = 100\,,\quad R = \frac{18}{\pi}$$

We can also calculate the feedback gain vector in (13), which is $\mathbf{k}^* = \begin{bmatrix} 4.178 & 2.416 \end{bmatrix}$.

Subsequently, the regulation process of the two state variables in system (11) is illustrated by Figure 5.

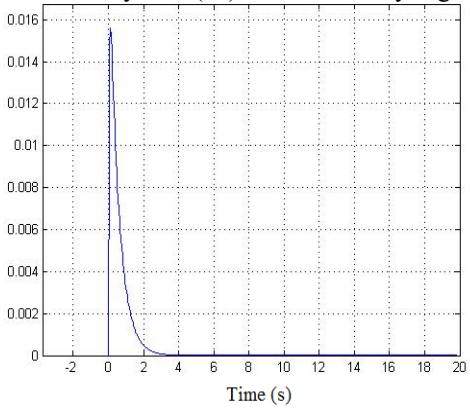

(a) Variable x_1

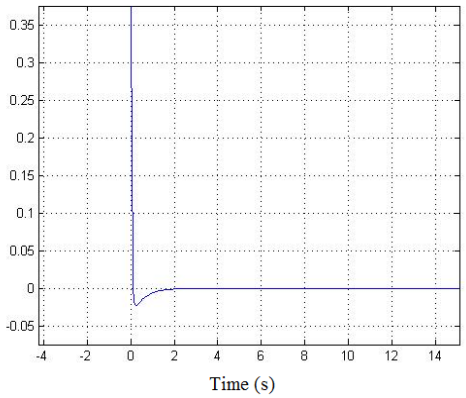

(b) Variable x_2

Figure 5. The regulation curves of state variables with q_1=100, where the unit of variable x_1 is m/s and the unit of variable x_2 is m/s^2

From Figures. 4-5, we can see that the designed controller can automatically generate the inverse yawing angle speed, in order to correct the effect resulted from the disturbance. Furthermore, if q_1 is chosen as a larger value, the faster regulation speeds of state variables will be presented. Until now, the simulation verification about the proposed controller has been completed.

5. CONCLUSIONS

The bicycle plant is a typical multi-variable, nonlinear and statically unstable system. Based on LQR optimal theory, a kind of automatic controller for the bicycle is proposed in this paper. Computer simulations are carried out to verify the effectiveness and the validity of the proposed controller. The results show that the designed controller can correct the effects resulted from the disturbance and then the standard yawing direction is recovered in a shorter time. Moreover, the proposed control approach can be extended into some other similar plants.

.

REFERENCES

[1]Wu L., Bao H., Du J.L. et al. A Learning Algorithm for Parameters of Automatic Disturbances Rejection Controller. Acta Automatica Sinica, 2014, 40(3): 556-560.

[2]Astrom K.J., Hagglund H. PID Controllers: Theory, Design and Tuning. NC: Instrument Society of America, 1995.

[3]Wang L.B, Ge Y., Hu D.W. Balance Control for Unmanned Bicycles Based on T-S Mode. Control Engineering of China, 2008, 15(S1): 109-112.

[4]Naidu D.S. Optimal control systems, Special Indian edition. FL: CRC Press, 2002.

[5]Shakir H. and Kim W.J. Nanoscale Path Planning and Motion Control with Maglev Positioners. IEEE/ASME Trans. Mechatronics, 2006, 11(5): 625-633.

[6]Basina M., Rodriguez-Gonzaleza J., Fridmanb L. Optimal and Robust Control for Linear State-Delay Systems. Journal of the Franklin Institute, 2007, 344(6): 830-845.

[7]Dragan V., Mukaidani H., Shi P. The Linear Quadratic Regulator Problem for A Class of Controlled Systems Modeled by Singularly Perturbed ito Differential Equations. SIAM Journal on Control and Optimization, 2012, 50(1): 448-470.

[8]Priess M.C., Conway R., Choi J. et al. Solutions to the Inverse LQR Problem with Application to Biological Systems Analysis. IEEE Transactions on Control Systems Technology, 2015, 23(2): 770-777.

Classification of Planting Structure in Remote Sensing Images Based on Semantic Segmentation Network Models

Weidong Li,Fanqian Meng, Ullah Inam*
College of Information Engineering, Henan University of Technology, Zhengzhou, 450001, China
**E-mail:3sadmin@gmail.com*

Abstract: This paper takes Xiaokaihe Irrigation Area as the research area, Landsat8 high resolution remote sensing image as the data source, select its 543 band for RGB synthesis, and the panchromatic band was fused to improve the resolution to 15 meters. According to the fusion image, make training set and test set, and verification set is made by using precise classification map of planting structure obtained by supervised classification. Three kinds of semantic segmentation network models are selected: FCN (full convolution neural network) model, SegNet model and U-Net model to classify planting structures and analyze the effects of different semantic segmentation networks on classification accuracy. The results showed that under the same conditions, the overall classification accuracy of U-Net model reached 90.7%, FCN model had the highest recognition rate of 78.7% for wheat, and SegNet had only 88.2% accuracy for plant structure extraction under similar spectral information. Therefore, the U-Net network model can get better classification results in areas with serious mixed features.
Keywords: deep learning; semantic segmentation network; remote sensing; classification

1. INTRODUCTION

Crop planting structure is the main basis for monitoring and estimating crop growth, analysing crop yield, adjusting and optimizing cropping structure, and managing crop irrigation [1]. Because agricultural land is dominated by farmers freely, the phenomenon of mixed planting is serious and spectral mixing is widespread, the application of high resolution remote sensing images can significantly improve the accuracy of crop classification [2-4]. Crop classification method based on Multi-temporal image can make full use of seasonal rhythm characteristics of crops, clearly reflect the changing trend of different crops with time, and effectively reduce crop misclassification, it is the mainstream method of crop planting structure remote sensing extraction [5-10]. However, there is little research on crop planting structure classification using deep learning method.

Deep learning has become a hotspot in the development of large data and artificial intelligence on the Internet. The biggest difference between deep learning and traditional machine learning methods is that it has the characteristics of automatic learning from large sample data sets rather than manual design. In addition, the deep network structure also makes it have strong learning and expression ability [11]. Convolutional neural network (CNN) is one representative algorithms of deep learning, with its advantages of automatic feature extraction and classification, it has significant advantages in the field of remote sensing [12-14]. At present, full convolutional network (FCN), as a very important network model in semantic segmentation research, is widely used in high resolution remote sensing images [15-22]. FCN improves the traditional convolution neural network models (AlexNet, VGG-Net, Google LeNet, etc.), it replaces the full connection layer with convolution layer, which contains huge parameters, and accepts image input of any size, the output results are consistent with the size of the input image, it is a real end-to-end network [23]. Many scholars have reformed the FCN model. Badrinarayanan et al. proposed SegNet network, it follows the idea of image semantics segmentation based on FCN. The network combines the characteristics of coding-decoding structure and jumping network, which enables the model to obtain more accurate output feature map and more accurate classification results under the condition of limited training samples [24]. Ronneberger O et al. proposed U-Net network based on FCN. The most important modification of this network is that there are a large number of characteristic channels in the upper sampling part, which allows the network to propagate the context information to a higher resolution layer. The expansion path and contraction path are symmetrical, forming a U-shaped structure, enabling the network to run with fewer training images and to perform more accurate segmentation operations [25]. But most of these studies are about single network model. It is still a question about which model training can get better training results for image sample input. For this reason, this paper analyses the influence of different network models on the classification effect of high-resolution remote sensing images.

2. RESEARCH AREA AND EXPERIMENTAL DATA

The research area of this paper is Xiaokaihe Irrigation District, Binzhou City, Shandong Province. Xiaokaihe Irrigation Area is a large-scale irrigation area for the

Yellow River diversion, it covers 420,000 people in six counties of Binzhou Yellow River. Its designed irrigation area is 1.1 million mu and its designed diversion flow is 60 cubic meters per second. At the end of 1998, the main canal was built with a total length of 96.5 kilometers, including 51.3 kilometers of sand channel, 4.2 kilometers of sediment sink, 41 kilometers of water channel and 163 key buildings. It is the first ecological irrigation area of Yellow River diversion in China.

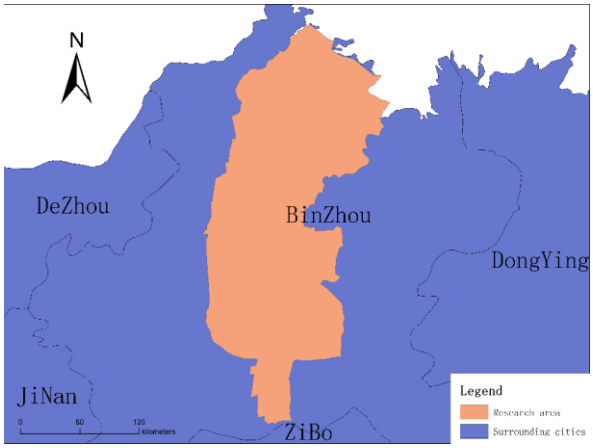

Figure 1 Location map of research area

The data mainly include: (1) Remote sensing image: Landsat 8 remote sensing image on April 17, 2018, The data description is shown in Table 1; (2)The classification data of planting structure obtained by manual interpretation (consisting of five categories of rivers, urban areas, woodlands, cotton and wheat as label data, as shown in Figure 2); (3) Fusion image: In order to preserve the vegetation information in remote sensing image to the greatest extent, 543 band RGB composite image and panchromatic band image are fused by HIS(Intensity, Hue, Saturation) panchromatic sharpening fusion method to realize the fusion of Landsat 8 multi-spectral and panchromatic images, as shown in Figure 3.

3. METHODOLOGY

3.1. Semantic Segmentation Network Classification Method

IHS transform fusion method has the advantages of improving texture and maintaining better space. Therefore, this study uses IHS transform fusion method for image fusion. Firstly, the multispectral image is resampled to have the same resolution as the panchromatic image. Then convert the R, G and B bands of multispectral images into IHS space, and the I, H and S components are obtained. The histogram matching of panchromatic image is carried out by using I component as reference, replace I component by panchromatic image matched by histogram. Finally obtain the fusion image by inverse transformation to RGB space with H and S components.

Table 1 Introduction to Landsat8 Data

Sensor	Band	Wavelength range/μm	Signal-to-noise ratio	Spatial resolution /m
OLI	1-COASTAL/AEROSOL	0.43-0.45	130	30
	2-Blue	0.45-0.51	130	30
	3-Green	0.53-0.59	100	30
	4-Red	0.64-0.67	90	30
	5-NIR	0.85-0.88	90	30
	6-SWIR1	1.57-1.65	100	30
	7-SWIR2	2.11-2.29	100	30
	8-PAN	0.50-0.68	80	15
	9-Cirrus	1.36-1.38	50	30
TIRS	10-TIR	10.60-11.19	0.4K	100
	11-TIR	11.50-12.51	0.4K	100

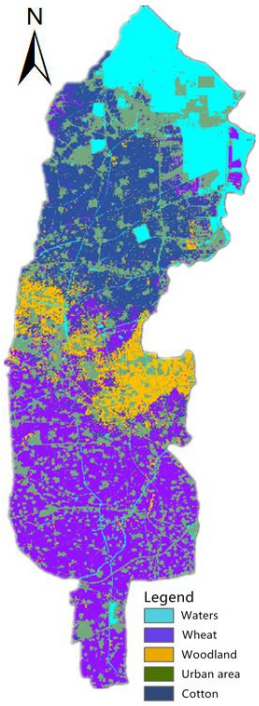

Figure 2 Label image

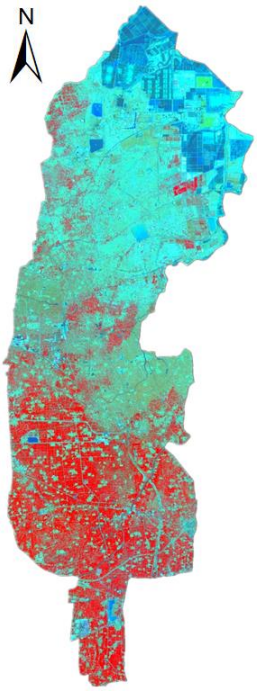

Figure 3 Fusion image

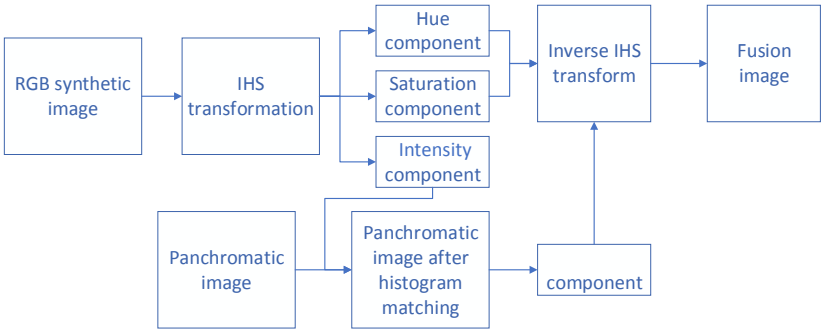

Figure 4 Flow chart of image fusion

3.2. Semantic Segmentation Network Classification Method

Remote sensing image classification method based on deep semantic segmentation network mainly includes two parts: network model training and prediction of classification. The training data set is trained by the network model, and adjust the hyperparametric optimization model until converges. Finally, apply the trained model to predict the test set, obtain the classification results. The classification process is shown in Figure 5.

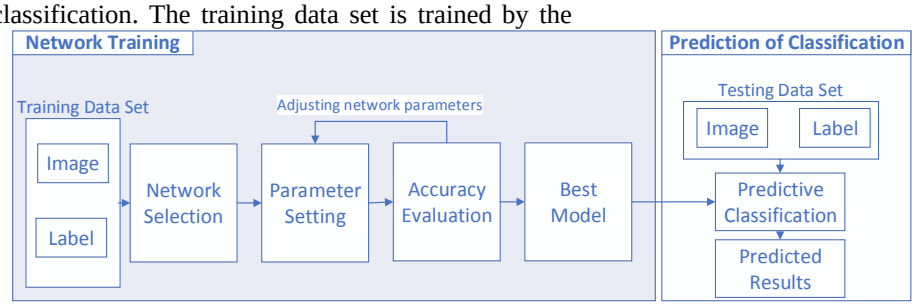

Figure 5 Flow chart of image classification

3.3. FCN Full Convolution Neural Network Model

In FCN classification model, all the connection layers in traditional CNN are changed into convolution layers. The image is sampled up by deconvolution operation, mainly including convolution layer, activation layer and deconvolution layer. The convolution layer uses a convolution core as a template, slides on the image and calculates value of corresponding point in the centre of the template. Activation layer transforms the linear output of the former layer into non-linear one by using activation function, which enhances the network's characterization ability. Deconvolution carries out bilinear sampling on feature map, which is implemented in the form of convolution and restored it to the size of the original image.

FCN uses a jumping architecture, combines the deep semantic information with the shallow representation information, assigns a semantic label to each pixel in the image, and obtains accurate and precise classification results. The FCN architecture diagram is shown in Figure 6.

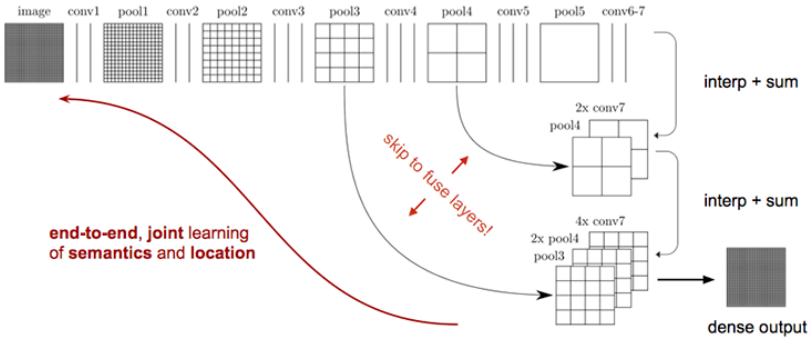

Figure 6 Structure Diagram of FCN Model

3.4. SegNet Model

Classification model based on SegNet is a method based on Encoder-Decoder. It includes convolution layer, batch standardization layer, activation layer, pooling layer, upper sampling layer and Softmax layer. The convolution layer and activation layer are the same as those based on FCN classification model. The pooling layer and upper sampling layer deal with information loss and use Softmax function to classify. Batch standardization accelerates the convergence of the model, greatly improves the training speed, improves the generalization ability of the network and restrains the over-fitting situation through transformation and reconstruction. The essence of

Pooling is to sample, compress the input feature map, reduce the complexity of network calculation, and better adapt to small-scale pixel migration. The structure of SegNet model is shown in Figure 7.

3.5. U-Net Model

In order to locate accurately, the U-Net model combines the high-pixel features extracted from the shrinkage path with the new feature map in the upsampling process to preserve some important feature information in the downsampling process to the greatest extent. In order to make the network structure run more efficiently, the structure cancels the fully connected layers, greatly reduces the training parameters, and benefits from the special U-shaped structure can retain the information in the picture very well. The structure of U-Net network model is shown in Figure 8.

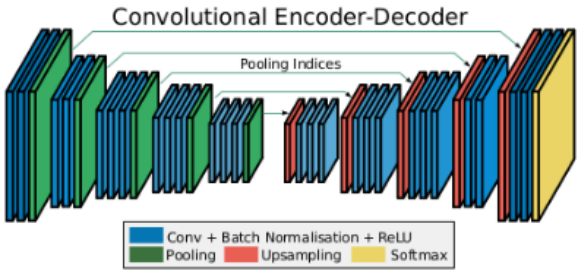

Figure 7 Structure Diagram of SegNet Model

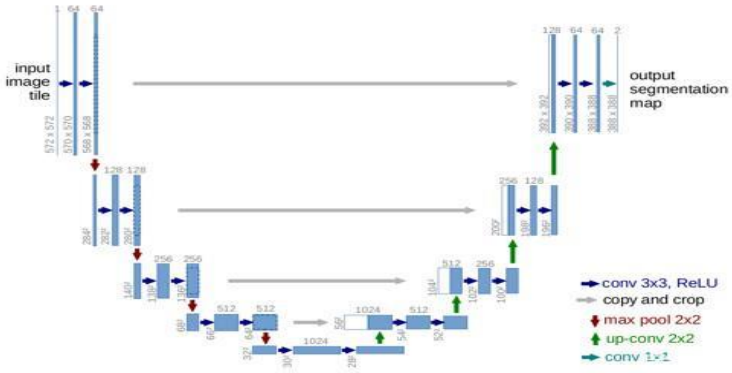

Figure 8 Structure Diagram of U-Net Model

4. RESULTS AND DISCUSSION

4.1. Results

Label graph and training results of different networks are shown in Fig. 9. From left to right are FCN model prediction result graph (left one), SegNet model prediction result graph (right two) and U-Net model prediction result graph (right one).

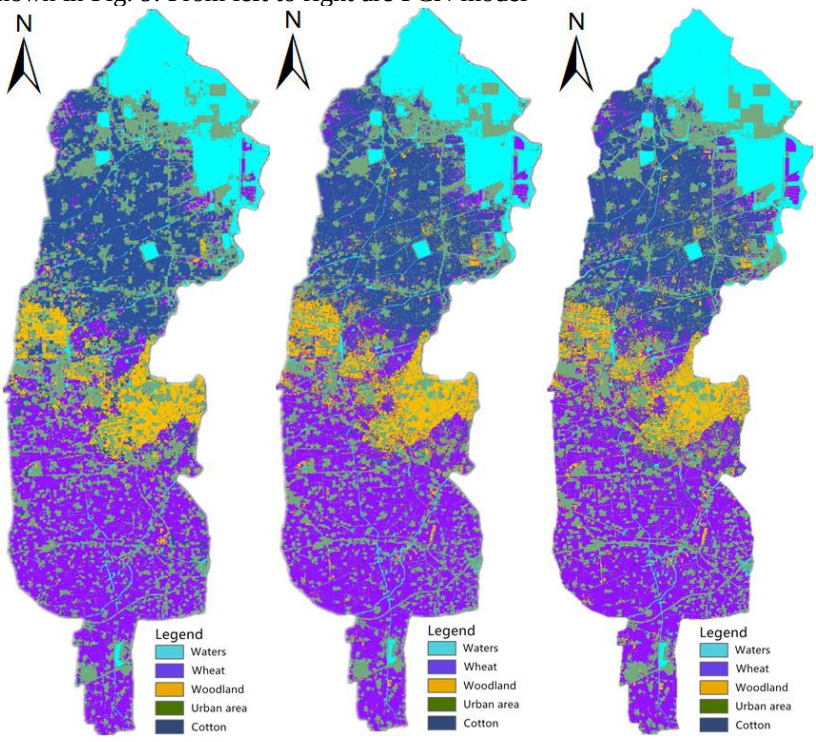

Figure. 9 Result Image

According to different network training, the classification results of remote sensing images predicted by corresponding optimal weight files are obtained, and the classification accuracy of each

category is analyzed by superimposing them with label images. Table 1 shows the classification accuracy of each category.

Table 2 Statistical tables of prediction accuracy for different networks

Category / Accuracy / Networks	Waters	Urban area	Woodlands	Cotton	Wheat	Whole
FCN	92.5%	84.2%	56.9%	74.1%	78.7%	88.2%
SegNet	86.2%	80.4%	48.5%	61%	75%	84.2%
U-Net	94.4%	87.9%	77.6%	80%	76.8%	90.7%

4.2. Discussion

According to Table 2, the prediction accuracy of different types of ground objects in each network model can be summarized as follows:

(1) The accuracy of river regional classification is over 86% in the three models.

(2) The classification accuracy of rivers and cities with obvious characteristics is higher than that of other types;

(3) Woodland, cotton and wheat belong to vegetation with similar characteristic information, the classification accuracy of them is low;

(4) Compared with FCN model and SegNet model, U-Net model can get better classification results, the overall accuracy rate is 90.7%.;

(5) FCN network has the best recognition effect on wheat, reaching 78.7%;

(6) Under the condition of serious mixed planting structure, the identification accuracy of SegNet is only 84.2%.

5. CONCLUSION

Based on three commonly used semantic segmentation models, this paper classifies and predicts high-resolution remote sensing fused images. Taking Xiaokaihe Irrigation District of Binzhou City, Shandong Province as the research area, use different semantic segmentation networks to predict and classify various types of land features, and analyse the corresponding results. It is concluded that under the same conditions, the overall classification accuracy of U-Net is the highest, FCN is the best for wheat recognition, and SegNet is not ideal in the case of serious mixing of objects. Because of the complexity of crop cultivation in the study area, there is a serious mix of different plant types. It is necessary to further improve the correlation between adjacent pixels and consider the influence of different network models on the classification accuracy of remote sensing images under different sizes, and provides a high accuracy and applicability image preprocessing flow for remote sensing image classification based on depth learning.

ACKNOWLEDGMENTS

The authors express gratitude to Henan Science and Technology key Project (NO.182106000025).

REFERENCES

[1]ARVOR D, JONATHAN M, MEIRELLES M S P, et al. Classification of MODIS EVI time series for crop mapping in the state of MatoGrosso, Brazil. International Journal of Remote Sensing, 2011, 32(22):7847-7871.

[2]SONG Qian, ZHOU Qingbo, WU Wenbin, et al. Recent progresses in research of integrating multi-source remote sensing data for crop mapping, Scientia Agricultura Sinica, 2015, 48(6):1122-1135.

[3]WU Bingfang, LI Qiangzi. Crop acreage estimation using two individual sampling frameworks with stratification, Journal of Remote Sensing, 2004, 8(6):551-569.

[4]LIU Jia, WANG Limin, YAO Baomin, et al. Ningxia rice area remote sensing estimation on large scale based on multi-temporal OLI data, Transactions of the Chinese Society of Agricultural Engineering, 2017, 33(15):200-209.

[5]HU Qiong, WU Wenbin, SONG Qian, et al. Recent progresses in research of crop patterns mapping by using remote sensing, Scientia Agricultura Sinica, 2015, 48(10):1900-1914.

[6]MA Li, XU Xingang, LIU Liangyun, et al. Study on crops classification based on multi-temporal NDVI and characteristic Bands, Remote Sensing Technology and Application, 2008, 23(5):520-524.

[7]KANG Jun, HOU Xuehui, NIU Zheng, et al. Decision tree classification based on fitted phenology parameters from remotely sensed vegetation data, Transactions of the Chinese Society of Agricultural Engineering, 2014, 30(9):148-156.

[8]ZHANG Huanxue, CAO Xin, LI Qiangzi, et al. Research on crop identification using multi-temporal NDVI HJ images, Remote Sensing Technology and Application, 2015, 30(2):304-311.

[9]LI Xiao, JIANG Qigang. Extraction of farmland classification based on multi-temporal remote sensing Dada, Transactions of the Chinese Society of Agricultural Engineering, 2015, 31(7):145-150.

[10]CHEN Junying, TIAN Qingjiu. Vegetation classification based on high-resolution satellite image, Journal of Remote Sensing, 2007, 11(2):221-227.

[11]BALL J E, ANDERSON D T, CHAN C S. A comprehensive survey of deep learning in remote sensing: theories, tools and challenges for the community, Journal of Applied Remote Sensing, 2017,

11(4): 042609.
[12]ZHANG L, ZHANG L, DU B. Deep learning for remote sensing data: a technical tutorial on the state of the art, IEEE Geoscie nce and Remote Sensing Magazine, 2016,4(2):22-40.
[13]CHENG G, HAN J, LU X. Remote sensing image scene classification: benchmark and state of the art// Proceedings of the IEEE. [S.l.:s.n.]2017, 105(10):1865-1883.
[14]ZHU X X, TUIA D, et al. Deep learning in remote sensing: a comprehensive review and list of resources, IEEE Geoscience and Remote Sensing Magazine, 2017, 5(4):8-36.
[15]MOU L, ZHU X X. RiFCN: Recurrent network in fully convolutional network for semantic segmentation of high resolution remote sensing images [EB/OL]. (2018-05-16). https:// arxiv.org/abs/1805.02091.
[16]ZHAO W Z, DU S H, EMERY W J. Object-based convolutional neural network for high-resolution imagery classification, IEEE Journal of Selected Topics in Applied Earth Observations and Remote Sensing, 2017:1-11.
[17]XUAN Yongcang. Research on the Semantic segmentation of complex scene image of field based on fully convolutional networks, Xi'an: Northwest A & F University, 2017.
[18]FANG Xu, WANG Guanghui, YANG Huachao, et al. High resolution remote sensing image classification combining with mean-shift segmentation and fully convolution neural network, Laser & Optoelectronics Progress, 2018(55):446 -454.)
[19]CHEN Guangsheng, CHEN Shouyu, JING Weipeng, et al. Remote sensing image pixel -level classification with genetic algorithm and fully convolu-tional network, Journal of Chinese Computer Systems, 2018, 39(7):1590-1595.
[20]SHRESTHA S, VANNESCHI L. Improved fully convolutional network with conditional random fields for building extraction, Remote Sensing, 2018, 10(7):1135.
[21]FU G, LIU C J, ZHOU R, et al. Classification for high resolution remote sensing imagery using a fully convolutional network, Remote Sensing, 2017, 9(5):498.
[22]MOU L, ZHU X X. Vehicle instance segmentation from aerial image and video using a multitask learning residual fully convolutional network, IEEE Transactions on Geoscience and Remote Sensing, 2018, 56(11): 6699 – 6711.
[23]LONG J, SHELHAMER E, DARRELL T. LONG J, DARRELL T. Fully convolutional networks for semantic segmentation, IEEE, Transactions on Pattern Analysis & Machine Intelligence, 2014, 39(4):640-651.
[24]Badrinarayanan V, Kendall A, Cipolla R. SegNet: a deep convolutional encoder -decoder architecture for image segmentation [EB/OL]. (2015-11-02). https://arxiv.org/abs/ 1511.00561.
[25]Ronneberger O, Fischer P, Brox T.U-Net: Convolutional networks for biomedical image segmentation, Medical Image Computing and Computer-Assisted Intervention (MICCAI) , 2015 , 93 51: 234-241.

Design of Playground Ticketing Scheme Based on Logit Model Algorithm

Yanan Zhang
Jincheng Campus, Taiyuan University of Science and Technology, Jincheng, Shanxi, China, 048011
E-mail: 1209043309@qq.com

Abstract: With the improvement of living standards, people are increasingly demanding leisure and entertainment. Large-scale playgrounds have become an important place for people to entertain and entertain. At the same time, people are thinking about how to save time and spend their time. In some large playgrounds, there are usually a variety of ways to buy tickets for people to choose. One is the pass: you can play all the facilities in the playground; one is the ticket: you can only enter the gate of the playground, and the corresponding items need to buy tickets. At the same time, there are two kinds of play rules in the playground: the items that need to be reserved and the items that can be played at any time. This paper analyzes the statistical analysis of the large-scale playground project charging standards and the number of participants in some projects, using gray prediction, least squares method and linear programming. The horizontal numerical analysis of the large-scale playground project reception statistics table was carried out, and the MATLAB model was established. The data change law and development trend were summarized. The numerical estimation was carried out and the corresponding data and laws were obtained. Through the longitudinal numerical analysis of the number of receptions of large-scale playground projects, the number of visitors on the day of the corresponding date is extracted, and the queuing theory is used to establish a model for the charging standards of large-scale playground projects. According to the analysis of the charging situation of large-scale playground items and the waiting time, the relevant number arrangement is obtained. In the ideal state and the normal state, and considering the queuing time, correspondingly establish the relevant model of the selection order, perform a selected Logit model algorithm in the Probit calculation, determine the optimal budget plan, and realize the suitability of the play.

Keywords: grey prediction, least squares method, curve fitting, fare, theoretical study

1. INTRODUCTION

With the improvement of living standards, people's quality of life is getting higher and higher, people's requirements for leisure and entertainment are getting higher and higher. Large amusement parks have become an important place for people to enjoy leisure and entertainment, and they can enjoy life. Corresponding to the issue of pass and ticket fees in the large-scale playground, the issue of the order of the items when playing, and the higher the benefits of the playground while making the tourists have a good gaming experience.

Almost all economic theories remind that property rights should be clearly defined before making decisions, thereby avoiding unclear responsibilities due to unclear property rights and improving the efficiency of resource allocation. The same is true for tourist attraction pricing [1]. The distribution of benefits is an important means to balance and coordinate the distribution of benefits during the duration of the scenic spot, and it is also a guarantee for balancing and coordinating the rights of stakeholders. Zhang Yufeng and Wu Kaichao pointed out that under the traditional planning system of China, the ownership of scenic resources is owned by the state or collectively. With the continuous expansion of China's tourism market and the rapid development of the tourism industry, various interest groups have seen the resource asset characteristics of scenic resources, and have struggled to compete for the rights of scenic resources. However, the authors of many articles recognize that the reform of the property rights system of scenic spots is a multi-party game process full of contradictions and conflicts.

Many researchers believe that the government has a positive role in the management of scenic spots, including ticket pricing. However, there are also voices that local governments have too much intervention in scenic area management in the context of unclear property rights [2]. Wang Zanxin believes that the development of county tourism industry depends on the complementarity and behavior coordination of the government and the market. Zhang Yufeng and Wu Kaichao realized that the state's ownership of scenic resources became a kind of illusion, and the local government became the actual representative of the ownership of scenic resources. Due to the inconsistency of the strength and status of the stakeholders in the scenic resources during the game, the acquisition of the interests of the institutional change is also quite unequal. The capital owners and local governments become the greatest interests, national interests and community residents. The benefits are weaker. Some scholars have compared the way of price management of foreign tourist attractions. Xiang Rong pointed out that the

United States and other developed countries have adopted specialized institutions (such as national parks) for vertical management, which have the following characteristics: (1) centralized functions; (2) basic use of national income for the maintenance of scenic spots, regardless of ticket income; 3) The manager is a national public official, not a corporate employee. As a result, the national ticket prices in the United States are low and the protection is doing very well. Of course, due to the nature of tourism resources and the number of tourists, foreign policies have only a reference for our research and have no decisive reference value.

2. THE MECHANISM AND STATUS QUO OF TICKET PRICING

As a commodity, the pricing of tourist attraction tickets requires not only the cost of maintaining the daily operation of the scenic spot, but also the value of tourism resources as a commodity and the regulation of market demand. Pan Qiuling and Cao Sanqiang believe that the pricing of tourist attractions should be considered from the following five dimensions: (1) resource value; (2) cost input; (3) market supply and demand; (4) property rights of scenic spots; (5) quality of service. Xu Feng and Shi Xiaoyan believe that due to the nature of quasi-public products in tourist areas, the ticket prices of tourist attractions are formed during the game of market competition and government intervention. The final decision of price depends on the autonomy of enterprises and the control. In the government's public welfare goal, every price fluctuation is a multiple game at different levels. Generally speaking, in the traditional sense, the price of tourist attraction tickets mainly includes three major items: operating costs, taxes and profits.

For the current situation of scenic spot tickets, most researchers believe that most of the tourist attractions in this stage are overpriced. Song Zhanghai believes that the ticket prices of many scenic spots in China are already higher than the social best price or even the monopoly price. The practice of rising ticket prices in scenic spots is not a measure for the sustainable development of tourist attractions. It will not only ruin the value of the scenic spot as a public good, but will also damage the rights enjoyed by some low-income tourists and cause unfairness in the public interest[3]. Xiang Rong also believes that tourist attractions are not only unreasonable in pricing basis, but also do not reflect fairness in pricing procedures. They should avoid unfair pricing through reasonable and open means.

3. MODELING

Following in table 1 is the symbol description.

Table 1 Symbol Description

Symbol	Symbol Description
μ	Number of customers served per unit of time
λ	Number of customers coming in per unit time
Ls	Number of customers in the system (n) expected value
Lq	The number of customers queued for service in the system
Ws	Stay time
Wq	Waitting Time
s	Number of service desks
ρ	Service strength,
x	Average arrival rate / minute / person
y	Average service rate / minute / person
M/M/S	A type of queuing service model
L	Corresponding to the date in the curve fit
Wi	Number of playground visitors (i is an integer from 1-5)

3.1 MODEL ESTABLISHMENT AND SOLUTION

Using the appendix given data, use MATLAB to establish a gray prediction model (gray prediction: prediction made by the gray system. The so-called gray system is a transition system between the white system and the black box system. Its specific meaning Yes: If all the information of a system is known as a white system, all information is unknown as a black box system, some information is known, some information is unknown, then this system is a gray system.) Statistics on the number of tourists in July and August 2018, Get the chart below (Figure 1):

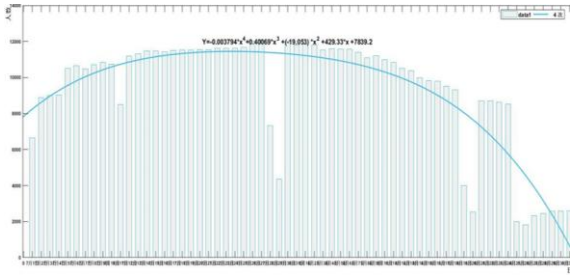

Figure 1 Statistics of the number of visitors in July and August 2018

Curve fitting is performed on the data from 2018 to June 2019, and the images are as follows in figure 2:

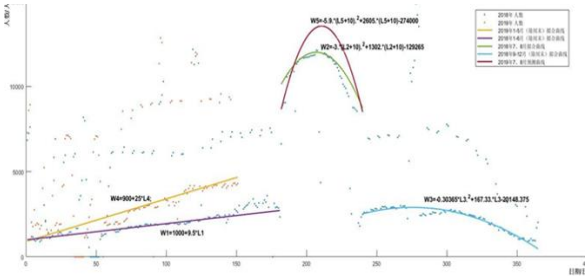

Figure 2 Number of people fitting curve

The data in the appendix will be analyzed. The data in 2018 can be roughly divided into three types: the first category is the weekend travel traffic with the number of people around 6000, and the second category is the work with the number of people below 5000. The traffic flow of the day; the third category is the peak of the summer vacation in July and August; some data have mutations, namely May Day and China Holiday [4]. After fitting the above data, using the MATLAB image fitting, the function expression is obtained:

W1=1000+9.5*L1

W2=-3.*(L2+10).^2+1302.*(L2+10)-129265

W3=-0.30365*L3.^2+167.33.*L3-20148.375

W4=900+25*L4

W5=-5.9.*(L5+10).^2+2605.*(L5+10)-274000

An effective line segment is taken from the above curve, and an analysis can be used to obtain a list of July-August 2019 data, which is the number of visitors predicted for each of the playgrounds in July and August 2019 (in Table 2):

Table 2 The number of visitors predicted for each of the playgrounds in July and August 2019

7.1	**8662**	7. 16	**12425**	8. 1	**13513**	8.16	**11790**
7.2	**8996**	7. 17	**12582**	8.2	**13481**	8.17	**11581**
7.3	**9317**	7. 18	**12727**	8.3	**13437**	8.18	**11360**
7. 4	**9627**	7. 19	**12860**	8.4	**13381**	8.19	**11127**
7. 5	**9925**	7. 20	**12981**	8.5	**13313**	8.20	**10882**
7. 6	**10211**	7. 21	**13090**	8.6	**13234**	8.21	**10625**
7. 7	**10486**	7. 22	**13187**	8.7	**13143**	8.22	**10357**
7. 8	**10749**	7. 23	**13273**	8.8	**13040**	8.23	**10077**
7. 9	**11000**	7. 24	**13347**	8.9	**12925**	8.24	**3429**
7. 10	**11239**	7. 25	**13409**	8.10	**12789**	8.25	**3453**
7. 11	**11466**	7. 26	**13459**	8.11	**12659**	8.26	**3476**
7. 12	**11681**	7. 27	**13498**	8.12	**12509**	8.27	**4212**
7. 13	**11885**	7. 28	**13540**	8.13	**12347**	8.28	**3520**
7. 14	**12077**	7. 29	**13543**	8.14	**12173**	8.29	**3541**
7. 15	**12257**	7. 30	**13534**	8.15	**11987**	8.30	**3562**
		7. 31	**13534**			8.31	**3582**

Available from the image: Maximum value is available in the W5 image: 13598 person-times. According to the statistics of tourists in 2018, the number of visitors reached the maximum on October 5th. According to the image display, it is predicted by gray. The maximum number of people in 2019 is about July 28 or October 5.

Through the vertical numerical analysis of the number of people in the large-scale playground project, the number of visitors on the day of the corresponding date is extracted. According to the charging standard of the large-scale playground project, the relevant formula of queuing theory is used to synthesize relevant data and information. At the same time, by establishing a MATLAB model, the number of players in the four projects A4, B5, B12, and B25 in the past period of time is counted, and the data law is observed. The queuing theory formula is used to

calculate the average number of queues and the average waiting time [5].

There are four projects. When someone has the same time, they can reach the location of the four projects at the same time. The examples are subject to the Poisson distribution. The average arrival rate is x people per minute. The service time is subject to the exponential distribution. The average service rate is y per minute. Suppose people arrive in a queue and then queue up to idle items. Obviously, the capacity and customer source of the system are not limited, and it belongs to the M/M/S type queuing service model [6]. As can be seen from the above, the model is constructed as shown below in Figure 3.

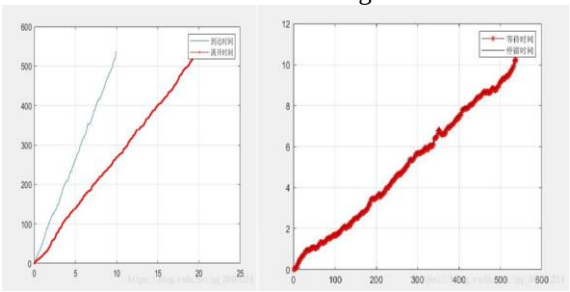

Figure 3 M/M/S type queuing service model

From the queuing theory formula, the number of play, waiting number and waiting time of the four items A4, B5, B12 and B25 on August 5, 2018 are calculated from the data provided by the above formula and appendix.

$$Wq = \frac{\lambda}{\mu(\mu-\lambda)} \quad (1)$$

$$\rho = \frac{\lambda}{\mu} \quad (2)$$

$$Ls = \frac{\lambda}{\mu-\lambda} = \frac{\rho}{1-\rho} \quad (3)$$

$$Ws = \frac{1}{\mu-\lambda} \quad (4)$$

$$Wq = \frac{\lambda}{\mu(\mu-\lambda)} = Ws\rho \quad (5)$$

Using the above method, the average waiting time and the average number of queuing people are calculated for each item, and the obtained values are curve-fitted, and then the number of people playing A4, B5, B12, and B25 on August 5, 2019 is 11236, 11118. 407, 9931. (Unit: person-time), each project is divided into two types of indoor and outdoor models to establish a three-dimensional model, combined with the (1) question to obtain the prediction curve of August 2019, further predicting the various projects on this day The number of players, the model fits as follows in Figure 4 and Figure 5:

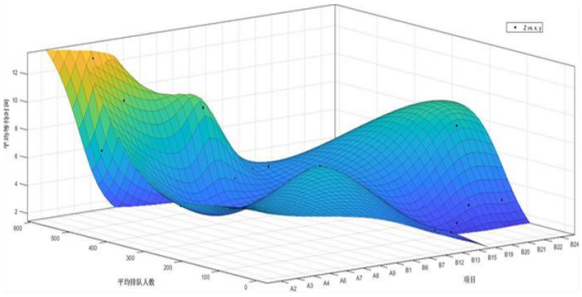

Figure 4 Average number of queues and average waiting time for indoor projects in 2019

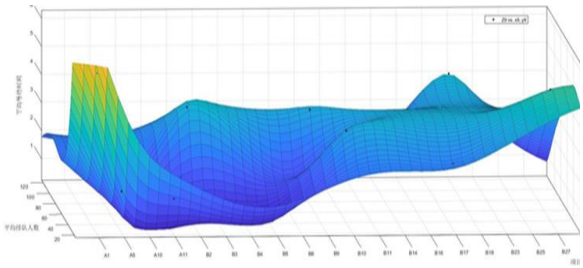

Figure 5 Average number of queues and average waiting time for outdoor projects in 2019

4. CONCLUSION

When considering the total social welfare, the optimal pricing strategy under the sub-voting system (that is, adopting the multi-level charging model) can obtain greater social total welfare than the optimal pricing strategy under the universal ticket system. When the policy makers only consider their own interests, there is no difference in the results of the two types of booking methods, but the results are inferior to the consideration of the total social welfare [7].

For newer projects, it is necessary to limit the price to attract tourists, so a certain amount of ticket fees always makes sense.

In the case of the sub-vote system over the pass system, we also understand the reasons behind the price-makers' enthusiasm for the pass system and higher ticket prices. The advantage of this model is that it compares two ticketing systems through a simple model and the role of government pricing in it. The model setting is basically in line with the characteristics of the Chinese playground. It is assumed that although it is more, it is more reasonable. In the model derivation, various parts of social welfare can be graphically represented, which is intuitive [8].

Due to the increasing marginal negative externalities, the negative externalities of the square are related to the "most comfortable visitors" of the square. When the number of people exceeds the most comfortable number, the square will become more and more crowded and the negative externalities will become larger and larger. However, when the marginal negative externalities are less than the marginal positive externalities, the admission to the park is still socially optimal. When the marginal negative

externality exceeds the marginal positive externality, it is necessary to collect admission tickets.

Since the number of tourist areas will fluctuate according to the season, tickets should also be floated according to the off-season season. In addition, considering the pricing process as a game model between policy makers (governments) and policy benefits/victims (tourists) can better overcome the trade-offs between different utilities in the model, and more in line with the actual pricing process is more realistic.

If policy makers (governments) have stronger game power, balanced pricing results are still better than the pass system; if policy makers (governments) only consider income, due to the existence of tourist power, the vote system The optimal result will be better than the pass system, but the gap will be narrowed, and the degree of reduction will be determined by the relative size of the two game forces.

5. COUNTERMEASURES

Establish and improve a sound management system, clarify the distribution of property rights of tourism resources, realize the rational distribution of management rights and management rights; rationally classify resources in the scenic area, find ancient cultural relics and ecological environment that need to be protected, and implement multi-level management; Through the use of historical data research, market research to determine the market supply and demand relationship, and comprehensive benefits, in multiple parties (government, tourists, businesses) in the equal game and negotiation of multi-level reasonable pricing of attractions; improve tourist attractions from a single The transition from sightseeing to comprehensive service industry development.

REFERENCES

[1]Wen C H, Chen T N, Fu C. A factor-analytic generalized nested logit model for determining market position of airlines. Transportation Research Part A, 2014, 62(4):71-80.

[2]Srinivasan K K, Mahmassani H S. A Dynamic Kernel Logit Model for the Analysis of Longitudinal Discrete Choice Data: Properties and Computational Assessment. Transportation Science, 2005, 39(2):160-181.

[3]Oshagbemi T, Ocholi S A. Influences on leadership behaviour: a binomial logit model. International Journal of Social Economics, 2013, volume 40(2):102-115.

[4]Luca A D. A Logit Model with a Variable Response and Predictors on an Ordinal Scale to Measure Customer Satisfaction. Quality & Reliability Engineering International, 2010, 22(5):591-602.

[5]Yi Liu, Jiawen Peng, and Zhihao Yu. 2018. Big Data Platform Architecture under the Background of Financial Technology: In the Insurance Industry As An Example. In Proceedings of the 2018 International Conference on Big Data Engineering and Technology (BDET 2018). ACM, New York, NY, USA, 31-35.

[6]Lu J, Feng T, Timmermans H, et al. An integrated Markov decision process and nested logit consumer response model of air ticket pricing. Transportmetrica A Transport Science Transportmetrica A Transport Science, 2017, 13(6):1-3

[7]Kruger J W, Anna-Marie. Forecasting Ticket Sales – the Case of Commuter Rail in South Africa. Ssrn Electronic Journal, 2011.

[8]Kekana S L. The impact of rapid urban growth on the commuter rail sector: the case of Gauteng province. 2013.

On the English Translation of Song of a Pipa Player from the Perspective of Three Beauties Principle

Du Zenghui , Cheng Xiongyong
Henan University of Technology, School of Foreign Languages Zhengzhou, Henan 450001, China
Email:1773729027@qq.com

Abstract: Poetry is a unique literary art. Poetry translation, as a bridge of intercultural communication, plays an important role in transmitting the aesthetic beauty and the ideas of the original poem. Bai Juyi's poetry is a product in the specific historical period with particular characteristics. Bai's poetry illustrates the beauty of sound, form, and sense of Chinese classical poetry, which requires that the English translation of classical poetry should not only follow the meaning of the original text faithfully and smoothly, but also convey the poetic imagery beauty of the original poetry. On the basis of the previous English translation studies on classical Chinese poetry, this thesis conducts the qualitative analysis of Xu Yuanchong's English translation of Bai's *Song of a Pipa Player* from the perspective of the "Three Beauties" Theory. According to the characteristics of *Song of a Pipa Player* in the aspects of sound, form and sense, this thesis analyzes how Xu presents the beauty of sound, form, and sense of the original poem in the translation process from the perspective of translation aesthetics, which indicates that the "Three Beauties" Theory has a clear guiding significance and great theoretical contribution to the English translation practice of Chinese classical poetry.

Key words: the "Three Beauties" Theory; *Song of a Pipa Player*; poetry translation

Introduction

With its long history and profound culture, China is gradually entering into the center of the world in the well-rounded aspects. Poetry, a unique form of language, has its ingenious literature style expressing the culture and society of a nation. Poetry translation plays an increasingly important role in the dissemination of the various cultures of China, which facilitates the cultural transmission and benefits China and the whole world. Translating Chinese poems into other languages is not only regarded as the process of Chinese literature going to the world, but also the necessary way of developing Chinese culture itself.

Bai's poetry occupies an important position in Chinese poetry history. Bai's personality and characters are vividly shown in his poems, and the charm of Bai's poems is mainly derived from the originality of the images. Although the English translation of Bai's poems has a history of decades, the related research has not been focused continuously, which leads to the fact that it has not been a major breakthrough in the field, and has not been rooted deeply and theoretically. Although some Chinese scholars touch the related research, it is still in the initial stage with lacking systematisms, comprehensiveness and profundity.

When it comes to the translation of poems, Xu Yuanchong cannot be neglected because of his outstanding contributions to this field. His supereminence in poem translation field is not only attributed to his rich and beautiful translation works, but also because of his outstanding contribution to translation theory. Most of his translation theories and principles come from his rich translation practice. His ideas on literary translation, especially on poetry translation, have made great repercussions in the translation field, of which the most important is the "Three Beauties" theory which gains the most popular theory in poem translation. Professor Xu Yuanchong is the expert in English translation of ancient Chinese poetry. He advocated in the translation theory of "Three Beauties" that the original poetry should be kept and transmitted from the three levels of sense, sound and form. The theory of "Three Beauties" has made a very important contribution to poetry translation studies.

Literature Review

Chinese poem translation has been emphasized for a long time since China has launched the reform and opening up policy, which is regarded as the symbol of the development and prosperity of Chinese culture. However, the related research on poem translation has been paid less attention than the poem translation itself, even though the scholars are gradually realizing this situation and trying to do more studies in this field. According to the research contents, the related studies are mainly categorized into four aspects: poem translation practice, poem translation theory, the research on poem translation versions, and the research on translators.

As for the research on poem translation practice, many scholars focus on the ideas about how to translate Chinese poems, and what kind of skills should be involved to poem translation. In details,

different dimensions are emphasized by different scholars on poem translation. For instance, Gao (2017) emphasizes the cultural factors which influences the translation qualities, and in the research poem translation is regarded as the way of communication between different cultures, in which the relevance theory is introduced to the poem translation to deal with the cultural influences on poem translation. Li (2009) carry out the study on the ideology that takes effects in translating poems to deliberate that poem translation is not only about the exchange of different languages, and not about being confined to the words themselves, but also about the macroscopical context in which the outside factors, such as the ideology of the author, should be taken into consideration when doing poem translation. And some scholars are still having the argument about whether the poems can be translated or not. However, the mainstream about this is holding the viewpoint that although it is difficult to translate Chinese poems into other languages considering the culture, history, and traditions, Chinese poem translation is still possible, which needs a tough journey to go.

As to the poem translation theory, the related translation theories and ideas are flourishing dramatically. Chinese poem translation is deeply affected by the translation theories put forward abroad. For example, Nida's functional equivalence theory is one of the most popular translation theories adopted in Chinese poem translation. There is another translation theory which is also popular in poem translation theory in China, namely, domestication and foreignization theory that is put forward by Lawrence Venuti (1995). Zheng (2014) analyzes the translation strategies of Du Fu's poetry from the perspective of domestication and foreignization theory. In the research, the author suggests that compared with the western countries, Chinese culture and literature are not that strong nowadays, so the translators should be encouraged more to adopt foreignization strategy to translate Chinese poems into other languages. There are still other scholars trying to propose another theoretical perspectives to Chinese poem translation, such as ecological translation, reception aesthetics theory, and so on.

All the previous studies reviewed above illustrates the fact that the research on the English translation of Chinese poems are gradually flourishing during the recent decades. However, the related translation theory developed or created by Chinese translators are not paid more attention than those abroad. Generated and nourished by the development of Chinese economy, culture, and society, Chinese translation theory owns its unique merits in doing the research on the English translations of Chinese poems. To enhance and enrich the study of English translation of Chinese poems under the help of Chinese translation theory, this thesis mainly adopts Xu Yuanchong's "three beauties" theory to analyze Xu's English translation of Bai's landscape poems to justify the application of "Three Beauties" theory in Bai's poems and try to provide the applicable strategies of Chinese poetry translation.

Theoretical Foundation

Since the birth of Xu Yuanchong's "Three Beauties" theory, the comprehensive changes have taken place in carrying out the analysis of poem translation. This part deliberates the theoretical foundation of this thesis with the brief introduction to Xu Yuanchong.

A Brief Introduction to Xu Yuanchong

Professor Xu Yuanchong is outstanding in the translation field because of his rich and beautiful translation works, and his prominent contribution to translation theory. Most of his translation theories come from his rich translation practice. For literary translation, especially in poetry translation, his ideas have made great repercussions in the translation field, of which the most important is the "three beauties" theory. On the basis of the "three beauties" theory, Xu Yuanchong also put forward the theory of "superiority" and "competition theory". His achievements in translation practice are also obvious to all. He translated the world masterpieces such as "Reminiscence", "John Christoph", "Red and Black" and "Mrs. Bovary" into Chinese, and translated "the Book of Songs", "Chu Ci", "Romance of the Western Chamber" and "Three Hundred Tang Poems" into English or French. Indeed, Mr. Xu has achieved remarkable achievements both in translation practice and in translation theory.

"Three Beauties" Theory

The "Three Beauties" theory refers to the beauty of sense, the beauty of form and the beauty of sound. The "Three Beauties" theory is inspired by Lu Xun about how to write articles. However, Mr. Xu applies this theory to literary translation. According to Xu, when translating poems, the beauty of sound and form should be concerned as much as possible without breaking the beauty of sense. Then in "Journal of Foreign Languages", Xu added the relationship between the "Three Beauties". The beauty of sense is the most important factor, the beauty of sound is the secondary, and the beauty of form follows them, which means the beauty of sound should be pursued as much as possible without breaking the beauty of sense, and the beauty of form should be improved as much as possible on the conditions of pursuing the beauty of sense and sound (Xu, 1979). Those three beauties are indispensable. Mr. Xu actively advocates the use of the "Three Beauties" theory to guide the translation of poetry, and to carry out his translation standards in the practice of translation.

With regard to the beauty of sense, Mr. Xu explained that the historical factors or associative factors are usually involved in dealing with the beauty of sense. When translating the poems into another language,

without the similarly historical and associative experiences, it is not easy to convey the sense beauty of the original poem. Therefore, when translating the meaning of the original poems, it is not only to express the meanings of its surface, but also to express its underlying meanings. In translation, the proper words in meaning should be chosen in the target language to meet with the sense of beauty in source language, and sometimes the beauty of sense can be realized by the sense of form and sound.

Regarding the beauty of form, Xu Yuanchong believes that this is mainly in terms of the length and the integrity of the poem. In his "Art of Translation" and many other papers on translation studies, Mr. Xu has repeatedly emphasized the importance of the beauty of form combining with the different rhyme patterns, which indicates his insistence that the structural factors should be paid more attention when doing translation. Mr. Xu also insists that length and symmetry should be included when dealing with the beauty of form. Generally speaking, it is difficult to follow the similar structure from source language when doing the translation to meet with the beauty of forms in target language. However, Xu has never been afraid of overcoming the difficulties, and has been brave to try and translate countless outstanding works.

As for the beauty of sound, the different rhyme patterns can be deployed according to the common usage of target language to meet with the source language, in which the rhymes in target language can be correspondingly chosen according to the rhymes in source language. Reduplication, repetition, and alliteration can be also employed to accomplish the beauty of sound. Mr. Xu is also very concerned about rhymes. Chinese ancient poetry is very strict in tone, rhyme and number of sentences, just like dancing with handcuffs and fetters. In his translation, he put on the "handcuffs and fetters", trying to make the translation with strict rhythm, sound step and number of sentences, so that the translation had the same harmony and aesthetic feeling as the original.

Analysis of the Translation of *Song of a Pipa Player* from "Three Beauties" Theory

The previous parts of this thesis have been deliberated the literature review of the English translation of Chinese poems, the features of Bai's poems, and the theoretical framework of Xu's "Three Beauties" Theory. This part conducts the specific analysis of the Xu Yuanchong's English translation of *Song of a Pipa Player* from "Three Beauties" Theory with taking the concrete examples to illustrate the justification of the employment of the "three beauties" when translating *Song of a Pipa Player*.

Analysis from the Beauty of Sense

According to the "Three Beauties" Theory, the beauty of sense involves dealing with the connotative meaning of a poem. The underlying meaning of a poem should be put into the first place to be considered when translating a poem. The beauty of sense is to achieve the faithful conveying of the sense. Mr. Xu once analyzed the "sense beauty" in the translation of poetry in a TV program: Tang poetry emphasizes "the combination of poetry and painting", with painting in the poem and poetry in the painting. The poet is very particular about artistic conception, and only a few words or phrases are used to depict the beautiful "artistic conception". It is this artistic beauty that he tries his best to embody in his translation.

In maple leaves and rushes autumn seemed to sigh

This poem explained the story of the time - maple leaves, flowers, rustling autumn wind night. Through three kinds of natural scenery - maple leaf, flower and autumn wind - the author reposed the feeling of desponding sadness in his heart. Xu not only faithfully translate the maple leaves, autumn, flowers, but also add a verb 'sigh'. The maple leaves howl in such a somber autumn wind, but the reality is the poet sighing. The use of the verb sigh seems to make the "sense" more beautiful. Here is another example extracted from this poem

Without flute songs we drank our cups with heavy heart;
The moonbeams blent with water when we were to part.

'With heavy heart' have combined the words "不成欢" and "惨" into one preposition phrase. In his translation, the moonbeams blend with water in the boundless river and the reflection of a bright moon in the water. Perhaps the reflection in the autumn wind is still moving and quiet. This gives people a sense of emptiness, loneliness and frustration.

Silence reigned left and right of the boat, east and west;
We saw but autumn moon white in river's breast.

These two poems write pipa player's performance effect. Silence reigned and left and right of the boat, east and west mesmerized the listeners, who were still immersed in music and the silence surrounding them was well expressed. The word "breast" in Xu's translation is commonly used to express the human or animal breast or refer to the human breast. Here, river's breast reminds people of the bright moon, which is printed not only in the river, but also in the poet's heart.

Analysis from the Beauty of Form and Sound

Chinese traditional poetry emphasizes rhyme which accords to the law, level and contrast. While modern English poetry are relatively free, no rules, no level and oblique tones, antithesis, refined language, image clear. The huge differences between the two languages make it difficult to translate Chinese metrical poems into English. In his translation, Xu not only needs "sense beauty", but also needs sound beauty (with sound ruler, tonal pattern and rhyme)

and shape beauty (with symmetrical pattern and even sentence). *Song of a Pipa Player is* the original poem for the seven-word poem, rhyme between sentences. In Xu's English translation, it can be seen that the translated poem has a neat rhyme, a neat step, and the number of sentences is equal to that of the original poem.

The thick strings loudly thrummed like the pattering rain;
The fine strings softly tinkled in a murmuring strain.

These two sentences describe the image of music of pipa music. The original poem rhymes with neat contraptions. The onomatopoeia of "snappy" and "sharp" are used to describe the sound of large strings and small strings popping up. In terms of sound beauty, rain rhymes with strain, and the original poem is also used to make thick strings and fine strings, intensive thrummed and josh tinkled, the pattering rain and murmuring strain compare with each other in form, adding light and light tones, it is hard to find a sense of music beauty.

Suddenly we heard water burst a silver jar,
And the clash of spears and sabers come from afar.

This sentence means music burst out from the almost frozen place, reflecting the intense burst of pipa girl's feelings. Xu translated "乍" to mean "Suddenly" in the original text. However, there are similarities in the sound effect. The verb "burst" conveys the image of water bursting into an object, and "clash" is used to express the "shooting" of knives and guns. Rhyming with the jar in the previous sentence, the translator deliberately changed the sound of knives and guns to "come from afar", indicating the translator's determination to pursue "sound beauty".

Conclusion

The "Three Beauties" theory has exerted a great influence on poem translation studies. This thesis has discussed Xu's English translation of *Song of a Pipa Player* under the framework of the "Three Beauties" theory put forward by Xu Yuanchong who is the prominent poem translator. A general view can be arrived at that the "Three Beauties" theory is a successful and effective device to examine *Song of a Pipa Player* from the aesthetic aspect. Specifically, as for the beauty of sense, Xu follows the meaning of the original poems with using various rhetorical devices and he put the beauty of sense into the first place with taking the risk of losing the beauty of sound and the beauty of form. As to the beauty of form, Xu's translation on *Song of a Pipa Player* pursues the similarity of the structures in phrase and sentence with slightly changing the orders of the meanings in the lines. In terms of the beauty of sound, Xu's translation on *Song of a Pipa Player* deals with the rhymes and meter between lines with obeying the musical quality of *Song of a Pipa Player*. Although, it is difficult to completely fulfill the three principles in the "Three Beauties" theory, Xu's translation has been trying the best to meet with the all the principles to represent the beauty of the original poems in different dimensions, and to real the images and emotions of the author. Therefore, this thesis exemplifies the effectiveness of the "Three Beauties" theory as a tool of translating Chinese classic poems into English.

References:

[1] Yang Xianyi, Dai Naidie. *Chinese-English translation of ancient poetry garden*. Tang poetry. Foreign languages publishing house, 2003.

[2] Xu Yuanchong. *300 Tang Poems*. Higher education press, 2000.

[3] Xu Yuanchong. *Dare to be the first in translation studies*. Chinese translation, 1999, (2).

[4] Xu Yuanchong. *The art of translation*. China foreign translation publishing company, 1984.

[5] Rao Fanzi. *Chinese and western comparative literature and art*. Beijing: China social sciences press, 1999.

[6] Yao Kefu. *Human poetry and words*. Bibliographic literature publishing house, 1983.

[7] Liu Zhengguang. *Metaphorical thinking in the use of nouns* [J]. Foreign language teaching and research, 2000 (5):335-339.

[8] Mao Ronggui. *Translation aesthetics* [M]. Shanghai: Shanghai jiao tong university press, 2005:216.